SUPER-ORTHOGONAL SPACE-TIME TURBO CODED OFDM SYSTEMS

By

Ilesanmi Banjo Oluwafemi

Submitted in fulfillment of the academic requirement for the degree of Doctor of Philosophy in Electronic Engineering,

University of KwaZulu-Natal, Durban, South Africa

September 2012

THESIS TITLE

Super-Orthogonal Space-Time Turbo Coded OFDM Systems

Submitted by

Ilesanmi Banjo Oluwafemi

IN FULFILLMENT OF THE DEGREE OF

Doctor of Philosophy in Electronic Engineering at the University of KwaZulu-Natal, Durban, South Africa

Date of Submission

September 2012

Supervised by

Prof. S. H. Mneney

As the candidate's supervisor, I agree to the submission of this thesis

Signed: _____

Name: _____ Date: _____

DECLARATION

I, **ILESANMI BANJO OLUWAFEMI,** declare that:

(i) The research reported in this thesis, except where otherwise indicated, is my original work.

(ii) This thesis has not been submitted for any degree or examination at any other University.

(iii) This thesis does not contain other persons' data, pictures, graphs or information, unless specifically acknowledged as being sourced from other persons.

(iv) This thesis does not contain other persons' writings, unless specifically acknowledged as being sourced from other researchers. Where other written sources have been quoted, then:

(a) Their words have been re-written but the general information attributed to them has been referenced;

(b) Where their exact words have been used, their writing has been placed inside quotation marks, and referenced.

(v) Where I have reproduced a publication of which I am an author, co-author or editor, I have indicated in detail which part of the publication was actually written by myself alone and have fully referenced such publication.

(vi) This thesis does not contain text, graphics or tables copied and pasted from the internet unless specifically acknowledged, the source being detailed in the thesis and in the References section.

Signed: _____

DEDICATION

This thesis is dedicated to God: The Ancient of days and

the Qualifier of the unqualified.

PREFACE

The research work reported in this thesis was performed by Ilesanmi Banjo Oluwafemi, under the supervision of Professor Stanley H. Mneney, at the School of Electrical, Electronic and Computer Engineering, University of KwaZulu-Natal, Durban, South Africa. The research work was supported by Telkom South Africa as part of the Center of Excellence programme.

Part of this thesis has been presented at: the SATNAC 2010 conference held at Spier Estate, Stellenbosch, South Africa; the IEEE 2nd International Conference on Wireless Communication Society, Vehicular Technology, Information Theory and Aerospace & Electronics Systems Technology (Wireless VITEA'11) in 2011 in Chennai India; the IEEE AFRICON Conference in 2011 in Livingstone Zambia; and the 19th Telecommunication Forum (Telfor 2011) in 2011 in Belgrade, Serbia. Part of this thesis has been accepted for publication by the South African Institute of Electrical Engineers (SAIEE) research journal and part has been submitted to the EURASIP Journal of wireless communication and networking.

The whole thesis, unless otherwise indicated, is the author's work and has not been submitted in part, or in whole, to any other University for degree purposes.

ACKNOWLEDGEMENT

"I know the thought I think towards you, the thought of peace ....."Jeremiah 29:11
My heartfelt gratitude goes to my Creator and Savior, the Triune God for fulfilling His good pleasure in me concerning this PhD programme.

I am deeply indebted to my supervisor, Professor S. H. Mneney. It has been a pleasure working with him and I feel greatly privileged to have him as my supervisor. I thank him for his guidance, teaching, listening, help, and patience. He is a source of encouragement and motivation.

Special appreciation goes to my wife sweet heart, Grace Adekemi Oluwafemi, for her unparalleled support, sacrifice, supplication and encouragement throughout the research period. Obviously without your support, I could not have completed this hard work. To Tofunmi the Prince of the home, and Tamilore the Princess of the home I say thank you, for your endurance, affection and sacrifice that supported this dream.

Special thanks go to Dr. Oyerinde and Wojuola Olanrewaju for all their invaluable support, time, suggestions and encouragements for the success of this research.

I also wish to convey appreciation to my parents and siblings spiritually and physically for their constant support and prayers for the success of this research. Special thanks to my DLCF family in Durban and in Ekiti State.

Thanks to Telkom South Africa and Alcatel-Lucent and Exotic for their valued financial support in the form of research assistantship through the Center of Excellence in the School of Electrical, Electronic and Computer Engineering, UKZN, South Africa. I also appreciate the financial support of THRIP through the Center of Engineering Postgraduate Study (CEPS) in the form of a bursary.

Thanks also go to the government of Ekiti State, Nigeria for awarding me a postgraduate scholarship for my overseas training. My appreciation also goes to the Education Trust Fund for their financial support for this programme. I also wish to express my appreciation to the management of Ekiti State University, Ado Ekiti, Nigeria for approving my study leave application with pay during the period of this study.

Thanks to all the professors, and support staff of center of excellence (CoE) who offered me support and help in the course of my PhD programme.

I would like to thank my wonderful friends and colleagues in the journey of postgraduate research, Oluwumi Adetan, Jules Moualeu, Chrispin Mulangu, John Masumba, Remmy, Gbolahan Aiyetoro, Tunde Alonge who have become dear and treasured friends. It is a great privilege to work with you all.

ABSTRACT

The ever increasing demand for fast and efficient broadband wireless communication services requires future broadband communication systems to provide a high data rate, robust performance and low complexity within the limited available electromagnetic spectrum. One of the identified, most-promising techniques to support high performance and high data rate communication for future wireless broadband services is the deployment of multi-input multi-output (MIMO) antenna systems with orthogonal frequency division multiplexing (OFDM). The combination of MIMO and OFDM techniques guarantees a much more reliable and robust transmission over a hostile wireless channel through coding over the space, time and frequency domains.

In this thesis, two full-rate space-time coded OFDM systems are proposed. The first one, designed for two transmit antennas, is called extended super-orthogonal space-time trellis coded OFDM (ESOSTTC-OFDM), and is based on constellation rotation. The second one, called super-quasi-orthogonal space-time trellis coded OFDM (SQOSTTC-OFDM), combines a quasi-orthogonal space-time block code with a trellis code to provide a full-rate code for four transmit antennas. The designed space-time coded MIMO-OFDM systems achieve a high diversity order with high coding gain by exploiting the diversity advantage of frequency-selective fading channels.

Concatenated codes have been shown to be an effective technique of achieving reliable communication close to the Shannon limit, provided that there is sufficient available diversity. In a bid to improve the performance of the super orthogonal space-time trellis code (SOSTTC) in frequency selective fading channels, five distinct concatenated codes are proposed for MIMO-OFDM over frequency-selective fading channels in the second part of this thesis. Four of the coding schemes are based on the concatenation of convolutional coding, interleaving, and space-time coding, along multiple-transmitter diversity systems, while the fifth coding scheme is based on the concatenation of two space-time codes and interleaving. The proposed concatenated

coding schemes in MIMO-OFDM systems achieve high diversity gain by exploiting available diversity resources of frequency-selective fading channels and achieve a high coding gain through concatenations by employing the turbo principle. Using computer software simulations, the performance of the concatenated SOSTTC-OFDM schemes is compared with those of concatenated space-time trellis codes and those of conventional SOSTTC-OFDM schemes in frequency-selective fading channels. Simulation results show that the concatenated SOSTTC-OFDM system outperformed the concatenated space-time trellis codes and the conventional SOSTTC-OFDM system under the various channel scenarios in terms of both diversity order and coding gain.

TABLE OF CONTENTS

LIST OF ABBREVIATIONS

3G	-	Third Generation Network
AGWN	-	Additive Gaussian White Noise
APP	-	a Posteriori Probability
BER	-	Bit Error Rate
BM	-	Branch Metric
BPS	-	Bit Per Modulated Symbol
BPSK	-	Binary Phase Shift Keying
BRAN	-	Broadband Radio Access Network
CC	-	Convolutional Code
CDMA	-	Code Division Multiplexing Access
CFR	-	Channel Frequency Response
CGD	-	Coding Gain Distance
CP	-	Cyclic Prefix
CSI	-	Channel State Information
DAB	-	Digital Audio Broadcasting
DFT	-	Discrete Fourier Transform
DS-SOSTTC	-	Double Serial Super-Orthogonal Space Time Trellis Code.
DVB-H	-	Digital Video Broadcasting for Handheld Terminal
DVB-T	-	Digital Video Broadcasting For Terrestrial Television
EDGE	-	Enhance Data for Global Evolution
ESOSTTC	-	Extended Super-Orthogonal Space-Time Trellis Code
FD	-	Frequency Domain
FDMA	-	Frequency Division Multiple Access
FER	-	Frame Error Rate
FFT	-	Fast Fourier Transform
GSM	-	Global System for Mobile Communication

HC-SOSTTC	-	Hybrid Concatenated Super Orthogonal Space-Time Trellis Code
HiperLAN/2	-	High Performance Local Area Network
ICI	-	Inter Carrier Interference
IDMA	-	Interleave Division Multiple Access
IEEE	-	Institute of Electrical and Electronic Engineering
IFFT	-	Inverse Fast Fourier Transform
IMT	-	International Mobile Telecommunication
ISI	-	Inter Symbol Interference
ISOVA	-	Improved Soft Output Viterbi Algorithm
ITU	-	International Telecommunication Union
LAN	-	Local Area Network
LCP-STBC	-	Linear Constellation Pre-coded Space-Time Block Code
LDPC	-	Low Density Parity Check Code
LLR	-	Log Likelihood Ratio
LOS	-	Line of Sight
LTE	-	Long Term Evolution
MAP	-	Maximum a Posteriori Probability
MIMO	-	Multiple/Input- Multiple/Output
ML	-	Maximum Likelihood
MLD	-	Maximum Likelihood Decoding
MMAC	-	Multimedia Mobile Access Communication
MMAC	-	Multimedia Mobile Access Communication
MPD	-	Minimum Product Distance
MRC	-	Maximum Ratio Combining
NRC	-	Non Recursive Code
OFDM	-	Orthogonal Frequency Division Multiplexing
OFDMA	-	Orthogonal Frequency Division Multiple Access

OSTBC	-	Orthogonal Space-Time Block Code
PAPR	-	Peak Average Power Ratio
PCCC	-	Parallel Concatenated Convolutional Code
PDC	-	Personal Digital Cellular
pdf	-	Probability Density Function
PEP	-	Pairwise Error Probability
QAM	-	Quadrature Amplitude Modulation
QPSK	-	Quadrature Phase Shift Keying
RS	-	Reel-Solomon
RSC	-	Recursive Systematic Code
SCCC	-	Serial Concatenated Convolutional Code
SF	-	Space Frequency
siso	-	Single Input Single Output
SISO	-	Soft Input Soft Output
SM	-	Spatial Modulation
SNR	-	Signal to Noise Ratio
SOST-CC	-	Super Orthogonal Space-Time Convolutional Code
SOSTFTC	-	Super Orthogonal Space-Time Frequency Trellis Code
SOSTTC	-	Super Orthogonal Space-Time Trellis Code
SOVA	-	Soft Output Viterbi Algorithm
SQOSTTC	-	Super-Quasi Orthogonal Space-Time Trellis Code
STBC	-	Space-Time Block Code
STC	-	Space-Time Coding
STF	-	Space-Time Frequency
STTC	-	Space-Time Trellis Code
TCM	-	Trellis Coded Modulation
TDMA	-	Time Division Multiple Access

TU	-	Typical Urban
VA	-	Viterbi Algorithm
VLEC	-	Variable Length Error Correcting
VoIP	-	Voice over Internet Protocol
WCDMA	-	Wideband Code Division Multiple Access
WLAN	-	Wireless Local Area Network

LIST OF NOTATIONS

$(.)^T$	Transpose
$(.)^*$	Complex conjugate
$(.)^H$	Transpose conjugate
$\|\|.\|\|_F$	The Frobenius of a matrix
τ_d	Delay spread
B_c	Coherent bandwidth
(f_d)	Doppler spread
(T_c)	Coherent time
v	Vehicular velocity
f_c	Carrier frequency
c	Speed of light
P_e	Error probability
γ	Received signal to noise ratio (SNR)
n_T	Number of transmit antennas
n_R	Number of receive antennas
$h_{i,j}$	Path gain from transmit antenna *i* to receive antenna *j*
η	Additive Gaussian noise
H	Channel matrix
K	Number of subcarrier
L	Number of channel multipath
$\mathcal{N}$	Noise matrix
det	Determinant of a matrix
$\mathbf{I}_{n_R}$	Identity matrix of dimension $n_R \times n_R$
ρ	Average SNR at each receiver

$\|H\|^2$	Normalized channel power transfer characteristic
C_{out}	Outage capacity
P_{out}	Outage probability
T_s	Sampling rate
T_g	Duration of the cyclic prefix
T_w	Duration of the window
Δ_k	Inter-subcarrier spacing
τ_l	lth path delay
G_d	Diversity gain
δ_H	Space-time symbol-wise hamming
d_p^2	Product of the Euclidean distances
G_c	Coding gain
λ_i	i-th eigenvalue
d_{free}	Minimum Hamming distance
E_s	Average symbol energy
N_0	Noise power spectra density
E[.]	Statistical average
rank(.)	The rank of a matrix
Γ	Gamma function
λ	Log-likelihood ratio

LIST OF FIGURES

LIST OF TABLES

CHAPTER 1

GENERAL INTRODUCTION

Modes of communication have evolved over the years from cable communication to wireless, from analog to digital and from speech to applications involving multimedia services. The convergence of communication technology and computer engineering, coupled with the ever increasing demand for broadband services, has led to an explosive growth in wireless communication engineering. The establishment of first generation cellular phones in the early 1980s has greatly inspired interest in wireless communication. The first generation mobile system used analog technology while the second generation mobile system introduced in the 1990s used digital technology [1]. Both the first and the second generation mobile systems were designed for speech transmission. With the success and the interest of the public in the first two generations of mobile communication systems, many researchers and industries concentrated their attention on improving the performance of wireless communication systems and extending them to cater for broadband services that combine speech and data. Industries have also been greatly involved in the introduction of new standards that led to new applications and the enhancement of the performance of the old applications. Examples of such standards include the personal digital cellular (PDC) global systems for mobile communication (GSM), the IS-54, IS-95, and IS-136. These standards designed for speech transmission support data services up to 9.6 kbits/s [1].

The 2.5 generation evolved from these standards and supports more advanced services of up to 100 kbits/s. The third generation was introduced in the 2000s, for high bit-rate services with multimedia applications in mind. The third generation systems supports transmission of up to 2 Mbits/s for slow moving users. International mobile telephone (IMT 2000) is the main body of the third generation standards which include enhanced data for global evolution (EDGE) standards and an enhancement of GSM. It also includes the wideband code division multiple access (WCDMA) and the code division multiple access (CDMA 2000). The third generation applications obviously demand high bit rates and multiple services.

The 3G-long term evolution (LTE) is the recent wireless technology that evolved from 3G technology. The 3G-LTE enables fixed-to-mobile migration of internet applications such as the voice over internet protocol (VoIP). The 3G-LTE supports high bit rates and the spectral efficiency of local area networks (LANs). Standards in the 3G-LTE include the IEEE802.11a, the IEEE802.11b, the IEEE802.11g, and the IEEE802.16-2004. The IEEE802.11a is based on orthogonal frequency division multiplexing (OFDM) and transmits up to 54 Mbits/s of data over 2.45 GHz unlicensed bands. The IEEE802.11g uses OFDM to provide data rates of up to 54 Mbits/s [1]. Other LAN standards include the high performance LAN (HiperLAN) and the multimedia mobile access communication (MMAC).

The fourth generation international mobile telecommunication (4G-IMT) advanced technology of the mobile communication family is the most recently defined technology by ITU and to be deployed in 2012 in the United State of America [2-3]. It is expected to combine OFDM with multiple-input/multiple-output (MIMO) technology to guarantee a data rate of up to 1 Gbits/s. Standards to be used in 4G-IMT include the IEEE802.16e, the IEEE802.11n and the 802.15.3a.

Wireless communication systems face many challenges with the ever increasing demand for high data rate and spectral efficiency. While the demand for data rates increases exponentially, the spectrum and available bandwidth are limited. The harsh nature of wireless channels combined with limited available bandwidth makes the provision of broadband services a challenging task.

1.1 Wireless Channels

Wireless channels are formed when electromagnetic waves are propagated from the transmitter to the receiver through free space [4]. There are usually different paths between the transmitter and the receiver [1]. As a result of obstruction in the path of the propagated electromagnetic wave, the propagation mechanism of electromagnetic wave can take the line of sight (LOS) path, the diffracted path, the reflected path and the refracted path between the transmitter and the receiver.

The effect of this propagation mechanism results in attenuation of the radiated waves (large scale fading and small scale fading). Large scale fading corresponds to the characterization of the signal power over a large distance or time-average behavior of

the signal while small scale fading is the rapid change in the amplitude and power of the signal [1].

Obstructions in the path of the transmitted wave result in reflection, diffraction, refraction and scattering of the transmitted wave which create several versions of the signal (*multipath*) at the receiver. Due to *multipath,* the signal suffers attenuation, distortion, delay and phase shift upon arriving at the receiver. The received signal could add up constructively or destructively. Fading occurs when the interference between the multipath signals add up destructively, which may cause temporary failure of communication systems. Small scale fading that occurs with multiple reflective paths and no line-of-sight signal component is called Rayleigh fading. The envelope of the received signal in this case is such that it can be described statistically by a Rayleigh probability density function (pdf) [5]. Rician fading is said to occur when there is dominant line-of-sight propagation, in addition to propagation from other reflective paths. The envelope of such fading can be illustrated by a Rician pdf [5]. Movement of the transmitter, receiver or the obstructions on the path of the signal in wireless communication systems also results in *Doppler shifts.* This property of the wireless channel creates varying fading channels. Fig 1.1 shows a wireless communication channel showing multipath. The obstructions in the path of the rays from the transmitter causes each of the rays arriving at the receiver to have different amplitudes, time delays, phase shifts and Doppler shifts.

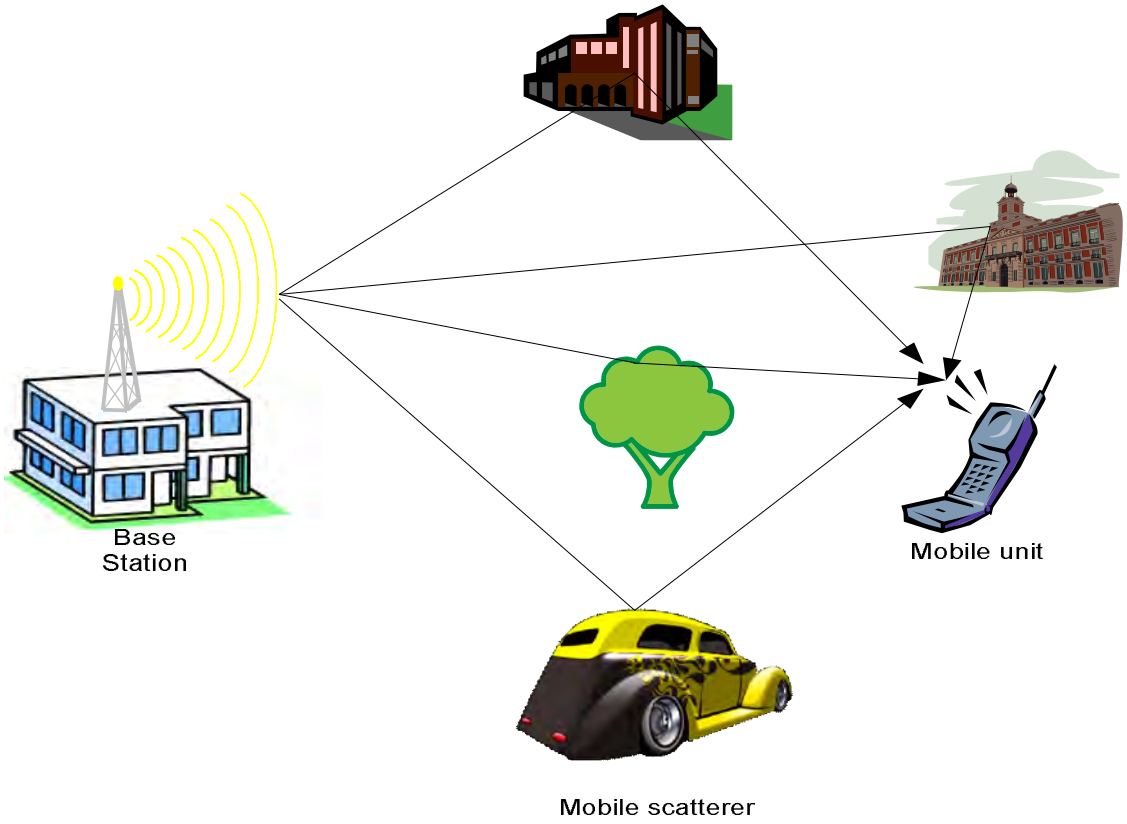

Fig.1.1: A wireless channel showing multipath between the transmitter and the receiver

1.1.1 Wireless Channels Parameters

Wireless channels are characterized by the following parameters [6], [7].

- *Delay Spread* (τ_d) and *Coherence bandwidth* (B_c): Delay spread and coherent bandwidth of a wireless channel describe the time disperse nature of the channel. Delay spread is the difference in propagation time between the longest and shortest paths, considering only paths with significant energy [4]. Coherent bandwidth is the frequency bandwidth over which the channel will experience the same degree of fading. It is related to the delay spread τ_d by

$$B_c \approx \frac{1}{\tau_d}. \qquad (1.1)$$

- *Doppler Spread* (f_d) *and Coherence Time* (T_c): Doppler spread and coherence time of a channel are parameters which describe the time-varying nature of the channel. Doppler spread is the range of frequencies whose Doppler spectrum is not zero. It is given as

$$f_d \approx f_c \frac{v}{c}, \tag{1.2}$$

where v denotes the vehicular velocity, f_c is the carrier frequency, and c is the speed of light. Coherence time of a channel is the period of time over which the channel impulse response remains the same. It is related to Doppler spread f_d by

$$T_c \approx \frac{1}{f_d}. \tag{1.3}$$

1.1.2 Wireless Channel Classifications

Fading channels can be classified based on time and frequency coherence:

- **Fading based on coherence bandwidth and delay spread:** This fading classification is based on frequency coherence of the channel and the symbol. It is based on how the signal bandwidth (B_s) compares with the coherence bandwidth and how the symbol duration (T_s) compares with the delay spread of the channel. Fading based on this classification are:
  - **Frequency non-selective (Flat fading):** In this type of fading, the coherence bandwidth of the channel is much larger than the bandwidth of the signal transmitted. In this fading scenario, the symbol duration is larger than the delay spread of the channel and a single channel filter tap is enough to represent the channel. In this case, all spectral components of the transmitted symbol experience the same fading attenuation.
  - **Frequency-selective fading:** In this type of fading, the channel coherence bandwidth is much smaller than the bandwidth of the transmitted signal. In this fading situation, the transmitted symbol duration is smaller than the delay spread of the channel, i.e. $T_s < \tau_d$ and the channel is represented by multiple taps.

- **Fading based on coherence time and Doppler spread**. This classification is based on the time coherence of the channel and the symbol. It is based on how the symbol period or duration compares with the channel coherence time. There are also two types of fading under these classifications which are fast fading and slow fading channels.
  - **Fast-fading channel:** In this type of fading the period of the transmitted symbol is greater than the channel coherence time. The channel impulse response changes rapidly within the symbol duration of the transmitted symbol and the symbol can be transmitted over multiple fades of the channel.
  - **Slow-fading channel:** Slow fading in wireless channels occurs if the period of the transmitted symbol is smaller than the coherence time of the channel. In this case, the rate of change of the transmitted symbols is faster than the rate of change of the channel impulse response.

The above classifications based on independent phenomena results in four types of fading channels summarized in Table 1.1 with their defining characteristics.

Table 1.1 Summary of types of fading channels and defining characteristics

Type of fading channels	Characteristics
Frequency non-selective (flat) slow fading	$B_s << B_c$ $T_s << T_c$
Frequency non-selective (flat) fast fading	$B_s << B_c$ $T_s >> T_c$
Frequency-selective slow fading	$B_s >> B_c$ $T_s << T_c$
Frequency-selective fast fading	$B_s >> B_c$ $T_s >> T_c$

1.2 Diversity Techniques

Fading can cause the effective signal-to-noise ratio (SNR) at the receiver of a communication system to drop drastically (deep fade) thereby making reliable recovery of the transmitted signal impossible [1]. The inability of a communication system to recover the transmitted signal at the receiver, results in loss of communication (outage) which is undesirable in any communication system. Diversity is a technique used in MIMO systems to combat channel impairments by providing replicas of the transmitted signal to the receiver, which fades independently [7-9]. If the multiple transmitted signals undergo independent fading, the probability that the entire transmitted signal will undergo simultaneous deep fade is minimized. As a result, the probability of outage is reduced in a system employing diversity. The diversity gain G_d is given as

$$G_d = -\lim_{\gamma \to \infty} \frac{log(P_e)}{log(\gamma)} , \tag{1.4}$$

where P_e is the error probability of the received signal and γ is the received signal-to-noise ratio (SNR).

Diversity techniques are classified according to the domain in which they are introduced as time, frequency and space.

1.2.1 Time Diversity

Time diversity is achieved when different time slots are used to transmit identical messages with the time separation between different transmissions being at least the coherence time of the channel to ensure independent fade [10]. This technique provides replicas of the transmitted signal across time by a combination of channel coding and time interleaving. In time diversity, the receiver suffers from time delay before receiving the entire transmitted signal for onward processing. This time delay results in bandwidth inefficiency.

1.2.2 Frequency Diversity

This technique uses different carrier frequencies to transmit identical messages [11]. To ensure independent fades across different replicas of the transmitted signal, the carrier

frequencies must be separated by more than the coherence bandwidth of the channel. Frequency diversity also suffers from bandwidth inefficiency.

1.2.3 Space Diversity

Spatial diversity is implemented by using multiple antennas separated enough to ensure that individual signals are uncorrelated [12]. Space diversity may be receive diversity in which multiple antennas are employed at the receive side, or transmit diversity in which multiple antennas are deployed at the transmit side. Two examples of spatial diversity are polarization diversity and angle diversity. Angular diversity uses directional antennas to achieve diversity in which different versions of the sent signals are collected from different angular directions. Polarization diversity method uses vertically and horizontally polarized signals to achieve diversity. Polarization diversity does not require a separate location of the antenna but its diversity is limited to two [1].

1.3 Multi-Antenna Transmission Systems

Wireless communication systems consisting of transmitter, channel and receiver are classified according to the number of input and output antennas. The simplest configuration involves the use of a single antenna at the receiving and the transmitting ends, also known as a single-input/single-output (SISO) communication system. When multiple antennas are employed at both the transmitting and receiving ends of a wireless communication system, it is called a multiple-input/multiple-output (MIMO) communication system. The main idea of MIMO is that multiple antennas at the transmitting and receiving ends of the communication system are combined in such a way that diversity is exploited to improve the performance of the transmission or the data throughput. Information theory results presented in [13-14] show that the channel capacity and the system performance of a communication system can be increased significantly by using multiple antennas at the transmitting and receiving ends of a communication system. With the MIMO technique, there is an increase in the data rates or diversity gain.

In a MIMO communication system, the availability of information on the MIMO channel parameters at the transmitting side determines the transmission and reception

strategies to be employed. If channel state information (CSI) is available at the transmitter, *beamforming* can be employed, but with no CSI at the transmitter, space-time coding (STC) or spatial multiplexing (SM) can be employed as the transmission technique. The data rates of the communication system are increased with the use of SM but with low reliability, while the STC technique, by exploiting the maximum diversity gain, achieves high performance and reliability.

1.3.1 MIMO Channel Model

Suppose there is a communication system with n_T transmit and n_R receive antennas as shown in Fig. 1.2. At time *t,* the signals $c_{t,j}$, $j = 1, \ldots, n_T$, are simultaneously transmitted from n_T transmit antennas. Each transmitted signal is affected by channel fading, and the response from each signal from each of n_T transmit antenna is received at each n_R receive antenna. If we consider a flat-fading channel with the channel gain between receive antenna *j* and transmit antenna *i* given as $h_{i,j}$, then the received signal at receive antenna j at time t is given by

$$r_{t,j} = \sum_{i=1}^{n_T} h_{i,j} c_{t,i} + \eta_{t,j} \quad , \tag{1.5}$$

where $\eta_{t,j}$ is the additive white Gaussian noise (thermal noise) at the receiving antenna j at time *t.* Consider that the channel is quasi-stationary, that is, the fading coefficients $h_{i,j}$ are constant over a certain time period *T'*, and from period to period they are varied independently. The rate of fading is determined by the value of *T'*. If the data block is transferred during the time *T*, less than *T'*, the fading is said to be slow. In this case the coefficients $h_{i,j}$ are constant during the entire transmission period. On the other hand, if *T* = *T'*, then the channel path gains $h_{i,j}$ change simultaneously with the transmission of data blocks. The signals transmitted during the time period *T* from n_T transmit antennas can be represented using the $(T \times n_T)$ matrix **C:**

$$\mathbf{C} = \begin{bmatrix} c_{1,1} & \cdots & c_{1,n_T} \\ \vdots & \ddots & \vdots \\ c_{T,1} & \cdots & c_{T,n_T} \end{bmatrix}. \tag{1.6}$$

Similarly, the received signal can be represented in the form of $(T \times n_R) -$ matrix **R:**

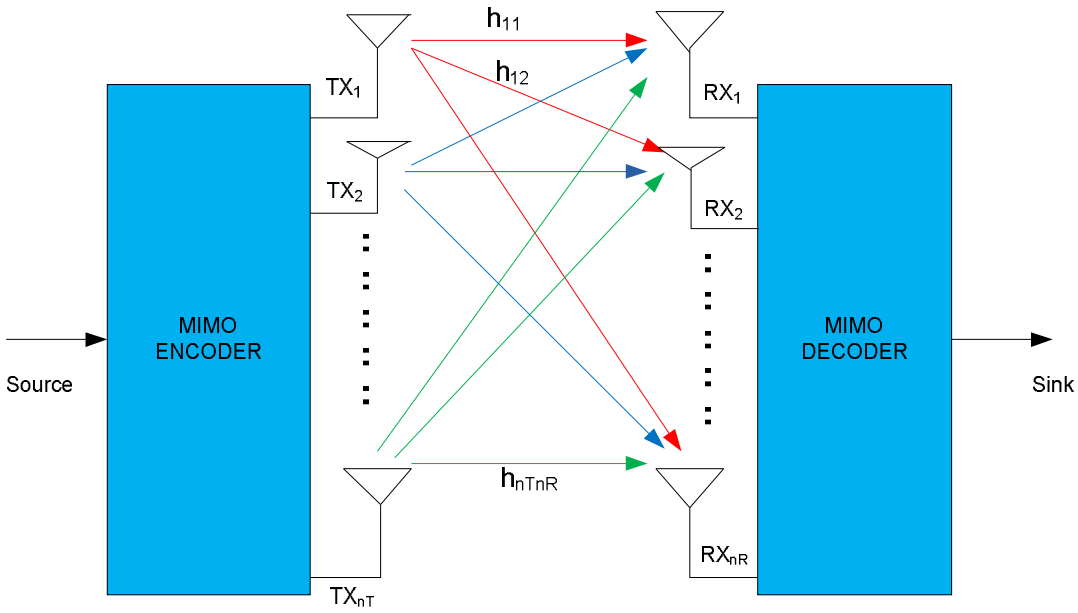

Fig. 1.2: A MIMO system with n_T transmit and n_R receive antennas

$$\mathbf{R} = \begin{bmatrix} r_{1,1} & \cdots & r_{1,n_R} \\ \vdots & \ddots & \vdots \\ r_{T,1} & \cdots & r_{T,n_R} \end{bmatrix}.$$

Assuming $T < T'$, that is, the channel fading coefficients are constant during the transmission period, these fading channel coefficients may also be written in the form of $(n_T \times n_R) -$ matrix **H:**

$$\mathbf{H} = \begin{bmatrix} h_{1,1} & \cdots & h_{1,n_R} \\ \vdots & \ddots & \vdots \\ h_{n_T,1} & \cdots & h_{n_T,n_R} \end{bmatrix}.$$

Then we can write (1.5) in matrix form as :

$$\boldsymbol{R} = \boldsymbol{H}.\boldsymbol{C} + \boldsymbol{\mathcal{N}}. \quad (1.7)$$

where $\boldsymbol{\mathcal{N}}$ is the matrix of noise given by :

$$\boldsymbol{\mathcal{N}} = \begin{bmatrix} \eta_{1,1} & \cdots & \eta_{1,n_R} \\ \vdots & \ddots & \vdots \\ \eta_{T,1} & \cdots & \eta_{T,n_R} \end{bmatrix}. \quad (1.8)$$

The noise is additive white Gaussian noise (AWGN) and its elements are independent of each other. For a complex baseband transmission, the AWGN has a complex Gaussian distribution.

Consider a Rayleigh fading channel whose path gains are modeled by independent complex Gaussian random variables. The channel gain at each time slot is independent, identically distributed (iid) Gaussian random variable with zero mean and 0.5 variance with the envelope of the channel gain $|h_{i,j}|$ having a Rayleigh distribution. Also, $|h_{i,j}|^2$ is a chi-squared random variable with two degrees of freedom, and the average channel energy is $E\left[|h_{i,j}|^2\right] = 1$. If we denote the average power of the transmitted symbol c_i as E_s and that of the variance of the zero mean complex Gaussian noise as $N_0/2$ per dimension, then the average signal-to-noise ratio (SNR) is $\gamma = n_T E_s / N_0$.

1.3.2 MIMO Channel Capacity

It has been shown in information-theoretical studies of wireless channels that MIMO channel capacity is increased significantly compared to the capacity of single-input/single-output (SISO) systems [13-14]. Recently, researchers have been actively engaged in an effort to exploit this new potential of MIMO channel capacity.

Channel capacity can be defined as the maximum error-free data rate that a channel can support. Claude Shannon in [15] derived the capacity of an AWGN channel as

$$C = \log_2(1 + \gamma), \quad (1.9)$$

where γ is the average received signal to noise ratio. The capacity of a deterministic SISO channel is given by [14]

$$C = \log_2(1 + \rho|H|^2), \tag{1.10}$$

where $|H|^2$ is the normalized channel power transfer characteristics and ρ is the average SNR at each receiver.

For a deterministic MIMO channel, the channel capacity is given by [14]

$$C = \log_2\left[\det\left(\mathbf{I}_{n_R} + \frac{\rho}{n_T}\mathbf{H}\mathbf{H}^H\right)\right], \tag{1.11}$$

while for an ergodic MIMO channel, the capacity is given by [13]

$$C = E_{\mathbf{H}}\left\{\log_2\left[\det\left(\mathbf{I}_{n_R} + \frac{\rho}{n_T}\mathbf{H}\mathbf{H}^H\right)\right]\right\}, \tag{1.12}$$

where $E_{\mathbf{H}}$ denotes expectation with respect to **H,** $\mathbf{I}_{n_R}$ is $n_T \times n_R$ identity matrix and det[**A**] is the determinant of matrix **A**. An increase in the number of antennas (assuming $n_T = n_R$) leads to increase in the ergodic capacity. In Fig. 1.3, the ergodic channel capacity, as a function of average SNR, is plotted for several uncorrelated MIMO systems with $n_T = n_R$. It is obvious from Fig. 1.3 that the capacity increases substantially with an increase in the number of antennas.

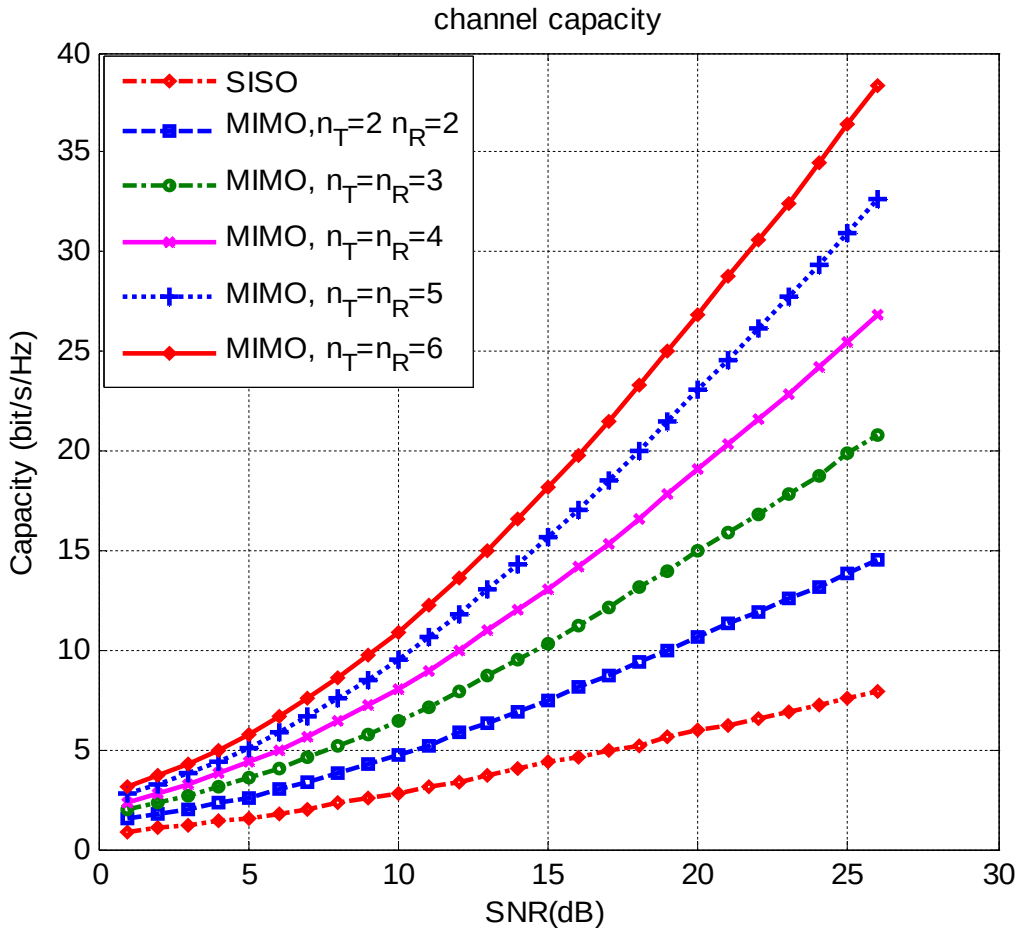

Fig. 1.3: The ergodic channel capacity of a MIMO channel

1.3.3 Outage Capacity

Outage capacity, defined in [14], is a more useful capacity concept of performance measurement for coding purposes. The outage capacity C_{out} is defined as a value that is smaller than the random variable C only with a probability P_{out} (outage Probability). P_{out} is related to C_{out} by

$$P_{out} = P(C < C_{out}). \tag{1.13}$$

The importance of P_{out} is that to transmit C_{out} bits/channel, the capacity of the channel is less than C_{out} with probability P_{out}. In other words, such a transmission is impossible with probability P_{out}. For a stationary channel, if a large number of frames

are transmitted, with a rate of C_{out} bits/channel, the number of failures is P_{out} multiplied by the total number of frames.

1.4 Space-Time Coding

The symbol transmitted over a MIMO channel in each symbol time is a vector because a MIMO channel has an input-output relationship of $\mathbf{r} = \mathbf{Hs} + \boldsymbol{\eta}$. Space-time coding occurs when the signal extends over both space (via the multiple antennas) and time (via multiple symbol times). Space-time coding (STC) is a coding technique designed for use with MIMO systems in which coding is performed in both spatial and temporal domains. Employing STC in a wireless channel can lead to a performance close to the capacity limit of a MIMO wireless channel [16]. STC can achieve transmit diversity and coding gain in a MIMO system without any loss in bandwidth.

1.5 MIMO - OFDM System

1.5.1 OFDM

Orthogonal frequency division multiplexing (OFDM) is a class of multicarrier modulation in which information is carried over many lower rate subcarriers. The concept of OFDM was first introduced in [17] and [18]. The frequency-domain (FD) bandwidth in classic parallel data transmission systems is divided into a number of non-overlapping sub-channels. Each subcarrier hosted by a sub-channel is modulated separately by a data symbol which results in a frequency-multiplexed signal across the entire sub-channel.

The individual sub-channels are orthogonal to one another which ensures non-interference of the subcarrier signals [19]. The early OFDM schemes [17], [18], [20-21] are highly complex because they required many sinusoidal subcarrier modulators and demodulators. The high complexity of the earlier OFDM systems limited the application of OFDM techniques at that time to only military applications. The introduction of the discrete Fourier transform (DFT) for OFDM modulation and demodulation reduced the implementation complexity of OFDM significantly in the early 1970s [22]. Since the reduction in complexity as a result of the introduction of DFT, much research has been carried out on OFDM systems. The performance of

OFDM in mobile communication channels was investigated by Cimini [23] and Kalet [24]. Summary of recent developments in OFDM technology is documented in [25].

OFDM possesses several merits over other wireless access technologies, such as frequency division multiple access (FDMA) [26], time division multiple access (TDMA) [27], and code division multiple access (CDMA) [26] [28-31]. The main advantage of OFDM is the fact that the wireless channel is divided into many narrowband, low-rate, non-selective frequency subcarriers that allow the transmission of multiple symbols in parallel, while maintaining high spectral efficiency. Another feature of the OFDM access technology is that it allows for a multi-user system called orthogonal frequency division multiple access (OFDMA) [32-33]. In the OFDM technique, different modulation signalling can be used for different subcarriers. OFDM is a highly attractive scheme for high data rate communication over frequency selective wireless channels because of its low complexity and high attainable performance. The OFDM system also exhibits high resilience against inter-symbol interference (ISI) introduced by multipath with the use of cyclic prefix symbols [34]. An OFDM system combined with channel coding combats frequency selective fading channels [35 - 36].

OFDM systems however are not without setbacks or disadvantages. One major disadvantage of the OFDM technique is that the envelope is not constant, because the summation is a sine wave. As a result there is a large peak-to-average power ratio (PAPR) [19]. Also due to sub-channel's narrow band, OFDM is sensitive to Doppler frequency and subcarrier offset [37].

OFDM has been widely accepted as a multi-carrier modulation technique over wireless channels. Many European standards are based on OFDM. Examples of such are the Digital Audio Broadcasting (DAB) [38], the Digital Video Broadcasting for Terrestrial Television (DVB-T) [39], the Digital Video Broadcasting for Handheld terminal (DVB-H) [40], the wireless local area networks (WLANs) [41], the Broadband Radio Access Networks (BRANs) [42], and the Long-Term Evolution (LTE) – the fourth-generation mobile communication technology.

Considering that the complex symbols to be transmitted in a K-subcarrier OFDM system with a pass bandwidth *B* are denoted by $\left(X_{-K/2}, \ldots, X_{-1}, X_1 X_2, \ldots, X_{K/2}\right)$, one *K*-subcarrier OFDM symbol can be represented mathematically by [43]

$$s(t) = \begin{cases} \sum_{k=K/2,k\neq 0}^{K/2} X_n e^{j2\pi f_k t}, & for\ kT - T_w - T_g \leq t \leq kT + T_{FFT} + T_w \\ 0 & otherwise \end{cases} \quad (1.14)$$

where f_k is the frequency of the *k*th subcarrier, $T_{FFT} = KT_s$ is the duration of the total number of FFT-points, T_s is the sampling rates, T_g is the duration of the cyclic prefix, and T_w is the duration of the windowing. The transmitted OFDM signal can be demodulated by applying inverse operations to (1.14) as

$$x_k = \frac{1}{T_{FFT}} \int_{t=0}^{T_{FFT}} s(t) e^{-2\pi f_k t} dt. \quad (1.15)$$

FFT operation ensures that the generated subcarriers are orthogonal because each bin of an IFFT corresponds to the amplitude and phase of a set of orthogonal sinusoid.

1.5.2 MIMO-OFDM System

The MIMO technique constitutes an effective and practical approach to high-throughput wireless communication. A MIMO system exploits both transmit and receive diversity to achieve significant improvement in the capacity of the system and its spectral efficiency. MIMO-OFDM forms the foundation of all the candidate standards proposed for IEEE 802.11n [44]. With the potentials of MIMO-OFDM, research efforts have been directed towards MIMO-OFDM in recent times for reliable broadband wireless communication.

Consider a MIMO-OFDM system with n_T transmit antennas, n_R receive antennas and a *K*-subcarrier OFDM modulator for each transmit antenna as shown Fig. 1.4, the input sequence $S = [s_1, s_2, \ldots, s_{K_s}]$ is encoded into codeword $\mathrm{C} \in \mathbb{C}^{\mathrm{KZ} \times \mathrm{n_T}}$, where s_i are modulated signals using some modulation signalling like BPSK or QPSK.

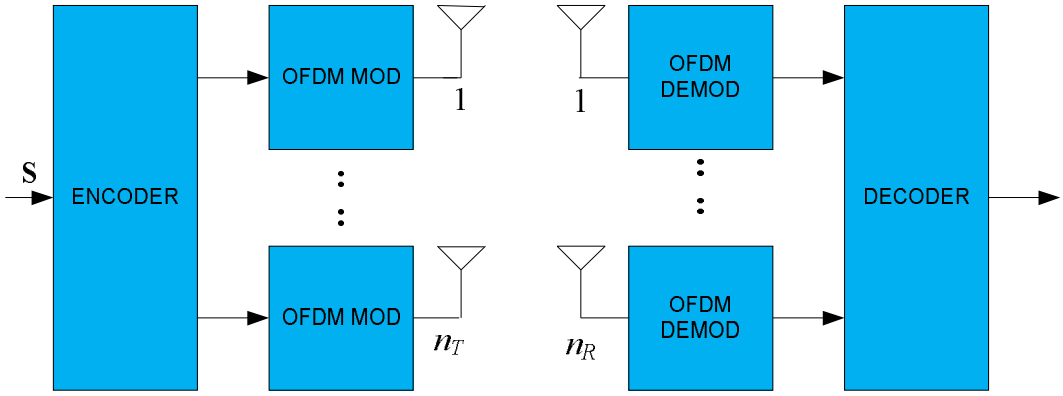

Fig. 1.4: MIMO-OFDM system

The Codeword $\boldsymbol{C}$ transmitted through n_T transmit antennas in Z OFDM symbols is given by

$$\boldsymbol{C} = \begin{pmatrix} c_1^1 & \dots & c_{n_T}^1 \\ \vdots & \ddots & \vdots \\ c_1^z & \dots & c_{n_T}^Z \end{pmatrix}, \tag{1.16}$$

where $c_i^1, c_i^2, \dots, c_i^Z$ will be transmitted from the i-th transmit antenna in OFDM symbols 1, 2, ...,Z respectively. Symbol c_i^Z is a K-length vector, where $i = 1, 2, \dots, n_T$ and $z = 1, 2, \dots, Z$.

Cyclic prefix is added on each OFDM symbol and the c_i^z is transmitted from the i-th transmit antenna at tth OFDM symbol duration. At the receiver, the appended CP is removed, the FFT process is performed and the received signal is decoded.

1.5.3 MIMO-OFDM Channel

The Channel Impulse Response (CIR) between transmit antenna i and receive antenna j in a MIMO-OFDM channel, has L independent delay paths on each OFDM symbol and an arbitrary power delay profile. The CIR can be expressed as

$$h_{i,j} = \sum_{l=0}^{L-1} \alpha_{i,j}(l)\delta(t - \tau_l), \tag{1.17}$$

where τ_l is the $l-$th path delay and $\alpha_{i,j}(l)$ are the fading coefficients at the delay τ_l. Each $h_{i,j}(l)$ is a zero mean complex Gaussian random variable with variance $\frac{\sigma_l^2}{2}$ on each dimension.

The Channel Frequency Response (CFR) which is the fading coefficient for the kth subcarrier between the ith transmit antenna and the jth receive antenna with a proper CP, a perfect sampling time and tolerable leakage can be expressed as

$$H_{i,j}(k) = \sum_{l=0}^{L-1} \alpha_{i,j}(l) e^{-2j\pi k \Delta_k \tau_l}, \tag{1.18}$$

where Δ_k is the inter-subcarrier spacing, $\tau_l = lT_s$ is the lth path delay and $T_s = \frac{1}{N\Delta_k}$ is the sampling interval of the OFDM system.

1.6 Research Motivations

The ever increasing demand for fast and efficient broadband wireless communication requires any future broadband communication system to provide high data rate, robust performance and low complexity within the limited available electromagnetic spectrum. With the spectrum limitation, size, cost and power consumption of the receiver terminal, future communication systems must be bandwidth and power efficient. One of the promising solutions to the challenges of future communication systems is to design efficient coding systems over time, space and frequency domain for MIMO-OFDM systems [45]. There have been increases in the throughput and reliability of wireless communication systems as a result of recent advances in such techniques.

It has been shown in [46] that space-time-frequency coding schemes can achieve a maximum diversity gain of $n_T n_R L\mathcal{T}$, where n_T and n_R are the number of transmit and receive antennas respectively, L is the number of channel paths, and $\mathcal{T}$ is the rank of the channel temporal correlation matrix over MIMO-OFDM systems. Over the years, much research efforts have been directed into obtaining space-time-frequency diversity and reducing the complexity of a space-time-frequency trellis coding system. To achieve this diversity, the length of the shortest error event path (minimum effective length) of the STF trellis system must be as large as possible. Also the coding gain of such a system depends on the channel response and thus it is not viable to optimize the coding

gain [47]. For the code to exploit the available frequency diversity, interleaving across frequency tones is a vital requirement because OFDM in the frequency domain is highly correlated and slowly varying.

Agrawal et al adapted Tarokh's space-time codes [16] to OFDM with multiple transmit antennas in [48]. However, these codes are not optimized for OFDM channels and cannot benefit from the available frequency diversity. Trellis coded modulation (TCM) was concatenated with a space-time block code (STBC) in [49] in order to simplify the design and reduce the complexity of the code. In the system, TCM achieved the desired frequency diversity while STBC guaranteed spatial diversity. The STTC-OFDM system was also proposed in [47] by optimizing the effective length of TCM and by employing a random interleaver. In both systems, the full diversity was achieved at the expense of the coding rate. The signal constellation was extended in [50] to propose a full diversity linear constellation pre-coded space-time block code (LCP-STBC) system at the cost of low power efficiency of the OFDM system. To overcome these drawbacks, super-orthogonal space-time-frequency trellis codes (SOSTFTC) which incorporate super orthogonal codes [51] were introduced. These codes were designed using QPSK constellations with 16, 32, 64-states trellis structure. To achieve multipath diversity, parallel transitions are avoided within the trellis of the SOSTFTC by increasing the trellis states and the schemes provided a lower coding gain on frequency selective channels.

As can be seen, all these proposals have several drawbacks such as not being optimized for MIMO-OFDM systems, having a low coding rate, low power efficiency and a low coding gain, among others. These drawbacks were the motivation behind the simple trellis coding systems proposed in this thesis. The proposed coding schemes offer more than one source of diversity and provide good performance in frequency- selective fading channels with low decoding complexity. The lower coding gain provided by the schemes in [51] further inspired the proposition of several concatenated versions of SOSTTC for MIMO-OFDM system in this thesis. The proposed schemes exploit the rich diversity of frequency-selective fading channels and significantly increase the coding gain of the SOSTTC-OFDM system.

1.7 Assumptions in this Thesis

A channel estimation problem is not addressed in this thesis. Perfect channel estimation is assumed throughout the thesis. Similarly, the problem of time and frequency synchronization between the transmitter and the receiver is not addressed in this thesis. Throughout the thesis, it is assumed that there is a perfect time and frequency synchronization between the transmitter and the receiver of the communication system. It is also assumed in all the simulations, that there is no correlation between all the antennas as well as between subcarriers. Also, only the case of a single user is considered.

1.8 Organization of the Thesis

This thesis is presented in seven chapters. The outline of each of the chapters is as follows. Chapter 1 gives the general introduction to the thesis.

Chapter 2 deals with space-time coding techniques and their performance in quasi-static and fast-fading MIMO channels. The design criteria of STC are examined, followed by a systematic discussion of space-time block code (STBC), space-time trellis code (STTC) and super-orthogonal space-time trellis code (SOSTTC). New SOSTTC that can exploit multipath diversity of frequency-selective fading channel proposed by the author is also presented in this chapter. In addition, this chapter presents the author's simulation results for evaluating the performance of these codes in both quasi-static and fast Rayleigh and Nakagami fading channels. The author's analytical results using coding gain distance are also presented.

Chapter 3 focuses on concatenation of convolutional and SOSTTC code in Rayleigh fading channels. Previous concatenated codes involving space-time code and convolutional code are reviewed. This chapter also presents two double concatenation codes with a constituent code of convolutional and SOSTTC proposed by the writer, with detailed descriptions of the encoding and the iterative decoding. The performance of the concatenated schemes is investigated in both quasi-static and fast Rayleigh fading channels. Pairwise error probabilities (PEP) for the two concatenated schemes are derived. Simulation results are presented to demonstrate the performance of the concatenated schemes and the results are compared with existing schemes in literature.

Chapter 4 reviews the space-time coded OFDM system. The performance of space-time coding in a frequency selective fading channel is discussed. The design criteria for a space-time coded OFDM system are also presented. An extended SOSTTC-OFDM system is proposed for two transmit antennas. Super quasi-orthogonal space-time trellis coding is proposed for a MIMO-OFDM system using four transmit antennas and simulation results of the two schemes are presented over various channel scenarios.

In Chapter 5, concatenated codes are proposed in frequency selective fading channels with an OFDM system. Four different concatenated schemes with a constituent code of convolutional and SOSTTC are presented for MIMO-OFDM systems. The encoding and the decoding of the schemes are described. Pairwise error probability (PEP) for the four proposed concatenated schemes is derived and simulation results describing the performance of the concatenated schemes are presented. The decoding complexity and memory requirements of the schemes are also presented.

Chapter 6 presents a Turbo-SOSTTC-OFDM system over a frequency selective fading channel which is a parallel concatenation of two SOSTTCs. Details of the decoding and encoding are presented and the simulation results for the Turbo-SOSTTC-OFDM system are also presented over various channel conditions.

Finally, in Chapter 7, a summary of the contributions of the work presented in this thesis are given. The chapter closes with suggestions of possible directions for future research.

1.9 Original Contributions

In this thesis, several coding techniques for transmission over flat and frequency selective fading channels are proposed. Analytical and simulation results for coded MIMO-OFDM systems under different channel scenarios are presented.

Combining the field of space-time coding and turbo coding, two concatenated topologies are proposed for the MIMO system in order to improve the coding gain of SOSTTC over fading channels. The two architectures, with *constituents* of SOSTTC and convolutional codes, benefit from iterative decoding to achieve high coding gain in flat fading channels.

Space-time trellis coding with two transmit antennas operating over frequency selective fading channels is also proposed. The proposition involves a coding technique which systematically combines an orthogonal space-time block code with trellis structures using rotated constellations. The designed space-time coded MIMO-OFDM system guarantees full diversity, high coding gain, full rate and multipath diversity with low decoding complexity. A space-time trellis coding scheme for a MIMO-OFDM system for four transmit antennas is also proposed. The scheme combines a quasi orthogonal space-time block code with a trellis code to offer a full rate, full diversity and high coding gain for four transmit antennas.

The principles of turbo and space-time coding is combined to propose four concatenated schemes with a constituent code of super orthogonal space-time trellis coding and convolutional coding for a MIMO-OFDM system. The concatenated schemes achieve high coding gain through concatenation with iterative decoding and achieve high diversity by exploiting multipath diversity.

Another concatenated architecture consisting of two super-orthogonal space-time trellis codes in parallel for MIMO-OFDM is also proposed. The scheme applies the turbo principle to achieve higher coding gain and multipath diversity in a frequency selective fading channel.

1.10 Publications

The following conference and journal papers have been published/ submitted from the results of the research work presented in this thesis.

1.10.1 Journal Papers

1. I. B. Oluwafemi and S. H. Mneney, "Iterative Decoding of Hybrid Concatenated Super-Orthogonal Space-Time Frequency Trellis Coded MIMO-OFDM Systems," *submitted to Eurasip J. of Wireless Commun. and netw, November* 2011.
2. I. B. Oluwafemi and S. H. Mneney, "Error Performance of Concatenated Super- Orthogonal Space-Time Trellis Coded OFDM System with Iterative Decoding," *South African Institute of Electrical Engineers Africa (SAIEE) Research Journal* (Accepted).

1.10. 2 Conference papers

1. I. B. Oluwafemi and S. H. Mneney, "Performance of Super-Orthogonal Space-Time Trellis Code over Nakagami fading Channels," *in Proceeding of IEEE 2nd International Conference on Wireless Communication Society, Vehicular Technology, Information Theory and Aerospace & Electronics Systems Technology (wireless VITEA'11),* Chennai, India, 5 pages, 28th February - 3rd March 2011.

2. I. B. Oluwafemi and S. H. Mneney, "Super-Quasi-Orthogonal Space-Time BPSK Trellis Coded OFDM System for Four Transmit Antennas ," *in Proceeding of IEEE 2nd International Conference on Wireless Communication Society, Vehicular Technology, Information Theory and Aerospace & Electronics Systems Technology (wireless VITEA'11),* Chennai, India, 5 pages, 28th February - 3rd March 2011 (**Best Paper Award**).

3. I. B. Oluwafemi and S. H. Mneney, "Hybrid Concatenated Super-Orthogonal Space-Time Trellis Codes Applying Iterative Decoding," *in Proceedings of IEEE AFRICON 2011,* Livingstone, Zambia, 5 pages, 13th-15th September 2011 .

4. I. B. Oluwafemi and S. H. Mneney, "Performance of Extended Super-Orthogonal Space-Time Trellis Coded OFDM system," *in Proceedings Southern African Telecommunications Networks and Applications Conference (SATNAC),* Spier Estate, Stellenbosch, South Africa, pp. 35-40, 5th- 8th September 2010.

5. I. B. Oluwafemi and S. H. Mneney, "Performance of Turbo Super-Orthogonal Space-Time Frequency Trellis Coded OFDM System" in proceedings 19th Telecommunication Forum (Telfor 2011), Belgrade Serbia, 4 pages, 22nd - 24th November 2011.

CHAPTER 2

SUPER-ORTHOGONAL SPACE-TIME TRELLIS CODES

2.1 Introduction

Space-time coding can improve significantly the error performance or the data rate of wireless communication systems. Super-orthogonal space-time trellis code (SOSTTC) is a recently introduced structure that provides full diversity while providing the highest possible rate and yields high coding gain. In this chapter, the performance of SOSTTC over flat fading channels is presented. The principles and concepts of space-time coding are discussed. The criteria for the optimal space-time code design are presented for flat fading channels. Earlier constructed space-time codes like space-time trellis code (STTC) and space-time block code (STBC) are discussed. The design of SOSTTC based on set partitioning and the generator matrix notation of SOSTTC is also discussed. New SOSTTC codes with 16-state, 32-state and 64-state designs using the set partitioning principle and generator matrix notation are proposed in this chapter. These codes are designed to exploit multipath diversity of frequency selective fading channels by avoiding parallel transition within their trellis. The coding gain distance for the three proposed SOSTTCs are analyzed. The pairwise error probability (PEP) for SOSTTC in Nakagami fading channels is derived. The performance of the newly proposed SOSTTC codes is evaluated by computer simulation in Rayleigh fading channels. Also, the performance of known SOSTTCs is evaluated by computer simulation over Nakagami fading channels. It is believed that these codes have not been analyzed in literature before.

Firstly, an overview of space-time coding is given in the next section. The design criteria for a space-time code are given in Section 2.3 while Section 2.4 describes the space-time trellis codes. Description of a space-time block code is given in Section 2.5 while Section 2.6 introduces the super-orthogonal space time trellis code. Section 2.7 presents an extended version of SOSTTC and the coding gain distance of the proposed codes is analyzed in Section 2.8. The performance of SOSTTC is described in Section

2.9 while the performance of the proposed SOSTTC and known SOSTTC are evaluated by comparative simulation over Rayleigh and Nakagami fading in Section 2.11.

2.2 Space-Time Coding

Space-time coding (STC) was first introduced in 1998 by Tarokh et al in [16]. STC involves coding in the space and time domains which differentiate it from channel coding that relies only on time-domain processing. For channel coding, redundancy is introduced in time-domain thereby leading to loss in bandwidth efficiency. The performance improvement achieved by channel coding is therefore at the cost of expansion in bandwidth. Space-time coding, on the other hand, is performed without necessarily sacrificing bandwidth efficiency by exploiting the space-domain provided by multiple antennas. STC requires well separated antennas for effectiveness and with no induced decoding delay.

2.3 Design Criteria for Space-Time Codes

Consider a space-time coded communication system equipped with n_T transmit and n_R receive antennas and assume that L symbols data frame length are transmitted from each transmit antenna. Then, by arranging the transmitted sequence in an array, the $n_T \times L$ space-time codeword matrix can be defined as

$$\boldsymbol{C} = [\boldsymbol{c_1}, \boldsymbol{c_2}, \dots, \boldsymbol{c_L}] = \begin{bmatrix} c_1^1 & \cdots & c_L^1 \\ \vdots & \ddots & \vdots \\ c_1^{n_T} & \cdots & c_L^{n_T} \end{bmatrix}, \tag{2.1}$$

where the transmitted data sequence from the i-th transmit antenna is denoted by the i-th row $\boldsymbol{C}^{\mathrm{i}} = \left[c_1^i, c_2^i, \dots, c_L^i\right]$, and the space-time symbol at time t is denoted by the t-th column $\boldsymbol{C}_t = \left[c_t^1, c_t^2, \dots, c_t^{n_T}\right]^T$. Dropping the time index t for brevity, and assuming CSI is known at the receiver, we define the pairwise block error event $\left(\boldsymbol{C} \to \widehat{\boldsymbol{C}}\right)$ as the event that when the block $\boldsymbol{C}$ was sent, it was erroneously decoded by the receiver as $\widehat{\boldsymbol{C}}$. Define $\boldsymbol{P}\left(\boldsymbol{C} \to \widehat{\boldsymbol{C}}\right)$ as the pairwise block error probability averaged over the fading channel. The objective of space-time coding is to design a space-time encoder that minimizes $\boldsymbol{P}\left(\boldsymbol{C} \to \widehat{\boldsymbol{C}}\right)$.

Define the matrix

$$\mathbf{D}(\mathbf{C}, \hat{\boldsymbol{C}}) = \mathbf{C} - \hat{\mathbf{C}}, \tag{2.2}$$

and matrix $\boldsymbol{A}(\boldsymbol{C}, \hat{\boldsymbol{C}}) = \boldsymbol{D}(\boldsymbol{C}, \hat{\boldsymbol{C}}).\boldsymbol{D}(\boldsymbol{C}, \hat{\boldsymbol{C}})^H$, where $(.)^H$ denote the Hermitian of a matrix.

At high SNR, it was shown in [16], [44] and [52] that $\boldsymbol{P}(\boldsymbol{C} \to \hat{\boldsymbol{C}})$ is upper bounded by

$$P(\boldsymbol{C} \to \hat{\boldsymbol{C}}) \leq \left(\prod_{i=1}^{r} \lambda_i\right)^{-n_R} \left(\frac{E_s}{4N_0}\right)^{-rn_R}, \tag{2.3}$$

where $\lambda_i, i = 1, \ldots, \text{rank}(\boldsymbol{A}(\boldsymbol{C}, \hat{\boldsymbol{C}}))$, are non-zero eigenvalues of $\boldsymbol{A}(\boldsymbol{C}, \hat{\boldsymbol{C}})$ and r is the rank of $\boldsymbol{A}(\boldsymbol{C}, \hat{\boldsymbol{C}})$. The diversity gain of the STC system from (2.3) is $G_d = r.n_R$, while the coding gain is

$$G_c = \left(\prod_{i=1}^{r} \lambda_i\right)^{1/r}. \tag{2.4}$$

Accordingly, we rewrite (2.3) as

$$P(\boldsymbol{C} \to \hat{\boldsymbol{C}}) \leq (G_c \gamma)^{-G_d}, \text{ where } \gamma = \frac{E_s}{4N_0}.$$

In order to minimize $\boldsymbol{P}(\boldsymbol{C} \to \hat{\boldsymbol{C}})$, the space-time code should be designed to maximize both diversity gain (G_c) and coding gain (G_d), which leads to the following two design criteria for space-time coding in quasi-static flat fading channels:

- **Rank Criterion**: To achieve the maximum possible diversity of $n_T n_R$, the matrix $\boldsymbol{A}(\boldsymbol{C}, \hat{\boldsymbol{C}})$ has to be full rank for any codeword $\boldsymbol{C}$, $\hat{\boldsymbol{C}}$. If the minimum rank of $\boldsymbol{A}(\boldsymbol{C}, \hat{\boldsymbol{C}})$ over all pairs of distinct codeword is r, then a diversity of rn_R is achieved.
- **Determinant Criterion**: Suppose $\boldsymbol{A}(\boldsymbol{C}, \hat{\boldsymbol{C}})$ is full rank, the minimum determinant of $\boldsymbol{A}(\boldsymbol{C}, \hat{\boldsymbol{C}})$ over all possible $\boldsymbol{C}$ and $\hat{\boldsymbol{C}}$, $\boldsymbol{C} \neq \hat{\boldsymbol{C}}$ should be maximized to achieve maximum coding gain.

For fast fading channels where the channel coefficient varies from one symbol to the next, the upper bound of the PEP at high SNR is given as [16]

$$P(\boldsymbol{C} \to \widehat{\boldsymbol{C}}) \leq \prod_{t \epsilon \rho(S,\hat{S})} |s_t - \hat{s}_t|^{-2n_R} \left(\frac{E_s}{4N_0}\right)^{-\delta_H n_R},$$

$$= d_p^{-2n_r} \left(\frac{E_s}{4N_0}\right)^{-\delta_H n_R}, \quad (2.5)$$

where δ_H is the space-time symbol-wise Hamming distance between the two codewords $\boldsymbol{C}$ and $\widehat{\boldsymbol{C}}$, $\rho(S,\hat{S})$ denotes the set of time instances *t=1, 2, ..., L,* where $\|s_t - \hat{s}_t\| \neq 0$ and d_p^2 is the product of the Euclidean distances between the two space-time symbol sequences given by

$$d_p^2 = \prod_{t \epsilon \rho(s,\hat{s})} |s_t - \hat{s}_t|^2. \quad (2.6)$$

The diversity gain of STC in this channel condition is given by the term $\delta_H n_R$ and the coding gain is given by

$$G_c = \frac{d_p^{2^{1/\delta_H}}}{d_u^2}, \quad (2.7)$$

where d_u^2 is the squared Euclidean distance of the uncoded reference system.

In order to minimize $P(\boldsymbol{C} \to \widehat{\boldsymbol{C}})$ in a fast fading channel, both G_c and G_d must be maximized, which leads to the following two design criteria for space-time code in a Rayleigh fast fading channel [9]:

- Maximum possible diversity for an STC code in fast fading channel is achieved with the maximization of the minimum space-time symbol-wise Hamming distance δ_H between all pairs of distinct codewords.
- Maximum coding gain is achieved by the maximization of the minimum product distance, d_p^2, along the path with the minimum Hamming distance δ_H.

For a STTC with the memory order *v*, the upper bound of the minimum symbol-wise Hamming distance δ_H is given by [9]

$$\delta_H \leq \lfloor v/2 \rfloor + 1. \quad (2.8)$$

2.4 Space-Time Trellis Code

Space-time trellis code (STTC) was proposed in [16] as an extension of the rate one delay diversity scheme of Wintteneben by jointly designing modulation, channel coding, transmit diversity and optional receive diversity. It is a trellis based STC that can realize maximum diversity gain and suboptimal coding gain at the cost of relatively high decoding complexity.

In order to guarantee full diversity by satisfying the rank criterion, the following two design rules were suggested in [16]:

- Transitions diverging from the same state should differ in the second symbol;
- Transitions merging to the same state should differ in the first symbol.

STTCs have been represented and analyzed in the literature in a number of ways. In [16] and [53-55], most codes are represented in their trellis form. In order to implement a systematic code search, the appealing trellis form of STTC was transformed into a more flexible generator matrix form in [56].

In the generator matrix form, the stream of coded complex phase-shift keying (PSK) symbol is given as

$$s_t = \text{Map}\left(u_t . G (\text{mod } M)\right), \tag{2.9}$$

where u_t denotes the input bits, M is the M-PSK constellations and the function Map*(x)* is given by

$$\text{Map}(x) = \exp\left(\frac{2\pi j x}{M}\right), \tag{2.10}$$

where G is the generator matrix with n_T columns and $m+s$ rows; s is the number referencing the memory element in the encoder and m represents information bits transmitted, given by $m = \log_2 M$.

STTC employs the Viterbi decoding algorithm [57-59] to implement maximum likelihood decoding of the received signal sequences. The branch metric *(BM)*, which is the degree of differences between the candidate sequences and the received signal, is calculated using

$$BM = \sum_{j=1}^{n_R} \left| r_t^j - \sum_{i=1}^{n_T} h_{j,i}^t s_t^i \right|^2 , \quad (2.11)$$

where $h_{j,i}^t$ is the channel response between the *j*-th receive antenna and the *i*-th transmit antenna at time *t*, r_t^j is the information signal sequence received at the *j*-th receive antenna at time *t* and s_t^i is the candidate information signal sequence from the *i*-th transmit antenna at time *t*.

2.5 Space-Time Block Code

Space-time trellis codes perform very well at the cost of relatively high decoding complexity. In resolving the issue of decoding complexity, a notable scheme for transmission using two transmit antennas, known as the Alamouti code, was proposed in [60]. For the scheme, the following transmission matrix is used for transmitting over the two antennas:

$$G_2 = \begin{pmatrix} s_1 & s_2 \\ -s_2^* & s_1^* \end{pmatrix}, \quad (2.12)$$

where columns signify transmit antennas and the rows signify time instances. Thus, at time $t = 1$, s_1 and s_2 will be transmitted from antennas 1 and 2 respectively, while at time $t = 2$, $-s_2^*$ and s_1^* will be transmitted from antennas 1 and 2 respectively. Assuming a single receive antenna, and that fading coefficients are constant over two consecutive time slots, the received signal is given by

$$r_1 = h_1 s_1 + h_2 s_2 + \eta_1, \quad (2.13)$$

$$r_2 = -h_1 s_2^* + h_2 s_1^* + \eta_2, \quad (2.14)$$

where h_1 and h_2 signify the coefficients of the channel, and η_1 and η_2 the channel noise. In order to extract the signals, both r_1 and r_2 are passed into the combiner which is

aided by the channel estimator. With perfect channel state information at the receiver, (2.13) and (2.14) can be maximum-likelihood (ML) decoded as [61]

$$\begin{aligned}\tilde{s}_1 &= h_1^* r_1 + h_2 r_2^* \\ &= (|h_1|^2 + |h_2|^2)s_1 + h_1^* \eta_1 + h_2 \eta_2^*, \end{aligned} \tag{2.15}$$

$$\begin{aligned}\tilde{s}_2 &= h_{21}^* r_1 - h_1 r_2^* \\ &= (|h_1|^2 + |h_2|^2)s_2 + h_2^* \eta_1 - h_2 \eta_2^*. \end{aligned} \tag{2.16}$$

Both $\tilde{s}_1$ and $\tilde{s}_2$ are then sent to the maximum likelihood decoder (MLD) to calculate the most likely values of transmitted symbols.

The simplicity and the performance of the code motivated the generalization of the Alamouti code to arbitrary numbers of transmit antennas, leading to the concept of space-time block codes (STBC). Tarokh et al invoked the theory of orthogonal code design to construct half-rate STBC [62], while Jafarkhani [63] and Foschini [64] also introduced the extended Alamouti code in a bid to improve the diversity gain achieved by the Alamouti code.

2.6 Super-Orthogonal Space-Time Trellis Code (SOSTTC)

The design of the earliest STCs was focused primarily on the implementation of full diversity order and not on optimal coding gain. The coding gain of STCs can be increased by introducing the orthogonal design of STBC into STTC. The coding gain of the STC in slow fading channels depends on the minimum determinant of a full rank codeword distance matrix [16]. The codeword distance matrix is a Hermitian matrix. As a result, the optimal determinant will be obtained if the codeword distance matrix is also a diagonal matrix with equal eigenvalues. A new class of STCs known as super-orthogonal space-time trellis codes (SOSTTC) was introduced in [65]. The STBC was combined with a trellis code in order to maximize the coding gain. This resulted in a new code that guarantees full diversity for any given rate and number of states [66-67]. The new structure also has lower decoding complexity than that of STTC [68-69].

The main idea of SOSTTC is to consider full rate STBCs as a modulation scheme for multiple antennas. With this, a STBC with a specific symbol constellation is assigned to transitions originating from a trellis state. Enough constituent orthogonal matrices are needed to achieve a desired rate b bits/sec/Hz. Enough constellation points are also needed for the transmission of $\log_2 M = b$ bits/sec/Hz per channel use, assuming that the matrix elements are from an M-PSK constellation.

Generally, for a STBC$\in \mathbb{C}^{T\times n_T}$, choosing a trellis branch emanating from a state is equivalent to transmitting Tn_T symbols from n_T transmit antennas in T time intervals. The class of orthogonal transmission matrices for two transmit antennas is obtained by multiplying (2.12) with the following unitary matrix u :

$$u = \begin{pmatrix} e^{j\theta} & 0 \\ 0 & 1 \end{pmatrix}. \tag{2.17}$$

This results in the orthogonal transmission matrix for SOSTTC given by

$$G(s_1, s_2, \theta) = \begin{pmatrix} s_1 e^{j\theta} & s_2 \\ -s_2^* e^{j\theta} & s_1^* \end{pmatrix}, \tag{2.18}$$

where s_1 and s_2 are selected by input bits. At the first symbol interval, $s_1 e^{j\theta}$ and s_2 are transmitted from the first and the second transmit antennas respectively. At the second interval, the symbols $-s_2^* e^{j\theta}$ and s_1^* are transmitted from the first and second antennas respectively. By varying the value of the rotation parameter, multiple orthogonal block codes are constructed, and a super-orthogonal code is formed from the union of these codes to provide necessary redundancy to achieve full rate. As a result of picking θ such that the resulting transmitted symbols are also from the same constellation, the constellation signal is not expanded. For M-PSK signalling with constellation signal represented by $s_i \in e^{j2\pi a/M}$, $i=1,2$, $a= 0,1, \ldots, M-1$, one can pick $\theta = 2\pi a'/M$, where $a' = 0,1, \ldots, M-1$ to avoid constellation expansion, and the resulting transmitted signals are also members of the M-PSK constellation. Specifically, the choice of θ that can be used in (2.21) is given as 0, π and 0, $\pi/2$, π, $3\pi/2$ for BPSK and QPSK respectively.

Also, super-orthogonal codes are parameterized and there is reduced complexity of the decoding process because of the orthogonality of the STBC building blocks.

Following the coding gain distance definition (CGD) from [65], the minimum determinant det($\mathbf{A_D}$) of the matrix $\mathbf{A_D = DD^H}$, where $\mathbf{D} = \boldsymbol{C} - \widehat{\boldsymbol{C}}$, over all possible pairs of distinct codeword $\boldsymbol{C}$ and $\widehat{\boldsymbol{C}}$, corresponds to the coding gain for a full diversity code,

$$CGD = \det(\boldsymbol{A_D}) = \prod_{i=1}^{n_T} \lambda_i , \tag{2.19}$$

where λ_i is the i-th eigenvalue.

In designing SOSTTC, the set partitioning principle proposed in [70] is used while CGD, instead of Euclidean distance, is employed and the coding gain of such SOSTTC is dominated by parallel transition. Fig. 2.1 and Fig. 2.2 illustrate the optimal set partitioning for BPSK and QPSK respectively, as demonstrated in [65]. Note that there is maximization of the CGD at each partitioning level. In the figures, the numbers at the leaves represent the indexes of the MPSK symbols in each codeword. For example, the possible indexes in the case of QPSK in Fig. 2.2 are m = (0, 1, 2, 3), whose complex points from the QPSK constellation are (1, j, -1, -j) respectively. The set partitioning process is done so that the CGD is maximized at each level, resulting in the coding gain of the designed SOSTTC being maximized.

A rule to maximize the coding gain is that all subsets should be used an equal number of times in the trellis, which is a similar rule given in [71] for the design of multiple trellis coded modulation (MTCM). The key design process for SOSTTC is that adjacent states are usually assigned to a different constellation of STBCs. Similarly, the same STBC can be assigned to branches that are merging into a state. Full diversity is achieved by every pair of codewords diverging from (or merging into) a state since the pair of codewords is from the same set of orthogonal codes. It is however possible that a codeword with a different parameter θ does not achieve full diversity. Since these codewords are assigned for different states, the resulting trellis code would provide full diversity despite the fact that a pair of codewords in a super-orthogonal code may not achieve full diversity [65].

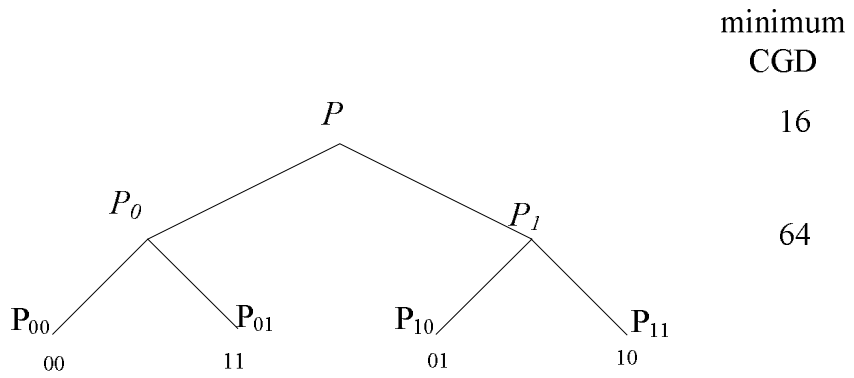

Fig. 2.1: Set partition for BPSK

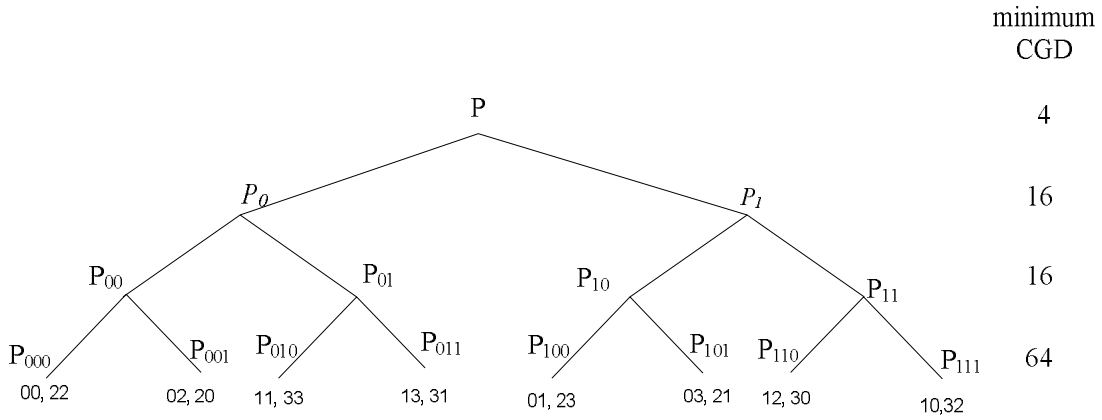

Fig. 2.2: Set partitions for QPSK

Fig. 2.3 shows a classical example of a four state SOSTTC to illustrate the design process. The rate of the code is (1/bit/s/Hz) for a set portioning for BPSK while the rate is 2 bits/s/Hz with QPSK. $G(s_1, s_2, 0)$ is used when departing from even states, and $G(s_1, s_2, \pi)$ is used when departing from odd states. The minimum CGD of this code is 64 and 16 for BPSK and QPSK respectively.

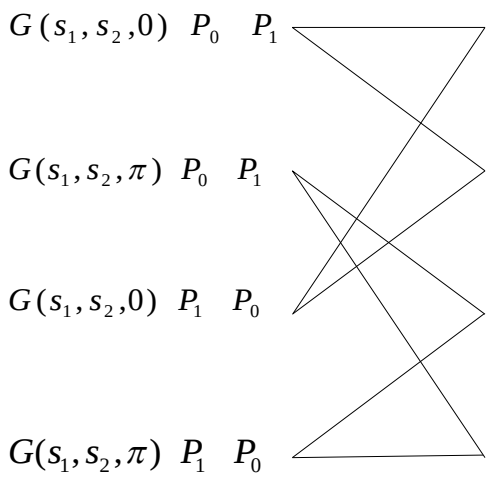

Fig. 2.3: A classical four state SOSTTC code, r = 1 bit/s/Hz using BPSK or r = 2 bits/s/Hz using QPSK

The generator matrix for SOSTTCs was recently introduced in [72], which is an extension of the generator matrix notation for STTC proposed in [56]. The generator matrix representation simplifies the implementation of the encoder and decoder for codes with a higher number of states because listing the outputs of all states is no longer required. The generator matrix representation allows for a systematic and exhaustive computer search for optimal codes with a higher number of states. The generator matrix notation of a full-rate SOSTTC for n_T transmit antennas consists of p rows by n_T columns where p is given by the sum of the number of input bits m at each trellis level and the number of bits s needed to represent each state. The symbol s is given by $s = log_2 N$, where N is the number of states. For M-PSK constellations with the highest possible rate, m is given by $m = 2log_2 M$. As an example, an eight-state SOSTTC with QPSK constellation with a rate of 2 bits/s/Hz and two transmit antennas is represented by seven rows and two columns as

$$G = \begin{Bmatrix} b_1 & b_2 \\ b_3 & b_4 \\ \vdots & \vdots \\ b_{13} & b_{14} \end{Bmatrix}, \tag{2.20}$$

where $b_x = 0, 1, 2$ or 3 and $x = 1, 2, \ldots, 14$. For an M-PSK modulation, $b_x = 0, 1, \ldots, M-1$. Let the n-bits information sequence to be transmitted be $\boldsymbol{u} = (u_1, \ldots, u_n)$, where $u_i = 0 \; or \; 1$. The number of bits influencing the transmission matrix (2.18) of a given

trellis level is equal to the number of rows of *G* or $(m + s)$. The *m* bits come from the information sequence *u* and the *s* bits represent the current state. If we represent $(m + s)$ bits by a vector $\boldsymbol{u}^l$, where *l* is the trellis level, two symbols s_1 and s_2 are obtained by multiplying $\boldsymbol{u}^l$ (modulo *M*) by *G*. These two symbols, by using the mapping schemes described by (2.18), are then mapped to a transmission matrix. All possible outputs from the SOSTTC can therefore be obtained from $\boldsymbol{u}^l G$, and this simplifies the implementation of the encoder and the decoder.

For example, for an 8-state code with two parallel branches, the bits of u^l can be considered as follows

$$\boldsymbol{u}^l = \left[\overbrace{u_7\ u_6\ u_5}^{Next\ state} \quad \overbrace{u_4}^{Parallel\ Branch} \quad \overbrace{u_3\ u_2\ u_1}^{Current\ State}\right]. \tag{2.21}$$

Upon moving to the next transition, four new input bits are shifted into the $\boldsymbol{u}^l$ vector. The next state is determined from the current state and the input bits by using a lookup table.

2.7 Extended Super-Orthogonal Space-Time Trellis Code (ESOSTTC)

The extended SOSTTC was proposed in [73] to improve the coding gain performance of the original SOSTTC by utilizing one extra rotation parameter ϕ, in addition to θ, to expand the inner STBCs. By replacing s_1 and s_2 with $s_1 e^{j\phi}$ and $s_2 e^{j\phi}$ in the transmission matrices in (2.18), the transmitted matrices of ESOSTTC, which are an extended class of orthogonal designs, is given by

$$G(s_1, s_2, \phi, \theta) = \begin{pmatrix} s_1 e^{j\phi} e^{j\theta} & s_2 e^{j\phi} \\ -s_2^* e^{-j\phi} e^{j\theta} & s_1^* e^{-j\phi} \end{pmatrix}. \tag{2.22}$$

The extra rotational parameter ϕ can be any real value between 0 and 2π. The set partitioning for extended super-orthogonal code is identical to that of the super-orthogonal code. In [74], the design rule for ESOSTTC was proposed. This rule is an extension of the generator notation of SOSTTC of [72]. In the following, the set partitioning principle and the generator matrix notation is combined with the design rule to design 16, 32 and 64 trellis state SOSTTC, and by extension, ESOSTTC.

The second design criteria for SOSTTC are optimized by an exhaustive code search using the generator matrix representation of SOSTTC [72], [74] with details from [75]. With the application of the search procedure, the following generator matrix for the 16, 32, and 64-state SOSTTC respectively are obtained:

$$G^T = \begin{Bmatrix} 1 & 2 & 0 & 0 & 2 & 3 & 1 & 0 \\ 2 & 0 & 1 & 2 & 2 & 1 & 1 & 3 \end{Bmatrix}, \tag{2.23}$$

$$G^T = \begin{Bmatrix} 2 & 0 & 1 & 0 & 1 & 2 & 1 & 2 & 0 \\ 2 & 1 & 1 & 2 & 0 & 1 & 2 & 0 & 0 \end{Bmatrix}, \text{and} \tag{2.24}$$

$$G^T = \begin{Bmatrix} 2 & 1 & 0 & 1 & 2 & 1 & 2 & 0 & 2 & 1 \\ 0 & 1 & 2 & 0 & 0 & 1 & 1 & 2 & 1 & 2 \end{Bmatrix} \tag{2.25}$$

The trellis diagram for the newly proposed 16-state ESOSTTC in this chapter is shown in Fig 2.4. The rotation parameter θ is shown as 0 and π. An optimum additional rotation parameter value of $\phi = 0$ and $\phi = \pi/4$ for even and odd states respectively are used to multiply the SOSTTCs to obtain the ESOSTTC.

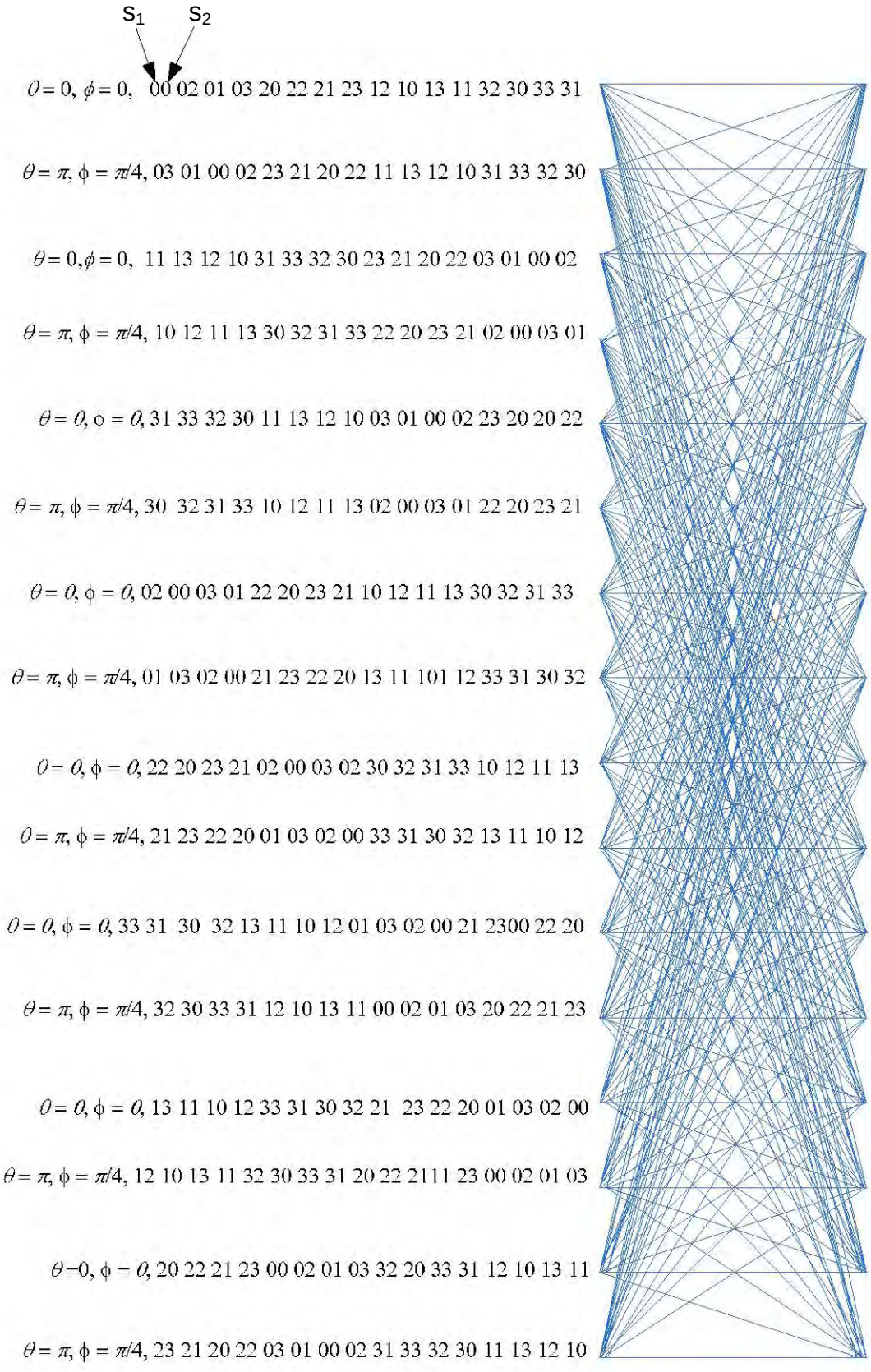

Fig. 2.4: A 16-state ESOSTTC at a rate of 2 bits/s/Hz using QPSK [76]

2.8 Coding Gain Distance Analysis (CGD)

In this section, the coding gain analysis for the 16-, 32 and 64-state SOSTTCs proposed in Section 2.7 is calculated. Parallel transition constraint in the trellis structure is avoided in order to increase the performance of the code in multipath channels. To avoid parallel transition using M-PSK signalling, at least M^2 states are needed in the trellis structure of the ESOSTTC. An optimal rotational parameter value that maximizes the minimum product (CGD×MPD) for ESOSTTC with QPSK is $\emptyset = \pi/4$. From Fig. 2.4, any valid codeword starts from state one and ends at state one. Due to the trellis structure, two codewords may differ in two or more trellis transitions. Then the smallest number of transitions (coding steps) is two. Considering that the path of an ESOSTTC codeword F stays in state one during both transitions (i.e. the path $1 \rightarrow 1 \rightarrow 1$), the corresponding codewords to be sent are

$$F^1\left(e^{j\frac{\pi}{2}(0)}, e^{j\frac{\pi}{2}(0)}, \emptyset = 0, \theta = 0\right), F^2\left(e^{j\frac{\pi}{2}(0)}, e^{j\frac{\pi}{2}(0)}, \emptyset = 0, \theta = 0\right). \quad (2.26)$$

By analyzing another possible codeword Q to be transmitted in two transitions, the minimum product CGD.MPD of the 16-state codeword in two transitions is 24×42, which is obtained if codeword F follows the paths $1 \rightarrow 10 \rightarrow 1$ and $1 \rightarrow 14 \rightarrow 1$.

In Fig. 2.5, the case when Q goes through $1 \rightarrow 10 \rightarrow 1$ is illustrated. From Fig. 2.4, we can see that the codewords to be transmitted in Q are

$$Q^1\left(e^{j\frac{\pi}{2}(1)}, e^{j\frac{\pi}{2}(0)}, \emptyset = 0, \theta = 0\right), Q^2\left(e^{j\frac{\pi}{2}(2)}, e^{j\frac{\pi}{2}(1)}, \emptyset = 0, \theta = 0\right). \quad (2.27)$$

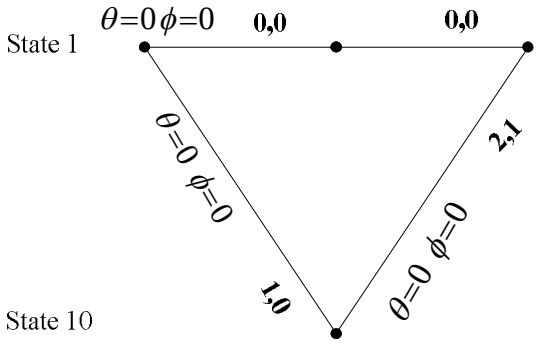

Fig. 2.5: Two typical paths differing in 2 transitions

The minimum CGD.MPD for this case is calculated as follows

$$CGD = det\,(B^1 + B^2) = 24. \tag{2.28}$$

$$MPD = (1 + \|C^1\|^2)(1 + \|C^2\|^2) = 42. \tag{2.29}$$

where

$$C^1 = F^1 - Q^1,$$

$$C^2 = F^2 - Q^2,$$

$$B^1 = (C^1)^H C^1,$$

$$B^2 = (C^2)^H C^2.$$

The minimum product occurs in the case of two transitions and $\delta_H = 2$ for the ESOSTTC. The CGD and MPD for the 32-state ESOSTTC are 32 and 48 respectively, while for the 64 states, the CGD and MPD are 36 and 48 respectively.

2.9 SOSTTC over Nakagami Fading Channel

The Nakagami fading model is a more versatile fading model that is based on Nakagami distribution, which is also called the *m*-distribution [77-78]. The Nakagami distribution includes the Rayleigh distribution and the one-sided Gaussian distribution as two special cases. Therefore, Nakagami distribution can model a fading channel that is more or less severe than that of the Rayleigh fading channel. Since Rayleigh fading cannot account for the large-scale effect of shadowing in mobile wireless communications, Nakagami-distributed fading may be encountered [77].

In [77], the performance of STTC in Nakagami fading channels was investigated and an upper bound was obtained for the pairwise error probability. It was shown that the diversity order achieved by STTC over a Nakagami fading channel is *m*-times that achieved over a Rayleigh fading channel and that the coding gain varies with the general Nakagami fading channel. In [79], the performance of an STTC design based on the Euclidean distance criteria (EDC) was also investigated and it was shown that

STTCs designed for a Rayleigh fading channel are suitable for a Nakagami fading channel. In [80], the performance of the space-time block code (STBC) over a Nakagami-m fading channel and a closed form expression for the exact symbol error rate for orthogonal space-time block code over an independent identically distributed (iid) Nakagami-m fading channel was obtained. In addition in [81], the pairwise error probability (PEP) for space-time codes in Rician-Nakagami channels was obtained, while in [82], the performance of MIMO systems through Nakagami fading channels with arbitrary fading parameter was conducted. In the following section, the PEP for STTC is extended to derive the PEP for SOSTTC over Nakagami fading channels. The performance of SOSTTC over Nakagami slow fading channels is also evaluated.

2.10 Pairwise Error Probability for SOSTTC in Nakagami Fading Channels

In this section, the PEP for STTC from [77] and [79] is extended to derive the PEP for SOSTTC as follows.

Consider a quasi-static Nakagami fading channel having fading amplitude of μ with the probability distributed function of the fading amplitude defined by [83]

$$P(\mu) = \frac{2}{\Gamma m}\left(\frac{m}{\upsilon}\right)^{m} \mu^{2m-1} e^{-\mu^2 \frac{m}{\upsilon}}, \tag{2.30}$$

where Γ is the Gamma function, $\upsilon = E[\mu^2]$,

$$m = \frac{\upsilon^2}{E[(\mu^2 - \upsilon)^2]}, \quad m \geq 0.5$$

and E[.] denotes statistical average.

Assuming that the channel amplitude $h_{i,j}$, $i = 1,2,\ldots,n_T$, $j = 1,2,\ldots,n_R$ is modeled as an identically independent m-distributed random variable, the probability of transmitting codeword $\boldsymbol{C}$ and the receiver deciding in favor of the codeword $\widehat{\boldsymbol{C}}$ assuming ideal CSI at the receiver is given by

$$P\left(\boldsymbol{C} \rightarrow \widehat{\boldsymbol{C}} \middle| h_{i,j}\right) = Pr\left[m(\boldsymbol{r}, \boldsymbol{C}) - m\left(\boldsymbol{r}, \widehat{\boldsymbol{C}}\right) > 0 | h_{i,j}\right], \tag{2.31}$$

where $m(\boldsymbol{r}, \boldsymbol{C})$ is the ML metric related to the correct path given by

$$m(\boldsymbol{r}, \boldsymbol{C}) = \sum_{j=1}^{n_R} \sum_{t=1}^{l} \left| r_t^j - \sum_{i=1}^{n_T} h_{i,j}\, C_t^i \right|^2 \tag{2.32}$$

and $m(\boldsymbol{r}, \widehat{\boldsymbol{C}})$ is the ML metric related to the decided path given by

$$m(\boldsymbol{r}, \widehat{\boldsymbol{C}}) = \sum_{j=1}^{n_R} \sum_{t=1}^{l} \left| r_t^j - \sum_{i=1}^{n_T} h_{i,j}\, \hat{C}_t^i \right|^2 \tag{2.33}$$

Substituting (2.32) and (2.33) in (2.31) and simplifying in terms of the Q-function yields

$$P(\boldsymbol{C} \to \widehat{\boldsymbol{C}} | h_{i,j}) = Q\left(\sqrt{\frac{E_s}{2N_0} D} \right), \tag{2.34}$$

where

$$D = \sum_{j=1}^{n_R} \sum_{t=1}^{l} \left| \sum_{i=1}^{n_T} h_{i,j} \left(\boldsymbol{C}_t^i - \widehat{\boldsymbol{C}}_t^i \right) \right|^2 . \tag{2.35}$$

Using the *Q*-function $Q(x) = \frac{1}{2} e^{-\frac{x^2}{2}}$, the PEP given in (2.34) can be upper bounded as

$$P(\boldsymbol{C} \to \widehat{\boldsymbol{C}} | h_{i,j}) \leq \exp\left(-\frac{\mathrm{E_S}}{4\mathrm{N_0}} \mathrm{D} \right). \tag{2.36}$$

If a matrix $\boldsymbol{A}$ is defined as $\boldsymbol{A} = (\boldsymbol{C} - \widehat{\boldsymbol{C}})(\boldsymbol{C} - \widehat{\boldsymbol{C}})^{\boldsymbol{H}}$, where $(.)^H$ is the Hermitian transpose function, and denoting the non-negative eigenvalues and eigenvectors of $\boldsymbol{A}$ by λ_i, and $\boldsymbol{v}_i = (v_{1,i}, \ldots, v_{n_T,i})$, $i = 1, 2, \ldots, n_T$ respectively, then

$$D = \sum_{j=1}^{n_R} \sum_{i=1}^{n_T} \lambda_i \left| \alpha_{i,j} \right|^2, \tag{2.37}$$

where

$$\alpha_{i,j} = \sum_{k=1}^{n_T} h_{k,j}\, v_{k,i} . \tag{2.38}$$

Since $\boldsymbol{v}_i = (v_{1,i}, \dots, v_{n_T,i})$ is an orthogonal unitary basis vector of $\mathbb{C}^{n_T}$ and the amplitude of $h_{i,j}$ are identically independent m-distributed, the amplitude of $\alpha_{i,j}$ is still m-distributed with same m and Ω. The pdf of $|\alpha_{i,j}|^2$ is given by

$$P\left(|\alpha_{i,j}|^2\right) = \frac{1}{\Gamma m}\left(\frac{m}{\Omega}\right)^m |\alpha_{i,j}|^{2(m-1)} e^{-|\alpha_{i,j}|^2 \frac{m}{\Omega}}, \tag{2.39}$$

where

$$\Omega = E[|\alpha_{i,j}|^2], \quad \text{and}$$

$$m = \frac{E^2[|\alpha_{i,j}|^2]}{Var[|\alpha_{i,j}|^2]} = \frac{\Omega^2}{E\left[\left(|\alpha_{i,j}|^2 - \Omega\right)^2\right]}. \tag{2.40}$$

To evaluate the upper bound for PEP, we average equation (2.38) with respect to the distribution of $|\alpha_{i,j}|^2$

$$P(\boldsymbol{C} \to \widehat{\boldsymbol{C}}) = \int_0^\infty exp\left(-\frac{E_s}{4N_0}\lambda_i\right) P\left(|\alpha_{i,j}|^2\right) d\left(|\alpha_{i,j}|^2\right). \tag{2.41}$$

$$P(\boldsymbol{C} \to \boldsymbol{C}) = exp\left(-\frac{E_s}{4N_0}\lambda_i\right)\frac{1}{\Gamma m}\left(\frac{m}{\Omega}\right)^m |\alpha_{i,j}|^{2(m-1)} e^{-|\alpha_{i,j}|^2 \frac{m}{\Omega}} d\left(|\alpha_{i,j}|^2\right). \tag{2.42}$$

From the Euler's integral of the second kind [83]

$$\Gamma x = \int_0^\infty t^{x-1} e^{-t}\, dt,$$

The PEP becomes

$$P(\boldsymbol{C} \to \widehat{\boldsymbol{C}}) = \frac{\left(\frac{m}{\Omega}\right)^m}{\Gamma m} \prod_{j=1}^{n_R} \prod_{i=1}^{n_T} \frac{\Gamma m}{\left(\frac{E_s}{4N_0}\lambda_i + \frac{m}{\Omega}\right)^m}. \tag{2.43}$$

Denoting the rank of $\boldsymbol{A}$ by r, and assuming that the nonzero eigenvalues of $\boldsymbol{A}$ are denoted by $\boldsymbol{\lambda_1}, \boldsymbol{\lambda_2}, \dots, \boldsymbol{\lambda_r}$, then from [77]

$$P(\boldsymbol{C} \to \widehat{\boldsymbol{C}}) \leq f(m)\left(\prod_{i=1}^{r}\lambda_i\right)^{-mn_R}\left(\frac{E_s}{4N_0}\right)^{-rmn_R}, \quad (2.44)$$

where

$$f(m) = \left(\frac{m}{\upsilon}\right)^{m-mn_R(n_T-r)}\Gamma(\upsilon)^{-\mathrm{n_T n_R}-1}.$$

From (2.44), it can be concluded that a diversity order of rmn_R is achieved for general c and $\hat{c}$, which is the diversity order in a Rayleigh fading channel times *m*, while the coding gain is $f(m)^{-1/rmn_R}(\prod_{i=1}^{r}\lambda_i)^{1/r}$. At high SNR, the minimum values of rmn_R and $f(m)^{-1/rmn_R}(\prod_{i=1}^{r}\lambda_i)^{1/r}$ over all pairs of distinct codewords asymptotically dominate the system error rate performance.

2.11 Simulation Results and Discussions

In this section, the FER performance of the proposed SOSTTCs are presented for both Rayleigh and Nakagami fading channels and some comparison is made with the performance of STTC and some known SOSTTCs. The transmission rate of the system is 2 bits/s/Hz.

2.11.1 Performance of SOSTTC over Rayleigh Fading Channels

The performance results of SOSTTC are presented in this section in terms of FER over a Rayleigh fading channel using computer simulation. The results for both quasi-static and rapid fading channels for two transmit and one receive antenna with QPSK modulation is presented. For the simulation, 10,000 frames were transmitted per antenna, each frame comprising 130 symbols, which, using QPSK modulation corresponds to 520 bits per frame. It was assumed that the antennas are well-spaced to ensure that the fading is statistically independent from one transmit-receive antenna pair to any other. Perfect CSI was also assumed at the receiver.

Fig. 2.6 shows the FER performance of the proposed new codes for 16-, 32- and 64-state SOSTTC in a slow-fading channel. In this figure, the performance of the codes is also compared with that of 4-state SOSTTC by Jafarkhani and Sashadri [65] and 16-state SOSTTC by Aksoy [51]. It can be observed from the performance curves that all

the three codes achieve full diversity order while the higher states also achieve better coding gain. Evaluating the slope of the FER curve as $G_d = \frac{10(\log(FER_2) - log(FER_1))}{SNR_2 - SNR_1}$, where FER_i is the frame error probability at SNR_i (dB), $i = \{1, 2\}$, gives a practical calculus of the diversity gain. A look at Figure 2.6 shows that the curve for Aksoy's 16-state code [51] overlaps the writer's, thus indicating that the two codes have similar performance. It should be noted that the proposed codes are primarily designed for multipath diversity and the essence of the investigation here is simply to know how they perform over flat fading. In terms of coding gain, the 16-state code achieves additional coding gain of about 1dB more than the 4-state SOSTTC, and 64-state SOSTTC is about 1.6 dB from the outage probability. Fig. 2.7 shows the FER performance of the proposed ESOSTTC as compared with the performance of SOSTTC and 16-state STTC by Tarokh, et al [16] in a quasi-static fading channel. As can be observed from the performance curves, the ESOSTTC provides additional coding gain of about 0.2 dB and 1.4 dB when compared with that of SOSTTC and the STTC codes respectively.

The FER performance curves of these codes over a fast-fading channel are shown in Fig. 2.8. In the same figure, the performance of the 4-state SOSTTC from [65], the 16-state code SOSTTC from [51], and 4- and 16-state STTCs from [16] are compared. There is performance degradation for the 4-state SOSTTC in a fast fading channel because the code has parallel transitions within its trellis which restrict the error performance in fast fading channels [84]. The performance curve shows that the 16-, 32-, and 64-state codes achieve the diversity order of three over a fast fading channel. The new 16-state SOSTTC also has the same error performance as the 16-state SOSTTC code from [51] in a fast fading channel. In comparison with the STTC code, the 16-state code is seen from the performance curve to provide additional coding gain of about 1.8 dB when compared with the 16-state STTC code. The FER performance of 16-state ESOSTTC, SOSTTC, and STTC over a fast fading channel is compared in Fig. 2.9. As can be observed from the performance curves, the ESOSTTC exhibits a coding gain advantage of about 2 dB and 0.2dB over the STTC and SOSTTC respectively.

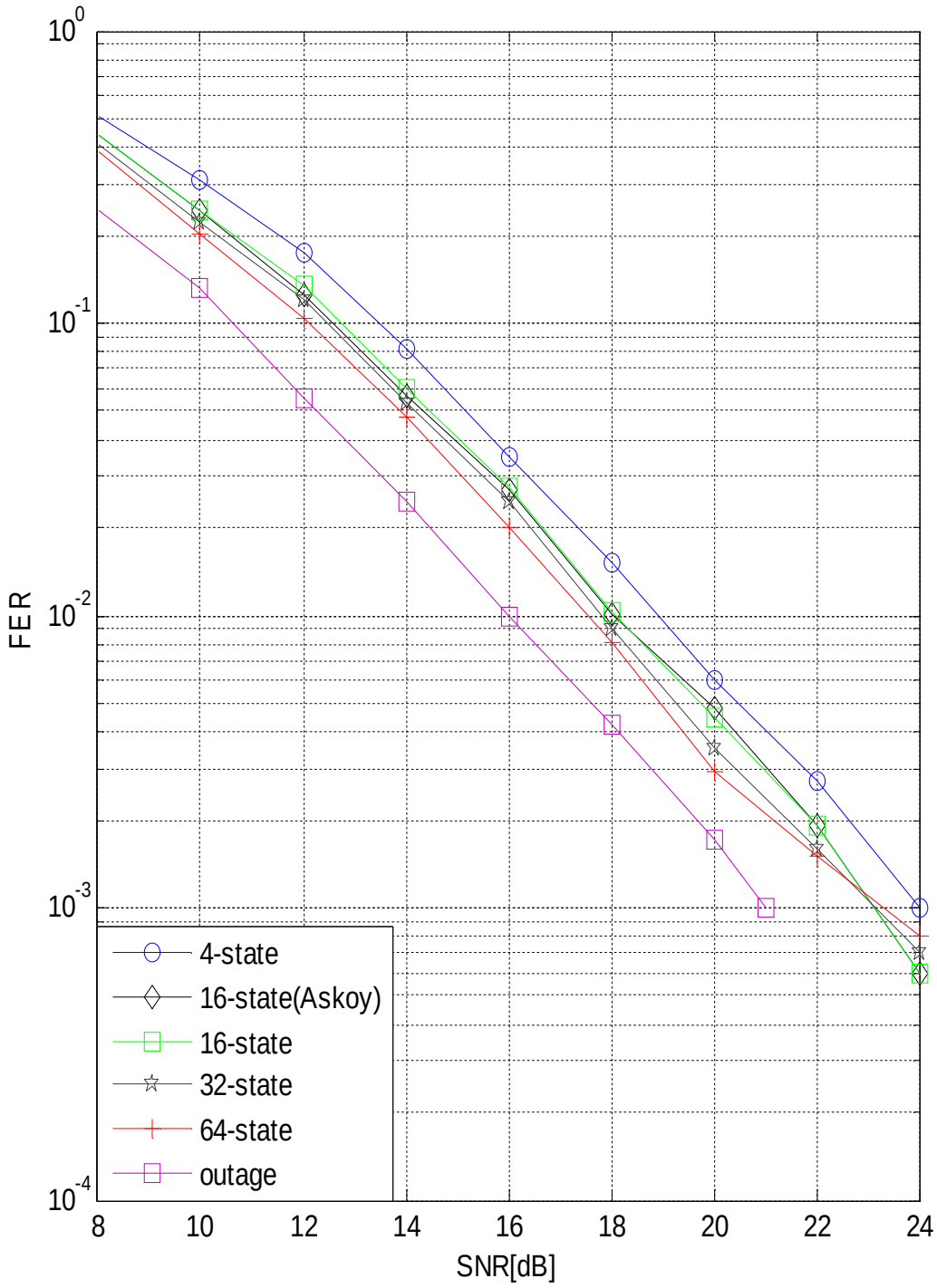

Fig. 2.6: FER performance for SOSTTC in a quasi static Rayleigh fading channel with one receive antenna

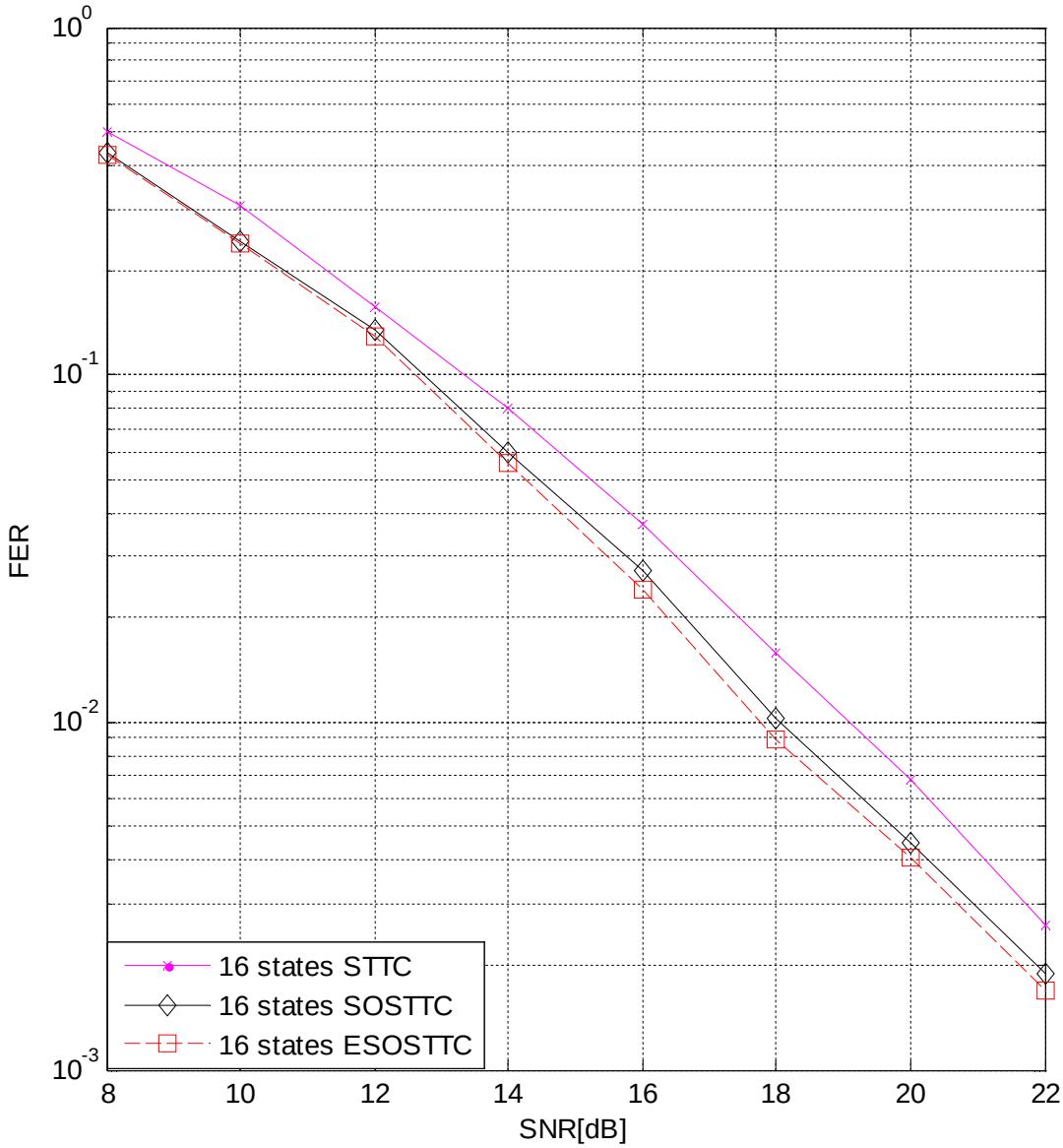

Fig. 2.7: FER performance for STTC [16], SOTTC [51] and ESOSTTC in a Rayleigh quasi-static fading channel with one receive antenna

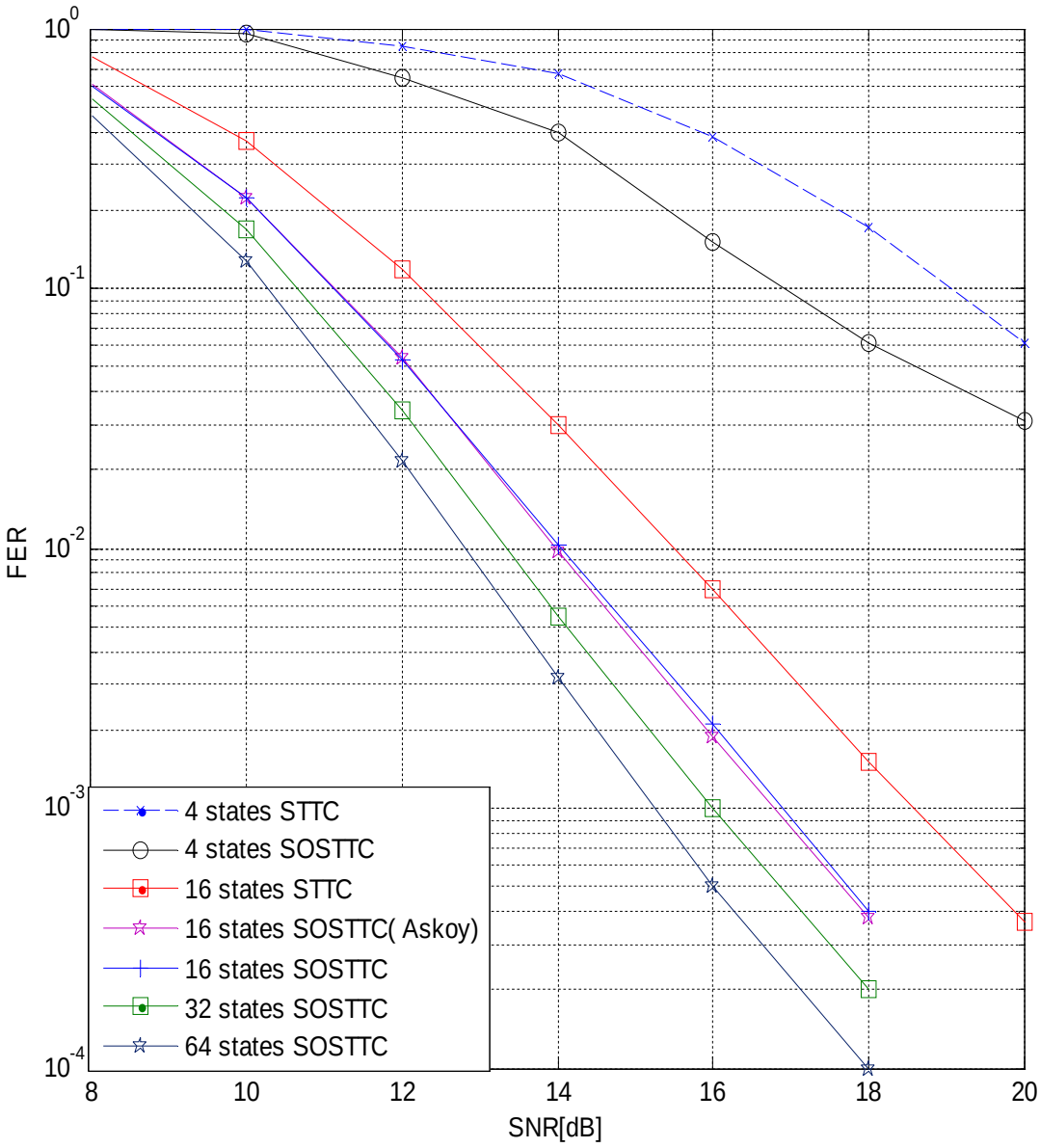

Fig. 2.8: FER performance for STTC [16], and SOSTTC in a Rayleigh fast fading channel with one receive antenna

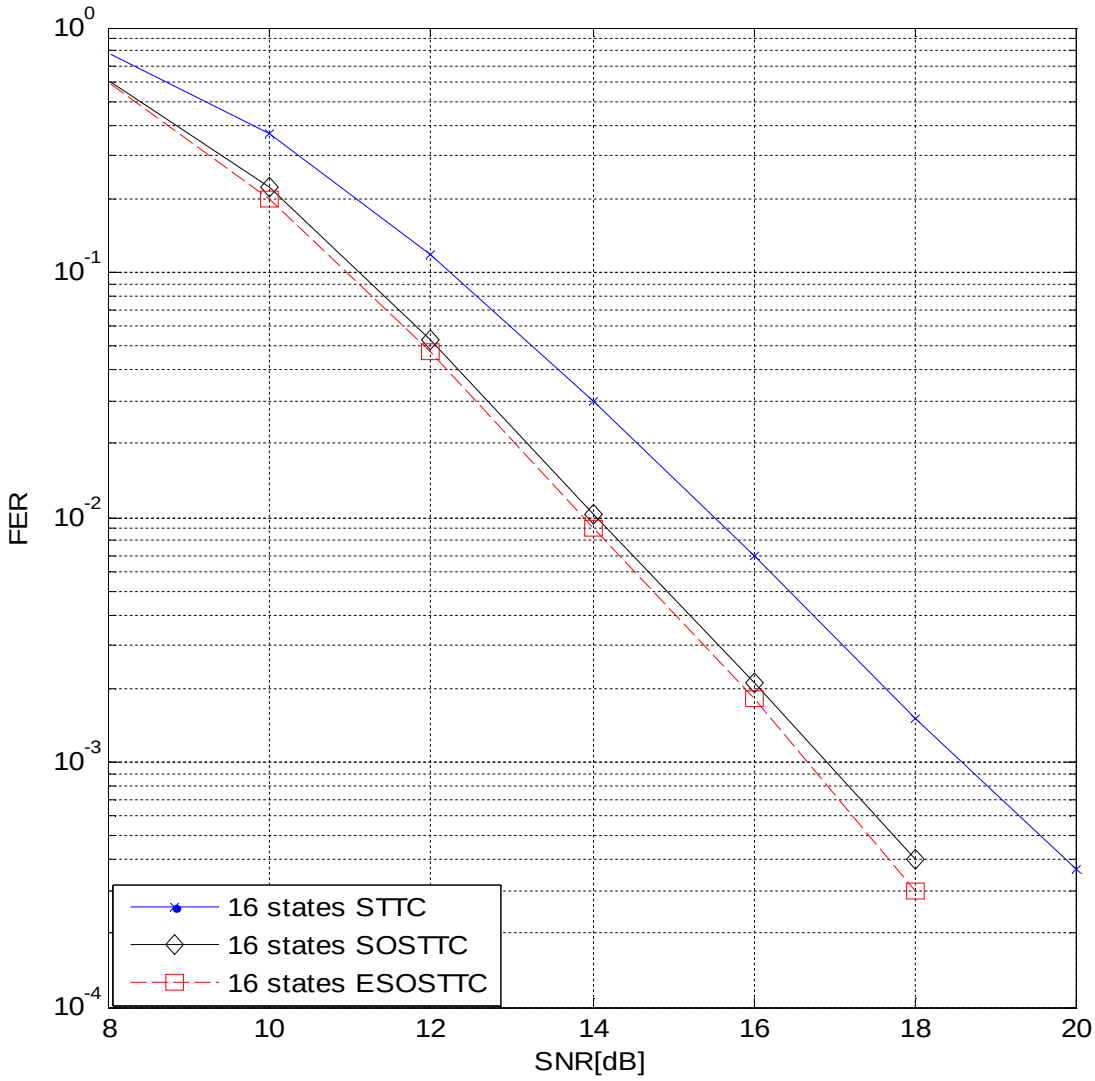

Fig. 2.9: FER performance for STTC [16], SOSTTC [51] and ESOSTTC in a Rayleigh fast fading channel with one receive antenna

2.11.2 SOSTTC over Nakagami Fading Channels

Table 2.1: Generator matrix for SOSTTC [72]

No of states	Generator Matrix
16	$G^T = \begin{pmatrix} 1 & 1 & 0 & 2 & 0 & 1 & 0 & 1 \\ 0 & 1 & 2 & 0 & 1 & 0 & 1 & 1 \end{pmatrix}$
32	$G^T = \begin{pmatrix} 1 & 0 & 0 & 2 & 0 & 0 & 1 & 0 & 0 \\ 1 & 2 & 1 & 2 & 1 & 2 & 1 & 2 & 3 \end{pmatrix}$
64	$G^T = \begin{pmatrix} 3 & 2 & 2 & 3 & 2 & 1 & 2 & 3 & 0 & 0 \\ 2 & 0 & 3 & 0 & 0 & 0 & 1 & 2 & 3 & 1 \end{pmatrix}$

In this section, the frame error rates (FER) performance of QPSK SOSTTC for 16-, 32- and 64-states given in Table I using two transmit antennas in a Nakagami fading channel are presented. For all the simulations, 130 symbols are transmitted from each transmit antenna and channel state information is assumed at the receiver. For the simulation, 10,000 frames were transmitted per antenna, each frame comprising 130 symbols, which, using QPSK modulation, corresponds to 520 bits per frame. It is assumed that the fading channel is quasi-static i.e. the fading channel coefficient is constant over one frame but varies from one frame to another.

Figs. 2.10, 2.11 and 2.12 present FER performance curves for 16-, 32- and 64-state QPSK SOSTTC for one receive antenna over Nakagami fading channels with fading parameters m = 0.5, 1, and 2, respectively. In Fig. 2.10, the simulation result for 16-state STTC from [79] for m = 2 using 1 receive antenna is also shown.

From the FER performance curve, it is observed that the diversity order of the system in a Rayleigh fading channel is a multiple of the fading parameter m in a Nakagami fading channel. Also, the coding gain achieved by the system is also seen to increase with a multiple of m. The 16-state SOSTTC is observed to maintain its superior coding gain advantage over the STTC counterpart over Nakagami-m fading with no diversity order advantage.

In Figs. 2.13, 2.14 and 2.15, the FER performance of 16-, 32- and 64-state QPSK SOSTTC using two transmit and two receive antennas is presented. The FER

performance curve shows that higher diversity and coding gain is achieved by using two receive antennas as compared with a single receive antenna. The diversity order of the system in a Rayleigh fading channel is observed to be a multiple of the fading parameter *m* which is consistent with the analysis presented in Section 2.9. Also, an increase in the number of states of the SOSTTC leads to an increase in achieved coding gain.

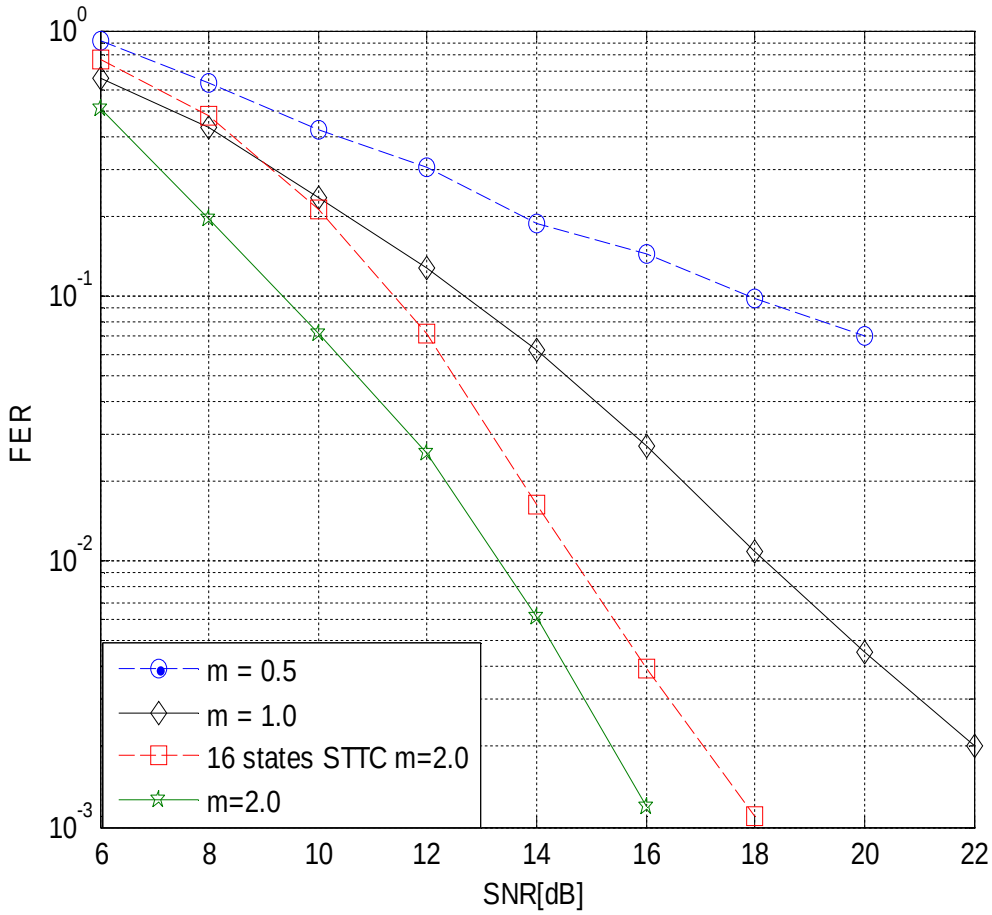

Fig. 2.10: FER performance for a 16-state SOSTTC and a 16-state STTC [79] in a Nakagami fading channel with one receive antenna

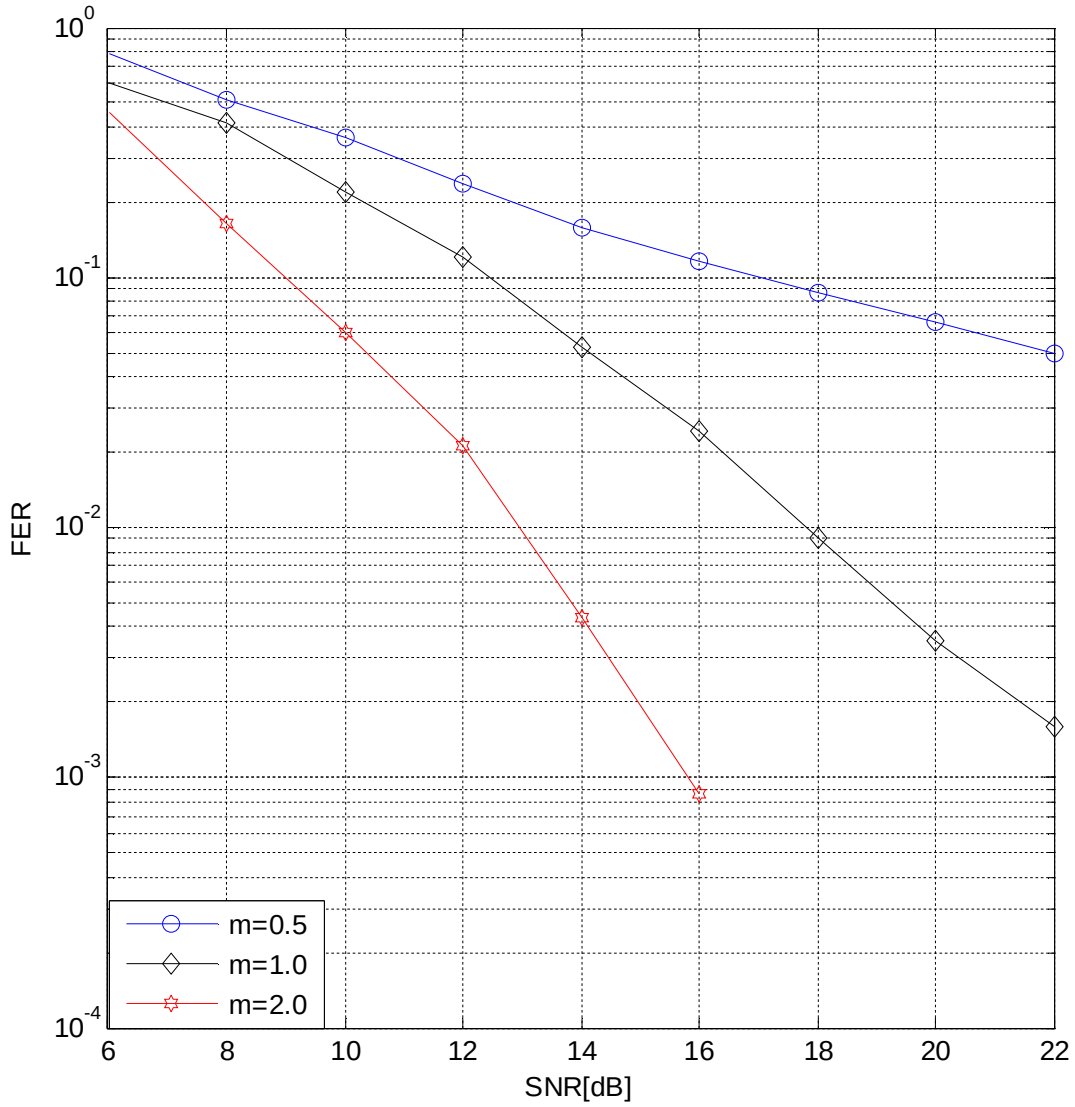

Fig. 2.11: FER performance for a 32-state SOSTTC in a Nakagami fading channel with one receive antenna

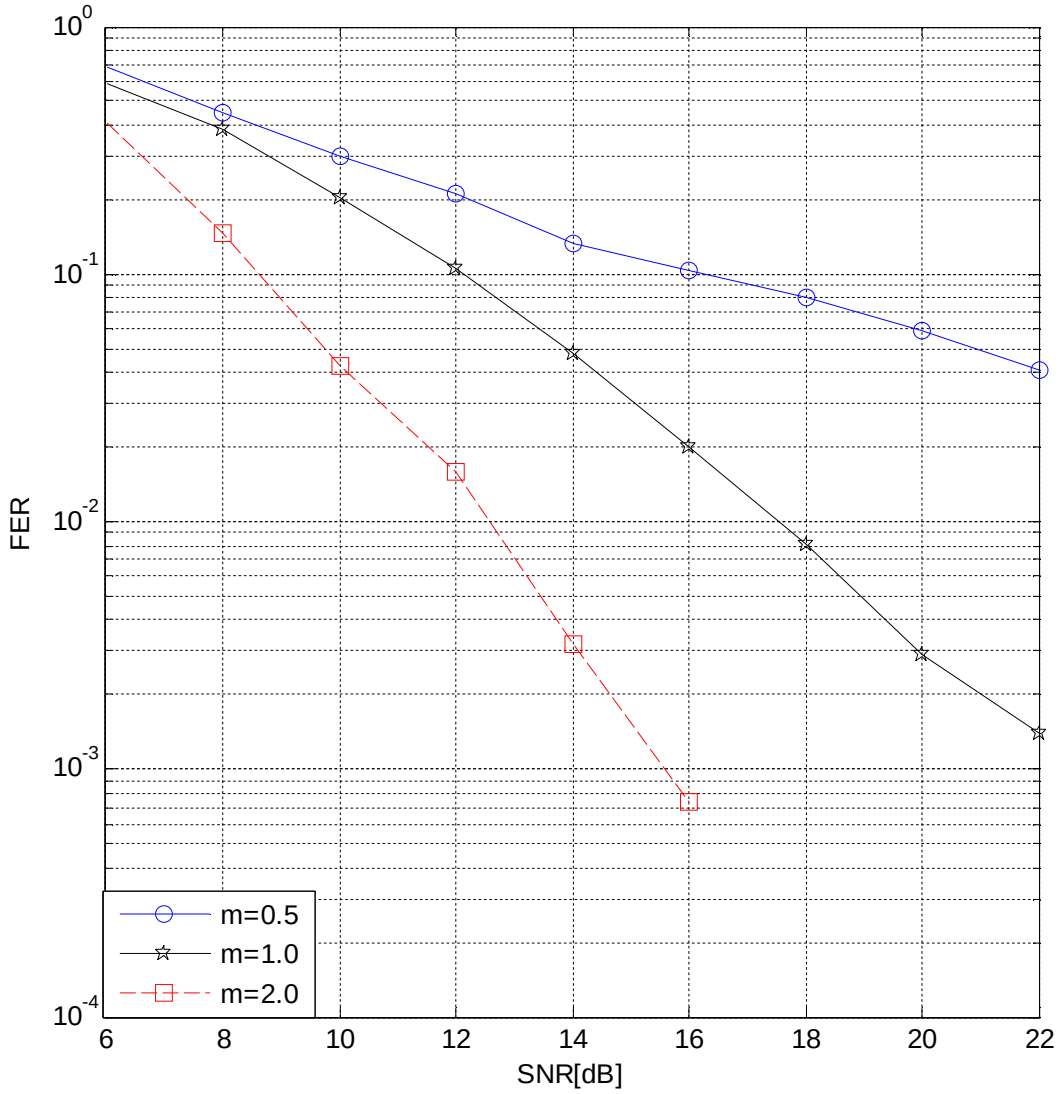

Fig. 2.12: FER performance for a 64-state SOSTTC in a Nakagami fading channel with one receive antenna

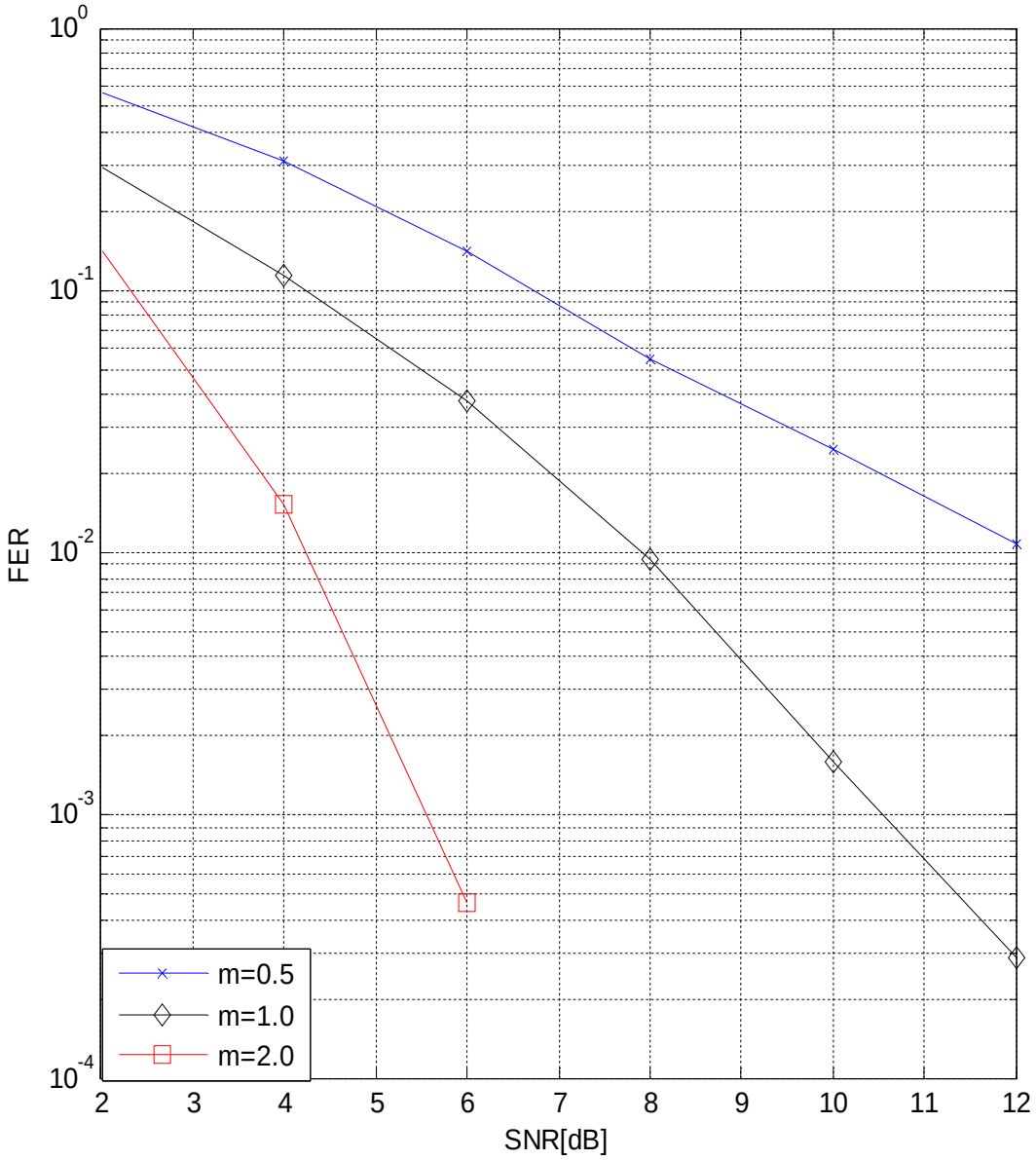

Fig. 2:13: FER performance for a 16-state SOSTTC in a Nakagami fading channel with two receive antennas

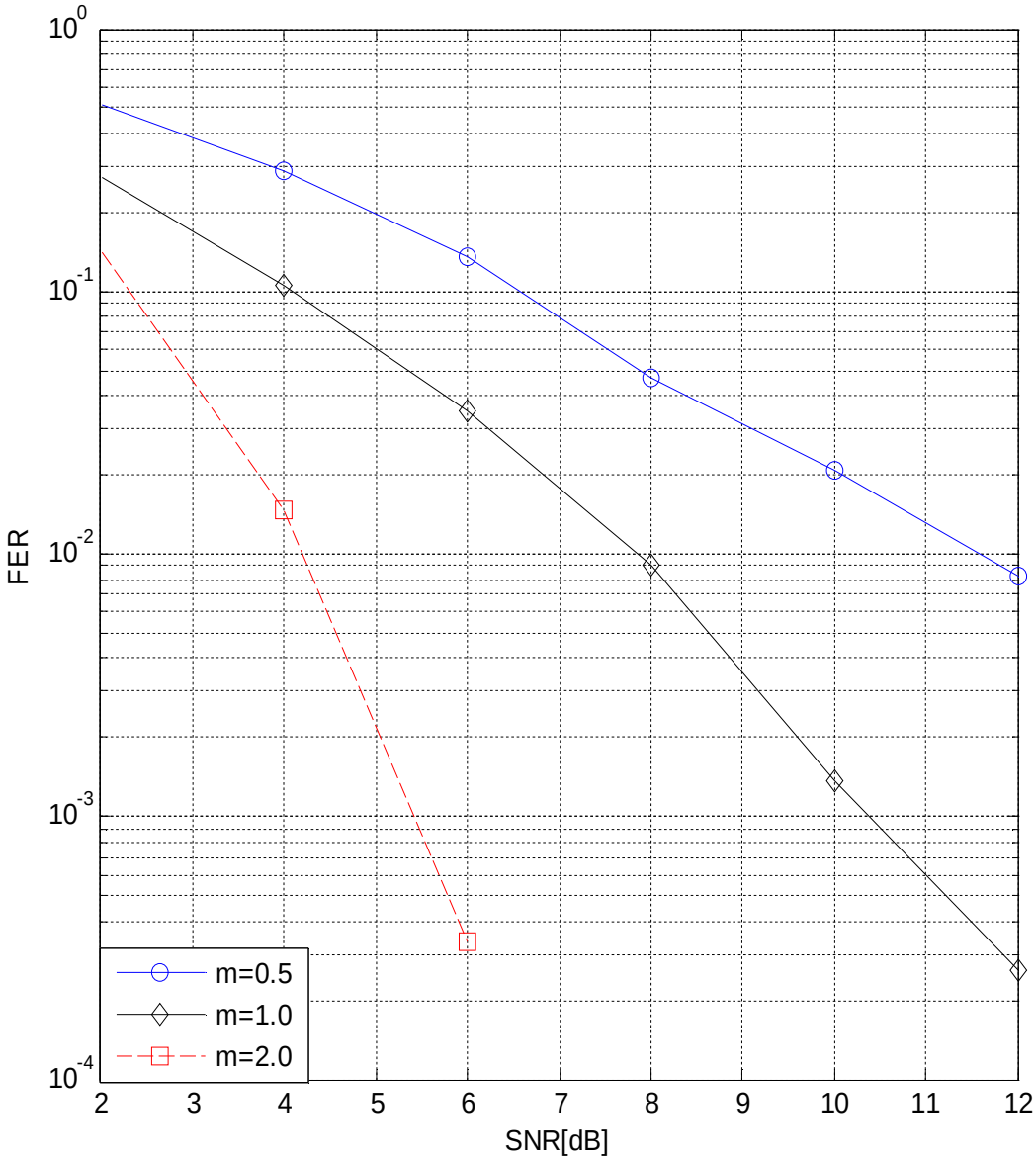

Fig. 2.14: FER performance for a 32-state SOSTTC in a Nakagami fading channel with two receive antennas

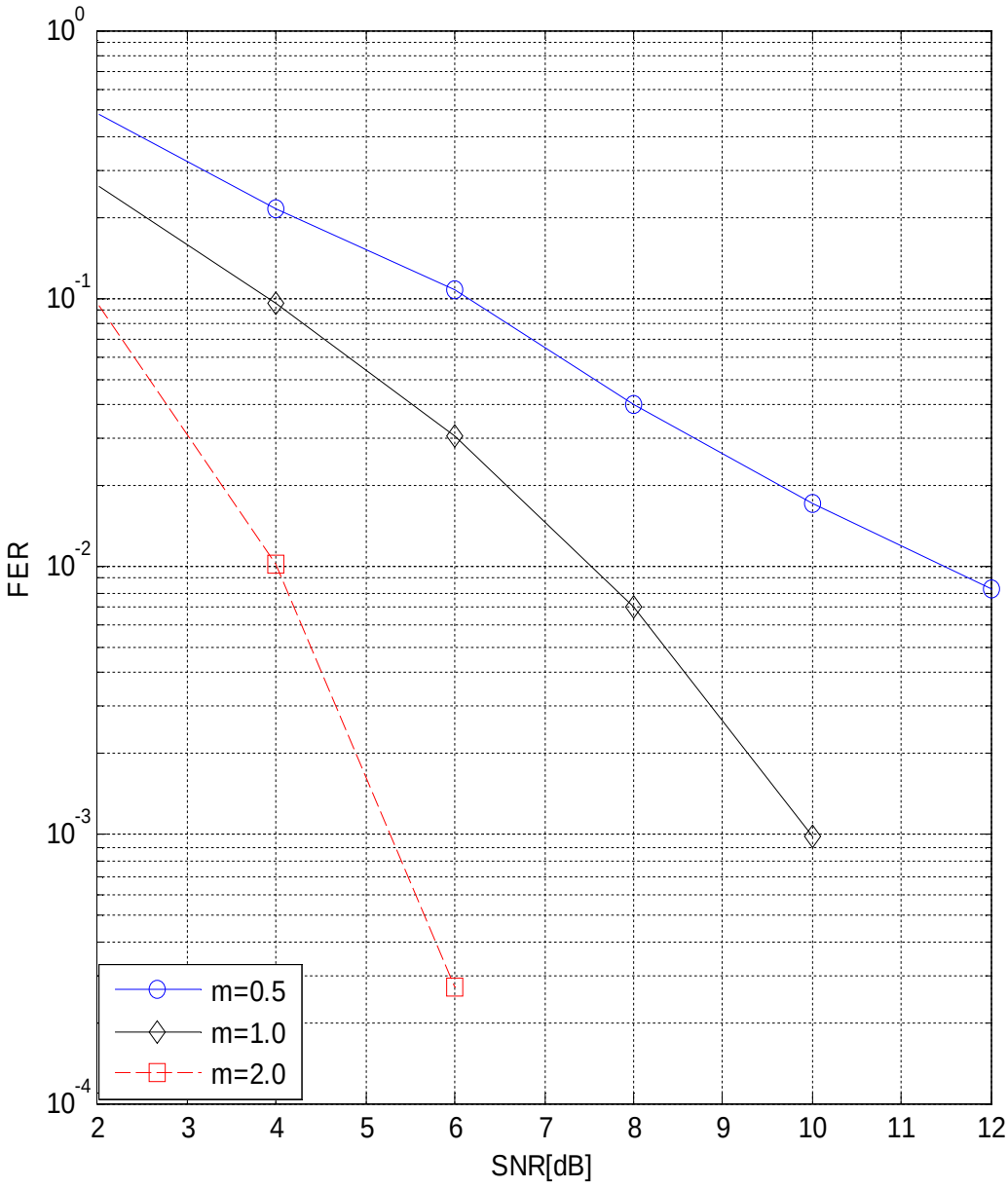

Fig. 2.15: FER performance for a 64-state SOSTTC in a Nakagami fading channel with two receive antennas

2.12 Chapter Summary

In this chapter, the performance of STCs in both fast and slow fading channels was investigated. First, an in-depth overview of space-time coding and design criteria of space-time codes over both fast and slow fading channels was provided. Various types of space-time coding schemes namely: space-time block codes (STBC), space-time trellis codes (STTC) and super orthogonal space-time trellis codes (SOSTTC) were introduced in detail.

New 16-state, 32-state and 64-state SOSTTCs, and by extension, ESOSTTC that can exploit multipath diversity of a frequency-selective fading channel with an OFDM system was designed using the set partitioning principle and the generator matrix notation. Parallel transitions were avoided in the trellis of the proposed SOSTTC in order to exploit the multipath diversity of the frequency-selective fading channel. The CGDs of the new SOSTTCs were also analyzed.

An overview of STC over a Nakagami fading channel was given and the PEP for STTC in [77] was extended to derive the PEP for SOSTTC. As in the case of STTC, it was shown that the diversity order achieved by SOSTTC in a Nakagami-m fading channel is a multiple of the *m* fading parameter. It was also shown that the coding gain of SOSTTC increases with an increase in the *m* fading parameter.

Simulation results evaluating the performance of SOSTTC and the ESOSTTC were presented for the case of quasi-static and rapid Rayleigh fading channels. The simulation results indicated that the proposed SOSTTC achieved full diversity over both quasi-static and rapid fading Rayleigh channels. Comparative simulation results were shown for a 4-state STTC, a 16-state STTC, a 4-state SOSTTC and a 16-state SOSTTC and it was shown that the proposed 16-state ESOSTTC achieves the lowest FER for quasi-static and rapid Rayleigh fading.

Simulation results evaluating the performance of SOSTTCs from literature were also presented for the case of quasi-static Nakagami fading channels for one and two receive antennas. Simulation results show that the diversity order achieved by SOSTTC in a Nakagami-m fading channel is a multiple of the *m* fading parameter. It was also shown that the coding gain of SOSTTC increases with an increase in the *m* fading parameter. Comparative simulation results were shown for a 16-state STTC for fading parameter *m*

= 2 for one receive antenna. The 16-state SOSTTC was shown to achieve the same diversity order as that of a 16-state STTC but the former achieved a coding gain advantage of about 2 dB over the latter.

CHAPTER 3

CONCATENATED SOSTTC OVER RAYLEIGH FLAT FADING CHANNELS

3.1 Introduction

Concatenated coding was first proposed in [85] by Forney where two codes were concatenated serially. The concatenated scheme consists of a convolutional code as the inner code and the Reed-Solomon (RS) code as the outer code. The Forney concatenated code achieved a very promising performance improvement and led to further research that resulted in several concatenated schemes employing iterative decoding in literature.

Space-time coding leads to an increase in both the bandwidth efficiency and the reliability of wireless communication channels by combining spatial and temporal diversity. A combination of channel coding and STC with iterative turbo decoding is a technique that has led to improved performance of STC in MIMO fading channels. The use of channel coding with STC has the advantage of providing additional time diversity especially in fast fading channels.

This chapter focuses on concatenated topology with constituents of SOSTTC and convolutional codes. Some concatenated schemes have been proposed in literature with improved performance over conventional STCs [86-96]. In this chapter, two concatenated schemes built from SOSTTCs and convolutional codes (CC) with iterative decoding are proposed in a bid to further improve the coding gain of SOSTTC over fading channels.

Firstly, an overview of concatenated schemes involving convolutional codes and space-time codes is given in the next section. The decoding algorithm employed in the systems is described in Section 3.3. Parameters influencing the performance of concatenated codes are explained in Section 3.4. The system models for the proposed hybrid concatenated SOSTTC are presented where the encoding and the decoding procedures are explained. A brief explanation of the bitwise additive SISO algorithm is

also presented. The PEP of the two proposed schemes is derived in Section 3.8. Lastly, the system performance is evaluated by computer simulations in Section 3.9 for quasi-static and rapid fading channels.

3.2 Concatenated Space-Time Codes

Deng and Costello were motivated by the concatenated scheme of Forney and that of Ungerboeck [70] on TCM to propose another concatenation scheme involving serial concatenation of TCM and RS code [97]. In [98], two convolutional codes were concatenated serially with a pseudorandom interleaver. The decoder employs Soft-Output Viterbi Algorithm (SOVA) that sends soft information to the outer Viterbi decoder. One of the most important breakthroughs in coding theory is the discovery of turbo codes in 1993 [99]. The discovery of turbo codes led to new ways by which concatenated codes can be exploited to achieve further improvements. Another concatenation scheme is introduced in [100] [101] involving two convolutional codes in serial concatenation with an interleaver. The new concatenated topology, which is inspired by the performance of turbo codes, employs an iterative decoding principle. The hybrid concatenated code was introduced in [102]. In the hybrid architecture, two serially concatenated CC codes are concatenated in parallel with a single convolutional code. The *constituent* codes are connected via two interleavers, one for the serial part and the second one for the parallel connection. All these earlier mentioned schemes were however proposed for AWGN channels.

Several research groups have proposed different versions of turbo coding topology for MIMO systems in recent times. In [103], a standard binary turbo code was concatenated with an inner space-time block code. In [104], serial and parallel concatenated topology was proposed with recursive component codes. In the serial concatenated topology, CC was used as the outer code while recursive STTC was used as the inner encoder. The parallel concatenated topology employed a self-concatenated STC. In [105], two parallel concatenated recursive convolutional codes were used in conjunction with a multiple transmit antenna system with BPSK modulation while in [106] a turbo coded modulation scheme for a wireless communication system with multiple antennas was proposed. The code achieved full coding rate but was not

guaranteed to achieve full diversity. In [107] a double concatenated scheme was proposed using two convolutional codes with inner STTC while in [108] a hybrid concatenated scheme involving parallel concatenation of two serial concatenated architectures was proposed. Other concatenated schemes involving STC were proposed in [86-96]. In [109], [110] and [111] concatenated schemes involving SOSTTC and convolutional codes were introduced. These involve serial concatenations of convolutional codes with SOSTTC as the inner code.

3.3 Decoding Algorithm for Concatenated Codes

Maximum likelihood decoding algorithms can be employed in decoding concatenated codes based on the entire code trellis. However, this is too complex to be implemented in a realistic system with medium to large interleaver size. The use of a suboptimal, yet powerful, iterative decoding algorithm in which the constituent codes are decoded separately and iteratively by the exchange of soft information between decoders is a reasonable way of implementing the decoder of a concatenated scheme with realizable complexity. An iterative decoding algorithm for concatenated schemes is derived from the Viterbi algorithm [112] or the maximum *a posteriori* algorithm (MAP) [113]. The Viterbi algorithm differs from the MAP algorithm in that the Viterbi algorithm minimizes FER by finding the most likely state sequence while MAP algorithm minimizes BER by finding the most likely individual state.

The soft-output Viterbi algorithm (SOVA), which is an extension of the Viterbi algorithm, was proposed in [114]. SOVA computes a reliability estimate of each bit and this estimate can be improved upon by the improved soft-output Viterbi algorithm (ISOVA) [115].

The MAP algorithm was first applied to turbo codes in [116]. Computation of the MAP algorithm in the log domain by using either log-MAP or the max-log-MAP algorithm was introduced to minimize the computational intensity and the sensitivity to the round-off error of the MAP algorithm. The algorithms discussed thus far only give an estimate of the uncoded bits and therefore are only suitable for turbo codes or multiple turbo codes. However, in the serial concatenated code and the hybrid code, improved estimates of the coded bits and the uncoded bits are required. The soft-input soft-output

(SISO) module was proposed to provide an estimate of the coded and the uncoded bits. The SISO module is a four-port module that accepts the input LLRs of the coded and the uncoded bits and generates an update of these LLRs based on the code constraints. The SISO module can be implemented in either additive mode which is an extension of log-MAP algorithm or multiplicative mode which is an extension of the MAP algorithm. The SISO in additive mode is described in Section 3.6

3.4 Performance Parameters for Concatenated Codes

The performance of concatenated codes depends on several parameters. Some of these parameters are presented in [117] for turbo codes and in [118] for serial concatenated convolutional codes (SCCC) and turbo codes. An overview of these parameters affecting the performance of concatenated codes is presented as follows.

3.4.1 Decoding Algorithm

The constituent decoding algorithm to be employed can be chosen by trading improved performance for increased complexity or vice-versa. In terms of computational complexity, the MAP decoding algorithm is the most complex, followed by the log-MAP, then the max-log-MAP and finally the SOVA. However, in terms of performance the log-MAP algorithm is marginally inferior to the performance of the MAP algorithm. The max-log-MAP algorithm offers a worse performance than the log-MAP, but better than the SOVA algorithm. In terms of good tradeoff between complexity and performance, the log-MAP algorithm is therefore a good decoding algorithm.

3.4.2 Trellis Termination

Termination of all or some of the constituent encoders of concatenated systems can improve performance. This can be achieved by forcing the encoders to the all zero state with the aid of tail bits. SCCCs can easily be terminated by adding tail bits to the end

of the frame while a turbo code can be terminated by calculating tail bits for the first encoder and leaving the second un-terminated.

3.4.3 Number of Decoding Iterations

The performance of concatenated codes improves with an increase in the number of decoding iterations until a saturation point is reached when further increase in the number of iterations will achieve no further improvement. Increasing the number of iterations beyond the saturation point adds no further improvement to the system performance. The decoding saturation point depends on the size of the interleaver employed, with codes having a longer interleaver length requiring a larger number of iterations before saturation.

3.4.4 Interleavers

Interleavers play a significant role in the performance of concatenated schemes. They generate long block codes from short constraint length constituent codes and, by de-correlating the input encoders, allow for the application of an iterative decoding algorithm which can exchange soft information between decoders. The size of the interleaver employed in a concatenated scheme has a strong influence on the performance of such codes, especially at low SNRs, while the structure of the interleaver is negligible. At high SNRs however, both the structure and the size of the interleaver influence the code's performance. With a longer interleaver, improved code performance is achieved as the BER is lowered to a level where the error floor region is reached. Details of interleaver structures are documented in [118].

3.4.5 Constituent Codes

The performance of a concatenated scheme largely depends on the type, the constraint length and the polynomial of the constituent code employed. For turbo codes, a recursive code results in higher interleaving gain than a non-recursive code. Due to the effect of the interleaver, a convolutional code achieving the largest minimum free

distance may not result in a minimum free distance concatenated code. Increasing the constraint length of the constituent codes improves the overall code's performance at high SNRs but leads to performance degradation at low SNRs. In designing concatenated codes therefore, the joint effect of the interleaver and the constituent code must be considered.

3.5 System Model for PC-SOSTTC and SOST-SC

SOSTTC has been shown to achieve higher coding gain when compared with earlier STTC constructions for both fast fading and slow (quasi-static) fading channels [65]. Concatenation of space-time codes through serial, parallel and hybrid means have also led to improved coding gain over conventional space-time coding. The potential for improved performance motivates the propositions of two concatenation schemes that combine the field of space-time and turbo coding in order to improve the performance of SOSTTC. The double concatenated structure of [107] and the hybrid architecture in [108] is modified here to incorporate a SOSTTC encoder. The first concatenated topology consists of two outer convolutional codes in parallel concatenated serially with a SOSTTC inner code to give PC-SOSTTC. The second scheme, referred to as a hybrid concatenated SOSTTC (HC-SOSTTC), involves parallel concatenation of two serially concatenated convolutional and SOSTTC codes. The decoding of these concatenation schemes is done iteratively with turbo decoders. The encoding and the decoding of these two proposed schemes over flat fading channel are explained in this section. The SISO decoding algorithm used in the decoding of the constituent CC and SOSTTC is also described.

3.5.1 PC-SOSTTC Encoding

A block diagram of the PC-SOSTTC system is shown in Fig. 3.1 where the input bits are encoded by CC1 as well as by CC2 after interleaving by π_p. All the output bits from CC1 and CC2 are converted to a single serial stream. The serial stream is then interleaved by π_s and finally SOSTTC-encoded to produce the complex symbols that are transmitted according to the SOSTTC transmission matrix at each of the transmit

antennas. The interleavers are all pseudo-random and operate on bits and not symbols. The convolutional encoders are either both recursive systematic convolutional (RSC) or non-recursive convolutional (NRC) encoders. All the encoders are terminated with tail bits and to ensure uncorrelated fading, all the antennas are separated by at least half of the wavelength of the signal.

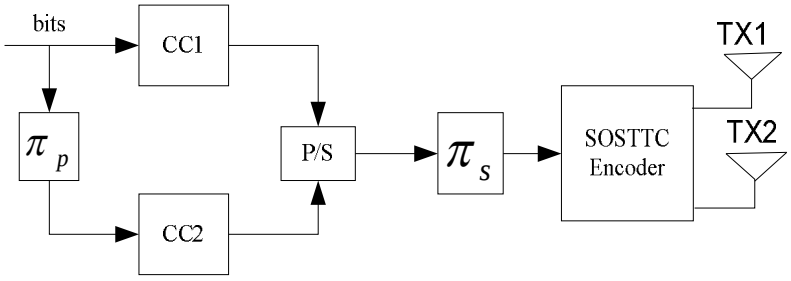

Fig. 3.1: Encoder block diagram of the PC-SOSTTC system

3.5.2 HC-SOSTTC Encoding

In Fig. 3.2 the transmitting block diagram of the HC-SOSTTC system is shown. The HC-SOSTTC topology consists of a parallel concatenation of two serially concatenated schemes. Each of the serial concatenated schemes consists of an outer convolutional code concatenated via an interleaver with an inner SOSTTC encoder. In the system, a block of *N* independent bits is encoded by the convolutional outer encoder (CC1) of the upper serial part of the scheme. The output of the upper convolutional encoder is then passed through a random bit interleaver (π_1). The permuted bits from the interleaver are then fed to the upper SOSTTC encoder to generate a stream of complex data that are transmitted from each of the transmit antennas using the SOSTTC transmission matrix.

In the lower serial part of the encoding, the lower convolutional encoder (CC2) receives the permuted version of the block of *N* independent bits and generates blocks of coded bits which are passed through another interleaver (π_2) to the lower SOSTTC encoder. The complex data from the output of the lower SOSTTC encoder are transmitted from the transmit antennas. It should be noted that the same convolutional and SOSTTC codes are used in the upper and lower encoding of the systems. Each of the encoders is

terminated using appropriate tail bits. All the four transmit antennas are well separated by at least half of the wavelength of the signal.

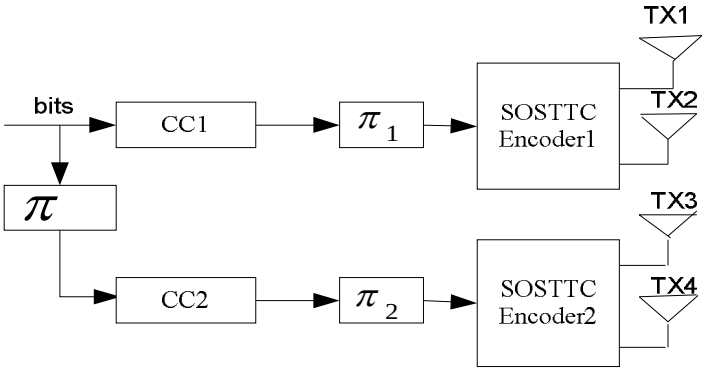

Fig. 3.2: Encoder block diagram of the HC-SOSTTC system

3.6 Bitwise Additive SISO Algorithm

The Soft-Input Soft-Output (SISO) [119] module is the core of the employed iterative decoding algorithm [100]. The algorithm is implemented in its bitwise additive form in this thesis [120]. In its bitwise additive form, soft information is exchanged between decoders in the form of a bit logarithm likelihood ratio (LLR) and this makes the process of interleaving and de-interleaving straightforward because the conversion between bit LLR and symbol LLR is not required.

Consider a typical trellis encoder with L input symbols u, m memory elements and L output symbols c. The input symbols, each consisting of k bits, are drawn from an alphabet of $n_u = 2^k$, where $u = \{u^1, \dots, u^k\}$ and k is the number of encoder input bits at each time instance. For convolutional codes, the symbols output is drawn from an alphabet of $n_c = 2^n$ symbols, each consisting of n bits, where $c = \{c^1, \dots, c^n\}$ and denotes the number of encoder output bits at each time instance. In the case of SOSTTCs, the output symbol is drawn from an alphabet of $n_c = M^{n_T}$ symbols, each consisting of n_T M-PSK symbols where $c = \{c^1, \dots, c^{n_T}\}$.

Fig 3.3a shows the four-port SISO module. The SISO module, based upon the code constraint, receives the input LLRs of the code bits and the uncoded bits, $\lambda_t(c^j, I)$

and $\lambda_t(u^j, I)$, and generates at the output an update of these LLRs, $\lambda_t(c^j, O)$ and $\lambda_t(u^j, O)$.

A single trellis section that gives all possible transitions or edge between the encoder state at time *t* and time *t*+1 can be used to describe a trellis code. Each trellis section of a trellis code is described by a set of $n_s = 2^m$ states, with the state of the trellis at time *t* given as $S_t = s$ and a set of $n_e = n_u.n_s$ edges connecting the states. Fig 3.3b shows a single trellis section of a trellis code having an edge *e* that describes the transition from the initial state s^S(e) to the final states s^E(e) with corresponding output symbol *c*(e) and input symbol *u*(e).

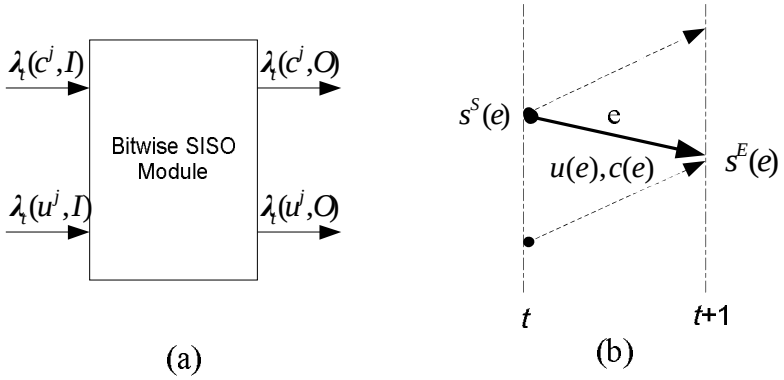

Fig. 3.3: (a) SISO module (b) Trellis section for edge e

In the following, we define the input-output relationship of the SISO module for a frame length of *L* symbols with an input frame size of $L * k$ bits as given in [121].

For $t = \{1, \ldots, L\}$,

$$\lambda_t(c^j, O) = \max_{e: c^j(e) = 1}{}^{*} \left\{ \alpha_{t-1}(s^S(e)) + \lambda_t(u(e), I) + \sum_{i=1, i\neq j}^{n} c^i(e)\lambda_t(c^i(e), I) + \beta_t(s^E(e)) \right\}$$

$$- \max_{e: c^j(e) = 0}{}^{*} \left\{ \alpha_{t-1}(s^S(e)) + \lambda_t(u(e), I) + \sum_{i=1, i\neq j}^{n} c^i(e)\lambda_t(c^i(e), I) + \beta_t(s^E(e)) \right\}. \quad (3.1)$$

$$\lambda_t(u^j, O) = \max_{e: u^j(e) = 1}{}^{*} \left\{ \alpha_{t-1}(s^S(e)) + \lambda_t(c(e), I) + \sum_{i=1, i\neq j}^{n} u^i(e)\lambda_t(u^i(e), I) + \beta_t(s^E(e)) \right\}$$

$$-\underset{e:\,u^j(e)\,=\,0}{\overset{*}{max}}\left\{\alpha_{t-1}\left(s^S(e)\right)+\lambda_t(u(e),I)+\sum_{i=1,i\neq j}^{n}u^i(e)\lambda_t(u^i(e),I)+\beta_t(s^E(e))\right\}. \quad (3.2)$$

The $\overset{*}{max}$ performs the following operation:

$$\underset{p}{\overset{*}{max}}(a_p)\triangleq log\left[\sum_{p=1}^{P}e^{a_p}\right].$$

The output LLRs in this algorithm do not depend on their corresponding simultaneous input. The output LLRs $\lambda_t(c^j,O)$ and $\lambda_t(u^j,O)$ are an update of the input LLRs $\lambda_t(c^j,I)$ and $\lambda_t(u^j,I)$.

The forward metrics $\alpha_t(.)$ is calculated as

$$\alpha_t(s)=\underset{e:\,s^E(e)\,=\,s}{\overset{*}{max}}\left\{\alpha_{t-1}\left(s^S(e)\right)+\lambda_t(u(e),I)+\lambda_t(c(e),I)\right\}, \quad (3.3)$$

while the backward metrics is calculated as

$$\beta_t(s)=\underset{e:\,s^S(e)\,=\,s}{\overset{*}{max}}\left\{\beta_{t+1}\left(s^E(e)\right)+\lambda_{t+1}(u(e),I)+\lambda_{t+1}(c(e),I)\right\}. \quad (3.4)$$

The forward and the backward metrics are initialized at the start of the decoding. The forward metrics are initialized as follows:

$$\alpha_0(s)=\begin{cases}0 & \text{if } s=S_0\\ -\infty & \text{otherwise}\end{cases}, \quad (3.5)$$

while the backward metrics is initialized as

$$\beta_L(s)=\begin{cases}0 & \text{if terminated and } s=S_0\\ 1/n_s & \text{if non}-\text{terminated}\\ -\infty & \text{otherwise}\end{cases}. \quad (3.6)$$

The max operator calculates addition recursively, in the log domain. To calculate $\underset{p}{\overset{*}{\max}}(a_p)$, we evaluate (3.7) recursively with δ_1 initialized to a_1 and max (.) taking the maximum of the two arguments. For $p = \{2, ..., P\}$,

$$\delta_p = \max(\delta_p, \delta_{p-1}) + \ln[1 + exp(|\delta_p - \delta_{p-1}|)]. \quad (3.7)$$

On the final iteration *P*,

$$\overset{*}{\underset{p}{max}}(a_p) = \delta_J. \quad (3.8)$$

The uncoded bits input symbol LLRs for both the CCs and SOSTTC are calculated as follows.

$$\lambda_t(u = u_l, I) = \sum_{i=1}^{k} u_l^i \lambda_t(u^i, I), \quad (3.9)$$

where $l = \{1, \dots, n_u\}$.

The input LLRs of the coded bits for the CCs are not received from the demodulator but are always received from other SISO modules and can be calculated as

$$\lambda_t(c = c_l, I) = \sum_{i=1}^{n} c_l^i \lambda_t(c^i, I), \quad (3.10)$$

where $l = \{1, \dots, n_c\}$.

The input LLRs of the coded M-PSK symbols for the SOSTTCs is only received from the soft output of the demodulator. The received signal at time *t* on the receive antenna *j* after matched filtering is given by (1.5). Let $\underline{s_l}$ be one of the possible output symbol vectors of the SOSTTC encoder where $l = \{1, \dots, n_c\}$. Let $\underline{s_1}$ be the reference symbol, then the input LLR of the coded M-PSK for the SOSTTC can be calculated as

$$\lambda_t(c = \underline{s_l}, I) = \hat{\lambda}_t(c = \underline{s_l}, I) - \hat{\lambda}_t(c = \underline{s_1}, I), \quad (3.11)$$

where

$$\hat{\lambda}_t(c = \underline{s_l}, I) = -\frac{1}{2\delta_r^2} \sum_{j=1}^{n_R} \left| r_t^j - \sum_{i=1}^{n_T} h_{ij}^t s_l^i \right|^2 . \quad (3.12)$$

3.7 PC-SOSTTC and HC-SOSTTC-Decoder

In this section, the iterative decoding process of the PC-SOSTTC and the HC-SOSTTC is described. The PC-SOSTTC decoder employs three SISO module decoders that exchange soft information iteratively between themselves. Also, four SISO decoders are used for the HC-SOSTTC scheme and each of the SISOs exchanges soft information iteratively between themselves.

3.7.1 Decoding of PC-SOSTTC

Fig. 3.4 shows a simplified diagram for the PC-SOSTTC decoder. For the purpose of simplification of description, the subscript *t* of λ and the superscript *j* of *c* and *u* are dropped. The decoder is specified by the subscript of *c* or *u* where the SOSTTC encoder is represented by *st,* the convolutional encoder CC1 is represented by 1 and the convolutional encoder CC2 is represented by 2. Since *a priori* information is unavailable on the first iteration, the SISO inputs $\lambda(u_{st}, I)$, $\lambda(u_1, I)$ and $\lambda(u_2, I)$ are all set to zero. The coded intrinsic LLR for the SOSTTC SISO module is computed as in (3.11).

The SOSTTC SISO takes the intrinsic LLR $\lambda(c_{st}, I)$ and the *a priori* information from both the CC1 SISO and CC2 SISO which are initially set to zero and computes the extrinsic LLR $\hat{\lambda}\,(u_{st}, O)$. The extrinsic LLR is then passed to the inverse interleaver π_s^{-1} from where the information pertaining to the coded bits of CC1 and CC2, $\lambda(c_1, I)$ and $\lambda(c_2, I)$ respectively, are extracted. The output LLRs $\lambda(c_1, O)$ and $\lambda(u_1, O)$ are calculated by the CC1-SISO. The LLR $\lambda(u_1, I)$ is subtracted from $\lambda(u_1, O)$ to obtain the LLR $\tilde{\lambda}(u_1, O)$ which is sent through the interleaver π_p to obtain the intrinsic information $\lambda(u_2, I)$ for the CC2-SISO. The output LLRs $\lambda(c_2, O)$ and $\lambda(u_2, O)$ are also calculated by the CC2-SISO. The LLR $\lambda(u_2, I)$ is subtracted from $\lambda(u_2, O)$ to obtain the LLR $\tilde{\lambda}(u_2, O)$ which is then sent via the de-interleaver π_p^{-1} to obtain the intrinsic information $\lambda(u_1, I)$ for the CC1-SISO. A single LLR stream constructed from $\tilde{\lambda}(c_2, O)$ and $\tilde{\lambda}(c_1, O)$ is interleaved by π_s to become $\lambda(u_{st}, I)$ on the next iteration. The LLR $\lambda(u_2, O)$ is interleaved (π_p) to obtain $\tilde{\lambda}(u_2, O)$ which is added to $\lambda(u_1, O)$ on the final iteration upon which the decision device acts to determine the input bits.

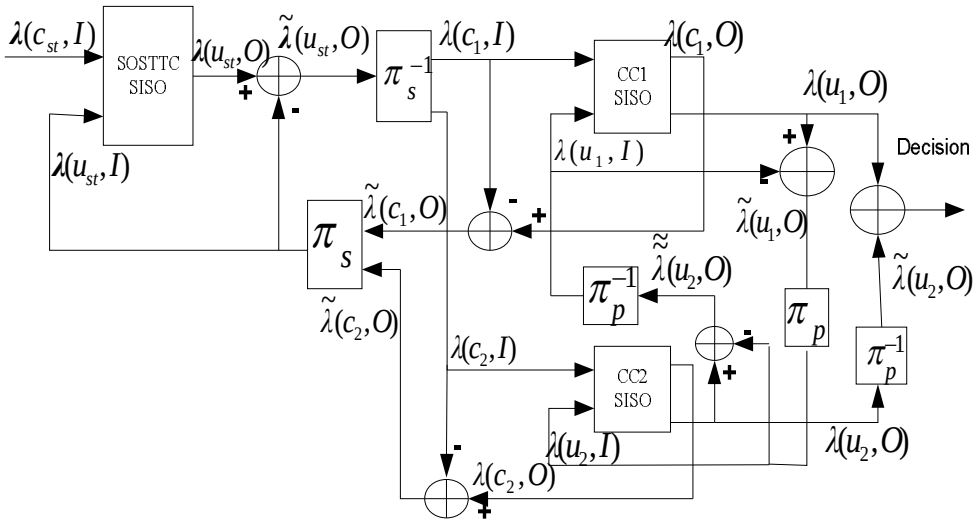

Fig.3.4: Decoding block diagram of the PC-SOSTTC system

3.7.2 Decoding of the HC-SOSTTC

The HC-SOSTTC decoder consists of two serial arms and one parallel sector as shown in Fig. 3.5. The decoder is specified by the subscript of the *c* or *u,* where for the upper SOSTTC encoder *st1* is used, and *st2* is used for the lower SOSTTC encoder, 1 is used for the upper convolutional encoder CC1 while 2 is used for the lower convolutional encoder CC2. The coded intrinsic LLR for the SOSTTC SISO module is computed as in (3.11)

The SOSTTC1 SISO takes the intrinsic LLR $\lambda(c_{st1}, I)$ and the *a priori* information from the CC1 SISO which is initially set to zero and computes the extrinsic LLR $\tilde{\lambda}(u_{st1}, O)$. This extrinsic LLR from the SOSTTC1 SISO is passed through the interleaver (π_1^{-1}) to obtain $\lambda(c_1, I)$.

The LLR's output of the CC1 SISO module which are $\lambda(c_1, O)$ and $\lambda(u_1, O)$ are calculated. The LLR $\lambda(c_1, I)$ is subtracted from $\lambda(c_1, O)$ to obtain the LLR $\tilde{\lambda}(c_1, O)$ which is then sent via interleaver π_1 to obtain the intrinsic information $\lambda(c_{st1}, I)$ for the SOSTTC1-SISO for the next iteration.

For the lower parallel arm, the SOSTTC2 SISO takes the intrinsic LLR $\lambda(c_{st2}, I)$ and the *a priori* information from the CC2 SISO, which is also initially set to zero, and computes the extrinsic LLR $\tilde{\lambda}(u_{st2}, O)$. This extrinsic LLR from the SOSTTC2 SISO is passed through the interleaver (π_2^{-1}) to obtain $\lambda(c_2, I)$. The LLRs $\lambda(c_2, O)$ and $\lambda(u_2, O)$ from the output of the CC2 SISO module are then calculated. The LLR $\lambda(c_2, I)$ is subtracted from $\lambda(c_2, O)$ to obtain the LLR $\tilde{\lambda}(c_2, O)$ which is then passed through the interleaver π_2 to obtain the intrinsic information $\lambda(c_{st2}, I)$ for the SOSTTC2-SISO.

For the parallel interconnection component of the iterative decoding process, the LLR $\tilde{\lambda}(u_2, O)$ obtained by subtracting the LLR $\lambda(u_2, I)$ from the LLR $\lambda(u_2, O)$ is sent via the de-interleaver π^{-1} to obtain the LLR $\lambda(u_1, I)$ which is the uncoded *a priori* information from the CC2 SISO into the CC1 SISO. Also the LLR $\tilde{\lambda}(u_1, O)$ obtained by subtracting LLR $\lambda(u_1, I)$ from the LLR $\lambda(u_1, O)$ is sent via the interleaver $\boldsymbol{\pi}$ to obtain the LLR $\lambda(u_2, I)$ which is the uncoded *a priori* information from the CC1 SISO into the CC2 SISO.

The process is iterated several times and the bit with the maximum APP is chosen by the decision device in the last iteration using the summed values of the output uncoded LLRs of both the CC1and CC2 SISO decoders.

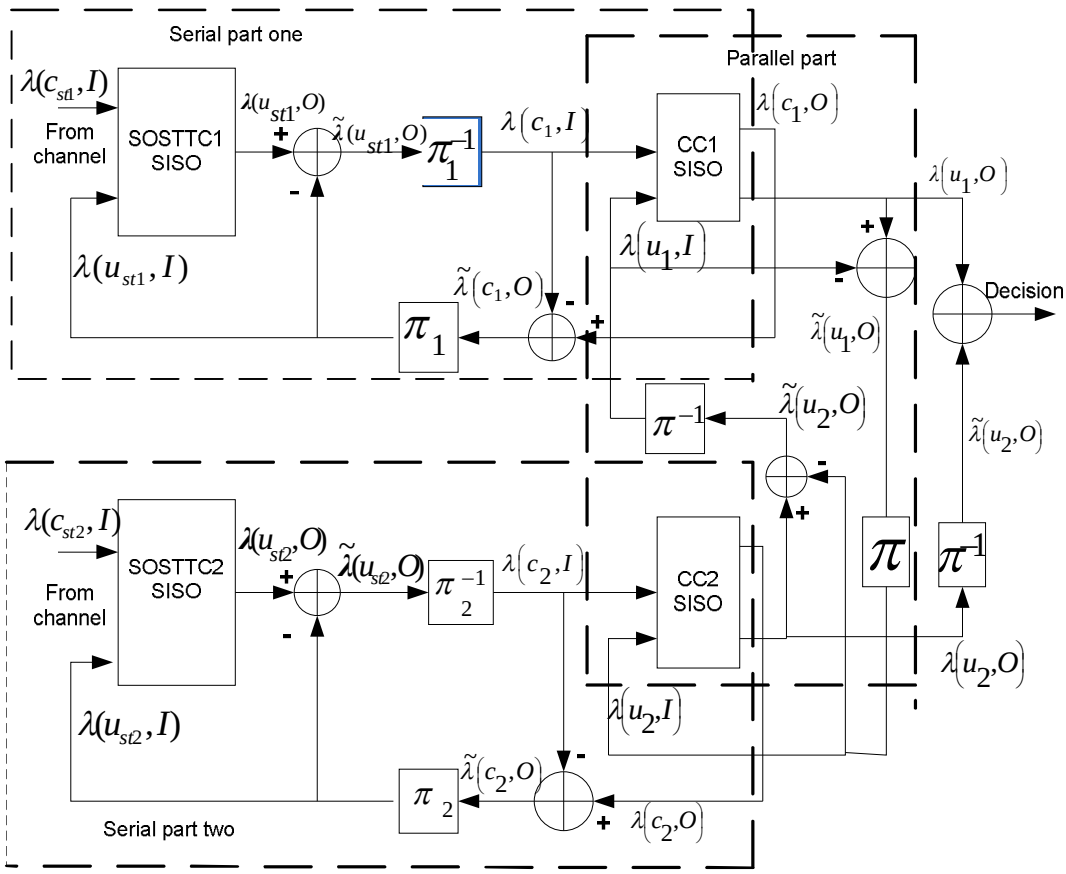

Fig. 3.5: Decoding block diagram of the HC-SOSTTC system [122]

3.8 Performance Analysis

In this section, the performance bound for the concatenated schemes is derived for the case of quasi-static and fast fading channels. It is believed that this derivation has not been done previously. For slow fading the entire frame is subjected to the same fade, while for fast fading, the symbols within the frames are assumed to be subjected to independent fades. For a fast fading channel, additional diversity is provided by the outer channel code while in slow fading channel, only coding gain is provided by the presence of the outer code.

3.8.1 Pairwise Error Probability for Quasi-Static Fading Channels

Let the transmitted codeword and the erroneously decoded codeword be denoted by $\boldsymbol{C}$ and $\widehat{\boldsymbol{C}}$ respectively. If we denote the symbol-wise Hamming distance between $\boldsymbol{C}$ and $\widehat{\boldsymbol{C}}$ by $d(\boldsymbol{C}, \widehat{\boldsymbol{C}})$ and assume ML decoding, the conditional PEP that the receiver will select $\widehat{\boldsymbol{C}}$ over $\boldsymbol{C}$, conditioned on the channel gains assuming perfect CSI at the receiver is given by

$$P(\boldsymbol{C} \rightarrow \boldsymbol{C}\,|\boldsymbol{H}) = \boldsymbol{Q}\left(\sqrt{\frac{E_s d^2}{2N_0}\sum_{i=1}^{n_T}\sum_{j=1}^{n_R}\left|h_{i,j}\right|^2}\right), \tag{3.13}$$

where

$$d^2 = \sum_{l=1}^{d(C,\hat{C})}\left|C(l) - \hat{C}(l)\right|^2. \tag{3.14}$$

is the squared Euclidean distance of the outer code.

By using $Q(x) = \exp\ (-\frac{x^2}{2})$, we have

$$P\left(\boldsymbol{C} \rightarrow \widehat{\boldsymbol{C}}\,|\boldsymbol{H}\right) = exp\left(-\frac{E_s d^2}{4N_0}\sum_{i=1}^{n_T}\sum_{j=1}^{n_R}\left|h_{i,j}\right|^2\right). \tag{3.15}$$

If Υ is defined as

$$\Upsilon = \sum_{i=1}^{n_T}\sum_{j=1}^{n_R}\left|h_{i,j}\right|^2 \tag{3.16}$$

Equation (3.16) is a chi-squared distributed random variable, each having $2n_T n_R$ degrees of freedom with the probability distributed function (pdf) given as

$$P_Y(y) = \frac{1}{(n_T n_R - 1)!}y^{(n_T n_R - 1)}e^{-y}, \quad y > 0. \tag{3.17}$$

In order to compute the average PEP, we average (3.15) with respect to the distribution of Υ,

$$P(\boldsymbol{C} \rightarrow \widehat{\boldsymbol{C}}) = \int_0^{\infty} exp\left(-\frac{E_s d^2}{4N_0} y \frac{1}{(n_T n_R - 1)!} y^{(n_T n_R - 1)} e^{-y}\right) dy. \quad (3.18)$$

Using the integral function [83]

$$\int_0^{\infty} x^n e^{-\mu x}\, dx = n!\, \mu^{-n-1}, \quad (3.19)$$

we have

$$P(\boldsymbol{C} \rightarrow \widehat{\boldsymbol{C}}) = \left(1 + \frac{E_s d^2}{4N_0}\right)^{-n_T n_R}. \quad (3.20)$$

At high SNR, (3.20) can be approximated as

$$P(\boldsymbol{C} \rightarrow \widehat{\boldsymbol{C}}) \approx \left(\frac{E_s d^2}{4N_0}\right)^{-n_T n_R} = \left(d^2(C, \hat{C}) \frac{E_s}{4N_0}\right)^{-n_T n_R}. \quad (3.21)$$

Equation (3.21) suggests that the diversity order of $n_T n_R$ is achieved in a quasi-static fading channel. For the HC-SOSTTC system therefore, the diversity order of 4 is achievable while for the PC-SOTTC, the diversity order of 2 is achievable. Therefore deploying an outer code only provides coding gain in a slow fading channel with no additional diversity benefit.

3.8.2 Pairwise Error Probability for Fast Fading Channels

In the case of a fast fading channel, the conditional PEP that the receiver will select codeword $\widehat{\boldsymbol{C}}$ over $\boldsymbol{C}$, assuming that CSI is known at the receiver and conditioned on the channel gain, is given by [16]

$$P\left(\boldsymbol{C} \rightarrow \widehat{\boldsymbol{C}} \,|\boldsymbol{H}\right) = \boldsymbol{Q}\left(\sqrt{\frac{E_s}{2N_0}\sum_{k=1}^{d(C,\hat{C})}\sum_{i=1}^{n_T}\sum_{j=1}^{n_R}\left|h_{i,j}(k)\right|^2\left|C(k)-\hat{C}(k)\right|^2}\right), \tag{3.22}$$

where $\left|C(k)-\hat{C}(k)\right|^2$ is the normalized squared Euclidean distance between the correct path signal and the error path signal at time index k. By using $Q(x) = \exp\left(-\frac{x^2}{2}\right)$, we have

$$P\left(\boldsymbol{C} \rightarrow \widehat{\boldsymbol{C}} \,|\boldsymbol{H}\right) = \prod_{\boldsymbol{k=1}}^{\boldsymbol{d(C,\,\widehat{C})}}\left\{exp\left(-d_k^2\sum_{j=1}^{n_R}\sum_{i=1}^{n_T}\left|h_{i,j}(k)\right|^2\right)\right\}, \tag{3.23}$$

where

$$d_k^2 = \frac{E_s}{4N_0}\left|C(k)-\hat{C}(k)\right|^2. \tag{3.24}$$

Y_k is defined as

$$Y_k = \sum_{j=1}^{n_R}\sum_{i=1}^{n_T}\left|h_{i,j}(k)\right|^2, \quad \text{for } k = 1, 2, \ldots, d\left(C, \hat{C}\right), \tag{3.25}$$

which are independent and chi-squared distributed, each with $2n_Tn_R$ degrees of freedom with a pdf given by (3.17).

In order to compute the average PEP, (3.23) is averaged with respect to the distribution of Y_k.

$$P\left(\boldsymbol{C} \rightarrow \widehat{\boldsymbol{C}}\right) = \prod_{k=1}^{d(C,\,\hat{C})}\int_0^{\infty} exp\left(-d_k^2 y_k \frac{1}{(n_Tn_R-1)!} {y_k}^{(n_Tn_R-1)} e^{-y}\right) dy_k. \tag{3.26}$$

Using (3.19), we have

$$P(\boldsymbol{C} \rightarrow \widehat{\boldsymbol{C}}) = \prod_{k=1}^{d(C,\ \hat{C})} (1 + d_k^2)^{-n_T n_R} \quad . \tag{3.27}$$

At high SNR, (3.27) can be approximated as

$$P(\boldsymbol{C} \rightarrow \widehat{\boldsymbol{C}}) \approx \prod_{k=1}^{d(C,\ \hat{C})} (d_k^2)^{-n_T n_R} \quad . \tag{3.28}$$

$$P(\boldsymbol{C} \rightarrow \widehat{\boldsymbol{C}}) = \prod_{k=1}^{d(C,\ \hat{C})} \left(\frac{E_s}{4N_0}\left|C(k) - \hat{C}(k)\right|^2\right)^{-n_T n_R} \quad . \tag{3.29}$$

$$P(\boldsymbol{C} \rightarrow \widehat{\boldsymbol{C}}) = \prod_{k=1}^{d(C,\ \hat{C})} \left(\left|C(k) - \hat{C}(k)\right|^2\right)^{-n_T n_R} \left(\frac{E_s}{4N_0}\right)^{-n_T n_R} \quad . \tag{3.30}$$

From (3.30), it is clear that the diversity order of $n_T n_R d_{\text{free}}$ is achieved in a fast fading channel, where d_{free} is the minimum Hamming distance of the outer convolutional code.

3.9 Simulation Results and Discussion

In this section, simulation results are presented to evaluate the performance of the concatenated scheme over a Rayleigh fading channel. The performance of the two proposed topologies is evaluated over both slow and fast fading channels. The results are presented in terms of FER versus E_b/No. In all the simulations, 130 symbols per frame are transmitted from each of the transmit antennas. For each simulation, 10,000 frames are transmitted from each of the transmit antennas. The Rayleigh channel coefficients are modelled as independent samples of the zero mean complex Gaussian random variable with variance 0.5 per dimension, while the noise is modelled as independent samples of the zero mean complex Gaussian random variable with variance No/2 per dimension. The signal-to-noise ratio (SNR) per receive antenna is defined as E_b/No where E_b is the energy per bit. A flat Rayleigh fading channel is considered and the fading is statistically independent from one transmit-receive antenna pair to any other. Unless otherwise stated, the number of iterations of the simulation is

set to six because the performance of the systems is observed to reach saturation at the sixth iteration.

The 4-state, QPSK SOSTTC from [65] is considered as the inner code. For the outer code, the RSC and NRC rate-1/2, 4-state convolutional codes are employed for the HC-SOSTTC while for the PC-SOSTTC the rate-2/3, 4-state RSC and NRC convolutional codes are used. In the two architectures, the outer convolutional codes are both either RSC or NRC.

Figs. 3.6 and 3.7 show the FER performance for the HC-SOSTTC and the PC-SOSTTC systems respectively for various numbers of decoding iterations in quasi-static fading channels. The performance of both schemes is observed to improve with an increase in the number of iterations, and it starts saturating at about the 4^{th} iteration. As can be observed from the FER performance curve, the HC-SOSTTC achieves a full diversity order of four, which is consistent with our observation from the PEP analysis. The concatenation adds no additional diversity to the scheme but achieves significant coding gain as seen by the horizontal shift of the FER performance curve. The significant improvement in the coding gain is as a result of the coding gain benefit of turbo decoding. Also from the FER performance curve of the PC-SOSTTC, no added diversity is achieved by the system but there is significant coding gain improvement by the concatenation.

In Fig 3.8, the FER performance for the HC-SOSTTC comparing the case of RSC outer code, NRC outer code, RSC with STTC inner code and NRC with STTC inner code is shown. On the same plot, the FER performance of SOST-CC from [109] is plotted. The SOST-CC concatenates convolutional code serially with SOSTTC, which is equivalent to one serial arm of the HC-SOSTTC system. For the STTC inner code, the four states of STTC from [16] is employed. As can be seen from the FER performance curve, the HC-SOSTTC system with RSC outer code outperformed the scheme with NRC outer code and the HC-STTC codes. The code with RSC outer code presented better coding gain when compared with the scheme with NRC outer code because recursive codes, unlike their non-recursive counterparts, achieve interleaving gain in iterative decoding. In comparison with the SOST-CC, the figure shows that the HC-SOSTTC outperforms the SOST-CC in terms of both diversity order and coding gain. The better diversity order of the HC-SOSTTC system is as a result of the number of

transmit and receive antennas involved while the better coding gain is as a result of the coding gain benefit of iterative decoding. The diversity order of SOST-CC is two while that of HC-SOSTTC is four. In terms of coding gain, the HC-SOSTTC outperforms the SOST-CC by 3.5 dB at an FER of 10^{-2}.

Fig 3.9 shows an FER performance comparison for the PC-SOSTTC system with an RSC outer code, NRC outer code and the PC-STTC code. As can be observed from the performance figure, the scheme with an outer RSC code achieves improved coding gain over the scheme with an outer NRC code. It can also be observed that the PC-SOSTTC achieves a higher coding gain than the PC-STTC code.

The FER performance of the HC-SOSTTC over a fast fading channel is shown in Fig. 3.10. The performance of the code is evaluated over this channel condition using both NRC and RSC outer codes. The scheme's performance is also compared with that of CC-SOSTTC [110] over the same channel condition. The scheme with outer RSC code is observed from the FER plots to achieve a higher coding gain when compared to the scheme with NRC outer code. In comparison with the CC-SOSTTC code, the HC-SOSTTC with outer a RSC code has a coding gain advantage of about 4 dB over the CC-SOSTTC at the FER of 10^{-3}.

The FER performance of the PC-SOSTTC system over a fast fading channel is shown in Fig. 3.11 using RSC and NRC outer convolutional codes. In the same figure the system with an inner STTC code is shown. The PC-SOSTTC is observed to achieve a very high diversity order in a fast fading channel but experiences the error floor phenomenon. Error floor at a higher SNR region is a peculiar characteristic of a parallel concatenation scheme [119]. The error floor phenomenon is more pronounced with the scheme with NRC outer code as can be observed from the FER performance plot.

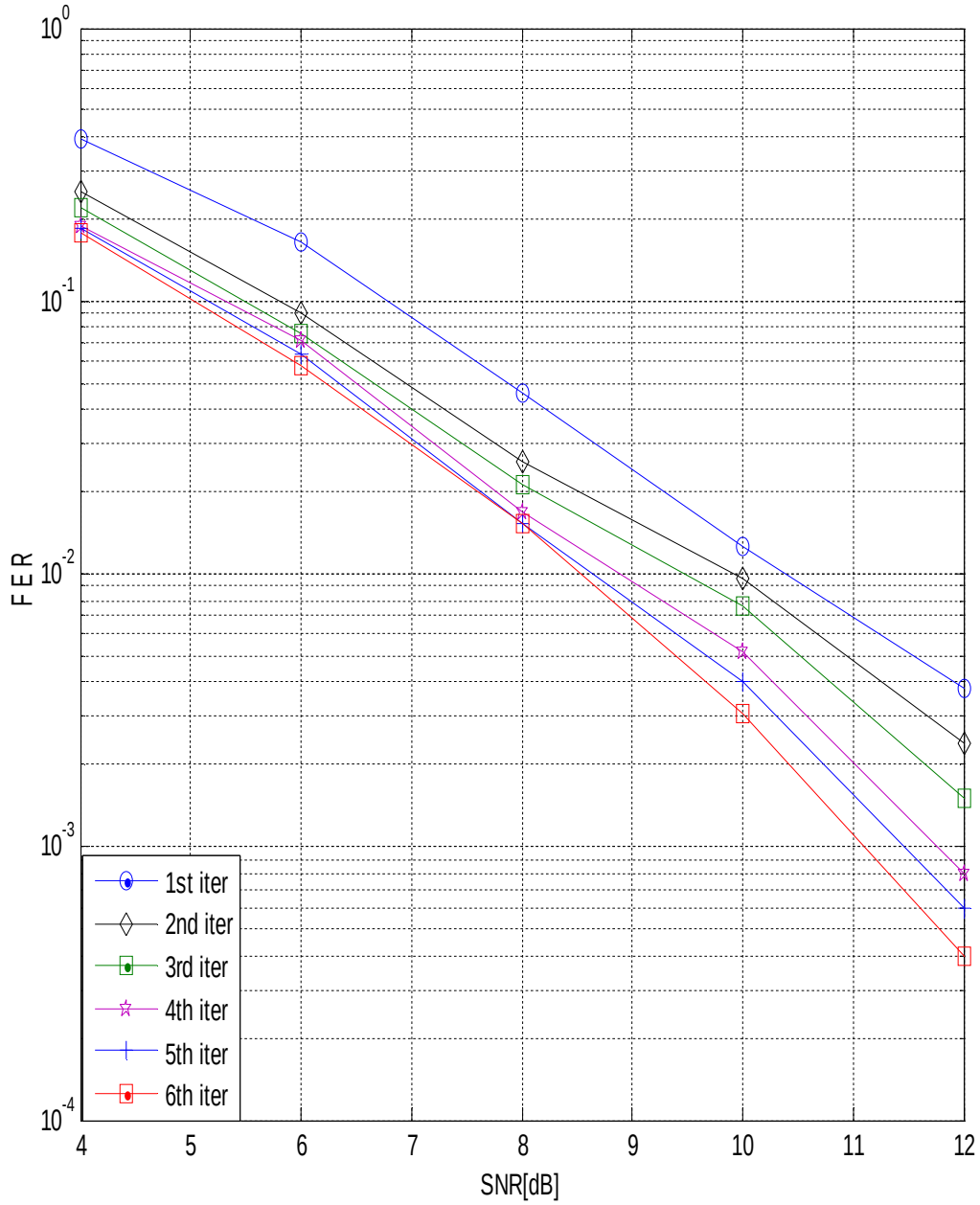

Fig. 3.6: FER performance of HC-SOSTTC for various numbers of decoding iterations

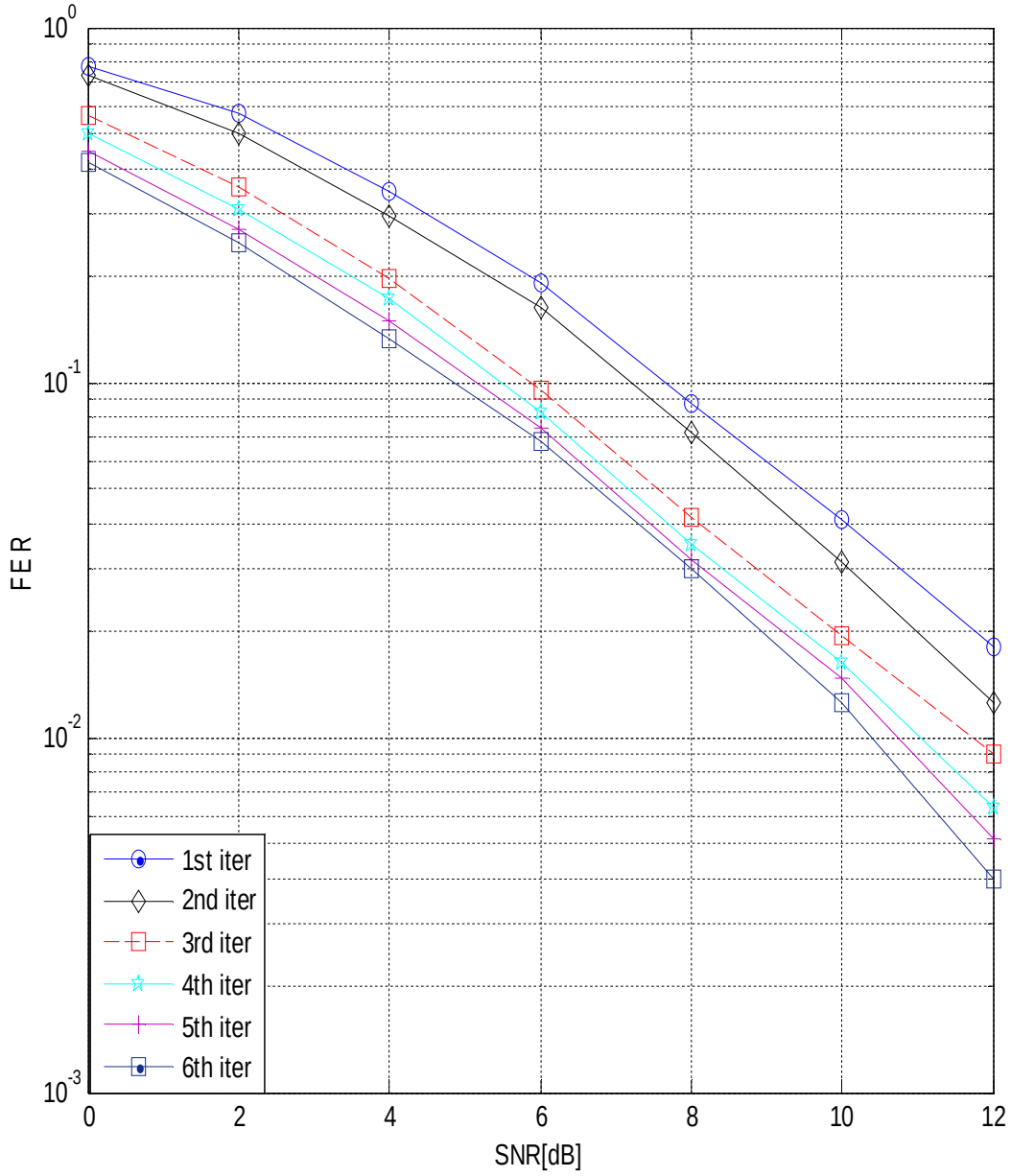

Fig. 3.7: FER performance PC-SOSTTC for various numbers of decoding iterations

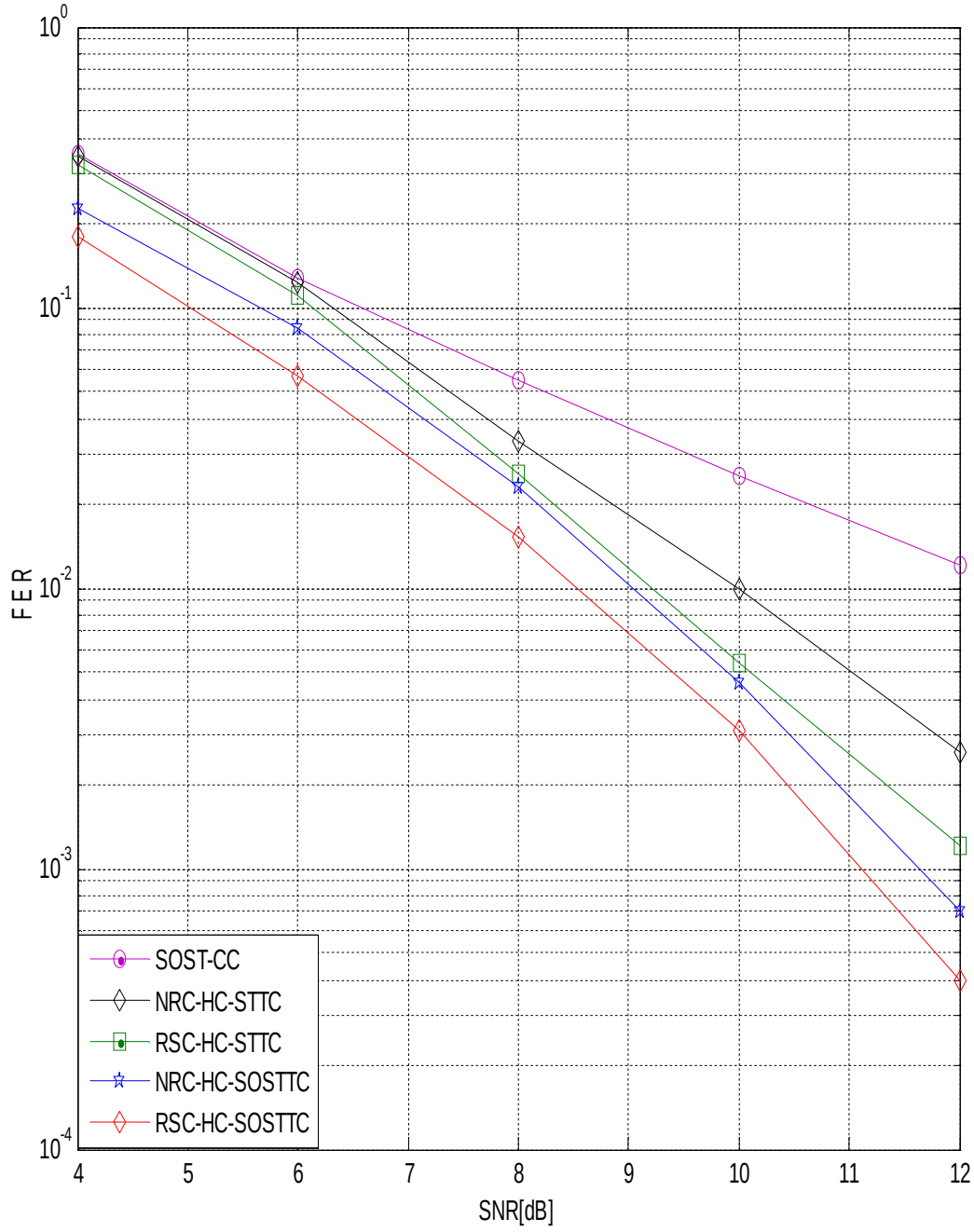

Fig. 3.8: FER performance of HC-SOSTTC over a quasi-static fading channel

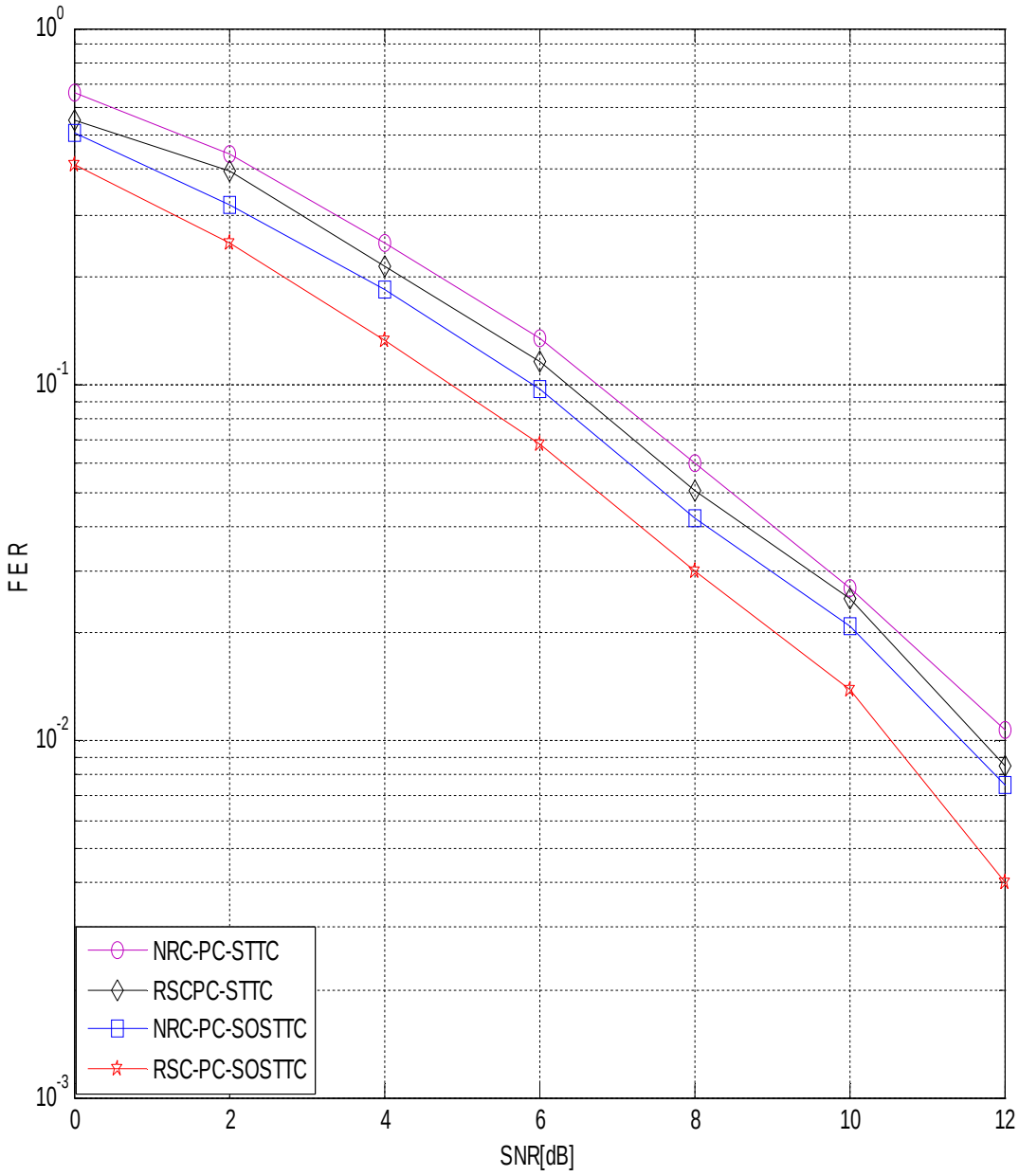

Fig. 3.9: FER performance for PC-SOSTTC over a quasi-static fading channel

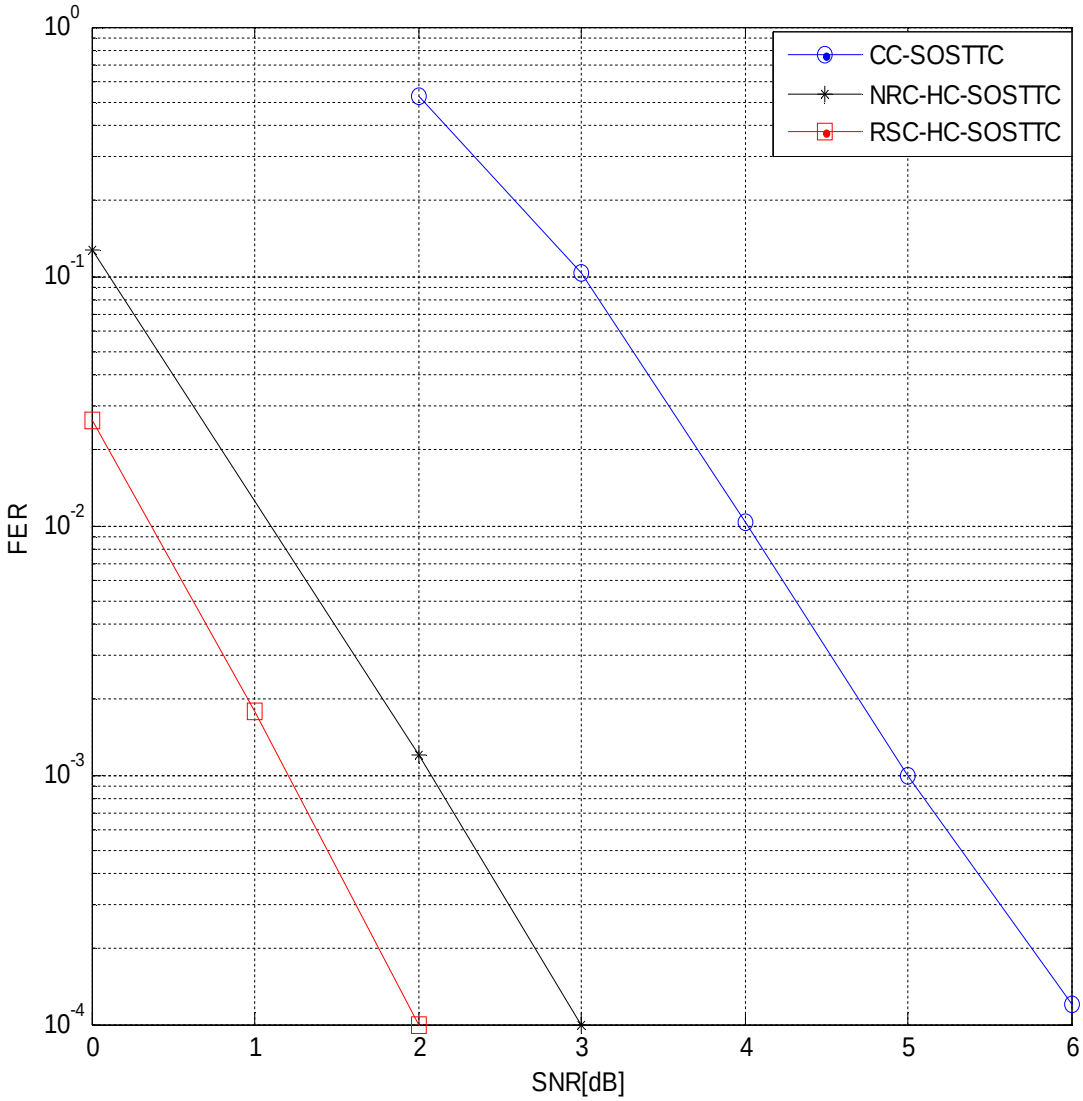

Fig. 3.10: FER performance for HC-SOSTTC over a fast fading channel

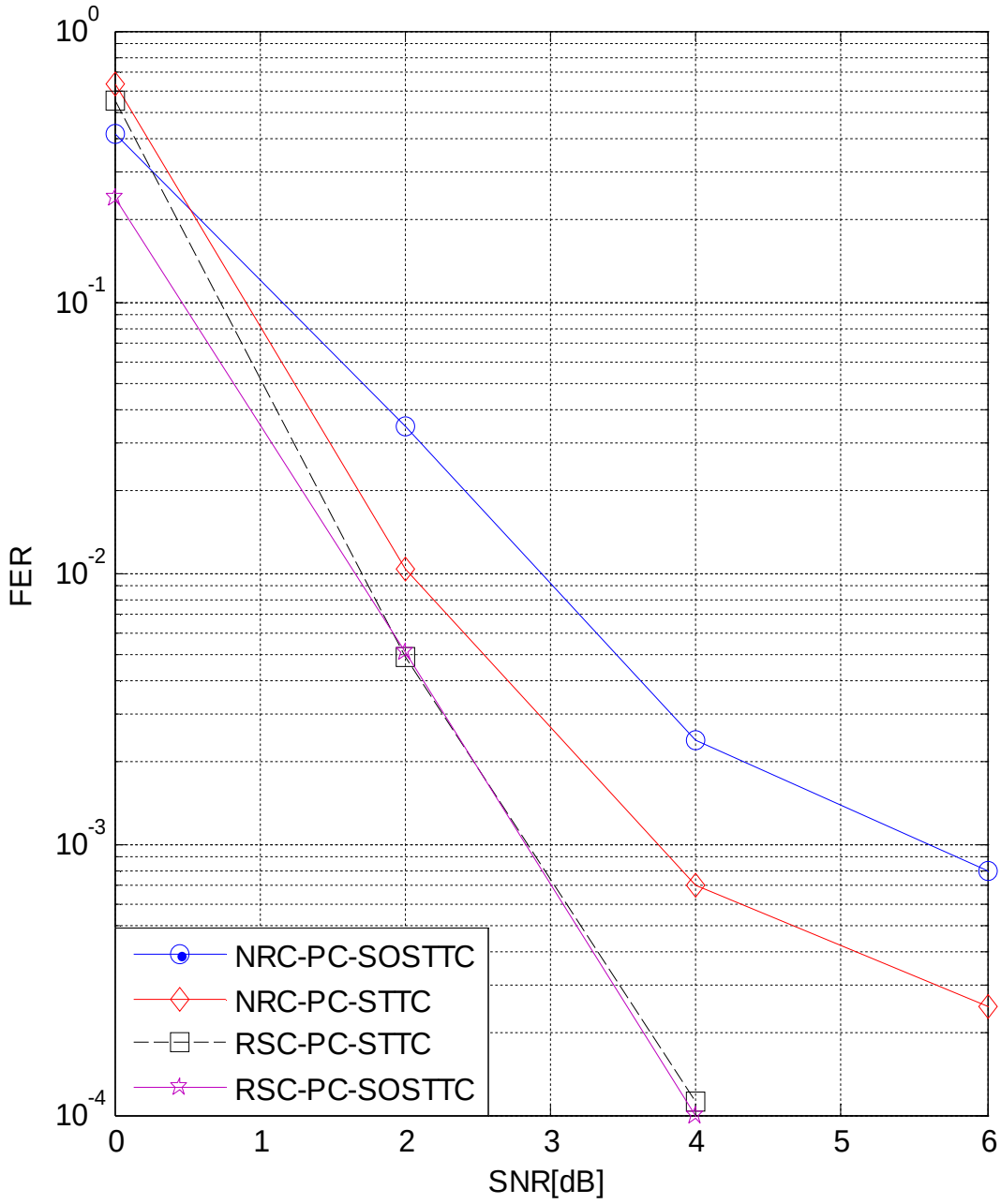

Fig. 3.11: FER performance for PC-SOSTTC over a fast fading channel

3.10 Chapter Summary

In this chapter, an overview of concatenated convolutional codes was given and recent literature in the field of concatenated STTCs and SOSTTCs was reviewed. Two hybrid concatenated topologies were proposed. The PC-SOSTTC system consisted of a PCCC outer code and a SOSTTC inner code, while the HC-SOSTTC system consisted of two serial combinations concatenated in parallel. Each serial combination consisted of a CC outer code and a SOSTTC inner code. The system model for these two systems was presented and the encoding and decoding of each were discussed. The PEP for the two proposed schemes was derived for both quasi static and fast Rayleigh fading channels.

Simulation results were presented for the cases of quasi-static and rapid Rayleigh fading, 130 QPSK symbol input frame size, recursive and non-recursive CCs and SOSTTCs. The FER performance of the HC-SOSTTC was compared with the performance of the SOST-CC over quasi-static Rayleigh fading. In each, 130 QPSK symbol input frame size was used from each transmit antenna. The HC-SOSTTC scheme was shown to achieve a higher diversity order because of the number of transmit antennas involved. Comparative simulation results were also shown for the hybrid scheme with STTC inner code. The scheme with SOSTTC inner code showed lower FER when compared with the scheme with inner STTC as a result of inherent better coding gain of SOSTTC. The HC-SOSTTC scheme with RSC outer code was shown to present a lower FER than the scheme with NRC outer code because of interleaving gain obtained by the RSC outer code.

In addition, the FER performance of the HC-SOSTTC was compared with the performance of the CC-SOSTTC [119] over a fast Rayleigh fading channel. The HC-SOSTTC also presents lower FER than the CC-SOSTTC over fast fading channels.

In general, it was shown that the HC-SOSTTC with recursive outer CC achieved higher diversity and coding gain than other concatenated schemes in both rapid and quasi-static fading channels.

CHAPTER 4

SUPER-ORTHOGONAL SPACE-TIME TRELLIS CODED OFDM SYSTEMS

4.1 Introduction

The performance of communication systems can be enhanced by using multiple transmit and/or receive antennas. SOSTTC was originally proposed for flat fading channels, but broadband services are normally subjected to frequency selective fading channels. SOSTTC combined with OFDM in frequency-selective fading channels enhances the performance of communication systems by exploiting diversity in a space, time and frequency domain to guarantee high data rate communication systems.

In this chapter, two new full-rate space-time coded OFDM systems are proposed, one for two transmit antennas and the other for four transmit antennas. The first one uses the rotated constellation concept from [73] and avoids parallel transition in the trellis design which restricts the performance of SOSTTC in multipath channels. The design of SOSTTC proposed in [65] for a flat fading channel is therefore extended to a case of a frequency selective fading channel by proposing the ESOSTTC-OFDM system for 16-, 32- and 64-states. Since there is no full rate orthogonal code for a case of more than two transmit antennas, the SQOSTTC proposed for four transmit antennas for flat fading is also extended to propose the SQOSTTC-OFDM system for four transmit antennas using BPSK signalling in this chapter. The scheme combines a quasi orthogonal space-time block code with a trellis code to offer a full rate, full diversity and high coding gain for four transmit antennas.

First, an overview of the performance of STC in a frequency-selective fading channel without any additional processing is presented in Section 4.2. In Section 4.3, the design criteria for a ST coded OFDM system for optimum performance is given. The proposed Extended-SOSTTC-OFDM is presented in Section 4.5, along with its codeword structure. Section 4.6 presents the proposed SQOSTTC-OFDM, along with its code

design. Finally the performance of the proposed schemes is evaluated by comparative simulation results.

4.2 STC over Frequency-Selective Fading Channels

In wideband wireless communication systems, the transmitted signal experiences frequency-selective fading because the channel delay spread is larger than the symbol period. Given a multipath fading channel having L different paths, the time variant impulse response is given by [53]

$$h(t;\tau) = \sum_{l=1}^{L} h^{t,l}\,\delta(\tau - \tau_l), \tag{4.1}$$

where τ_l denotes the time delay of the ι-th path and $h^{t,l}$ denotes the complex amplitude of the ι-th path. Consider a transmission system with n_T transmit and n_R receive antennas having the channel complex amplitude of $h_{i,j}^{t,l}$ between the i-th transmit antenna and the j-th receive antenna at time t at the l-th path, the received signal at antenna j after matched filtering is given by [123]:

$$r_t^j = \alpha \sum_{i=1}^{n_T} \sum_{l=1}^{L_p} h_{i,j}^{t,l} \mathrm{c_t^i} + I_t^j + \eta_t^j, \tag{4.2}$$

where I_t^j is a term representing the inter-symbol interference (ISI) and α is a constant dependent on the channel power delay profile, which can be computed as

$$\alpha = \frac{1}{T_s} \int_{-T_s}^{T_s} P(\tau)(T_s - |\tau|)d\tau, \tag{4.3}$$

η_t^j is the sum of the additive noise and the ISI which is a complex Gaussian random variable with a zero mean and single-sided power spectral density N_I+N_0, L denotes the number of multipath fading channels and $P(\tau)$ is the channel power delay profile.

The PEP for STC in this condition is given by [123].

$$P(\boldsymbol{C}, \widehat{\boldsymbol{C}}) \leq \left[\prod_{i=1}^{r}\left(\lambda_i \frac{\alpha^2}{N_I/N_0 + 1} i\right)\right]^{-n_R} \left(\frac{E_s}{4N_0}\right)^{-rn_R}, \quad (4.4)$$

where r is the rank of the codeword distance matrix, and $\lambda_i = 1, 2, \ldots, r$ are the non zero eigenvalues of the matrix. Equation 4.4 indicates that STC achieves the same diversity gain of rn_R over frequency-selective fading channels and flat fading channels. The coding gain achieved by STC in such a channel is reduced by a factor of $\left(\frac{\propto^2}{N_I/N_0+1}\right)$ compared to the coding gain achieved in a flat fading channel. It was also reported that at high SNRs, there exists an irreducible error rate floor for STC in frequency-selective fading channels, and that coding gain decreases considerably due to ISI which results in high performance degradation with an increase in the delay spread [123]. Results from [67] show about 4 dB performance degradation for a 2-state SOSTTC scheme in a frequency selective channel. This performance degradation is attributed to the increase in the number of parallel path transitions per state at the receiver. Improving the code performance in frequency-selective fading channels therefore requires additional processing to remove ISI. OFDM is an effective transmission technique that removes ISI and it has an additional edge over the use of multichannel equalization in removing ISI because of the decoding complexity in multichannel equalization.

4.3 Performance of Space-Time Coding in OFDM Systems

OFDM divides a communication channel into a number of equally spaced frequency bands with a center frequency subcarrier. Each subcarrier is orthogonal in the time domain with every other subcarrier.

The codeword from a STC-OFDM communication system with K subcarriers, n_T transmit antennas, n_R receive antennas at time t is given as [9]

$$\boldsymbol{C}_t = \begin{bmatrix} c_{t,1}^1 & c_{t,2}^1 & \cdots & c_{t,K}^1 \\ c_{t,1}^2 & c_{t,2}^2 & \ldots & c_{t,K}^2 \\ \vdots & \vdots & \ddots & \vdots \\ c_{t,1}^{n_T} & c_{t,2}^{n_T} & \ldots & c_{t,K}^{n_T} \end{bmatrix}, \quad (4.5)$$

where the *i*-th row $\boldsymbol{c}_t^i = c_{t,1}^i, c_{t,2}^i, \dots, c_{t,L}^i, i = 1, 2, \dots, n_T$ is the data signal for the *i*-th transmit antenna. The output of the *k*-th OFDM subcarriers, $k = 1, 2, \dots K$ at the receive antenna *j*, $j = 1, 2, \dots . n_R$ with perfect time and frequency synchronization between the transmitter and the receiver, is given by [11]

$$r_{t,k}^j = \sum_{i=1}^{n_T} H_{t,k}^{i,j} c_{t,k}^i + \eta_{t,K}^j, \tag{4.6}$$

where $H_{t,k}^{i,j}$ is the channel frequency response for the path from the *i*-th transmit antenna to the *j*-th receive antenna in the *k*-th OFDM sub-channel, $\eta_{t,K}^j$ is the noise samples at the *j*-th receive antenna and the *k*-th sub channel.

Given that there is ideal CSI at the receiver, the ML decoding rule for the STC-OFDM received signal is given by [32]

$$\widehat{\boldsymbol{C}}_t = \underset{\widehat{\boldsymbol{X}}}{\arg min} \sum_{j=1}^{n_R} \sum_{k=1}^{K} \left| r_{t,k}^j - \sum_{i=1}^{n_T} H_{t,k}^{i,j} c_{t,k}^j \right|^2, \tag{4.7}$$

while the channel impulse response between the *i*-th transmit antenna and the *j*-th receive antenna is given by

$$h_{i,j}(t;\tau) = \sum_{l=1}^{L} h_{t,l}^{i,j}\, \delta(\tau - \tau_l), \tag{4.8}$$

where L is the number of multipath, τ_l is the time delay of the ℓ-th path and $h_{t,l}^{i,j}$ is the complex amplitude of the ℓ-th path.

Performing Fourier transform on the channel impulse response results in the channel frequency response at time *t* given as

$$H_{t,k}^{i,j} = \sum_{i=1}^{L} h_{i,j}\,(t, n_l) e^{-j2\pi k n_l / k}. \tag{4.9}$$

Given the MLD rule in [39], and assuming that ideal CSI is available at the receiver, for a given realization of the fading channel H_t, the PEP of transmitting C_t and deciding in favor of $\hat{C}_t$ at the decoder conditioned on H_t is given by

$$P(\boldsymbol{C}_t, \widehat{\boldsymbol{C}}_t \,|\boldsymbol{H}_t\,) \leq exp\left(-d_H^2(\boldsymbol{C}_t, \widehat{\boldsymbol{C}}_t\,)\frac{E_s}{4N_0}\right), \tag{4.10}$$

where E_s is the average symbol energy, N_0 is the noise power spectral density, and $d_H^2(C_t, \hat{C}_t\,)$ is given by

$$d_H^2(\boldsymbol{C}_t, \widehat{\boldsymbol{C}}_t\,) = \sum_{j=1}^{n_R}\sum_{k=1}^{K}\left|\sum_{i=1}^{n_T} H_{t,k}^{i,j}\left(c_{t,k}^{i} - \hat{c}_{t,k}^{i}\right)\right|^2,$$

$$= \sum_{j=1}^{n_R}\sum_{k=1}^{K}\left|\boldsymbol{h}_j \boldsymbol{W}_k \boldsymbol{e}_k\right|^2, \tag{4.11}$$

where

$$\boldsymbol{h}_j = \left(h_{1,j}^{t}\right)^H, \left(h_{2,j}^{t}\right)^H, \ldots, \left(h_{n_T,j}^{t}\right)^H \times Ln_T,$$

$$\boldsymbol{W}_k = \begin{vmatrix} w_k & 0 & \cdots & 0 \\ 0 & w_k & \cdots & \vdots \\ \vdots & \cdots & \ddots & 0 \\ 0 & 0 & \cdots & w_k \end{vmatrix}_{L_p n_T \times n_T},$$

and

$$\boldsymbol{e}_k = \begin{bmatrix} c_{t,k}^{1} - \hat{c}_{t,k}^{1} \\ c_{t,k}^{2} - \hat{c}_{t,k}^{2} \\ \vdots \\ c_{t,k}^{n_T} - \hat{c}_{t,k}^{n_T} \end{bmatrix}_{n_T \times 1}.$$

Equation (4.11) can be rewritten as

$$d_H^2(\boldsymbol{C}_t, \widehat{\boldsymbol{C}}_t) = \sum_{j=1}^{n_R} \boldsymbol{h}_j \boldsymbol{D}_H(\boldsymbol{C}_t, \widehat{\boldsymbol{C}}_t) h_j^H, \tag{4.12}$$

where $\boldsymbol{D}_H(\boldsymbol{C}_t, \widehat{\boldsymbol{C}}_t)$ is an $Ln_T \times Ln_T$ matrix given by

$$\boldsymbol{D}_H(\boldsymbol{C}_t, \widehat{\boldsymbol{C}}_t) = \sum_{k=1}^{K} \boldsymbol{W}_k\, \boldsymbol{e}_k\, \boldsymbol{e}_k^H \boldsymbol{W}_k^H\,. \tag{4.13}$$

By averaging (4.10) with respect to the channel coefficients $H_{t,k}^{i,j}$, the PEP for STC-OFDM is upper bound by [9]

$$P(\boldsymbol{C}_t, \widehat{\boldsymbol{C}}_t) \leq \left(\prod_{j=1}^{r_h} \left\{ 1 + \lambda_j \frac{E_S}{4N_0} \right\} \right)^{-n_R}, \tag{4.14}$$

$$\leq \left(\prod_{j=1}^{r_h} \lambda_j \right)^{-n_R} \left(\frac{E_S}{4N_0} \right)^{-r_h n_R}. \tag{4.15}$$

From (4.15) it is obvious that the diversity gain of $r_h n_R$ can be achieved by STC-OFDM in a frequency-selective fading channel while the coding gain is given by

$$\frac{\left(\prod_{j=1}^{r_h} \lambda_j \right)^{1/r_h}}{d^2 u},$$

where $d^2 u$ is the squared Euclidean distance of the reference uncoded symbol.

Minimizing the code error probability requires choosing a code with the maximum diversity and coding gain. The maximum possible diversity gain for STC in frequency-selective fading channels is $Ln_T n_R$, which is the product of the transmit antenna, receive antenna and the number of multipath L.

According to [34], (4.15) provides some suggestion on STC coding design in OFDM systems:

1. The dominant exponent of the PEP in (4.15) that is associated with the structure of the code is r_k, the rank of the matrix. To achieve maximum possible diversity therefore, the effective length of the code must be greater than $n_T L$, which is the dimension of matrix D in (4.13).

2. Another quantity in the PEP is $\prod_{j=1}^{r_h} \lambda_j$, the product of the eigenvalues of matrix *D*. Since *D* changes with different channel set-ups, the optimal design of $\prod_{j=1}^{r_h} \lambda_j$ is not possible.

However, as observed in [13], the STC with higher state numbers (and effective length) has improved performance, which suggests that increasing the effective length of the STC beyond the minimum requirement may help to improve the factor $\prod_{j=1}^{r_h} \lambda_j$.

4.4 Recent Literature

The first STC-OFDM proposed in the literature is the STTC-OFDM presented in [48] where the 16-state STTC, QPSK 2 bits/sec/Hz from [16] was adapted to OFDM and became attractive for delay-sensitive applications. The scheme was also concatenated with a RS code and its performance was evaluated over 5μs and 40μs delay spread. After the initial work of [48], many other STC schemes were proposed in OFDM in order to obtain high diversity for OFDM systems.

A coding scheme which guarantees both frequency and spatial diversity by concatenating TCM with STBC was proposed in [49] while in [50] the concept of sub-channel grouping was incorporated in order to construct simplified designs for full diversity group-space time frequency trellis codes. In [124], STTC-OFDM was investigated with the STTC concatenated with a convolutional code to form a bit interleaved STC-OFDM scheme. The scheme was considered for a generalized block fading channel to achieve time-frequency diversity. The IEEE802.11a physical layer standard was employed in the investigation. Both PEP and error bound were derived and used with simulation to conduct the performance analysis of the system over a general block fading channel.

The scheme in [125] exploited the maximum transmit diversity gain and large coding gain of space frequency of turbo coded modulation where two 8-state recursive STTC concatenated in parallel via a bitwise interleaver scheme with puncturing was proposed in an OFDM system to achieve high performance. Investigations in [126] showed that the diversity gain of STTC-OFDM depends on the channel delay profile and that to reduce this dependence, an ideal interleaver is needed to scramble the code system [50], [127]. The scheme in [128] investigated the effect of various channel delay distributions on the code with the discovery that the higher memory order STTCs are more sensitive to the channel delay. The effect of antenna spacing and propagation parameters on STTC-OFDM were investigated in [129] and the author showed that the existing STTC cannot exploit the diversity available in frequency-selective MIMO channels, and suggested that a completely new code be developed for MIMO-OFDM. Later in [130], the scheme of [129] was modified to form a new STTC-OFDM scheme.

Space-time coded OFDM systems have been deployed in literature with their performances analyzed over different channel conditions in [50], [125], [128], [131-142].

Recently in [67], it has been shown that the error performance of SOSTTC designed for flat fading channel breaks down in a multipath environment because SOSTTC contains a large number of transitions within its trellis structure. To avoid such parallel transitions so that SOSTTC can exploit multipath diversity, it was shown in [51], [84], [143] that at least 16 states are needed for QPSK modulation. In [144] and [145], a 16-state SOSTTC was deployed in OFDM environments with delay spreads while in [51], a 16-, 32- and 64-state trellis was designed for SOSTFTC that fully exploited the spatial and multipath diversity of the code based on the pairwise error probability for the error difference symbol matrix.

However these earlier works have several drawbacks such as not being optimized for MIMO-OFDM systems, having a low coding rate, low power efficiency and low coding gain, among others.

To address these problems, in this chapter the extended SOSTTC for two transmit antennas with improved coding gain and with multipath diversity in addition to spatial diversity is proposed. To achieve a high coding gain, the concept of rotated constellation shown in [73] where the design of SOSTTC was extended for performance improvement is incorporated. However, the ESOSTTC proposed in [73] has a large number of parallel transitions which restricts its performance in a multipath channel. Hence to achieve multipath diversity ESOSTTC, parallel transitions are avoided within the trellis of the code.

4.5 Extended SOSTTC-OFDM Systems

In a bid to improve the performance of SOSTTC, ESOSTTC was proposed in [73]. In this section, an ESOSTTC-OFDM for frequency-selective fading channel is proposed. The 16-, 32- and 64-state ESOSTTC presented in Section 2.6 is deployed here in a frequency selective fading channel using OFDM, and the performance is investigated under various channel scenarios.

4.6 Codeword Structure for the ESOSTTC-OFDM System

In order to exploit the diversity advantage of wideband channels, it has been shown that an effective length and the use of random interleaving are two critical design parameters (for a trellis code over a MIMO-OFDM system) [146]. Furthermore, the code performance depends on both code structure and channel profile. The code structure of the proposed ESOSTTC-OFDM is as follows.

Let there be an extra-rotation parameter ϕ between 0 and 2π, in addition to the rotation parameter θ as proposed in [73]. Let us set $\theta = 0$, assuming that space goes horizontally and different rows are transmitted at consecutive OFDM symbols, the *k*-th codeword to be transmitted at the subcarrier $k = 1, 2, ..., K$ is defined as

$$C^k(s_1, s_2, \phi, \theta) = \begin{pmatrix} s_1 e^{j\phi} e^{j\theta} & s_2 e^{j\phi} \\ -s_2^* e^{-j\phi} e^{j\theta} & s_1^* e^{-j\phi} \end{pmatrix}. \quad (4.16)$$

Let N be the frame length and $\boldsymbol{C}^{\mathrm{n}}$ be the branch output at the *n*-th coding step of the trellis encoder. Let us consider that $\boldsymbol{C}^{\mathrm{n}}$ is an Alamouti codeword [60] for two complex symbols c_1 and c_2. Also let $\overline{\overline{\boldsymbol{C}}} = c_1 c_2 - c_2^* c_1^* \in \mathbb{C}^{(N\times 2)\times 2}$ be the transmitted coded sequence such that at a given symbol period, the OFDM symbol $c_1 = (c_1^1, c_1^2, \dots, c_1^N)^T$ is transmitted from the first antenna, and from the second antenna the symbol sent is $c_2 = (c_2^1, c_2^2, \dots, c_2^N)^T$; where $(.)^T$ denotes the vector transpose. In the next symbol period, the OFDM symbol $-c_2^* = (-c_2^{*1}, -c_2^{*2}, \dots, -c_2^{*N})^T$ is transmitted from the first antenna and the symbol $c_1^* = (c_1^{*1} c_1^{*2}, \dots, c_1^{*N})^T$ is transmitted from the second antenna. An ML decoder might decide erroneously in favor of the coded sequence $\overline{\overline{\hat{\boldsymbol{C}}}} = [\hat{c}_1 \hat{c}_2 - \hat{c}_2^* \hat{c}_1^*]$. As shown in [146], when the branch output is a symbol vector, the diversity order of a SF trellis code varies from rn_R to $\delta_H n_R$, where r is the minimum rank and δ_H is the minimum symbol Hamming distance over all pairs of distinct coded sequences. Moreover, it is a necessary condition that $\delta_H \geq n_T L$ in order to achieve the maximum diversity of $(n_T n_R L)$. Unlike the scheme in [146], the proposed ESOSTTC-OFDM scheme has orthogonal matrix branch output.

Let $\boldsymbol{D^n} = \boldsymbol{C^n} - \widehat{\boldsymbol{C}}^{\boldsymbol{n}}$ be a branch difference matrix between $\boldsymbol{C^n}$ and $\widehat{\boldsymbol{C}}^{\boldsymbol{n}}$, where $\boldsymbol{C^n}$ and $\widehat{\boldsymbol{C}}^{\boldsymbol{n}}$ is the *n*-th codeword in coded sequences $\overline{\boldsymbol{C}}$ and $\overline{\overline{\boldsymbol{C}}}$ respectively**.** The distance matrix of a codeword is defined as [146]

$$\boldsymbol{A^n} = (\boldsymbol{D^n})^{\boldsymbol{H}}\boldsymbol{D^n}, \tag{4.17}$$

where $(.)^H$ denotes transpose conjugate.

Next we define $\rho\left(\overline{\boldsymbol{C}}, \overline{\widehat{\boldsymbol{C}}}\right)$ as the set of instances $1 \leq n \leq N$ at which $\boldsymbol{C^n} \neq \widehat{\boldsymbol{C}}^{\boldsymbol{n}}$, and δ_H as the number of elements in $\rho\left(\overline{\boldsymbol{C}}, \overline{\widehat{\boldsymbol{C}}}\right)$.

If $\boldsymbol{A^n}$ is a rank two matrix for all $n \in \rho\left(\overline{\boldsymbol{C}}, \overline{\widehat{\boldsymbol{C}}}\right)$, it can be shown [146] that the diversity takes value from $2n_R$ to $2\delta_H n_R$, and the maximum diversity order that can be achieved by the ESOSTTC over a frequency-selective fading channel with two transmit antennas and L independent paths is

$$G_{dmax} = 2n_R.\min(\delta_H, L). \tag{4.18}$$

The distance criterion derived in [146] can be rewritten as the maximization of the minimum product of the CGD and the modified product distance MPD, which is denoted as

$$\text{maximize}(\min\{CGD.MPD\}), \tag{4.19}$$

where

$$CGD = \det\left(\sum_n A^n\right), \tag{4.20}$$

$$MPD = \prod_n (1 + \|D^n\|_F^2), \tag{4.21}$$

and $n \in (\overline{\boldsymbol{C}}, \overline{\widehat{\boldsymbol{C}}})$.

The δ_H of the ESOSTTC employed is two and therefore the maximum achievable diversity is $2n_R.\min(2, L)$.

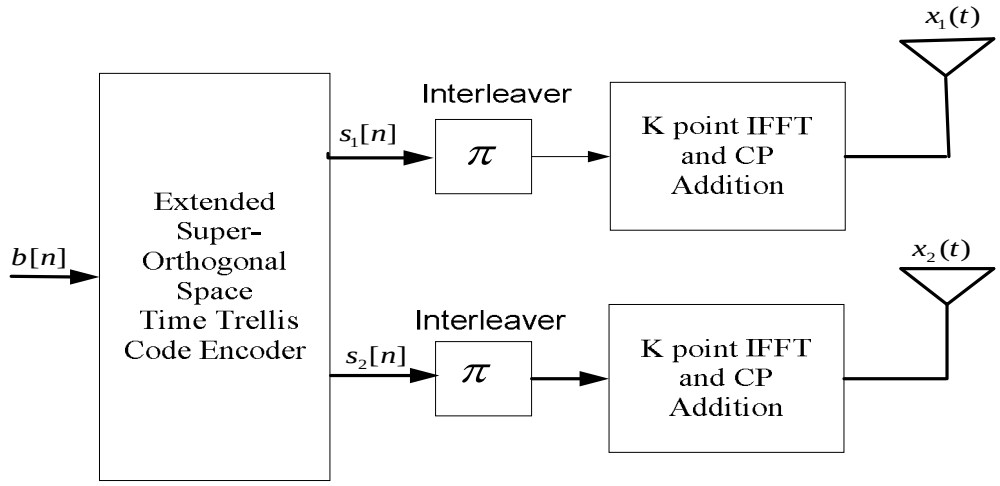

Fig. 4.1: The encoding block diagram of the ESOSTTC-OFDM system for two transmit antennas

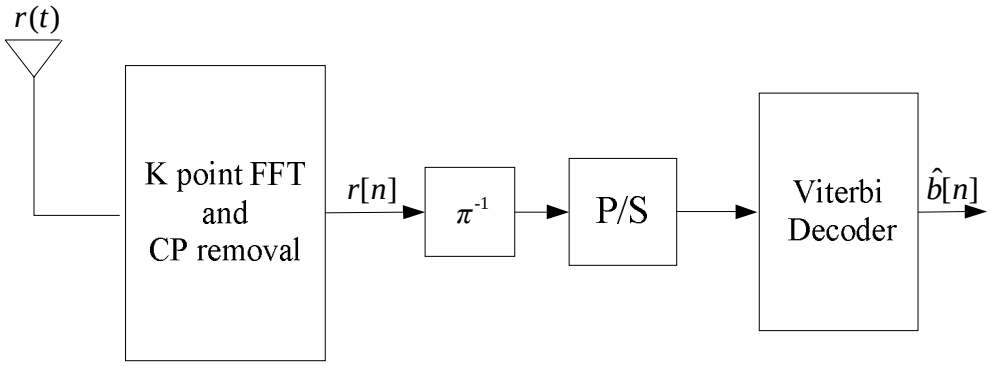

Fig. 4.2: The decoding block diagram of the ESOSTTC-OFDM system for one receive antenna

In Fig. 4.1 b[n] is the digitally modulated signal at time n. ESOSTTC operation is performed over b[n]. The ESOSTTC process starts at state zero. At n-th coding step, depending on the input information bits and the current state in the trellis encoder, a codeword $\boldsymbol{C}^n$ is selected from a constellation of possible codewords. Thereafter, there is a transition towards the next state in the trellis, and the encoding process is performed again to obtain a frame with N codewords. The last codeword to be sent must be selected to return the trellis state to zero. Thereafter, the N-length codeword (frame) is interleaved and then mapped to the K subcarriers. In order to prevent ISI, CP is added to the transformed symbols before they are transmitted from each of the transmit antennas. The sequence of the transmitted data blocks is shown in Table 4.1.

Table 4.1: Transmission sequence for ESOSTTC-OFDM

OFDM block	Transmit Antenna one	Transmit Antenna two
n	$s_1 e^{j\phi} e^{j\theta}$	$s_2 e^{j\phi}$
n+1	$-s_2^* e^{-j\phi} e^{j\theta}$	$s_1^* e^{-j\phi}$

The receiving block diagram of the ESOSTTC-OFDM is shown in Fig. 4.2. The received signals at the antennas, assuming that the channels are quasi-static over two OFDM blocks, are given by

$$r(t) = h_{11}(t) * x_1(t) + h_{21}(t) * x_2(t) + w(t), \quad (4.22)$$

$$r(t + T_s) = h_{11}(t) * x_1(t + T_s) + h_{21}(t) * x_2(t + T_s) + w(t + T_s), \quad (4.23)$$

where $h_{i,j}(t), i = 1,2\ j = 1$ are continuous-time impulse responses of the channels from the *i*-th transmit antenna to the *j*-th receive antenna. The inserted CP is removed from the received signal and the OFDM demodulation process is performed on the received symbols.

The received signal at the *k*-th subcarrier frequency after CP removal and the FFT operation can be expressed as

$$r_1[n,k] = \sum_{i=1}^{2} H_{i,j}[n,k] s_i[n,k] + w_j[n,k], \quad \text{and} \quad (4.24)$$

$$r_1[n+1,k] = \sum_{i=1}^{2} H_{i,j}[n,k] s_i[n+1,k] + w_j[n+1,k]. \quad (4.25)$$

These transformed received signals are then de-interleaved and converted to a serial stream before being sent to the ESOSTTC decoder. The Viterbi algorithm is employed for the maximum likelihood decoding of the ESOSTTC to find the most likely valid path in the trellis. Let $\mathbf{H}(k)$ be the channel matrix during the transmission of codeword $\boldsymbol{C}^k$, and $r(k)$ the received signal at two consecutive OFDM symbols over the

k-th subcarrier. Assuming perfect CSI at the receiver and that the channel is quasi-static over two OFDM symbol durations, the maximum-likelihood (ML) decoding rule is given by

$$\hat{\hat{\boldsymbol{C}}} = \arg \min_{(s1,s2)} \sum_{k=1}^{K} \|r(k) - \mathbf{H}(k)\boldsymbol{C}^k\|_F^2. \tag{4.26}$$

4.7 Super-Quasi-Orthogonal Space-Time Trellis Coded OFDM

SOSTTC combines the set partitioning principle and a super-set of orthogonal STBC in a systematic way to provide full diversity and improved coding gain, when compared with space-time trellis code (STTC). However, there is no full-rate code for orthogonal STBC for more than two transmit antennas [16].

To solve the problem of non-full-rate code for more than two transmit antennas, the quasi-orthogonal space-time block code (QOSTBC) is proposed in [147-148]. In [149], super-quasi-orthogonal space-time trellis code (SQOSTTC) is introduced for four transmit antennas. SQOSTTC combines the constellation rotation of SOSTTC with that of QOSTBCs to provide full-rate code for four transmit antennas providing full diversity, and very high coding gain. The transmission matrix for SQOSTTC is [149],

$$G(s_1, s_2, \phi_1, s_3, s_4, \phi_2, \theta_1, \theta_2) =$$

$$\begin{pmatrix} e^{j\theta_1}e^{j\phi_1}s_1 & e^{j\theta_2}e^{j\phi_1}s_2 & e^{j\phi_2}s_3 & e^{j\phi_2}s_4 \\ -e^{j\theta_1}e^{-j\phi_1}s_2^* & e^{j\theta_2}e^{-j\phi_1}s_1^* & -e^{-j\phi_2}s_4^* & e^{-j\phi_2}s_3^* \\ e^{j\theta_1}e^{j\phi_2}s_3 & e^{j\theta_2}e^{j\phi_2}s_4 & e^{j\phi_1}s_1 & e^{j\phi_1}s_2 \\ -e^{j\theta_1}e^{-j\phi_2}s_4^* & e^{j\theta_2}e^{-j\phi_2}s_3^* & -e^{-j\phi_1}s_2^* & e^{-j\phi_1}s_1^* \end{pmatrix}, \tag{4.27}$$

where for M-PSK signal constellations, the signals $\mathsf{s}_1, \mathsf{s}_2, \mathsf{s}_3, \mathsf{s}_4$ which are selected by input bits can be represented by $e^{\frac{j2\pi l}{M}}$, where $l = 0, 1, \ldots, M-1$. The rows correspond to transmitted symbols in a time instance while the columns correspond to transmitted symbols at the antenna instance. In time slot 1, the first row represents the transmitted symbol while in time slot 2, the second row represents the transmitted symbol. Similarly the third row is the transmitted symbol in time slot 3 and the fourth row is the transmitted symbol in time slot 4. For the column instance, the symbol transmitted by

antenna 1 is represented by the first column, while the second column corresponds to the symbol transmitted by antenna 2. The third column is the symbol transmitted by antenna 3 while the fourth column represents the symbol transmitted by antenna 4.

The SQOSTTCs in [149] are designed for frequency-flat fading channels and their trellises are characterized by parallel transitions. In [150], a new full-rate full diversity 16-state BPSK SOSTTC is designed for four transmit antennas in fast-fading channels. The work shows that, to avoid parallel transition that restricts the error performance of the code, at least a 16-state trellis is required for BPSK modulation.

4.8 Code Design for SQOSTTC

In this section, a BPSK SQOSTTC for frequency selective fading channels with four transmit antennas and an arbitrary number of receive antennas is considered. For four transmit antennas and in order to avoid parallel transitions, a trellis of at least 16 states should be considered for full-rate BPSK SQOSTTC based on the set partitioning principle given in [149].

The set partitioning principle given in [149] is extended in this thesis in designing the 16-state full rate full diversity code. To achieve full diversity using BPSK signalling, the rotation $\phi = \pi/2$ and the rotation θ take on the value of π.

The proposed 16-state SQOSTTC for BPSK modulation is given in Fig. 4.3 where the transmission matrices assigned to branches originating from each state are given on the left side of the trellis. To express the trellis more clearly and to reduce the complexity, the orthogonal matrix is denoted by S_j where j = 1,2,…,16 denotes all realizations of a binary codeword $x_1x_2x_3x_4$ as 0000, 1001, 1101, 0100, 0010, 1011, 1111, 0110, 1100, 0101, 0001, 1000, 1110, 0111, 0011, 1010, respectively, which are mapped to the BPSK symbols by the rule 0→ -1, 1→1. The minimum symbol Hamming distance (δ_H) of the code is 8 and the minimum coding gain CGC for the code with error event of 2 transitions is 4096. The maximum achievable diversity of the system is $n_R . \min(\delta_H, n_T L)$ [51].

The transceiver block diagram for the SQOSTTC-OFDM is shown in Fig. 4.4, where b[n] is the digitally modulated signal at time *n*. SQOSTTC operation is performed over

b[n]. The SQOSTTC process starts at state zero. At *n*-th coding step, depending on the input information bits and the current state in the trellis encoder, a codeword $\boldsymbol{C}^n$ is selected from a constellation of possible codewords. Thereafter, there is a transition to the next state in the trellis, and the encoding process is performed again to obtain a frame with *N* codewords. The last codeword to be sent must be selected to return the trellis state to zero. After, the *N*-length codeword (frame) is interleaved and then mapped to the *K* subcarriers. In order to prevent ISI, CP is added to the transformed symbols before they are transmitted from each of the transmit antennas. The sequence of the transmitted data blocks is shown in Table 4.2

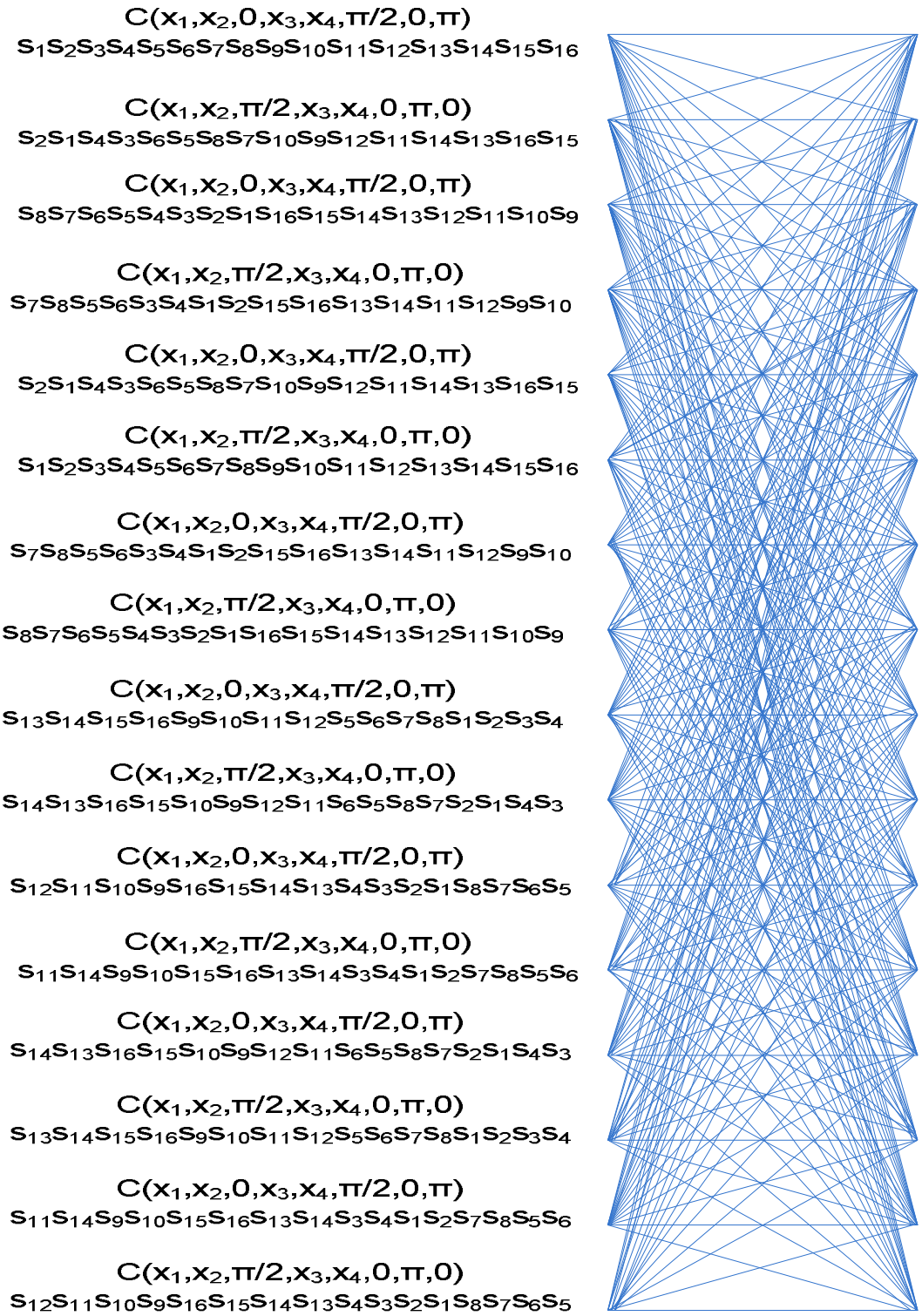

Fig. 4.3: A 16-state SQOSTTC at a rate of 1 bit/s/Hz using BPSK for four transmit antennas [151]

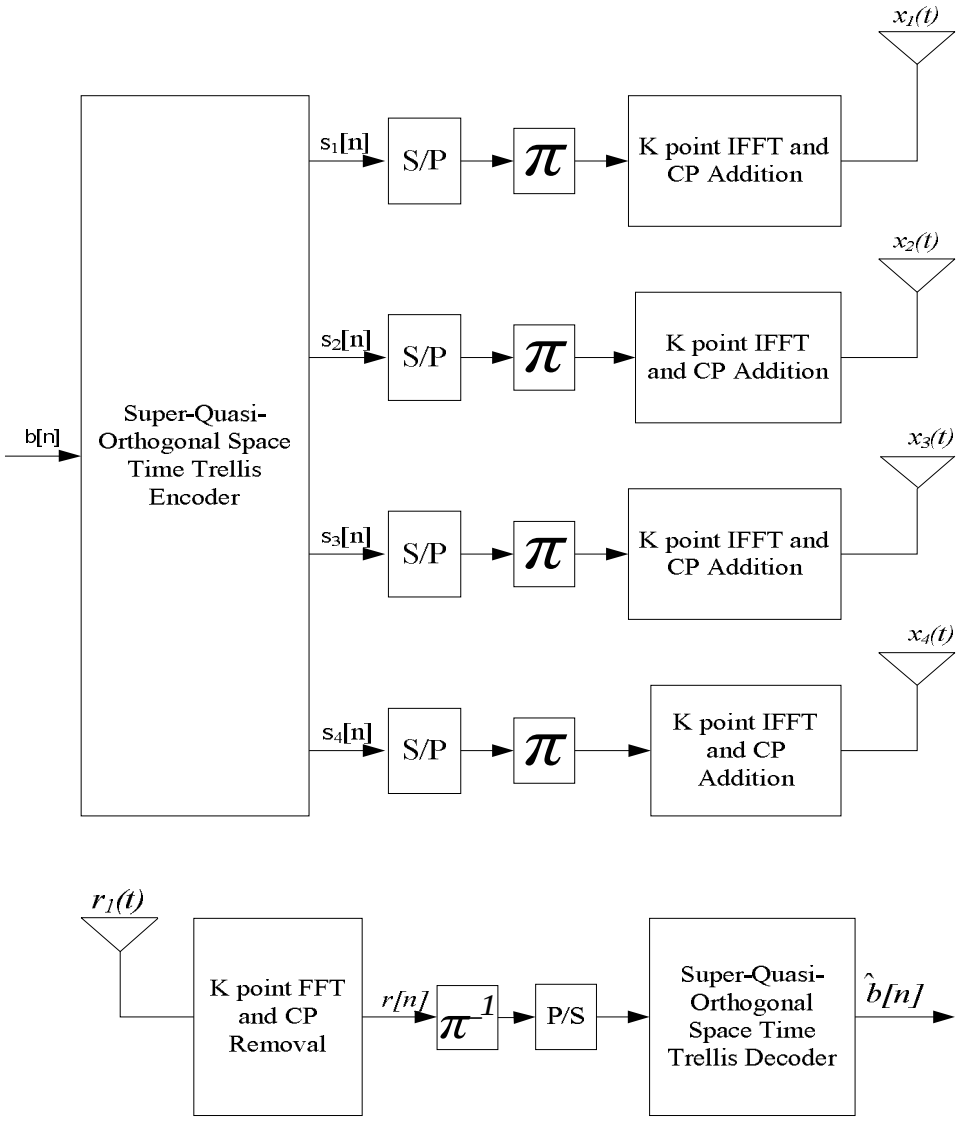

Fig. 4.4: Transceiver block diagram for the SQOSTTC-OFDM system

Table 4.2: Transmission sequence for SQOSTTC-OFDM

OFDM block	Transmit Antenna 1	Transmit Antenna 2	Transmit Antenna 3	Transmit Antenna 4
n	$e^{j\theta_1}e^{j\phi_1}s_1$	$e^{j\theta_2}e^{j\phi_1}s_2$	$e^{j\phi_2}s_3$	$e^{j\phi_2}s_4$
n+1	$-e^{j\theta_1}e^{-j\phi_1}s_2^*$	$e^{j\theta_2}e^{-j\phi_1}s_1^*$	$-e^{-j\phi_2}s_4^*$	$e^{-j\phi_2}s_3^*$
n+2	$e^{j\theta_1}e^{j\phi_2}s_3$	$e^{j\theta_2}e^{j\phi_2}s_4$	$e^{j\phi_1}s_1$	$e^{j\phi_1}s_2$
n+3	$-e^{j\theta_1}e^{-j\phi_2}s_4^*$	$e^{j\theta_2}e^{-j\phi_2}s_3^*$	$-e^{-j\phi_1}s_2^*$	$e^{-j\phi_1}s_1^*$

The received signal at the antennas assuming that the channels are quasi-static over four OFDM blocks are given by

$$r(t) = h_{11}(t) * x_1(t) + h_{21}(t) * x_2(t) + h_{31}(t) * x_3(t) + h_{41}(t) * x_4(t) + w(t) \quad (4.28)$$

$$r(t+T_s) = h_{11}(t) * x_1(t+T_s) + h_{21}(t) * x_2(t+T_s) + h_{31}(t) * x_3(t+T_s) + h_{41}(t) * x_4(t+T_s) + w(t+T_s) \quad (4.29)$$

$$r(t+2T_s) = h_{11}(t) * x_1(t+2T_s) + h_{21}(t) * x_2(t+2T_s) + h_{31}(t) * x_3(t+2T_s) + h_{41}(t) * x_4(t+2T_s) + w(t+2T_s) \quad (4.30)$$

$$r(t+3T_s) = h_{11}(t) * x_1(t+3T_s) + h_{21}(t) * x_2(t+3T_s) + h_{31}(t) * x_3(t+3T_s) + h_{41}(t) * x_4(t+3T_s) + w(t+3T_s) \quad (4.31)$$

where $h_{i,j}(t), i = 1,2,3,4\ j = 1$ are the continuous-time impulse response of the channels from the *i*-th transmit antenna to the *j*-th receive antenna. The inserted CP is removed from the received signal and the OFDM demodulation process is performed on the received symbols.

The received signal at the *k*-th subcarrier frequency after CP removal and the FFT operation can be expressed as

$$r_j[n,k] = \sum_{i=1}^{4} H_{i,j}[n,k]s_i[n,k] + w_j[n,k]. \quad (4.32)$$

$$r_j[n+1,k] = \sum_{i=1}^{4} H_{i,j}[n,k]s_i[n+1,k] + w_j[n+1,k]. \quad (4.33)$$

$$r_j[n+2,k] = \sum_{i=1}^{4} H_{i,j}[n,k]s_i[n+2,k] + w_j[n+2,k]. \quad (4.34)$$

$$r_j[n+3,k] = \sum_{i=1}^{4} H_{i,j}[n,k]s_i[n+3,k] + w_j[n+3,k]. \quad (4.35)$$

The outputs are then sent to the SQOSTTC decoder and the estimates of the transmitted OFDM symbols are computed.

4.9 Simulation Results and Discussions

In this section, the simulation results illustrating the performance of the proposed ESOSTTC-OFDM and the SQOSTTC-OFDM system over frequency-selective fading channels are provided. A MIMO-OFDM system equipped with two transmit antennas and one receive antenna is considered for the ESOSTTC-OFDM, while a MIMO-OFDM system with four transmit antennas and one receive antenna is considered for the SQOSTTC-OFDM system. Each of the OFDM modulators utilizes 64 subcarriers with a total system bandwidth of 1 MHz and FFT duration of 80 μs. The system's subcarrier spacing is 15 kHz with symbol duration of 64 μs while the guard band interval is 16 μs. The performance curves are described by means of frame error rate (FER) versus the receive SNR with QPSK constellation. The system is simulated over two channel scenarios: (1) Typical urban (TU) six paths COST 207 power delay profile reported in [152]. (2) A quasi-static channel with equal-power two-path channel impulse response (CIR). The system is simulated under no delay spread, 5μs delay spread and 40μs delay spread between the adjacent paths. The channel is assumed constant over two symbol periods (frame) and changes independently over each frame. Perfect channel state information at the receiver with perfect timing and frequency synchronization between the transmitter and the receiver is also assumed.

In Fig.4.5 the FER performance of the ESOSTTC-OFDM over a frequency selective fading channel is shown. It can be rightly observed from the FER plot that ESOSTTC systems achieve a diversity order of four. Also, the code with the higher state is observed to achieve a higher coding gain as can be observed by the performance of the 64-state code as compared with that of the 16- and 32-state codes.

Fig. 4.6, shows the effect of delay spread on the performance of the ESOSTTC-OFDM code. In this case the 16-state ESOSTTC code is employed to evaluate the performance of the scheme with two-path rays. It is observed from the performance curves that delay spread has a significant effect on the coding gain of the system. The coding gain of STC increases with an increase in the delay spread between adjacent paths because the

minimum determinant of STC in an OFDM system increases with the maximum tap delay of the channel. The scheme with a delay spread of 40μs is observed to have a coding gain advantage of about 2 dB over the scheme with no delay spread between the adjacent paths.

The effect of mobile speed on the performance of the ESOSTTC-OFDM system is shown in Fig. 4.7. The result is presented for various normalized Doppler frequencies of 0.1, 0.05, 0.01 and 0.002 Hz, which correspond to mobile speed of 300 m/s, 150 m/s, 60 m/s, 30 m/s and 15 m/s respectively. The FER plot in this channel condition shows that variation in the mobile speed has no effect on the diversity order of the proposed trellis coded OFDM system but affects its coding gain. The coding gain advantage of the system is seen to increase with reduction in mobile speed.

Fig. 4.8 shows performance comparison of the proposed ESOSTTC-OFDM with other space-time coded OFDM systems with a simulation parameter from [51]. The number of subcarriers in this case is 48 and the multipath gains were assumed to be statistically independent, identically distributed complex Gaussian variables with variance N_0 for L = 4. The 4-state SOSTTC code from [65] and the 16-state STTC from [48] is deployed over an OFDM system for comparison. In order to have the same number of symbols per frame and the same delay length for both systems, the number of subcarriers for the STTC-OFDM is chosen to be 96, which is twice that of the ESOSTTC-OFDM. The performance result of the 16-state [51] SOSTTC-OFDM is also replicated and shown for comparison in the same plot.

As can be rightly observed from the FER plot, the proposed ESOSTTC achieves a diversity order of 4 in this channel scenario while the 16-state SOSTTC achieves a diversity order of 3. Also from the FER plot, it can be observed that the 4-state SOSTTC code could not exploit the diversity advantage of the frequency selective fading channel because of parallel transition within it trellis. Parallel transitions break down the error performance of SOSTTC in frequency-selective fading channels [51]. Therefore, the 4-state SOSTTC presents no additional diversity order by employing it in an OFDM system over a frequency-selective fading channel. In terms of coding gain, the ESOSTTC-OFDM is seen to achieve additional coding gain of about 1 dB, 2 dB and 0.6 dB when compared with the STTC-OFDM, the 4-state SOSTTC-OFDM and the 16-state SOSTTC-OFDM respectively.

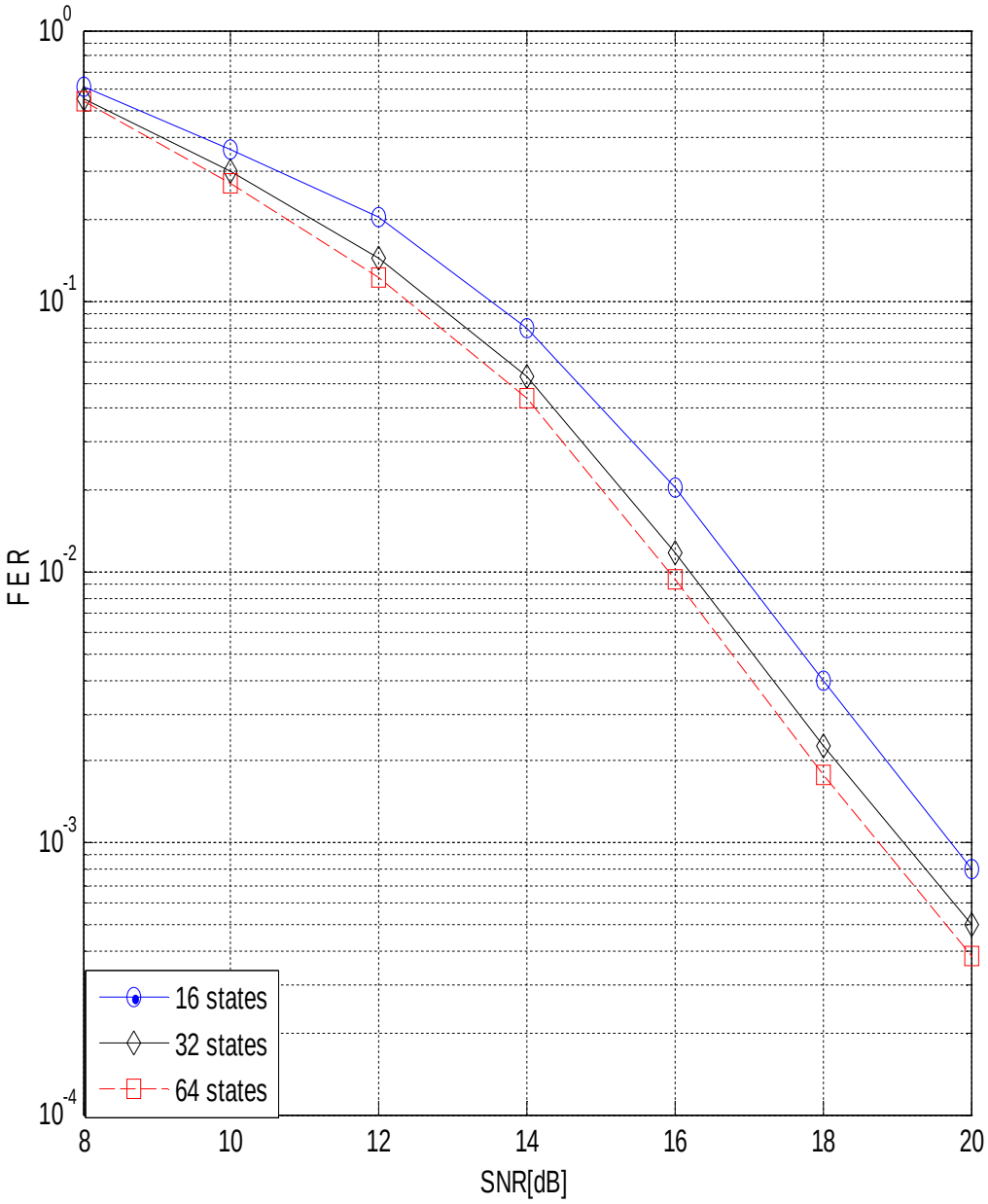

Fig. 4.5: FER performance of 16-, 32- and 64-state ESOSTTC-OFDM systems

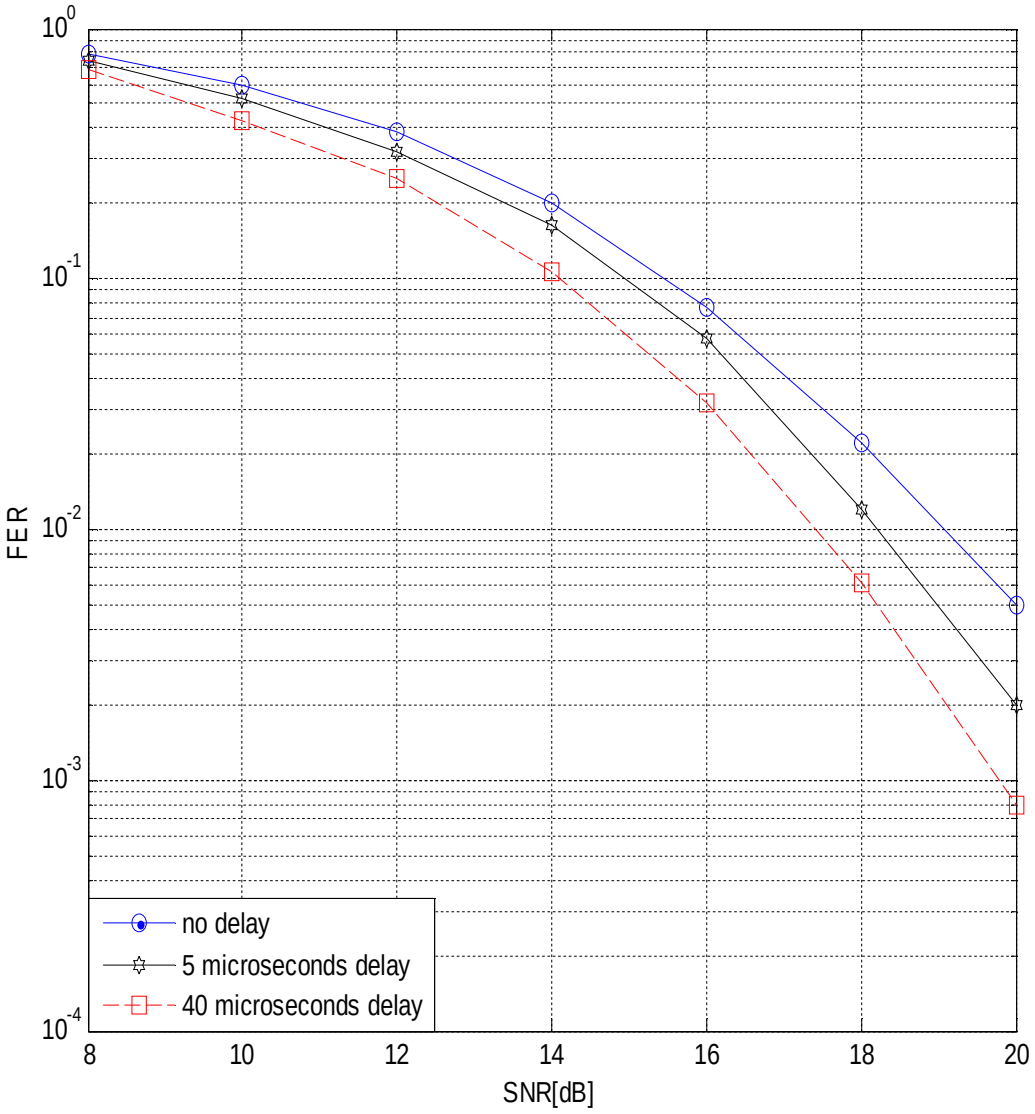

Fig. 4.6: Effect of Delay spread on the performance of the ESOSTTC-OFDM system

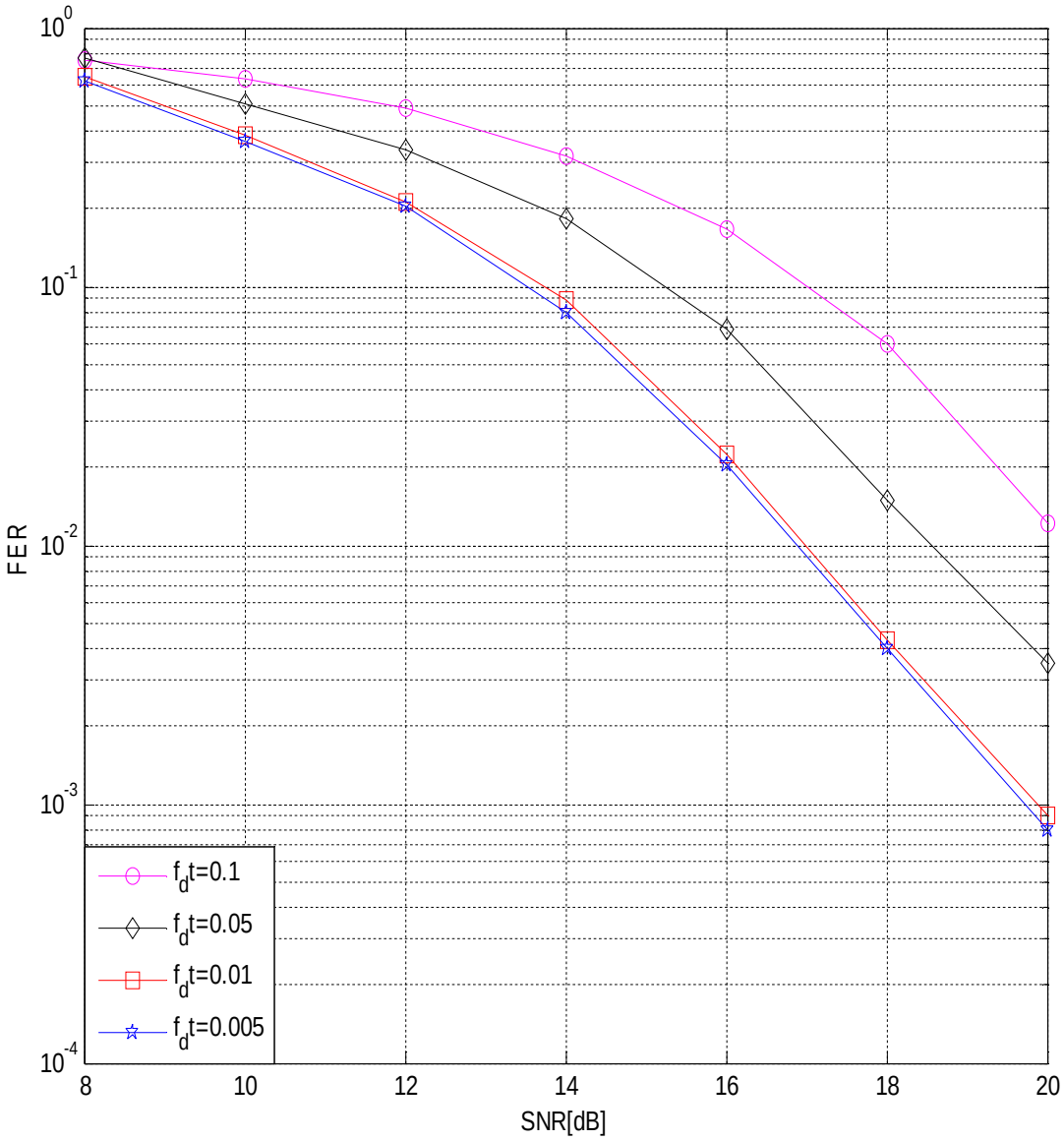

Fig.4.7: Effect of normalized Doppler frequency on the performance of the ESOSTTC-OFDM system

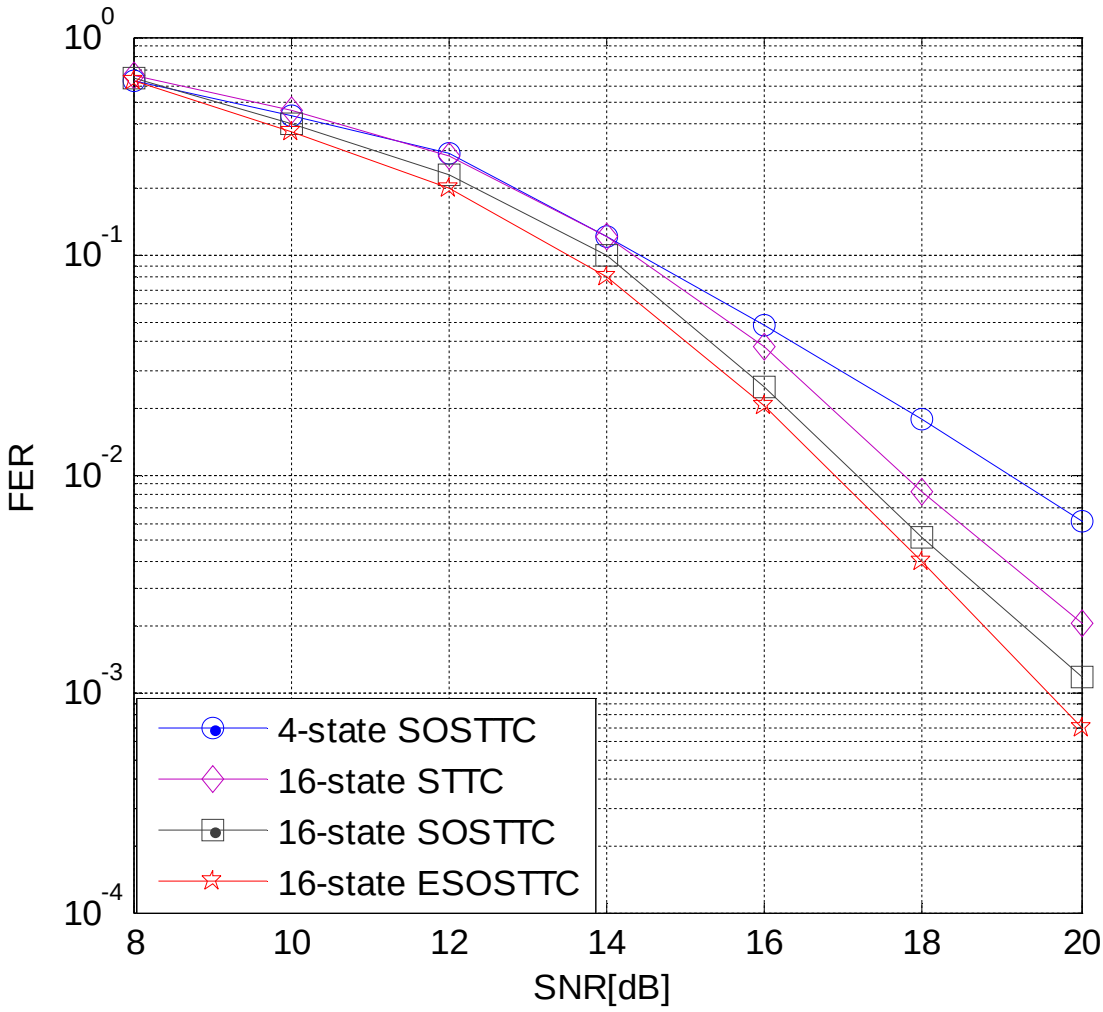

Fig. 4.8: FER performance comparison of a 4-state SOSTTC-OFDM [65], a 16-state STTC-OFDM [153], 16-state SOSTTC-OFDM [51] and 16-state ESOSTTC-OFDM (Four ray path)

Fig. 4.9 shows the FER performance of the SQOSTTC-OFDM system under the COST 207 channel condition. The result is presented over various normalized Doppler frequencies of 0.05, 0.01 and 0.002 which correspond to mobile speeds of 150m/s, 30m/s and 6m/s. The proposed trellis coded OFDM system is seen from the FER plot to achieve the maximum diversity of 8 with the various mobile speeds. However, the coding gain achieved by the system is seen to increase with a decrease in the mobile speed.

Fig. 4.10 shows the effect of delay spread on the performance of the SQOSTTC-OFDM. The result is shown using the two-ray channel model with delay spread of 5 μs, 40 μs and no delay spread between the adjacent paths. From the FER performance plot, increase in coding gain is achieved by increasing the delay spread within the adjacent path.

Performance comparison of the SQOSTTC-OFDM with other schemes is shown in Fig. 4.11. The performance of the system is compared with that of a 2-state SQOSTTC from [149] and the 4-state SOSTTC from [121]. As can be observed from the FER plot, the 2-state SQOSTTC code could not exploit the multipath diversity of frequency-selective fading channel because of parallel transition within its trellis. Also in comparison with the 4-state SOSTTC, the 2-state SQOSTTC is seen to outperform the SOSTTC in terms of both diversity order and coding gain. In terms of diversity order, the proposed schemes achieve a diversity order of 8, while the 2-state SQOSTTC and the 4-state SOSTTC achieve a diversity order of 4. The better diversity order achieved by the SQOSTTC system is because of the number of transmit antennas involved. At FER of 10^{-3}, the proposed scheme presents a coding gain advantage of about 2 dB over the 2-state SQOSTTC code under the same channel condition.

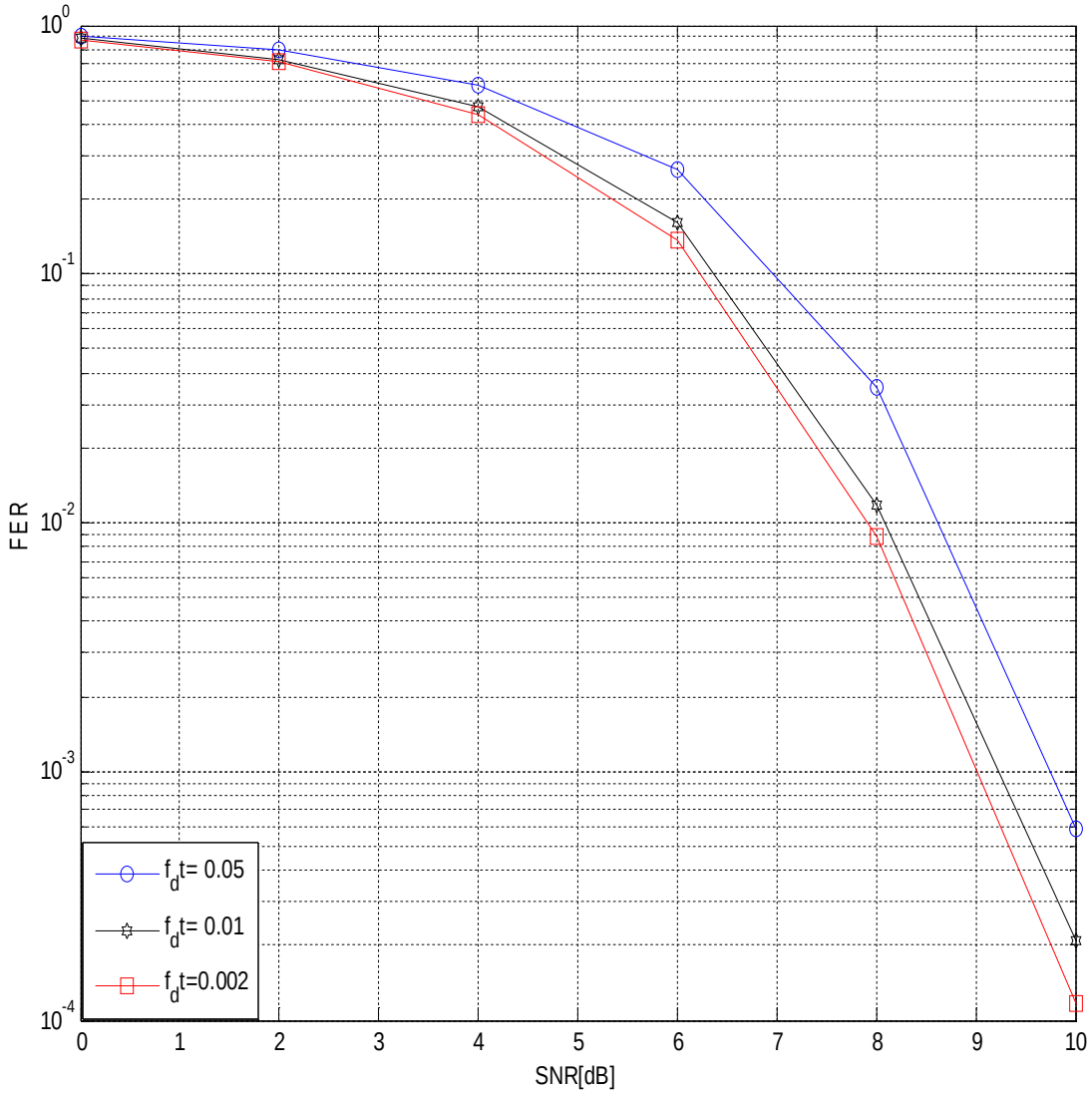

Fig. 4.9: FER performance of SQOSTTC-OFDM for various normalized Doppler frequencies

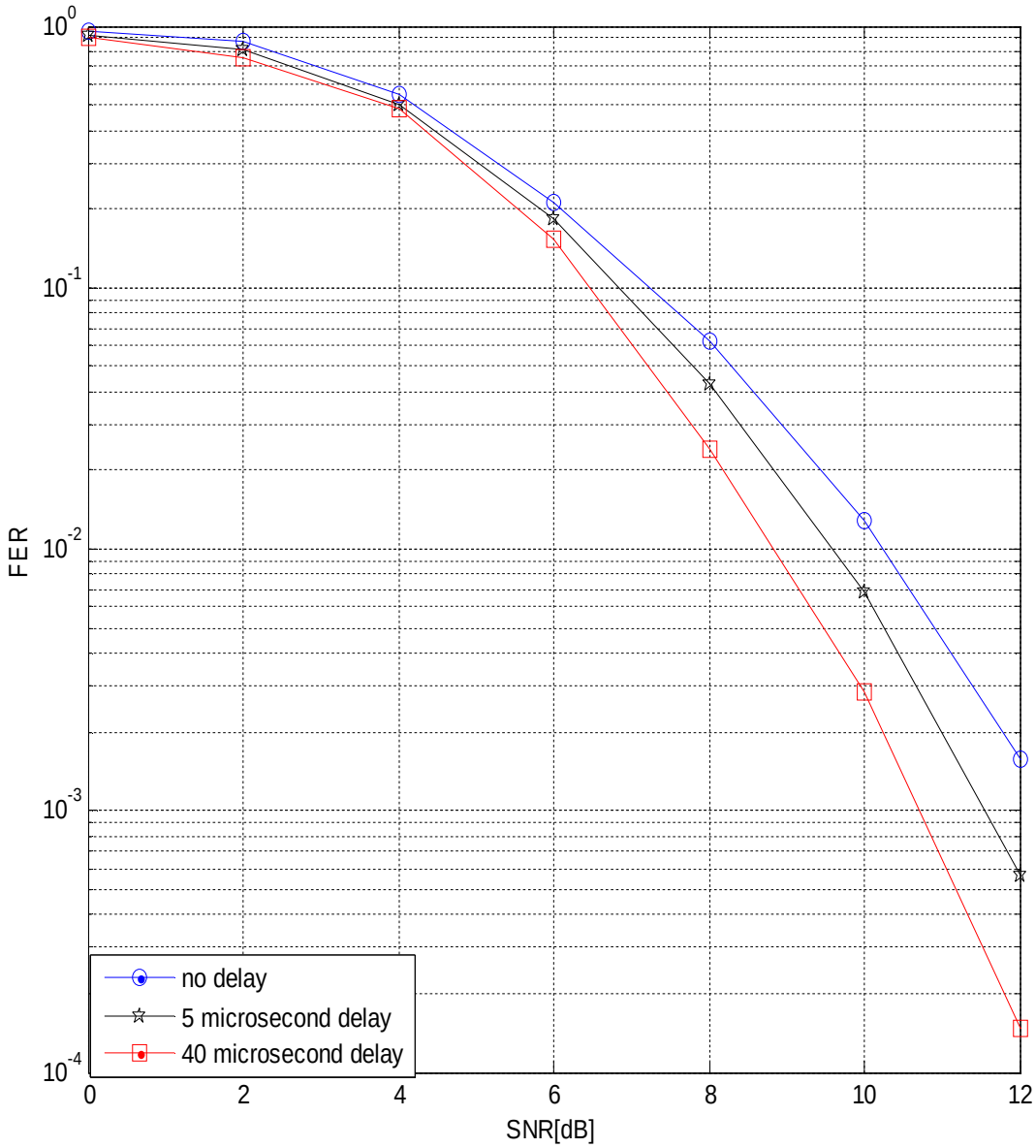

Fig. 4.10: Effect of delay spread on the performance of SQOSTTC-OFDM

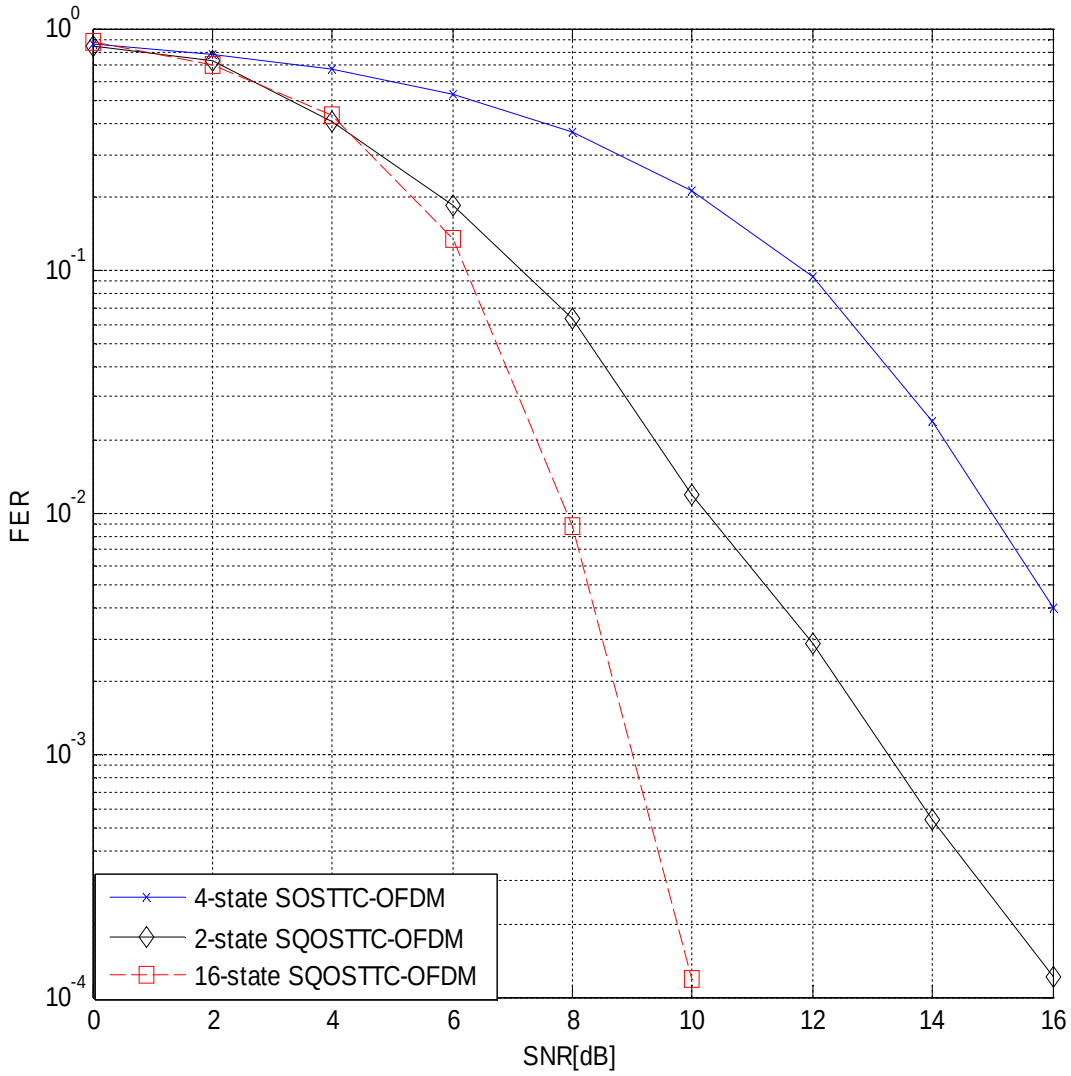

Fig. 4.11: FER performance of SQOSTTC-OFDM with other schemes

4.10 Chapter Summary

In this chapter, the performance of trellis code over an OFDM system in frequency-selective fading channel was presented. An overview of STC over frequency selective fading channels was given and the performance of space-time coding in OFDM systems was reviewed. Recent literature in the field of space-time coding and OFDM systems for a broadband communication system were reviewed.

Two new space-time coded OFDM schemes were proposed in this chapter. The first is the ESOSTTC-OFDM which used the rotated constellation concept from [73] and avoided parallel transitions in the trellis design which restrict the performance of SOSTTC in multipath channels. The design of SOSTTC proposed in [65] for flat fading channel was therefore extended in this chapter to a case of frequency-selective fading channels. The designed space-time coded MIMO-OFDM system guarantees full diversity, high coding gain, full rate and multipath diversity with low decoding complexity. The ESOSTTC-OFDM scheme was described with its encoder and decoder block diagrams for various antenna configurations. The codeword structure of the extended scheme was presented and the achievable diversity order over independent channel paths was derived.

Since there is no full rate orthogonal code for a case of more than two transmit antennas, the SQOSTTC proposed for four transmit antennas for flat-fading channels in [149] was extended in this chapter to give the SQOSTTC-OFDM system for four transmit antennas using BPSK signalling. The scheme combines quasi-orthogonal space-time block code with trellis code to offer a full rate, full diversity and high coding gain for four transmit antennas. Simulation results were presented for a frequency-selective fading channel for the case of delay spread between adjacent paths and variation in mobile speed. The system was shown to achieve full diversity over a frequency selective fading channel under the various channel conditions. The FER performance of the two proposed schemes showed that delay spread between adjacent paths improves the coding gain advantage of the system but not the diversity order. Also, the FER showed that the diversity order of the two systems is not affected by variation in mobile speed but that the speed affects the coding gain advantage.

Comparative simulation results were given with the 16-state SOSTTC [51], 4-state SOSTTC [65] and 16-state STTC [48]. It was shown that the ESOSTTC achieved the lowest FER under the channel condition considered. Comparative simulation results were presented for the proposed 16-state SQOSTTC and the 2-state SQOSTTC. The 2-state SQOSTTC could not exploit the multipath diversity of frequency selective fading channel because of parallel transitions within it trellis. The design of the SQOSTTC-OFDM was restricted to BPSK signalling because to avoid parallel transitions using QPSK modulation would require at least 256 trellis states which would be very complex.

In general, the proposed full-rate space-time coded OFDM schemes achieved full diversity under the various channel conditions considered.

CHAPTER 5

CONCATENATED SOSTTC-OFDM SYSTEMS

5.0 Introduction

One of the promising solutions to the challenges of future communication systems is to design efficient coding schemes over time, space and frequency domain for MIMO-OFDM systems. MIMO-OFDM communication systems have been shown to be a major access technique for next generation networks. SOSTTC deployed in frequency-selective fading channels through the OFDM system have shown improved performance over flat fading channels by exploiting the multipath diversity of frequency-selective fading channels, but it provides lower coding gain. Concatenated codes have been shown to be an effective technique of increasing the coding gain of coding schemes through the turbo principle.

This chapter focuses on concatenated codes in frequency-selective fading channels. In a bid to improve the performance of SOSTTC-OFDM systems in frequency-selective fading channels, four different and distinct concatenated codes with constituent SOSTTC and CC are proposed.

First, an overview of concatenated codes in an OFDM system is given in the next section. A detailed description of the encoding process of the proposed concatenated schemes is given in Section 5.2 while the decoding process of the concatenated schemes is given in Section 5.3. The PEP analysis of the concatenated schemes is derived in Section 5.4. The decoding computational complexity with the memory requirement for the concatenated schemes is calculated in Section 5.5. Finally, the performance of the proposed schemes is evaluated by comparative computer simulation in Section 5.6.

5.1 Overview of Concatenated STC-OFDM

There is limited literature on concatenated space-time coding in an OFDM environment. In [154], the performance of convolutional code concatenated serially with space-time trellis code is analyzed. The effects of the constituent codes and mobile speed were investigated. Also, in [61] and [155] the performance of concatenated STTC and STBC concatenated with turbo code and Reel Solomon (RS) code were investigated in an OFDM system. The effect of delay spread on the code performance was also investigated. RS code and CC was also concatenated serially in an OFDM environment in [9] and the system showed significant performance improvement over conventional STTC in a wideband environment.

5.2 The Encoder System Model

With achievable performance improvement from concatenated schemes, four concatenation schemes that combine SOSTTC and turbo coding in a bid to further improve the performance of SOSTTCs in frequency-selective fading channels are proposed.

The first concatenated topology consists of a convolutional code concatenated serially with SOSTTC inner code to give the CC-SOSTTC-OFDM. The second scheme, referred to as a double serial concatenated scheme (DS-SOSTTC-OFDM), involves an SCCC outer code and an SOSTTC inner code. The third concatenated topology modifies the PC-SOSTTC of Section 3.3.1 to incorporate an OFDM system and 16-state SOSTTC. It consists of PCCC concatenated serially with an SOSTTC inner code to give the PC-SOSTTC-OFDM. The fourth scheme is also an HC-SOSTTC scheme of Section 3.3.2 modified to incorporate an OFDM part with 16-state SOSTTC inner code. The fourth scheme referred to as HC-SOSTTC-OFDM involves parallel concatenation of two serially concatenated convolutional and SOSTTC codes. The decoding of these concatenation schemes is done iteratively with turbo decoders. The encoding and the decoding of these proposed schemes are explained in this section.

5.2.1 CC-SOSTTC-OFDM System Encoding

The encoder block diagram of the CC-SOSTTC-OFDM is shown in Fig. 5.1. In the system, a block of *N* independent data bits is encoded by the convolutional outer encoder and the output block of the coded bits is interleaved by using a random bit interleaver (π). The interleaved sequences are then passed to the SOSTTC encoder to generate a stream of QPSK symbols. Each of the symbols from the SOSTTC encoder is converted to a parallel output, and an inverse fast Fourier transform (IFFT) is performed on each of the parallel symbols. At the end, a cyclic prefix (CP) is added to each of the transformed symbols before transmission from each of the transmit antennas. Both RSC and NRC are considered as the outer code and the two encoders are terminated using appropriate tail bits.

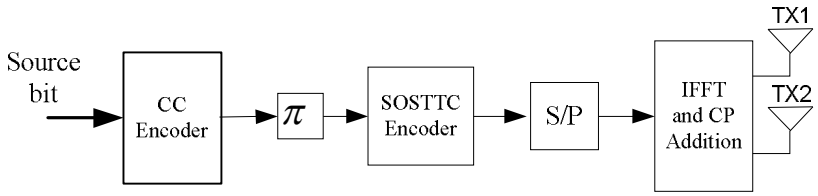

Fig. 5.1: Encoder block diagram of the CC-SOSTTC-OFDM system

5.2.2 DS-SOSTTC-OFDM System Encoding

The encoder structure of the double concatenated scheme is shown in Fig. 5.2. In the system, two outer serially concatenated convolutional codes are concatenated with an inner SOSTTC in a bid to improve the overall coding gain of the systems. The encoding process is similar to that of Section 5.2.1 above except for the addition of an extra convolutional outer encoder. In this system, a block of *N* independent data bits is encoded by the first convolutional outer encoder and the output block of the coded bits are interleaved by using a random bit interleaver (π_1). The interleaved sequences are then passed to the second convolutional outer code. The output stream from the second outer encoder are thereafter interleaved by the second interleaver (π_2) before the interleaved codes are passed to the SOSTTC encoder. The remaining process of encoding follows the description given in Section 5.2.1. Both the recursive systematic

(RSC) and the non-recursive convolutional (NRC) codes were considered as outer codes and each of the encoders was terminated using appropriate tail bits.

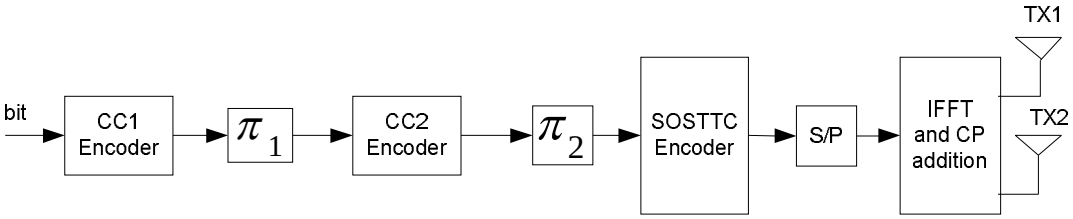

Fig. 5.2: Encoder block diagram of the DS-SOSTTC-OFDM system

5.2.3 PC-SOSTTC-OFDM System Encoding

The block diagram of the PC-SOSTTC-OFDM system is shown in Fig. 5.3 where the input bits are encoded by convolutional code 1 (CC1) as well as by convolutional code 2 (CC2) after interleaving by π_p. All the output bits from CC1 and CC2 are converted to a single serial stream. The serial stream is then interleaved by π_s and thereafter encoded by the SOSTTC to produce the complex symbols. The serial complex data are then converted to parallel streams upon which IFFT is performed. CP is then added to the transformed symbols before they are transmitted from each of the antennas. The convolutional encoders are either both RSC or both NRC encoder and all the encoders are terminated using appropriate tail bits.

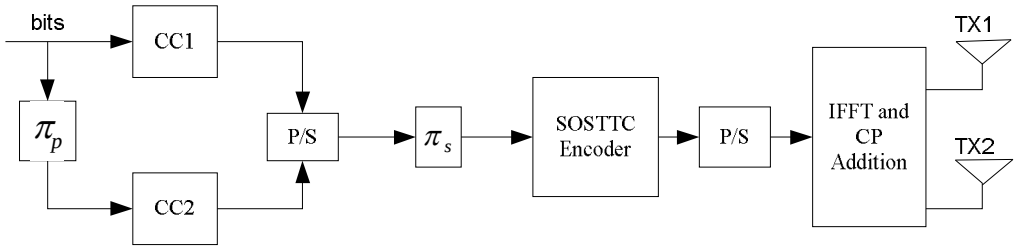

Fig. 5.3: Encoder block diagram of PC-SOSTTC-OFDM system

5.2.4 HC-SOSTTC-OFDM System Encoding

The encoder block diagram of the proposed hybrid concatenated scheme, shown in Fig.5.4, consists of a parallel concatenation of two serially concatenated schemes. Each of the serial concatenated schemes consists of an outer convolutional code concatenated via an interleaver with an inner SOSTTC. In the system, a block of *N* independent bits is encoded by the outer convolutional encoder of the upper serial part of the concatenated scheme. The output of the upper convolutional encoder is then passed through a random bit interleaver (π_1). The permuted bits from the interleaver are then fed to the upper SOSTTC encoder to generate a stream of complex data.

The complex symbol from the SOSTTC encoder is thereafter converted to a parallel output and IFFT is performed on each of the parallel symbols. In order to avoid ISI caused by multipath delay, Cyclic Prefix (CP) is added to each of the transformed symbols before transmission from each of the antennas.

In the lower serial part of the encoding, the lower convolutional encoder receives the permuted version of the block of *N* independent bits and generates blocks of coded bits which are passed through another interleaver (π_2) to the lower SOSTTC encoder. It should be noted that the same convolutional code and SOSTTC used in the upper encoding is used in the lower encoder. The complex data from the output of the lower SOSTTC encoder are then converted to parallel outputs and an IFFT is performed on each of the parallel symbols. Cyclic Prefix (CP) is added to the transformed symbols before transmission from each of the antennas from the lower arm of the encoder. Note that each encoder is terminated using appropriate tail bits.

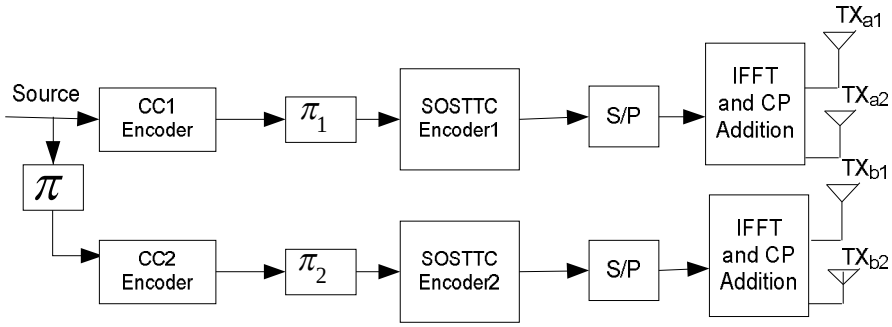

Fig. 5.4: Encoder block diagram of HC-SOSTTC-OFDM system

5.3 The Decoder Structures

In this section, the iterative decoding process of the proposed topologies is described. The decoder utilizes the SISO module. Each of the SISO decoders is matched to one of the component encoders and the SISO decoders work iteratively between themselves. The bitwise SISO algorithm described in Section 3.4 is used for the decoding of the four concatenated systems with some modifications. The subscript *t* of λ is replaced with subcarrier index *k* and equations (3.11) and (3.12) are modified to become matrix LLR as follows

$$\boldsymbol{\lambda}(k)\left(c = \underline{s}_l, I\right) = \hat{\boldsymbol{\lambda}}(k)\left(c = \underline{s}_l, I\right) - \hat{\boldsymbol{\lambda}}(k)\left(c = \underline{s}_1, I\right), \tag{5.1}$$

where

$$\hat{\boldsymbol{\lambda}}(k)\left(c = \underline{s}_l, I\right) = -\frac{1}{2\delta_r^2}\sum_{p=1}^{n_R}\left|r(k) - \sum_{q=1}^{n_T} H(k)s(k)\right|^2 . \tag{5.2}$$

5.3.1 CC-SOSTTC-OFDM Decoding

The simplified block diagram of the CC-SOSTTC-OFDM decoder is shown in Fig. 5.5. The subcarrier index of the LLR is dropped for simplicity of expressions. The subscript of the *c* or *u* specifies the decoder where *st* is used for the SOSTTC encoder and cc is

used for the convolutional encoder. As shown in Fig. 5.5, the inserted CP is first removed from each of the symbols and the fast Fourier transform (FFT) is performed on each of the symbols. The parallel transformed symbols are then converted to serial streams and the coded intrinsic LLR for the SOSTTC SISO module is computed as (5.1).

The SOSTTC SISO takes $\lambda(c_{st}, I)$ and the *a priori* information from the CC-SISO which is initially set to zero to compute the extrinsic information $\tilde{\lambda}(c_{st}, O)$. This extrinsic information is de-interleaved (π^{-1}) and fed to the CC-SISO to become its *a priori* information $\lambda(c_{cc}, I)$. The *a priori* information is then used to compute the extrinsic LLR $\tilde{\lambda}(c_{cc}, O)$ for the convolutional code SISO (CC-SISO). The extrinsic LLR is then interleaved to become the *a priori* information $\lambda(u_{st}, I)$ for the SOSTTC SISO for the next iteration. During the first iteration, $\lambda(u_{st}, I)$ is set to zero as no *a priori* information is available at the SOSTTC-SISO. The transmitted source symbols are assumed to be equally likely and therefore the input LLR $\lambda(u_{cc}, I)$ to the CC-SISO is permanently set to zero. The process is iterated several times and on the final iteration, a decision is taken on the extrinsic information $\lambda(c_{cc}, O)$ to obtain the estimate of the original transmitted bit stream.

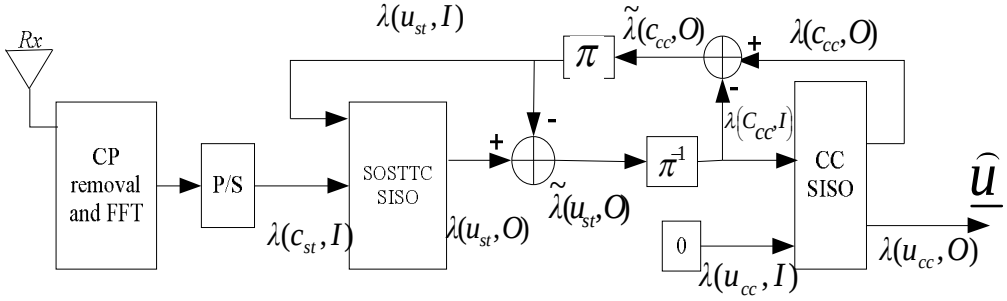

Fig. 5.5: The block diagram of the CC-SOSTTC-OFDM decoder

5.3.2 DS-SOSTTC-OFDM Decoding

Fig 5.6 shows the decoding block diagram of the DS-SOSTTC-OFDM system. The subscript of the *c* and *u* specifies the decoder as mentioned in Section 5.3.1, *st* is used for SOSTTC encoder, 1 for the convolutional encoder CC1 and 2 for the convolutional encoder CC2. During the first iteration the LLRs $\lambda(u_{st}, I)$ and $\lambda(u_2, I)$ are set to zero as

no *a priori* information is available. The source symbols transmitted are assumed to be equally likely and therefore the input LRR $\lambda(u_1, I)$ to the C1-SISO is permanently set to zero. The coded intrinsic LLR for the SOSTTC SISO $\lambda(c_{st}, I)$ is computed using (5.1).

The SOSTTC SISO takes $\lambda(c_{st}, I)$ and the *a priori* information from the C2-SISO which is initially set to zero and computes the extrinsic information $\tilde{\lambda}(u_{st}, O)$. The extrinsic LLR $\tilde{\lambda}(u_{st}, O)$ is then de-interleaved through π_2^{-1} to become the input LLR $\lambda(c_2, I)$ for the SISO decoder for the second outer convolutional code. The C2-SISO takes the input LLR $\lambda(c_2, I)$ and the *a priori* information from the C1-SISO and computes the extrinsic information for the C2-SISO for the coded $\tilde{\lambda}(c_2, O)$ and the un-coded LLR values $\tilde{\lambda}(u_2, I)$. The extrinsic information $\tilde{\lambda}(u_2, O)$ is then de-interleaved through π^{-1} to become the intrinsic LLR information to the C1-SISO decoder $\lambda(c_1, I)$. The intrinsic information is then used by the C1-SISO to compute the extrinsic information for the C1-SISO $\tilde{\lambda}(C_1, O)$.

The C1-SISO output LLR is thereafter passed through the interleaver π_1 to obtain the *a priori* information for the C2-SISO. The coded LLR output obtained from the C2-SISO $\tilde{\lambda}(c_2, O)$ is also passed through the interleaver π_2 to obtain the *a priori* information $\lambda(u_{st}, I)$ for SOSTTC- SISO for the next iteration. During the final iteration, decision is taken on $\lambda(u_1, O)$ from the C1-SISO output to obtain the estimate of the original transmitted symbol.

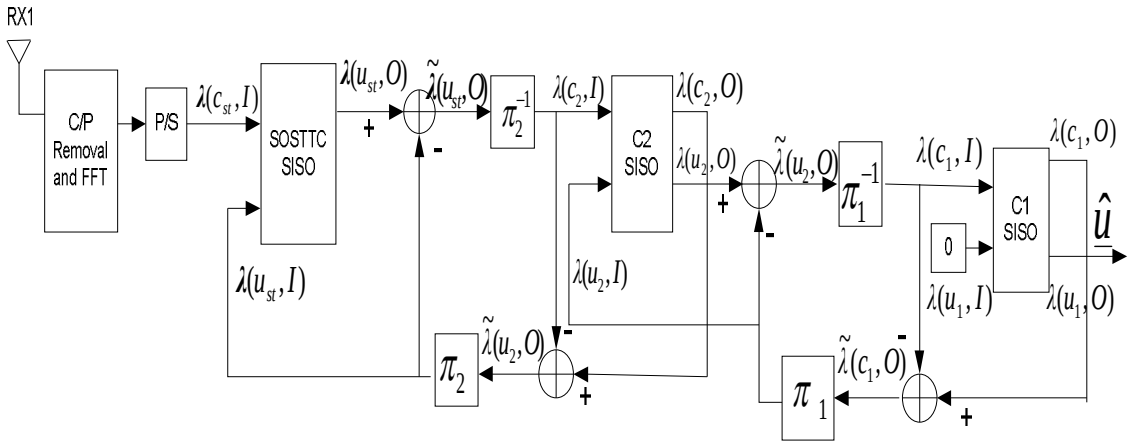

Fig. 5.6: The block diagram of the DS-SOSTTC-OFDM decoder

5.3.2 PC-SOSTTC-OFDM Decoding

The block diagram of the PC-SOSTTC-OFDM is shown in Fig. 5.7 which is a modification of Fig. 3.3. The subscript of *c* and *u* will specify the decoder where *st* is used for the SOSTTC encoder, 1 for convolutional CC1 and 2 for convolutional CC2.

The inserted CP is first removed from the symbol and FFT is performed on each of them. The parallel data streams are then converted to serial symbols. On the first iteration the SISO inputs $\lambda(u_{st}, I)$, $\lambda(u_1, I)$ and $\lambda(u_2, I)$ are all set to zero since no *a priori* information is available. By dropping the subcarrier index *k* for simplicity, the coded intrinsic LLR for the SOSTTC symbol-by-symbol SISO $\lambda(c_{st}, I)$ module is computed as (5.1).

The SOSTTC-SISO module takes the coded intrinsic LLR and computes the extrinsic LLR for the SOSTTC-SISO $\tilde{\lambda}(u_{st}, O)$. This extrinsic LLR is then passed to the inverse interleaver π_s^{-1} from where the information pertaining to the coded bits of CC1 and CC2, $\lambda(c_1, I)$ and $\lambda(c_2, I)$ respectively are extracted. Then the output LLRs $\lambda(c_1, O)$ and $\lambda(u_1, O)$ are calculated by the CC1-SISO. The LLR $\lambda(u_1, I)$ is subtracted from $\lambda(u_1, O)$ to obtain the LLR $\tilde{\lambda}(u_1, O)$ which is then passed through the interleaver π_p to obtain the intrinsic information $\lambda(u_2, I)$ for the CC2-SISO. The output LLRs $\lambda(c_2, O)$ and $\lambda(u_2, O)$ are also calculated by the CC2-SISO. The LLR $\lambda(u_2, I)$ is subtracted from $\lambda(u_2, O)$ to obtain the LLR $\tilde{\lambda}(u_2, O)$ which is then passed through the de-interleaver π_p^{-1} to obtain the intrinsic information $\lambda(u_1, I)$ for the CC1-SISO. A single LLR stream constructed from $\tilde{\lambda}(c_2, O)$ and $\tilde{\lambda}(c_1, O)$ is interleaved by π_s to become $\lambda(u_{st}, I)$ on the next iteration. On the final iteration, the LLR $\lambda(u_2, O)$ is interleaved by π_p to obtain $\tilde{\lambda}(u_2, O)$ which is added to $\lambda(u_1, O)$ upon which the decision device acts to determine the input bits.

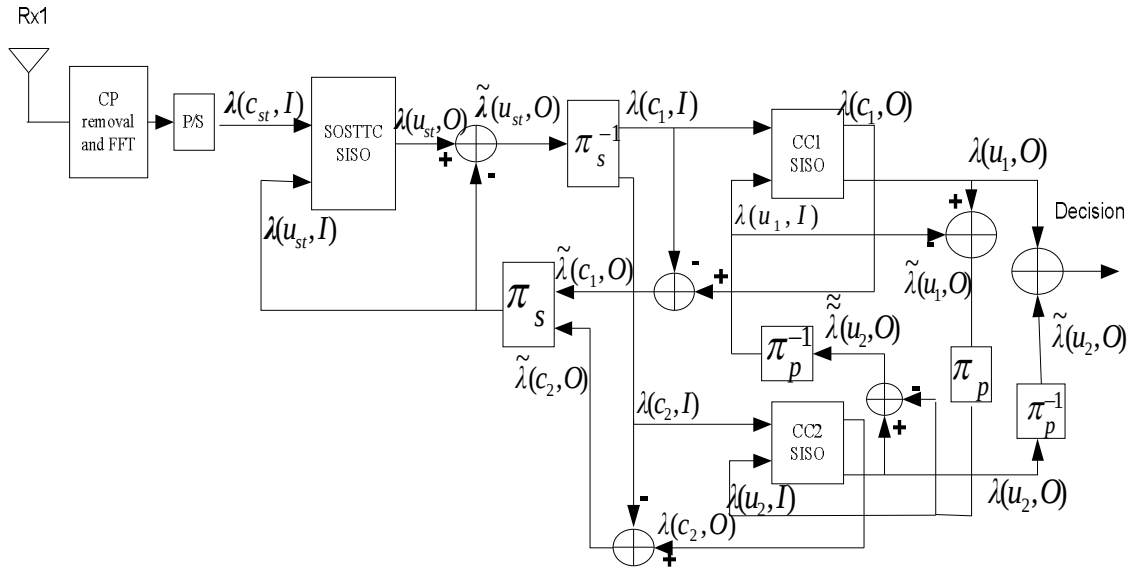

Fig. 5.7: The decoder block diagram of the PC-SOSTTC-OFDM system

5.3.3 HC-SOSTTC-OFDM Decoding

The decoding block diagram of the iterative decoding system of the HSOSTTC-OFDM system is shown in Fig. 5.8. The subscript of the *c* or *u* specifies the decoder where *st*1 is used for the upper SOSTTC encoder, *st*2 for the lower SOSTTC encoder, 1 for the upper convolutional code and 2 for the lower convolutional code. The decoder consists of two serial parts and one parallel sector. For the upper serial decoding, the inserted CP is first removed from each of the symbols and FFT is performed on each of the symbols. The parallel streams are then converted to serial symbols and the coded intrinsic LLR for the SOSTTC symbol-by-symbol SISO module is computed as in (5.2).

The SOSTTC SISO takes the intrinsic LLR $\lambda(c_{st1}, I)$ and the *a priori* information from the CC1-SISO which is initially set to zero and computes the extrinsic LLR given as

$$\tilde{\lambda}(u_{st1}, O) = \lambda(u_{st1}, O) - \lambda(u_{st1}, I), \tag{5.3}$$

where u denotes un-coded information, O denotes extrinsic, I denotes *a priori* information.

The extrinsic information is de-interleaved (π_1^{-1}) and fed to the CC1-SISO to become its *a priori* information. The *a priori* information is then fed to the CC1-SISO together with the uncoded *a priori* information from the parallel part to compute the extrinsic information for the CC1-SISO. The *a posteriori probability* (APP) output of the CC1-SISO consists of the extrinsic $\tilde{\lambda}(c_1, O)$) and *a priori* LLR given by

$$\tilde{\lambda}(c_1, O) = \lambda(c_1, O) - \lambda(c_1, I), \tag{5.4}$$

where c is the coded information, O denotes extrinsic and I denotes intrinsic information.

The APP outputs of the lower serial MAP decoders can be obtained by replacing the index 1 in (5.3) and (5.4) to index 2.

The parallel interconnection component of the iterative decoding process is described by (5.5) and (5.6):

$$\tilde{\lambda}(u_1, O) = \lambda(u_1, O) - \lambda(u_1, I). \tag{5.5}$$

$$\tilde{\lambda}(u_2, O) = \lambda(u_2, O) - \lambda(u_2, I). \tag{5.6}$$

The process is iterated severally and the bit with the maximum APP is chosen by the decision device in the last iteration using the summed values of the uncoded LLRs' output for both the CC1-SISO and CC2-SISO decoders.

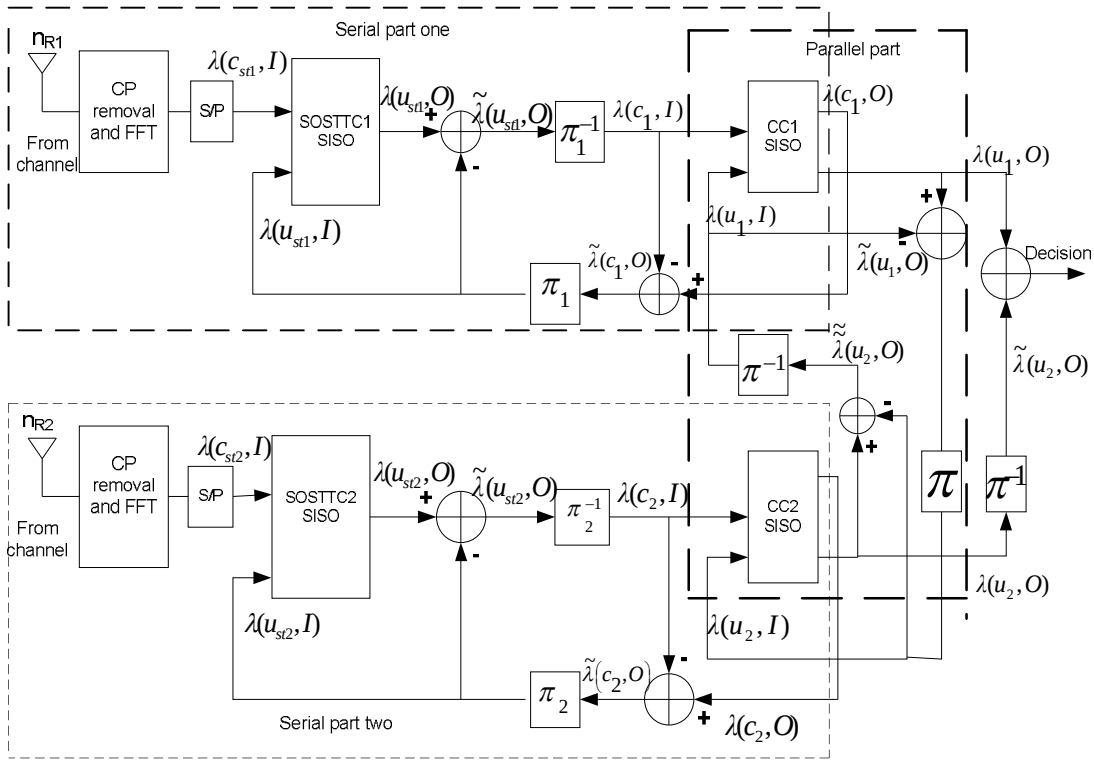

Fig. 5.8: The decoder block diagram of the HC-SOSTTC-OFDM system

5.4 Pairwise Error Probability Analysis

The PEP used for the analysis of STTC in [16], applied in [51] and [77] is extended here to the analysis of the proposed concatenated schemes. Assuming that the symbol matrix sequence $\boldsymbol{C} = \{c[1], \dots, c(Y)\}$ is transmitted, where Y is the trellis path length chosen to be smaller than K, and the Maximum Likelihood (ML) decoder decision is in favor of the coded sequence $\widehat{\boldsymbol{C}} = \{\hat{c}[1], \dots, \hat{c}(Y)\}$, where $m(\boldsymbol{r}, \widehat{\boldsymbol{C}}) \geq m(\boldsymbol{r}, \boldsymbol{C})$, then $m(\boldsymbol{r}, \widehat{\boldsymbol{C}})$ is the ML metric related to the decoded path given by

$$m(\boldsymbol{r}, \widehat{\boldsymbol{C}}) = \sum_{y=1}^{Y} \sum_{n=1}^{N_x} \sum_{j=1}^{n_R} \left| r_j^n(y) - \sum_{i=1}^{n_T} H_{ij}(y) \hat{c}_i^n(y) \right|^2 . \qquad (5.7)$$

and $m(\boldsymbol{r}, \boldsymbol{C})$ is the ML metric for the correct path given by

$$m(\boldsymbol{r}, \boldsymbol{C}) = \sum_{y=1}^{Y} \sum_{n=1}^{N_x} \sum_{j=1}^{n_R} \left| r_j^n(y) - \sum_{i=1}^{n_T} H_{ij}(y) c_i^n(y) \right|^2 , \tag{5.8}$$

where N_x is time interval.

Thus the PEP is given by

$$P\left((\boldsymbol{C} \to \widehat{\boldsymbol{C}}) \middle| \mathbf{H} \right) = \Pr\left[\mathrm{m}(\boldsymbol{r}, \boldsymbol{C}) - \mathrm{m}(\boldsymbol{r}, \widehat{\boldsymbol{C}}) > 0 \middle| \mathbf{H} \right]. \tag{5.9}$$

Substituting (5.7) and (5.8) in (5.9) and simplifying in terms of Gaussian Q-function yields

$$\boldsymbol{P}\left((\boldsymbol{C} \to \widehat{\boldsymbol{C}}) | \boldsymbol{H} \right) = Q\left(\sqrt{\frac{E_s}{2N_0} D} \right), \tag{5.10}$$

where N_0 is the variance of the noise, E_s is the symbol energy and D is defined as

$$D = \sum_{j=1}^{n_R} \sum_{y=1}^{Y} \sum_{n=1}^{N_x} D_n^j(y) ,$$

and

$$D_n^j(y) = \left| \sum_{i=1}^{n_T} [c_i^n(y) - \hat{c}_i^n(y)] H_{ij}(y) \right|^2 .$$

Using an upper bound for the Q-function $Q(x) \leq 1/2 e^{-x^2/2}$, PEP can be upper bounded as

$$\boldsymbol{P}\left((\boldsymbol{C}\rightarrow\widehat{\boldsymbol{C}})\middle|\boldsymbol{H}\right)\leq\frac{1}{2}exp\left(-\frac{E_s}{4N_0}D\right). \tag{5.11}$$

Since the expected value of $H_{pq}(y)$ is zero for all $H_{pq}(y)$'s, then the expected value of $D_n^q(l)$ is given as

$$E\left[D_n^j(y)\right]=\sum_{i=1}^{N_T}E\left[\left|c_i^n(y)-\hat{c}_i^n(y)\right|^2\left|H_{ij}(y)\right|^2\right].$$

The PEP upper bound average over all possible channel realizations is given from (5.11) as $\boldsymbol{P}(\boldsymbol{C}\rightarrow\widehat{\boldsymbol{C}})=E[\boldsymbol{P}\left((\boldsymbol{C}\rightarrow\widehat{\boldsymbol{C}})\middle|\boldsymbol{H}\right)$,

$$\leq\prod_{j=1}^{n_R}\prod_{i=1}^{n_T}\prod_{y=1}^{Y}E\left\{\frac{1}{2}exp\left[\frac{-E_s}{4N_0}\left(\sum_{n=1}^{N_x}\left|c_i^n(y)-\hat{c}_i^n(y)\right|^2\left|H_{ij}(y)\right|^2\right)\right]\right\}. \tag{5.12}$$

For all $\upsilon\in\mathbb{R}$,

$$E[\exp(\upsilon\varsigma^2)]=\int_0^{\infty}2\varsigma\exp(-\varsigma^2)\exp(\upsilon\varsigma^2)\,d\varsigma=\frac{1}{1-\upsilon}, \tag{5.13}$$

where ς is a random variable with Rayleigh distribution with variance ½. Assuming that the OFDM subcarrier gains $H_{ij}(y)$ are independent, complex, Gaussian-distributed variables, and taking $\varsigma=\left|H_{pq}(y)\right|^2$ in (5.13), then (5.12) yields

$$\boldsymbol{P}(\boldsymbol{C}\rightarrow\widehat{\boldsymbol{C}})\leq\prod_{j=1}^{n_R}\prod_{i=1}^{n_T}\prod_{y=1}^{Y}\frac{1}{1+\frac{E_s}{4N_0}\sum_{n=1}^{N_x}\left|c_i^n(y)-\hat{c}_i^n(y)\right|^2}, \tag{5.14}$$

$$\leq\prod_{j=1}^{n_R}\prod_{i=1}^{n_T}\prod_{y\epsilon\eta}\frac{1}{1+\frac{E_s}{4N_0}\sum_{n=1}^{N_x}\left|c_i^n(y)-\hat{c}_i^n(y)\right|^2}.$$

where η is the set of all y for which $c_i^n(y) \neq \hat{c}_i^n(y)$. Denoting the number of elements in η by l_η, then at high signal to noise ratio, Eqn. (5.14) can be expressed as [51]

$$\boldsymbol{P}(\boldsymbol{C} \rightarrow \widehat{\boldsymbol{C}}) \leq \frac{1}{\left[\left(\frac{E_s}{4N_0}\right)^{l_\eta} d_p(l_\eta)\right]^{n_R}}, \tag{5.15}$$

where

$$d_p(l_\eta) = \prod_{y}^{Y} \prod_{i=1}^{n_T} \sum_{n=1}^{N_x} |c_i^n(y) - \hat{c}_i^n(y)|^2$$

is the product sum distance along the error events $\boldsymbol{P}(\boldsymbol{C} \rightarrow \widehat{\boldsymbol{C}})$ path and l_η is called the effective length of this error event. The built-in frequency diversity of the SOSTTC is calculated as $L_\eta = \min(l_\eta)$ while the product sum distance is calculated as $d_p(L_\eta) = min[d_p(l_\eta)]$.

Assuming that the whole codeword of the concatenated scheme $\boldsymbol{X}$ is constructed from N_η different $\boldsymbol{C}$ sequences denoted by $\boldsymbol{C_\eta}$ for $\eta = 1, \ldots, N_\eta$, so that $\boldsymbol{X} = \boldsymbol{C_1}, \ldots, \boldsymbol{C_\eta}, \ldots, \boldsymbol{C_{N_\eta}}$. Then

$$\boldsymbol{P}(\boldsymbol{X} \rightarrow \widehat{\boldsymbol{X}}) = \prod_{\eta=1}^{N_\eta} P\left(\boldsymbol{C_\eta} \rightarrow \widehat{\boldsymbol{C}}_{\boldsymbol{\eta}}\right),$$

$$\leq \frac{1}{\left[\left(\frac{E_s}{4N_0}\right)^{l_\gamma(\boldsymbol{X},\widehat{\boldsymbol{X}})} d_p(l_\gamma)\right]^{n_R}}, \tag{5.16}$$

where, $l_\gamma(\boldsymbol{X}, \widehat{\boldsymbol{X}})$ is the effective length given by

$$l_\gamma(\boldsymbol{X}, \widehat{\boldsymbol{X}}) = \sum_{\eta=1}^{N_\eta} l_\eta\left(\boldsymbol{C_\eta}, \widehat{\boldsymbol{C}}_{\boldsymbol{\eta}}\right), \tag{5.17}$$

and $d_p(l_\gamma)$ is the product sum distance defined as

$$d_p(l_\gamma) = \prod_{\eta=1}^{N_\eta} d_p(l_\eta). \tag{5.18}$$

The space-frequency diversity of each arm of the concatenated scheme is therefore calculated from

$$L_\gamma = \min(l_\gamma). \tag{5.19}$$

The design criterion from (5.19) at high signal-to-noise ratio involves the maximization of the built-in space-frequency diversity of the concatenated code and the minimum product sum distance. Maximization of the build-in-space-frequency diversity of the concatenated code optimizes the diversity while the maximization of the minimum product sum distance optimizes the coding gain of the concatenated scheme.

If it is assumed that the bit interleaver maps different bits of the outer coded bit vector pairs into different groups, then the minimum number of different groups in a pair will be equal to the free distance d_{free} of the outer code. With this assumption, the built-in space-frequency diversity of each arm of the concatenated schemes becomes $L_\gamma = L_\eta d_{free}(\text{outer code})$.

The overall diversity of the concatenated code from (5.16) and (5.19) can then be written as

$$D_g = n_R \times min\{L_\eta d_{\text{free}}(\text{outer code}), n_T L\}, \tag{5.20}$$

where L denotes the number of multipath.

For the CC-SOSTTC-OFDM system,

$$d_{\text{free}}(\text{outer code}) = d_{\text{free}}(CC).$$

while for the CC-CC-SOSTTC-OFDM system,

$$d_{free}(\text{outer code}) = d_{\text{free}}(CC1) \times d_{\text{free}}(CC2).$$

The overall diversity achievable by the HC-SOSTTC-OFDM system is given by

$$D_g = 2 \times n_R \times min\{L_\eta d_{\text{free}}(\text{outer code}), n_T L\}. \quad (5.21)$$

where

$$d_{\text{free}}(\text{outer code}) = d_{\text{free}}(CC1) \ or \ d_{\text{free}}(CC2).$$

For the PC-SOSTTC-OFDM system,

$$d_{\text{free}}(\text{outer code}) = (d_{\text{free}}(CC1) + d_{\text{free}}(CC2)).$$

5.5 Comparative Decoding Complexity and Memory Requirements

In this section, the relative estimated complexity and the memory requirement of the proposed schemes in MIMO-OFDM systems are addressed. The approach used in [61] is adopted in analyzing the complexity and memory requirement of the various proposed schemes. In computing the estimated complexity, the estimated complexity of the whole systems is assumed to depend only on the channel decoder, i.e. the complexity associated with the modulator, demodulator, STC encoder are assumed to be insignificant compared with the complexity of the channel decoders. The complexity of the channel decoders which depends directly on the number of trellis transitions per information data bit is used as the basis of comparison.

For SOSTTC, the number of trellises leaving each state is equivalent to 2^{BPS}, where BPS is the number of transmitted bits per modulation symbols.

The approximate complexity of an SOSTTC decoder using the VA can therefore be given as

$$\text{Comp}\{SOSTTC\} = \frac{2^{BPS} \times \text{No of states}}{BPS}. \quad (5.22)$$

For the concatenated schemes, the Log-MAP decoding algorithm for iterative decoding is applied. Since the Log-MAP algorithm has to perform forward as well as backward recursion and soft output calculation, which results in traversing through the trellis

three times, the number of trellises in Log-MAP decoding algorithm is assumed to be three times higher than the conventional Viterbi Algorithm.

For the rate-2/3, 4-state CC decoder, the complexity is estimated as

$$\text{Comp}\{CC(3,2,K)\} = 3 \times 2^{K-1} \times 3 \times \text{number of iterations.}$$

For SOSTTC in the iterative decoding, the complexity is estimated as

$$\text{Comp}\{SOSTC_{\text{iter}}\} = \frac{3 \times 6 \times 2^{BPS} \times \text{number of states}}{BPS}. \qquad (5.23)$$

The memory requirement for SOSTTC using VA algorithm is given by

$$\text{mem}\{SOSTTC\} = \text{no of states} \times \text{block length}, \qquad (5.24)$$

while for SOSTTC involved in Log-MAP algorithm is given by

$$\text{mem}\{SOSTTC \text{ iter}\} = 3 \times \text{no of states} \times \text{block length}. \qquad (5.25)$$

For the CC used as constituent code in the concatenated scheme, the memory requirement is given by

$$\text{mem}(CC(2,1,K) = 3 \times 2K - 1 \times \text{block length}. \qquad (5.26)$$

Applying equations (5.22) to (5.26) and considering six iterations for all the concatenated schemes, the estimated complexity and memory requirement for all the proposed schemes in OFDM systems is summarized in Table 5.1. Here, it is explicitly assumed that 256 bits are needed for the 64 subcarriers without the tail bits. It is obvious from Table 5.1 that the diversity advantage and the high coding gain provided by the concatenated schemes comes with higher decoding complexity and memory requirement.

Table 5.1: Estimated decoder complexity and memory requirements for the proposed schemes

S/N	Scheme	Decoding Algorithm	CC	SOSTTC	Complexity	Memory Requirement
1	SOSTTC-OFDM	VA		16 states	64	4096
				32 states		
				64 states		
2	ESOSTTC-OFDM	VA		16 states	64	4096
				32 states		
				64 states		
3	CC-SOSTTC-OFDM	Log-MAP	rate2/3	16 states	1368	14,184
4	DS-SOSTTC-OFDM	Log-MAP	rate 2/3	16states	1584	15,504
5	PC-SOSTTC-OFDM	Log-MAP	rate 2/3	16 states	1584	14,160
6	HC-SOSTTC-OFDM	Log-MAP	rate 2/3	16 states	2592	27,408

5.6 Simulation Results and Discussion

In this section, simulation results illustrating the performance of the proposed concatenated schemes over frequency-selective fading channels are provided. For the simulation, a MIMO-OFDM concatenated scheme equipped with two transmit antennas and one receive antenna is considered. Each of the OFDM modulators utilizes 64 subcarriers with a total system bandwidth of 1 MHz and FFT duration of 80 μs. The system's subcarrier spacing is 15 kHz with symbol duration of 64 μs while the guard band interval is 16 μs. The performance curves are described by means of frame error

rate (FER) versus the receive SNR with QPSK constellation. The system is simulated over two channel scenarios: (1) A quasi-static channel with a two-path uniform power delay profile. The delay between these paths is one OFDM sample duration. (2) Typical urban (TU) six-path COST 207 power delay profile reported in [156]. The channel is assumed to be constant over two symbol periods (frame) and changes independently over each frame. Availability of perfect channel state information at the receiver with perfect timing and frequency synchronization between the transmitter and the receiver is also assumed throughout the simulations.

Fig. 5.9 shows the FER simulation results for the first concatenated scheme for various numbers of iterations. The system performance is seen to improve with increase in the number of iterations and achieve the maximum possible diversity of 6 at the 6^{th} iteration. Figure 5.10 shows the FER performance for the CC-SOSTTC using NRC and RSC outer code and that of RSC outer code with STTC inner code. The CC-SOSTTC with RSC outer code is observed to achieve additional coding gain of 1 dB and 2 dB at an FER of 10^{-3} when compared with its counterpart with NRC outer code and the scheme with STTC inner code respectively.

For the DS-SOSTTC-OFDM scheme, rate-2/3 outer codes are considered for the case of both recursive and non-recursive codes. Fig. 5.11 shows the FER variation with the number of decoding iterations using RSC outer code. The performance of the system improves with increase in the number of iterations and the scheme achieves the maximum achievable diversity of 12 at the sixth iteration. The FER performance of DS-SOSTTC-OFDM is also presented considering RSC and NRC outer codes and the case of STTC inner code with the RSC outer code in Fig. 5.12. As can be seen in the FER plot, the scheme with outer RSC code achieves additional coding gain of about 1.2dB and 0.6 dB at FER of 10^{-3} when compared with the scheme with STTC inner code and the scheme with NRC outer code respectively.

The performances of CC-SOSTTC-OFDM, DS-SOSTTC-OFDM, CC-STTC-OFDM, DS-STTC-OFDM and SOSTTC-OFDM from [51] are compared in Fig. 5.13. As can be seen from the performance curves additional diversity gain and coding gain are provided by the concatenating schemes. The CC-SOSTTC-OFDM achieves a diversity order of 6, while the DS-SOSTTC-OFDM and the SOSTTC-OFDM achieve a diversity order of 12 and 4 respectively. In terms of coding gain, the DS-SOSTTC-OFDM

system offers an additional coding gain of about 9.2 dB, 5.2 dB, 3 dB and 1.2 dB when compared with SOSTTC-OFDM, CC-STTC-OFDM, CC-SOSTTC-OFDM and DS-STTC-OFDM schemes respectively. The serial concatenated schemes provide significant diversity advantages and coding gain over the conventional SOSTTC-OFDM system but with a higher decoding complexity and a loss in bandwidth efficiency.

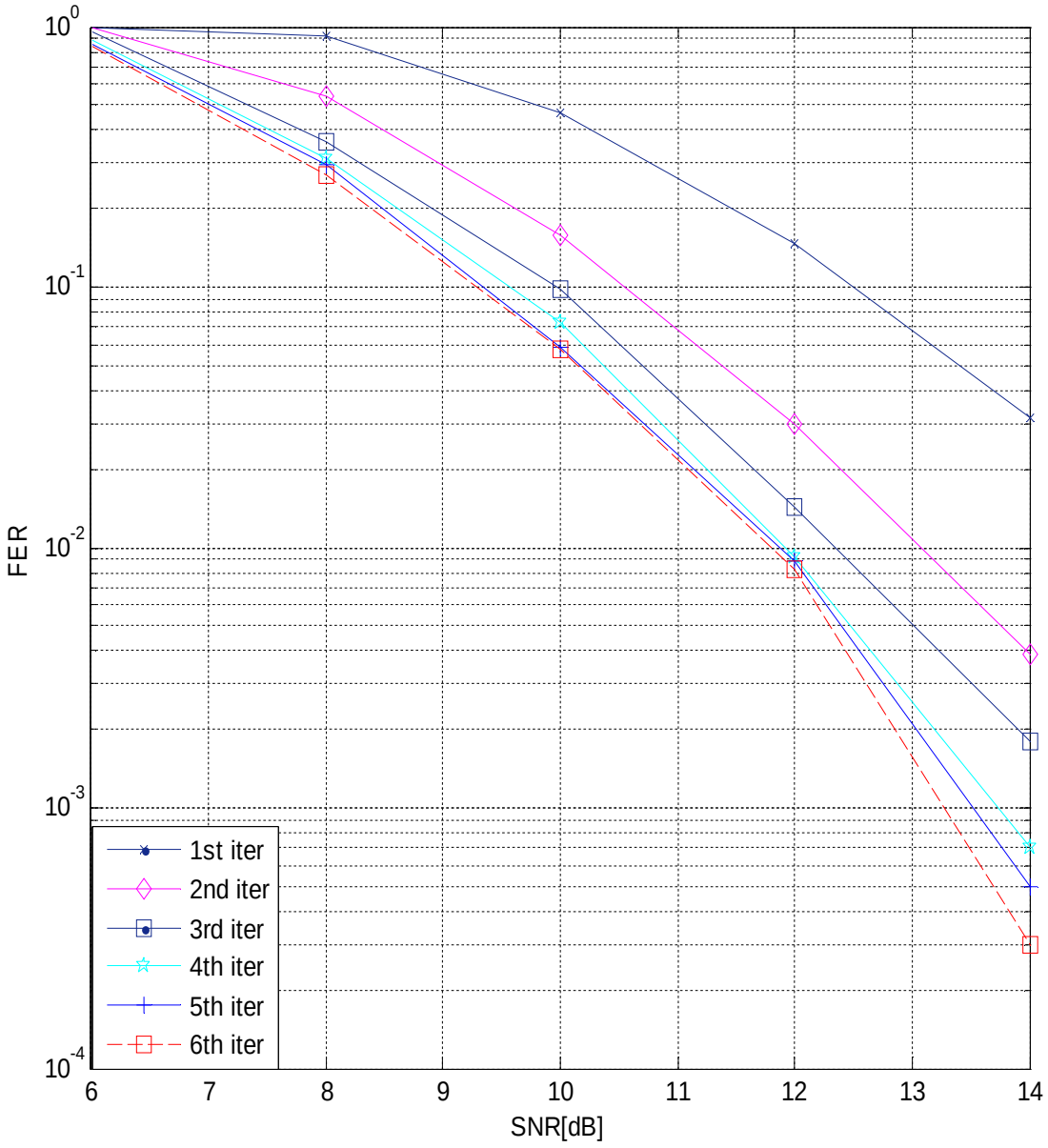

Fig. 5.9: FER performance of CC-SOSTTC-OFDM for various number of decoding iterations

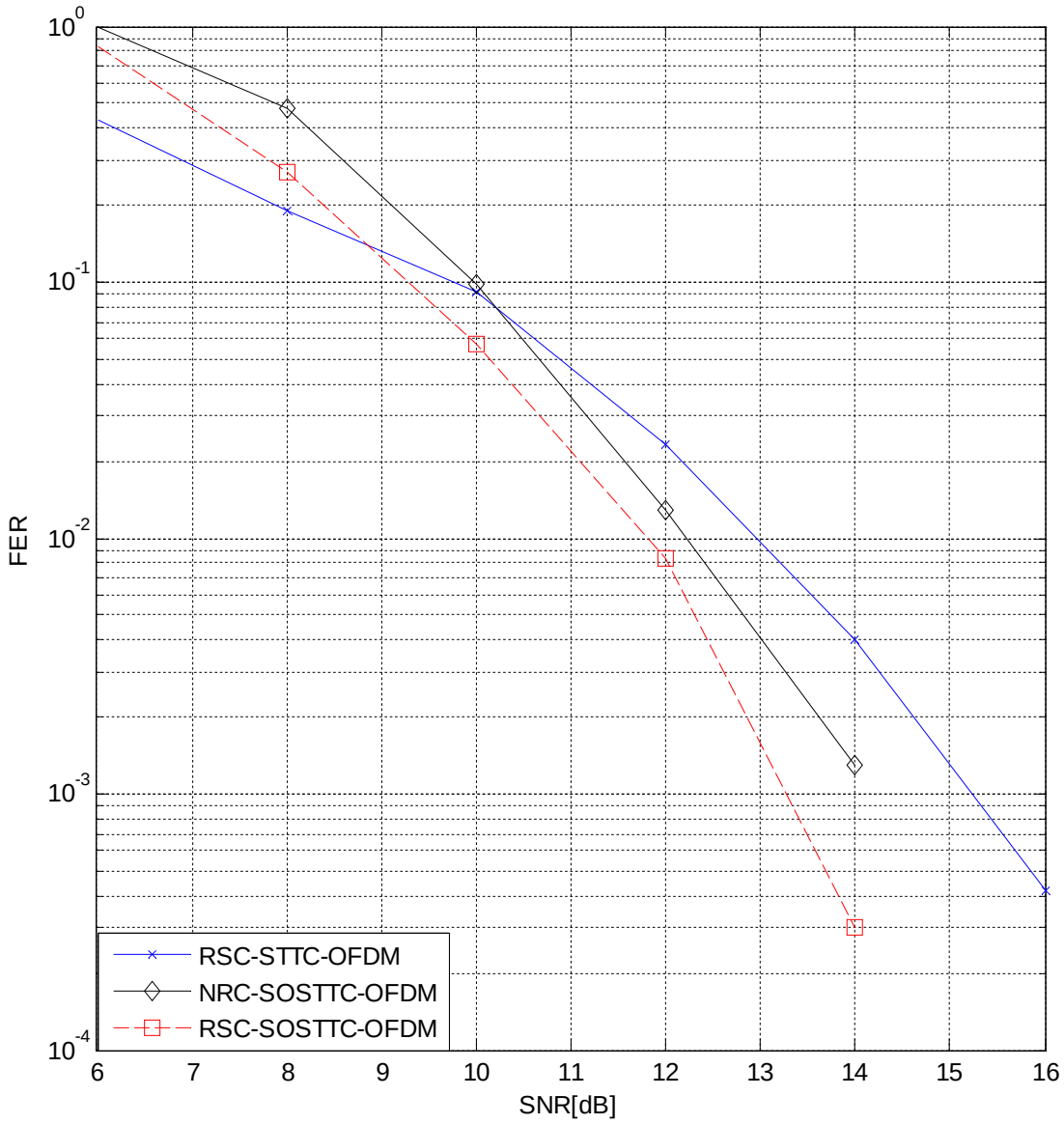

Fig. 5.10. FER performance of CC-SOSTTC-OFDM using NRC and RSC outer codes

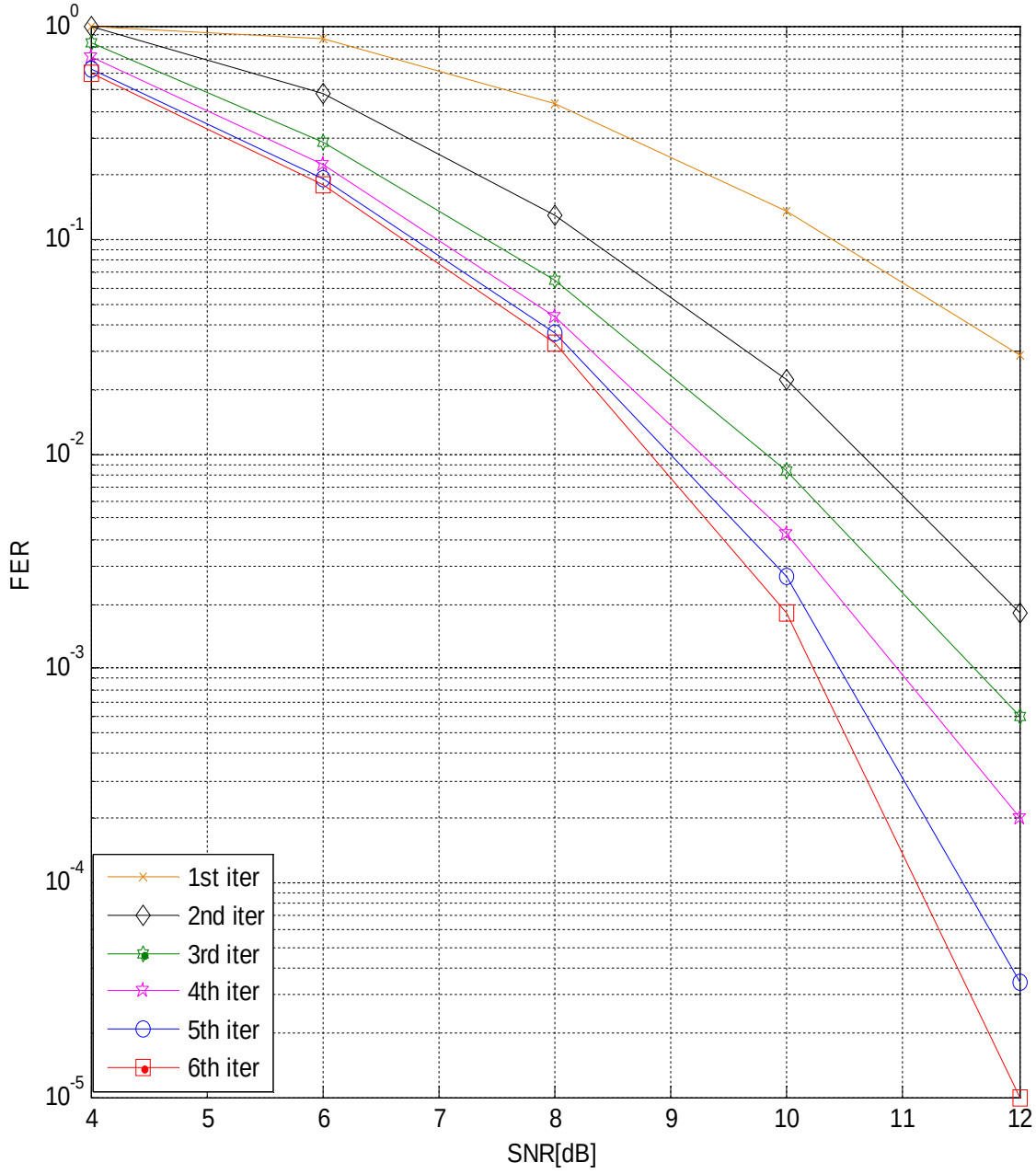

Fig. 5.11: FER performance of DS-SOSTTC-OFDM for various number of decoding iterations

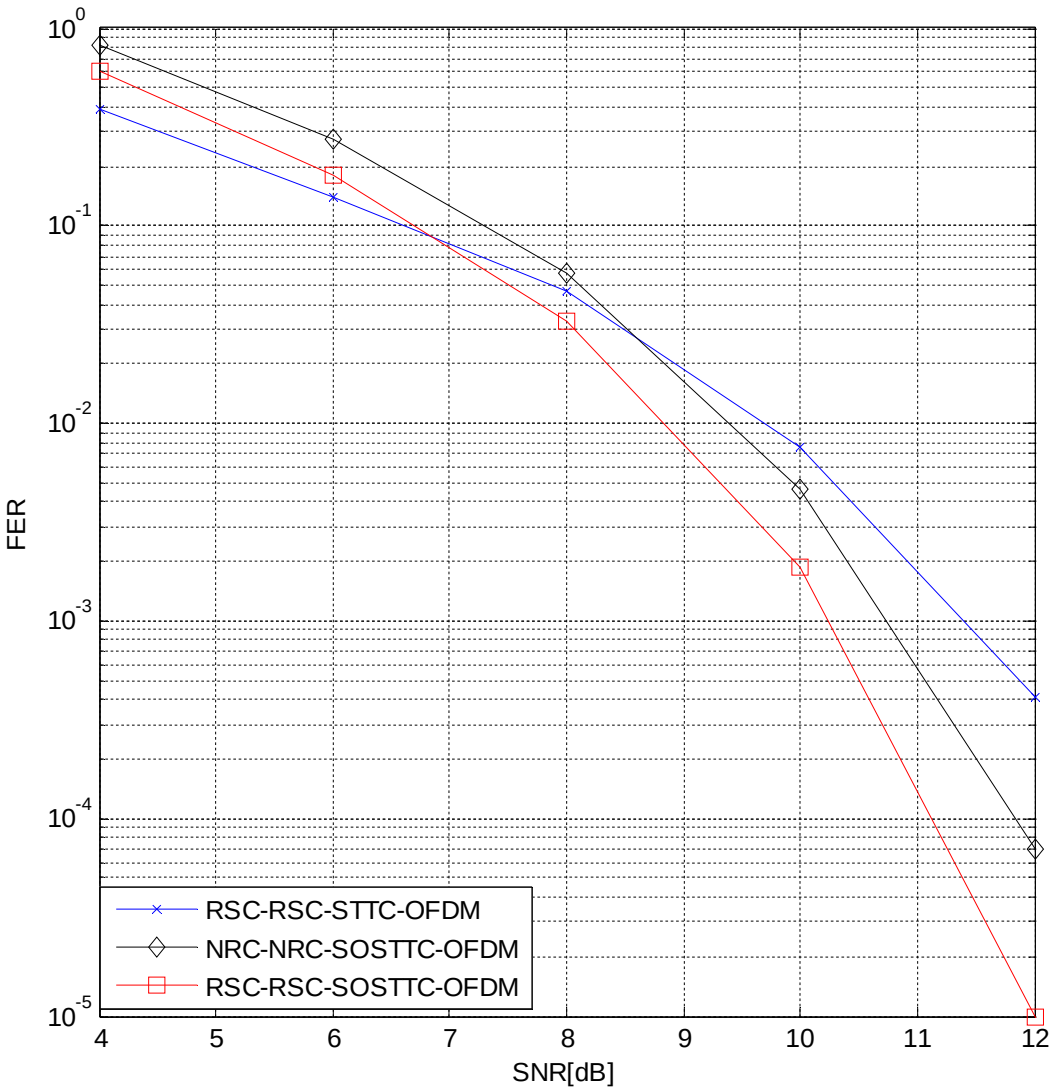

Fig. 5.12: FER performance of DS-SOSTTC-OFDM using NRC and RSC outer codes

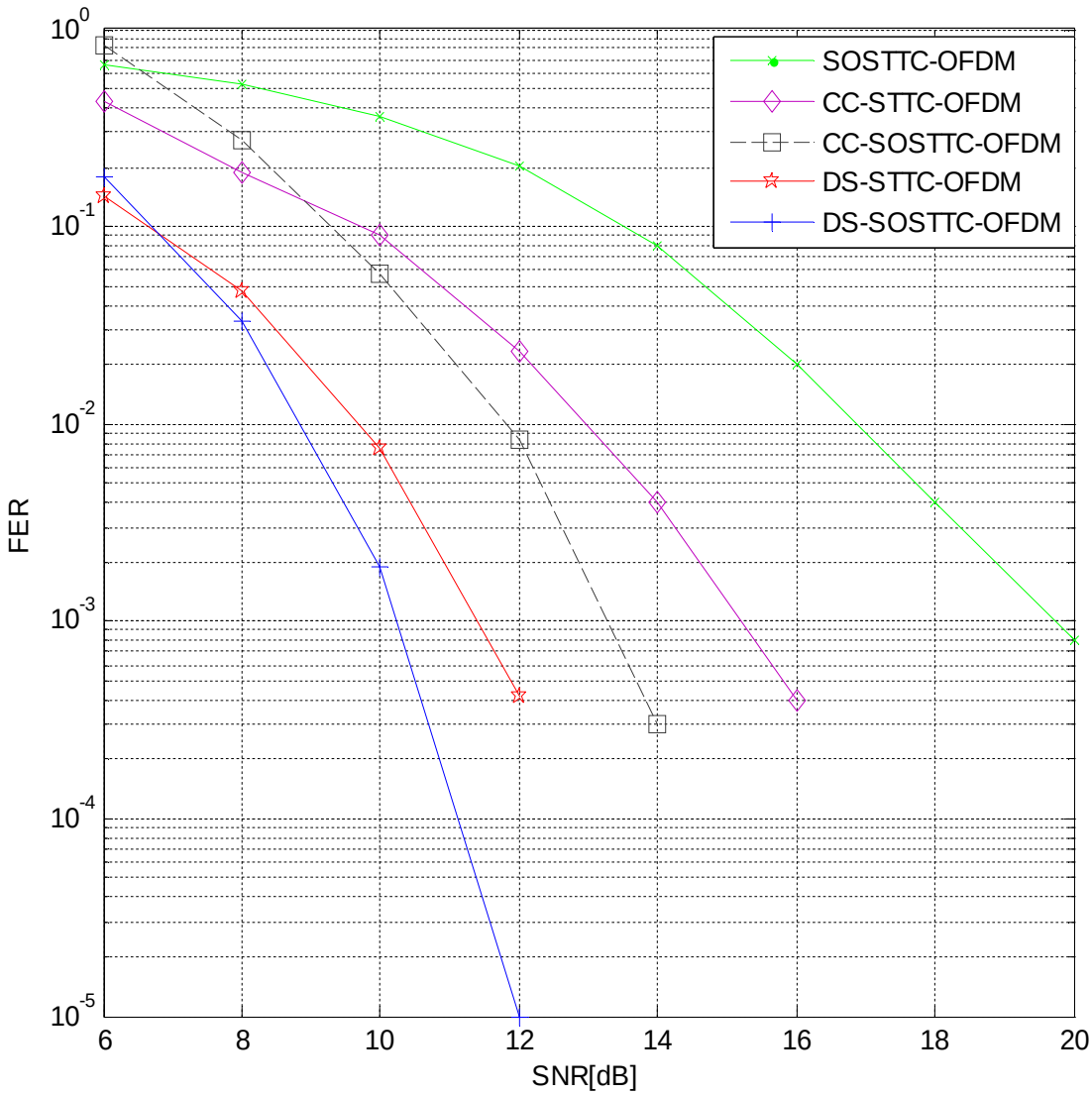

Fig. 5.13: FER comparison of SOSTTC-OFDM, CC-STTC-OFDM, CC-SOSTTC-OFDM, DS-STTC-OFDM and DS-SOSTTC-OFDM

For the PC-SOSTTC-OFDM, the 4-state, rate-2/3 both recursive and non-recursive convolutional codes are used as the outer codes. The code FER performance is evaluated for various numbers of iterations in Fig. 5.14. The rate-2/3 RSC is considered as the outer code in this case. The coding gain achieved by the system is seen to increase as the number of decoding iterations increase and starts saturating at the 4^{th} iteration. The system however did not achieve the maximum diversity order as a result of interleaver gain saturation (error floor). Error floor at a higher SNR region is a peculiar characteristic of a parallel concatenation scheme.

In Fig. 5.15, the FER performance of the PC-SOSTTC-OFDM is shown for both RSC and NRC outer codes and an inner STTC code with RSC outer code. The scheme with RSC outer code is seen to provide a coding gain of about 0.6 dB and 1.6 dB when compared with its counterpart with an STTC inner code and NRC outer code respectively. The FER performance of the PC-SOSTTC-OFDM is also evaluated in Fig. 5.16 using both the RSC and the NRC outer codes compared with PC-STTC-OFDM under the two rays channel model. Under this channel scenario, the scheme with RSC outer codes is observed from the FER performance curve to achieve a full diversity order of 4, as well as additional coding gain of about 0.6 dB and 1.4 dB when compared with its counterpart having STTC inner code and NRC outer code respectively.

The same 4-state rate-2/3 recursive and non-recursive convolutional codes are used as the outer code for the HC-SOSTTC-OFDM system. Each serial part of the HC-SOSTTC-OFDM scheme employs 64 subcarriers.

The FER performance of the HC-SOSTTC-OFDM system is shown in Fig. 5.17 for various numbers of iterations using channel condition 1. From the FER performance curve, it can be observed that the HC-SOSTTC-OFDM achieves a diversity order of 12 at the 6th iteration. The FER performance of the system is presented for both RSC and NRC outer code in Fig. 5.18. In the same Fig. 5.18, the FER performance with a case of STTC inner code is compared. The scheme with RSC outer code provides additional coding gain of about 0.8 dB and 1.7dB when compared with the scheme having STTC inner code and NRC outer code system respectively. Fig. 5.19 shows the FER for the HC-SOSTTC-OFDM system using the two-ray channel model. It can be seen from the slope of the performance curve that the HC-SOSTTC-OFDM with RSC outer code

achieves a full diversity order of 8 under this channel condition. It can also be observed from the FER curve of Fig. 5.19 that the code with RSC outer codes achieves additional coding gain of about 1.3 dB and 0.6 dB when compared with the HC-SOSTTC-OFDM having NRC outer code and HC-STTC-OFDM system respectively. Note that, to have the same number of symbols per frame and the same delay length for both systems, the number of OFDM subcarriers for the scheme with STTC inner code was selected as 128. In Fig. 5.20 the FER performance of HC-SOSTTC-OFDM is compared with that of CC-SOSTTC-OFDM, from where it is observed that the HC-SOSTTC-OFDM achieves a higher diversity order than the CC-SOSTTC-OFDM and also presents an additional coding gain of 5.0 dB but with double decoding complexity.

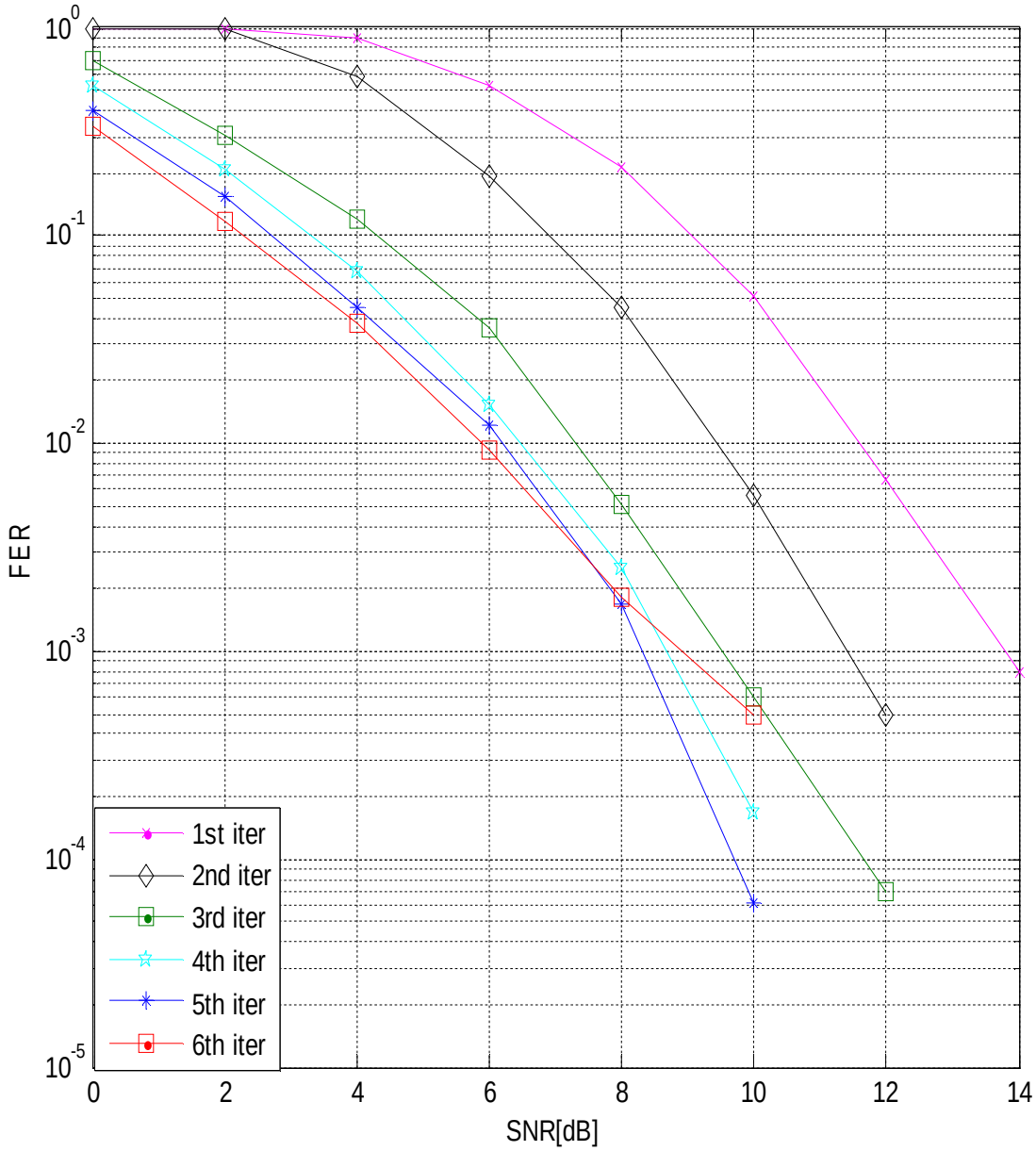

Fig 5.14: FER performance of PC-SOSTTC-OFDM for various numbers of decoding iterations over the typical urban (TU) six-path COST 207 channel model

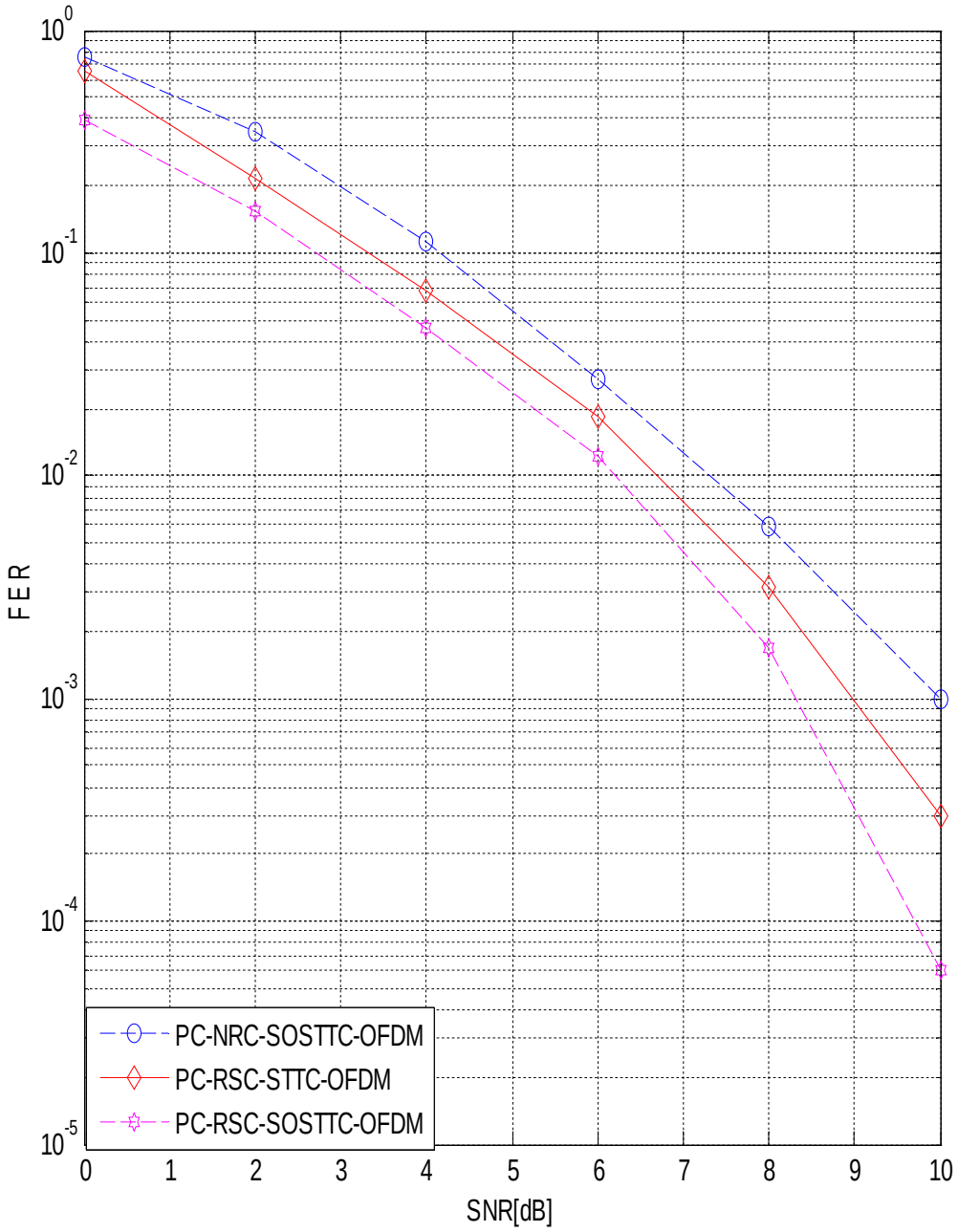

Fig. 5.15: FER performance of PC-NRC-SOSTTC-OFDM, PC-RSC-STTC-OFDM and PC-SOSTTC-OFDM over the typical urban (TU) six-path COST 207 channel model

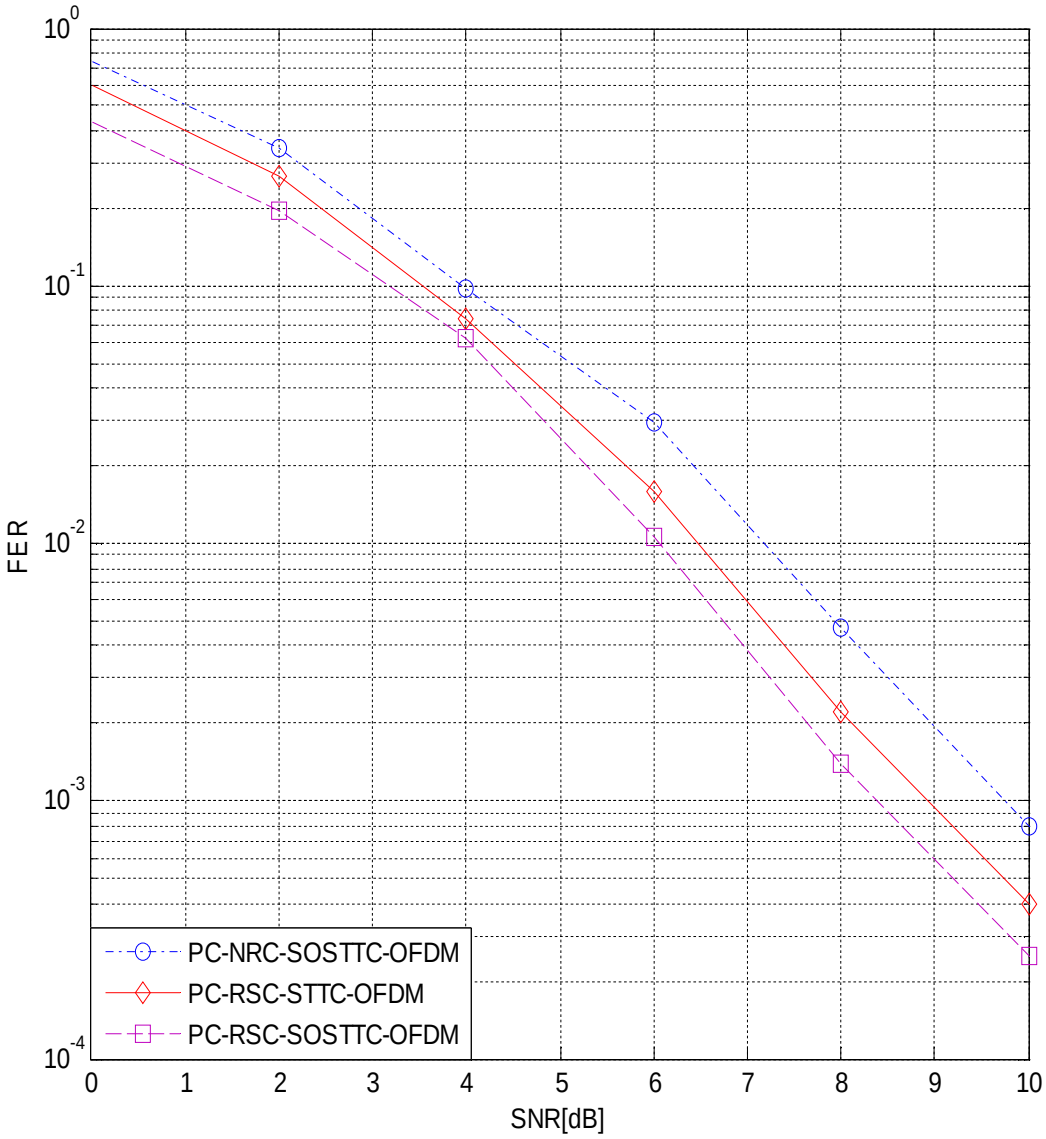

Fig. 5.16: FER performance of PC-NRC-SOSTTC-OFDM, PC-RSC-STTC-OFDM and PC-SOSTTC-OFDM over the two-ray channel model

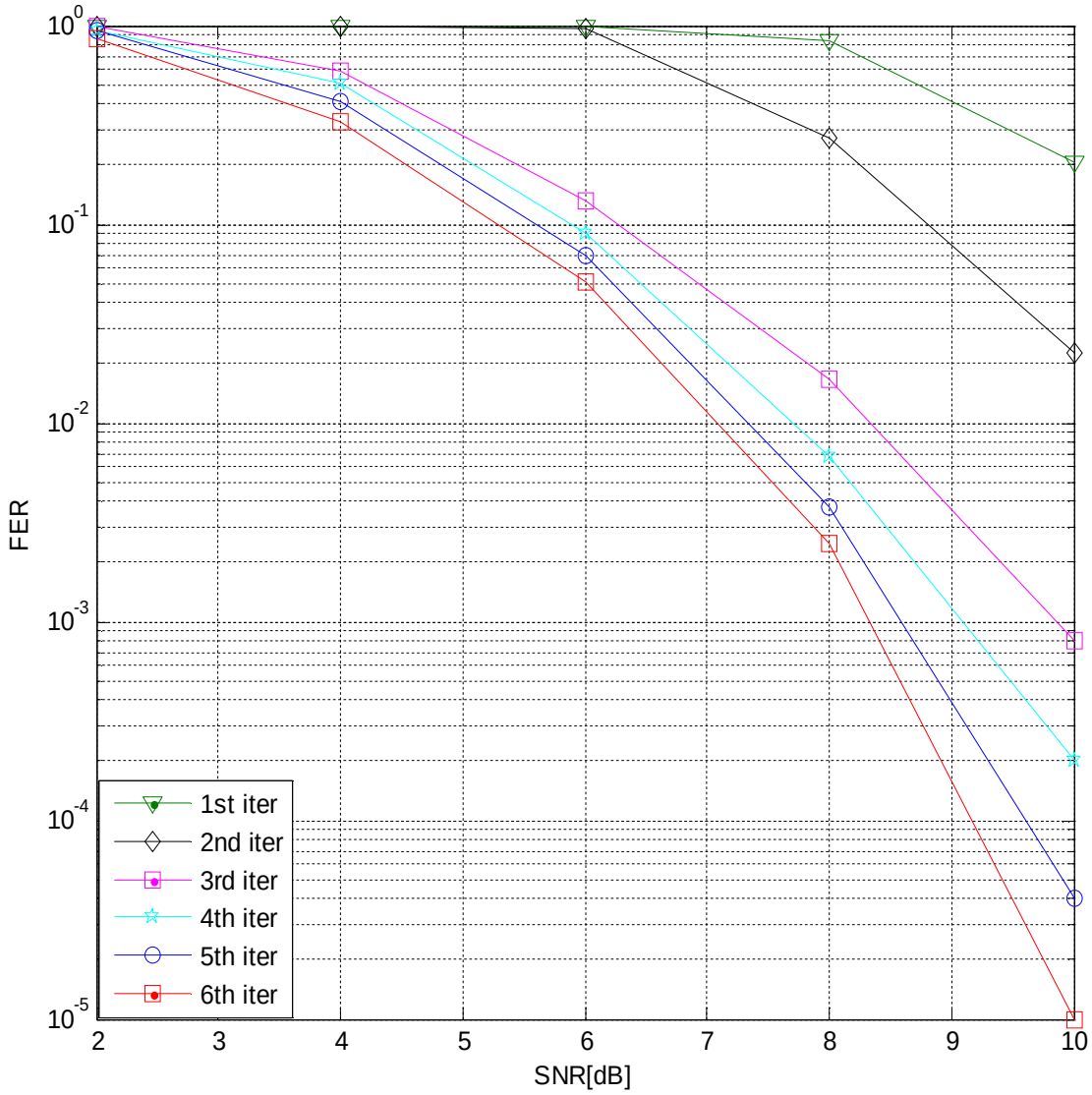

Fig. 5.17: FER performance of HC-SOSTTC-OFDM for various numbers of decoding iterations over the typical urban (TU) six-path COST 207 channel model

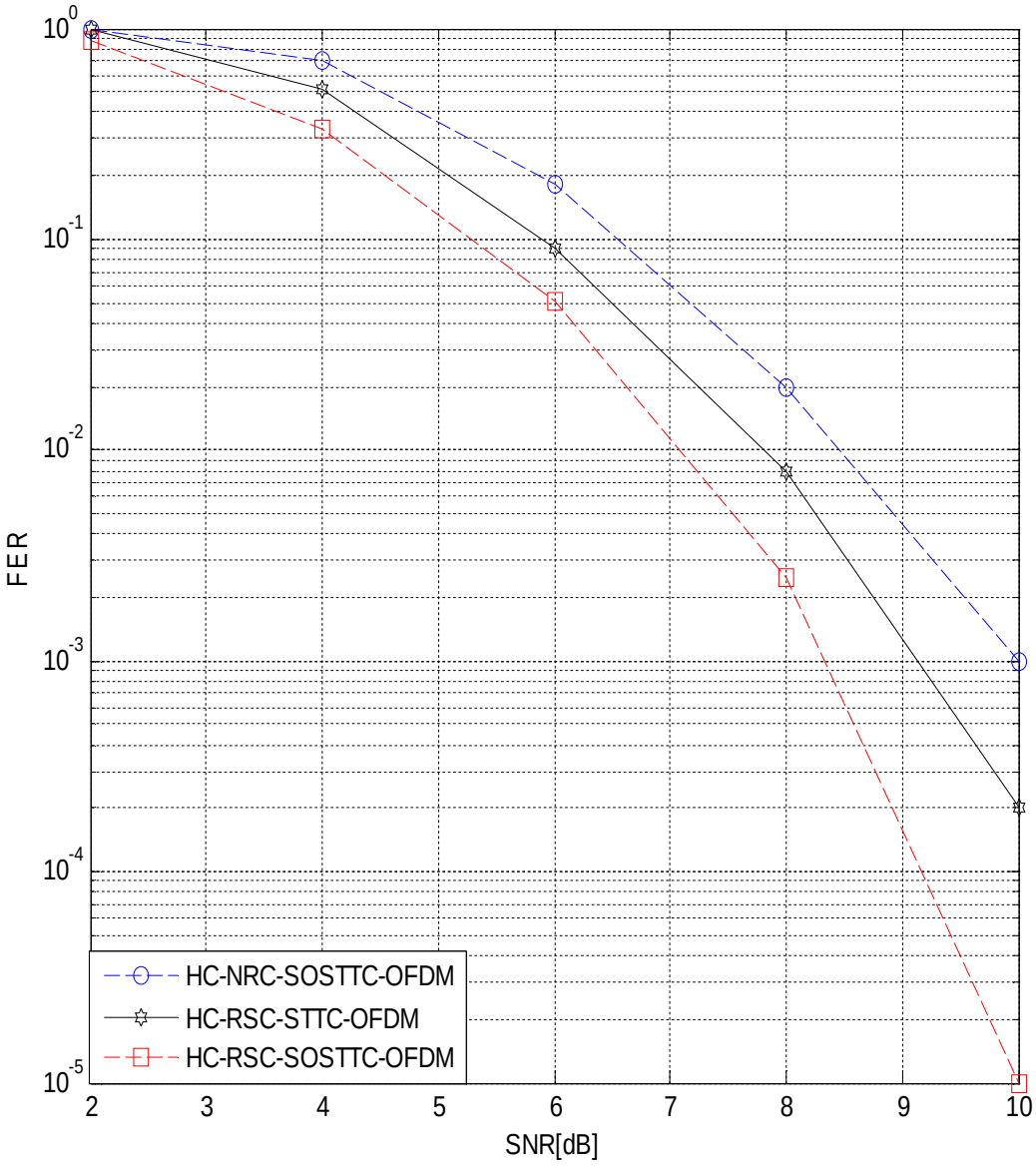

Fig. 5.18: FER performance of HC-NRC-SOSTTC-OFDM, HC-RSC-STTC-OFDM and HC-SOSTTC-OFDM over the typical urban (TU) six-path COST 207 channel model

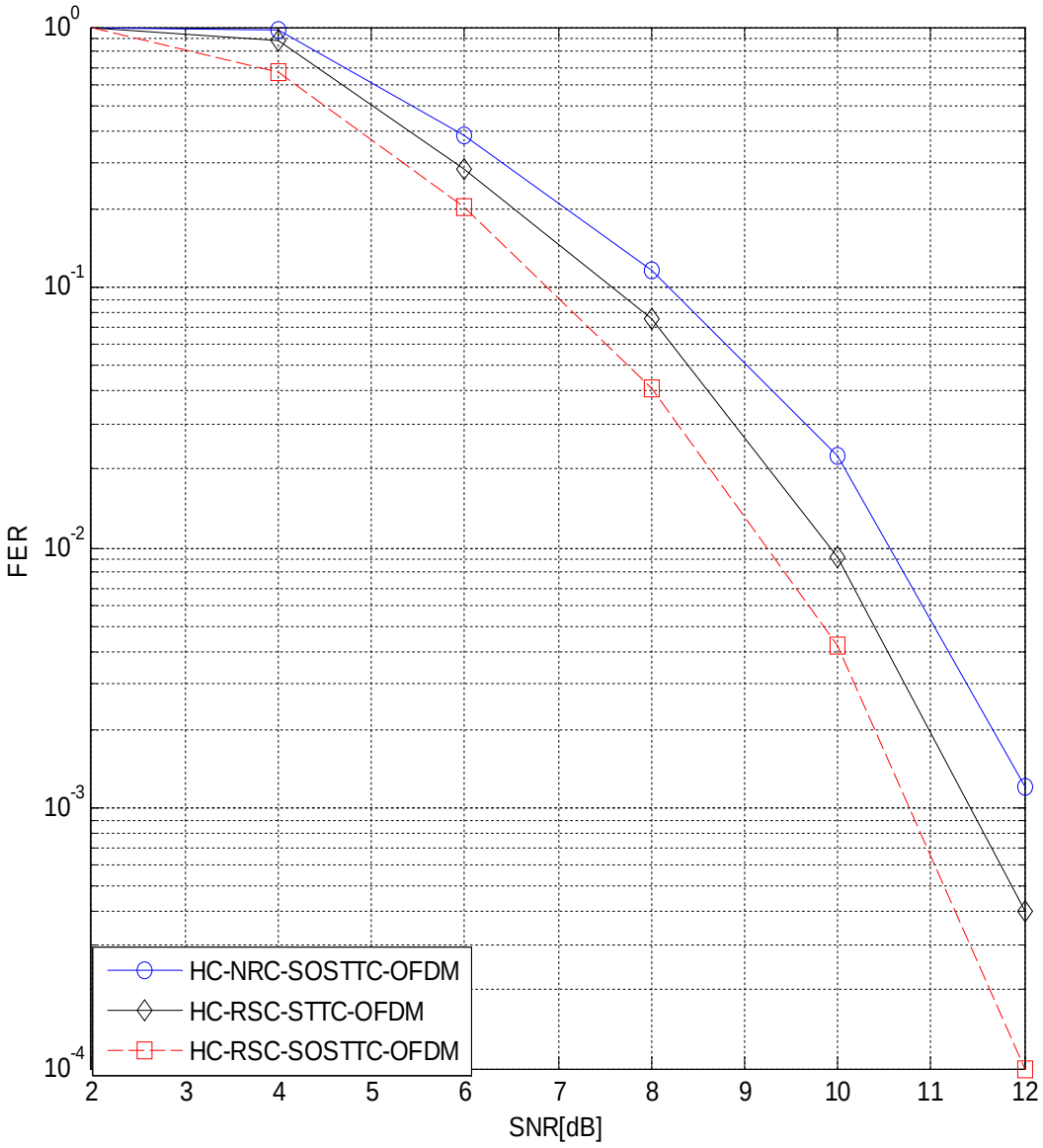

Fig. 5.19: FER performance of HC-NRC-SOSTTC-OFDM, HC-RSC-STTC-OFDM and HC-SOSTTC-OFDM over the two-ray channel model

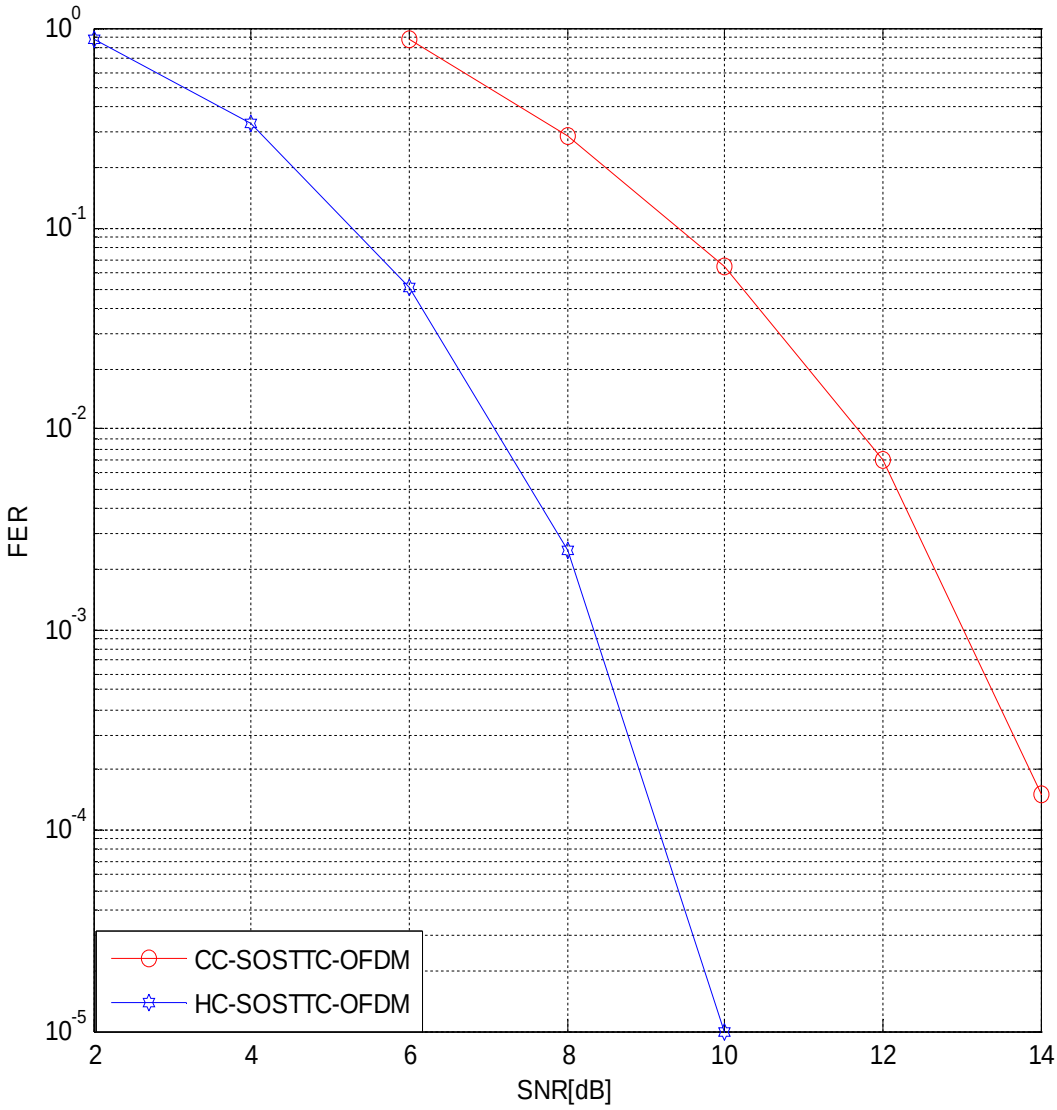

Fig. 5.20: FER performance comparison of CC-SOSTTC-OFDM and HC-SOSTTC-OFDM systems over the typical urban (TU) six-path COST 207 channel model

5.7 Chapter Summary

In this chapter an overview of concatenated convolutional codes was given and recent literature in the field of concatenated space-time coded OFDM systems was reviewed. Four concatenated topologies were proposed over a frequency-selective fading channel with OFDM technique.

The CC-SOSTTC-OFDM system consists of a convolutional outer code concatenated serially with SOSTTC inner code, while the DS-SOSTTC-OFDM system consists of a SCCC outer code with an inner SOSTTC code in an OFDM system. The third and the fourth are an extension of the concatenated schemes that were proposed in chapter 3, but with a different inner code and in an OFDM system. The schemes in chapter 3 employ 4-state SOSTTC from literature while the PC-SOSTTC-OFDM and the HC-SOSTTC-OFDM employ the 16-state SOSTTC designed in chapter 2. In order to exploit multipath diversity, a 16-state SOSTTC was employed as the inner code. The PC-SOSTTC system consists of a PCCC outer code and a SOSTTC inner code, while the HC-SOSTTC system consists of two CC-SOSTTC-OFDMs concatenated in parallel. Each serial combination consists of a CC outer code and a SOSTTC inner code. The system models for these four systems were presented and the encoding and decoding of each was discussed.

The PEP for the four proposed schemes was derived for frequency-selective Rayleigh fading channels and it was shown that the achievable diversity order of the concatenated schemes depends on d_{free} of the outer convolutional codes. The complexities of the four schemes were calculated together with their memory requirements, and these were compared with those of un-concatenated SOSTTC-OFDM systems. It was shown that the concatenation resulted in higher complexity and memory requirements but with much lower FER and high coding gain.

Simulation results were presented for the four schemes under two channel conditions, namely the typical urban (TU) COST 207 channel model and the two-path uniform power delay profile. Both RSC and NRC outer codes were considered for each of the proposed architectures. Comparative simulation results were also presented for each of the schemes with an STTC inner code and the un-concatenated SOSTTC-OFDM system. Simulation results showed that the schemes with RSC outer code presented a

lower FER because the recursive outer code benefited from interleaving gain in iterative decoding. Also, it was shown that the scheme with inner SOSTTC presented higher coding gain than the scheme with inner STTC because of the inherent better coding gain of SOSTTC. It was also shown that, at higher SNR, the PC-SOSTTC-OFDM scheme suffers from an error floor.

In all, the proposed schemes were shown to exploit the multi-path diversity of frequency-selective fading channels. The HC-SOSTTC-OFDM presented the lowest FER among the four schemes but also had the highest complexity among all the schemes that were proposed.

CHAPTER 6

TURBO SUPER ORTHOGONAL SPACE-TIME TRELLIS CODED OFDM SYSTEM

6.0 Introduction

Combining ST codes and turbo coding techniques is a natural way of improving the error performance of ST codes in MIMO fading channels. In this chapter, a Turbo-SOSTTC-OFDM system for MIMO-OFDM systems over wideband frequency-selective fading channels is proposed. The scheme, which is a parallel concatenation of SOSTTC, combines the field of SOSTTC and turbo coding to achieve a high diversity order by exploiting the multipath diversity advantage of frequency-selective fading channels. It also achieves high coding gain by the turbo principle.

First, an overview of recent literature involving turbo-space-time coding is given in Section 6.1. The system structure detailing the encoding and the decoding process of the concatenated trellis-coded MIMO-OFDM system is given in Section 6.2, and the performance of the proposed scheme is evaluated under various channel conditions by computer simulations in Section 6.3.

6.1 Recent Literature

Several space-time turbo coding schemes have been proposed in recent years. In [92], the recursive structure of STTC and the parallel concatenated encoder were introduced. The resulting scheme from [92] was a half-rate code because there was no puncturing of the coded symbols. Bandwidth efficient space-time turbo trellis coding schemes were developed in [86-88], [90], [157-163]. The bandwidth-efficient code consists of two recursive STTC concatenated in parallel. The schemes in [86] and [157] employed symbol interleaving and alternative parity symbol puncturing in constructing the coded sequence while bit interleaving and information puncturing were employed in [90]. It was shown that employing bit interleaving presents better error performance than using symbol interleaving. In [162], the constituent codes of the turbo STTC were constructed

by choosing the feed-forward coefficients to maximize the minimum square Euclidean distance and the feedback coefficient to minimize the iterative decoding threshold. In [164], the turbo coding principle was extended to parallel concatenation of two SOSTTCs to form the Turbo-SOSTTC scheme over a flat-fading channel. In this chapter, the Turbo-SOSTTC-OFDM for MIMO-OFDM over a frequency-selective fading channel is proposed and its performance evaluated over various channel scenarios.

6.2 System Model

In this section the encoding and the decoding system model for the Turbo-SOSTTC-OFDM system is described.

6.2.1 Encoding System Model

The encoder structure of the Turbo-SOSTTC-OFDM with two transmit antennas is shown in Fig. 6.1, consisting of two SOSTTC encoders with the transmission matrix given by (2.18). The 16-state SOSTTC presented in Section 2.6 is considered as the constituent codes. Each encoder operates on a message block of *b* information bits. The upper SOSTTC encoder in Fig. 6.1 maps the input sequence into streams of QPSK symbols according to the transmission matrix of (2.18). Prior to encoding by the lower encoder, the information bits are permuted by the random bit interleaver. The lower encoder also produces streams of QPSK symbols according to (2.18). The upper and the lower QPSK sequences from each of the encoders are multiplexed and thereafter converted to a parallel sequence upon which inverse fast Fourier transform (IFFT) is performed. The multiplexing is done in parallel across antennas so that at one time instant, one of the encoders has full access to two transmit antennas. Cyclic prefix (CP) is added to the symbol stream before transmission from each of the antennas in order to prevent inter symbol interference (ISI) which is produced by the multipath delay of the channel. The coding rate of the turbo encoder is 0.5 but it is possible to obtain a coding rate of one by alternate puncturing of the output of each of the SOSTTC encoders before the multiplexing operation.

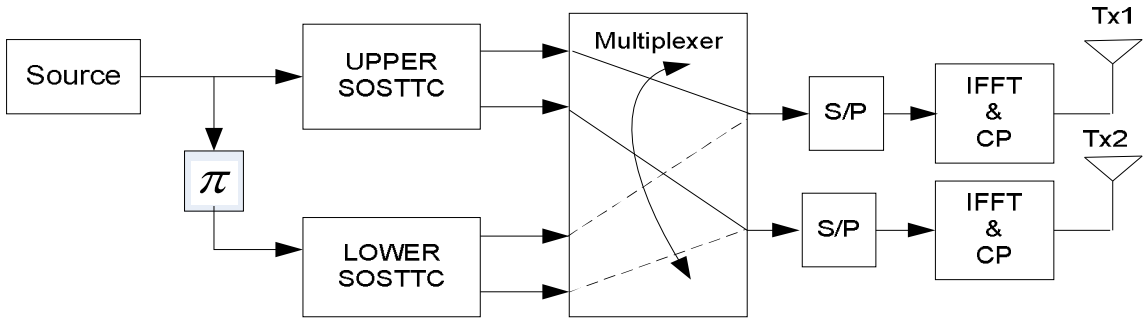

Fig. 6.1: Encoder block diagram of the Turbo-SOSTTC-OFDM system [165]

6.2.2 Decoding System Model

The decoder structure of the Turbo-SOSTFTC-OFDM is shown in Fig. 6.2. The inserted CP is first removed and fast Fourier transform (FFT) is performed on each of the symbols. The parallel symbols are converted to serial stream and de-multiplexed by the de-multiplexer. The iterative decoding process for the symbol-by-symbol log-MAP algorithm for the Turbo-SOSTTC-OFDM is similar to that of the Turbo-STTC [9] and Turbo-SOSTTC [164]. With the log-MAP decoder, the logarithm of the probability is computed and passed to the next decoding stage. Both systematic and extrinsic information is exchanged between the two component decoders.

Given that a single super-orthogonal symbol matrix denoted by $\boldsymbol{x}(k)$ is transmitted by a single OFDM subcarrier, then transmission of $\boldsymbol{x}(k)$ results in the reception of $\boldsymbol{r}(k)$ at the receiver, given by

$$\boldsymbol{r}(k) = \boldsymbol{x}(k)\boldsymbol{H}(k) + \boldsymbol{n}(k), \tag{6.1}$$

the input Log-Likelihood Ratio (LLR) $\lambda(c_{\mathrm{st}}(k), I)$ is computed according to [100]

$$\lambda_{\mathrm{st}}(\mathrm{c}(k), I) = \log \frac{\Pr[\mathbf{x}|\mathbf{r}(\mathrm{k})]}{\Pr[\mathbf{x}_0|\mathbf{r}(\mathrm{k})]}, \tag{6.2}$$

except that instead of a single symbol, we have symbol matrix $\boldsymbol{x}$ and any reference $\boldsymbol{x_0}$ given by (2.18). This input LLR is de-multiplexed into $\lambda(c_{\mathrm{st1}}(k), I)$ and

$\lambda(c_{\mathrm{st2}}(k), I)$ which corresponds to the input LLR for the SOSTTC1 and SOSTTC2 Soft-Input Soft-Output (SISO) module respectively. If the subcarrier index *k* is dropped for simplicity of description, the joint extrinsic and systematic information of the first log-Map decoder denoted as λ can be obtained as

$$\hat{\lambda}(u_{\mathrm{st1}}, O) = \lambda(u_{\mathrm{st1}}, O) - \lambda(u_{\mathrm{st1}}, I), \tag{6.3}$$

where $\lambda(u_{\mathrm{st1}}, I)$ is the de-interleaved joint extrinsic and systematic information of the second log-Map decoder. The extrinsic LLR $\hat{\lambda}(u_{\mathrm{st1}}, O)$ is used as the estimate of the *a priori* probability ratio at the next decoding stage. After de-interleaving, it is denoted by$\lambda(u_{\mathrm{st2}}, I)$. The joint extrinsic and systematic information from the second encoder is given by

$$\hat{\lambda}(u_{\mathrm{st2}}, O) = \lambda(u_{\mathrm{st2}}, O) - \lambda(u_{\mathrm{st2}}, I) \tag{6.3}$$

The process is iterated several times and on the final iteration, a decision is taken on the extrinsic LLR λ_2 to determine the estimate of the transmitted information.

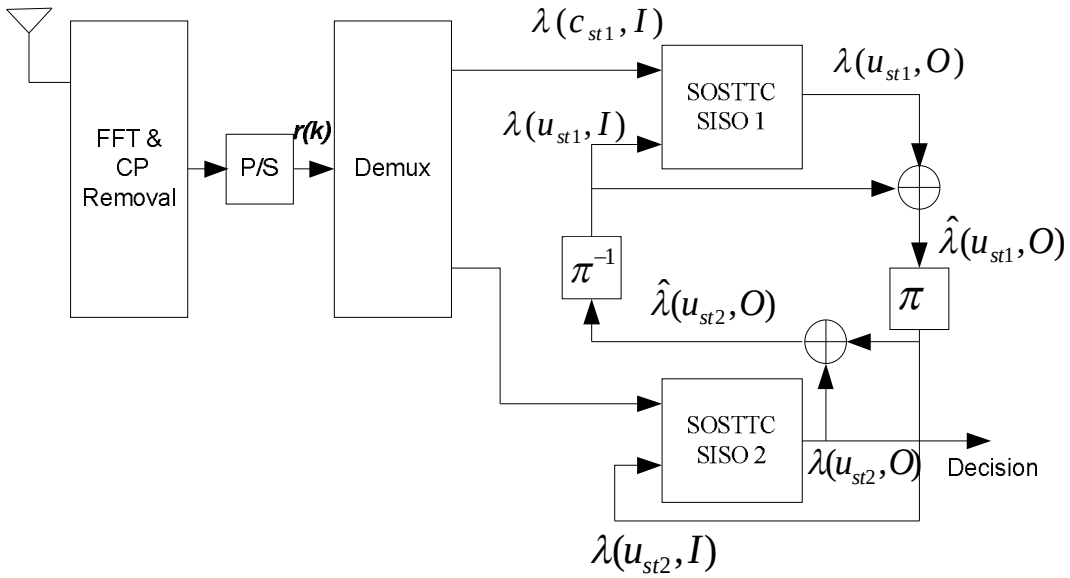

Fig. 6.2: Decoder block diagram of the Turbo-SOSTTC-OFDM system

6.3 Simulation Results and Discussion

In this section, simulation results illustrating the performance of the proposed Turbo-SOSTTC-OFDM scheme over frequency-selective fading channels are provided. For

the simulation, a MIMO-OFDM concatenated scheme equipped with two transmit antennas and one receive antenna is considered. The OFDM modulator utilizes 64 subcarriers with a total system bandwidth of 1 MHz and FFT duration of 80 µs. The system's subcarrier spacing is 15 kHz with symbol duration of 64 µs. Perfect channel state information is assumed at the receiver with perfect timing and frequency synchronization between the transmitter and the receiver. Cyclic prefixes that are equal to or greater than the delay spread of the channel are applied for the OFDM schemes to eliminate ISI. The performance of the system is described by means of frame error rate (FER) versus the receive SNR with QPSK constellation.

The code performance is evaluated in Fig. 6.3 for various numbers of paths. During the simulation, it is assumed that the channel parameters remain constant during the transmission of two consecutive OFDM frames where the taps are equally-weighted, Rayleigh-distributed variables. The FER plot for the system was obtained for six decoding iterations with different number of paths. It can be observed from the FER performance curve, that the diversity order achieved by the proposed system increases with an increase in the number of paths. It should be noted that because of the employed constituent code, the maximum achievable diversity order of the system is four and therefore, increasing the number of taps beyond two will yield no further diversity advantage though it can provide a coding gain advantage.

The proposed scheme's performance is also investigated under the delay spread scenario in Fig. 6.4. The channel in this case is modeled as two paths of equal power with no delay spread, 5 µs delay spread and 40 µs delay spread between the adjacent paths. Increasing the delay spread between the adjacent paths is observed, from the FER plot, to increase the coding gain advantage of the system.

The systems performance is also investigated under a time varying channel in Fig. 6.5. The system performance is evaluated using a typical urban (TU) six-path COST 207 power delay profile channel model. Results for normalized Doppler frequency of 0.02, 0.01, 0.005 and 0.002 which correspond to mobile speeds of 60, 30, 15 and 6 m/s are presented. As seen from the curve, the diversity order of the scheme remains unchanged with variation in mobile speed but the system presents some coding gain advantage at low mobile speeds.

In Fig. 6.6, performance comparison of the proposed Turbo-SOSTTC-OFDM scheme with that of Turbo-STTC-OFDM and Aksoy's SOSTTC-OFDM [51] is presented. For the Turbo STTC-OFDM, the 16-state STTC in [153] is used as the constituent code and the comparison was done under the TU six-path COST 207 channel condition. The Turbo-SOSTTC-OFDM scheme is seen to outperform the Turbo-STTC-OFDM scheme significantly in terms of coding gain with almost the same decoding complexity. The Turbo-SOSTTC-OFDM is also seen to outperform the SOSTFTC-OFDM significantly, but with a loss in bandwidth efficiency and increased decoding complexity.

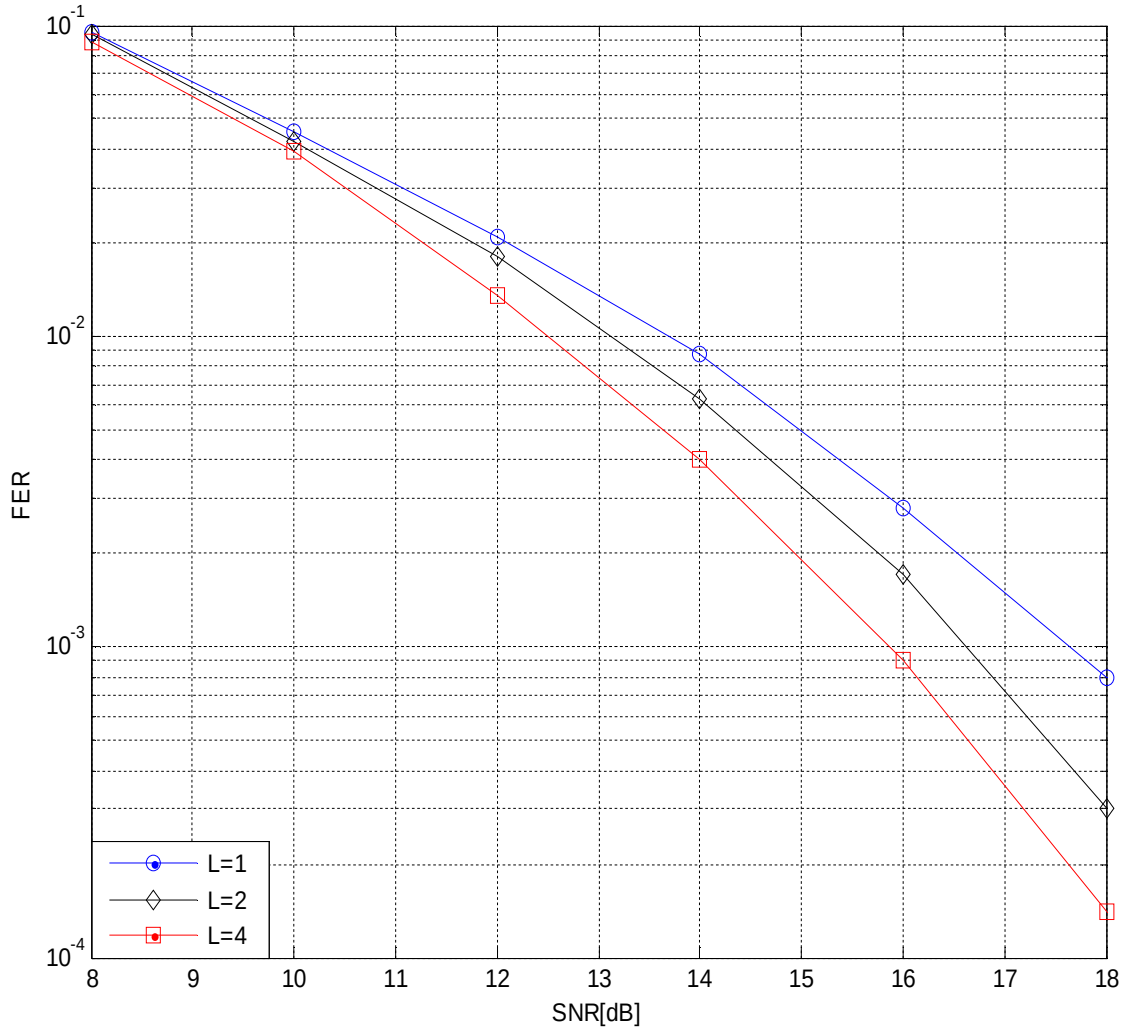

Fig. 6.3: FER performance of the Turbo-SOSTTC-OFDM with various numbers of paths

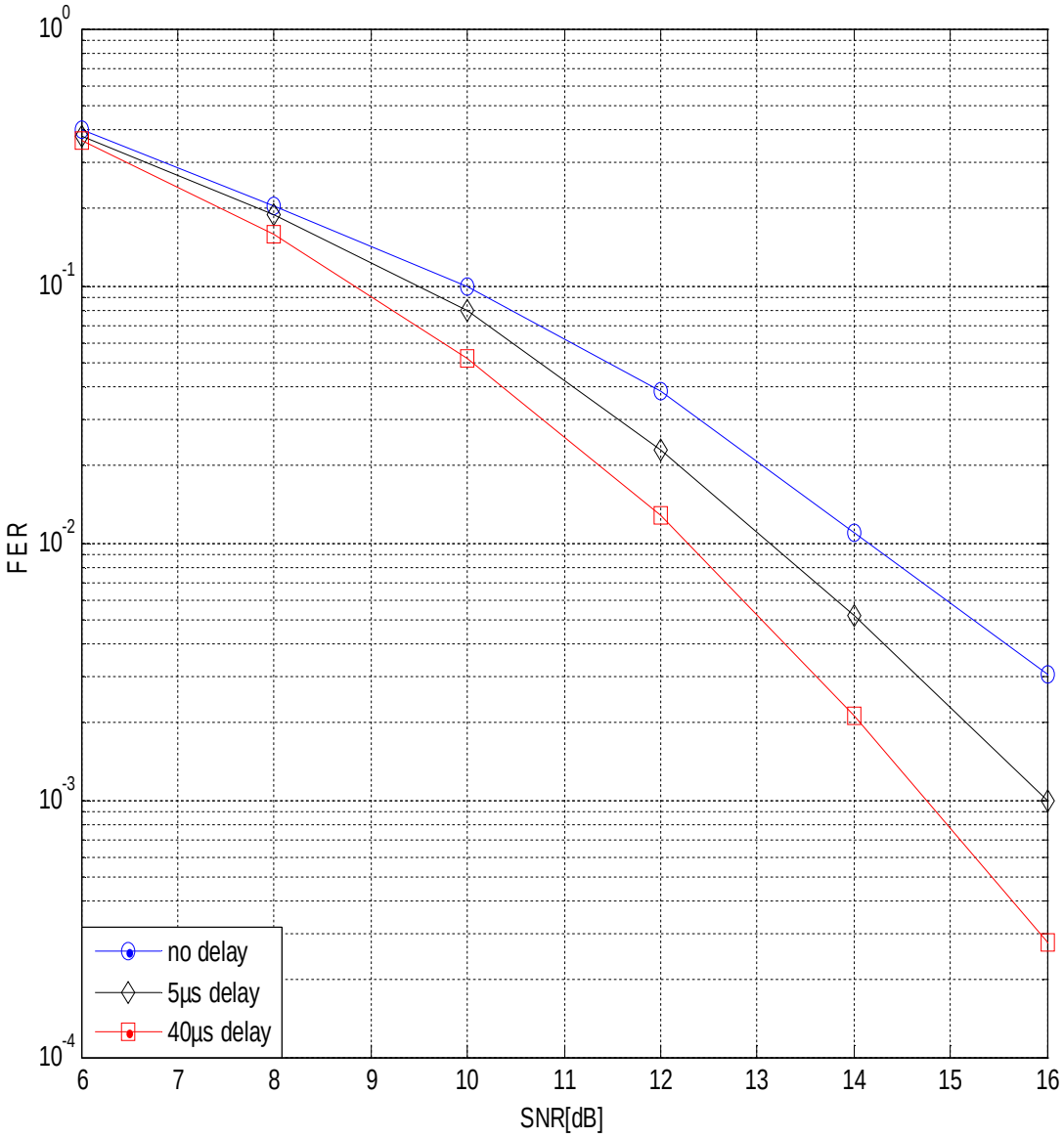

Fig. 6.4: FER performance of the Turbo-SOSTTC-OFDM with delay spread between adjacent paths

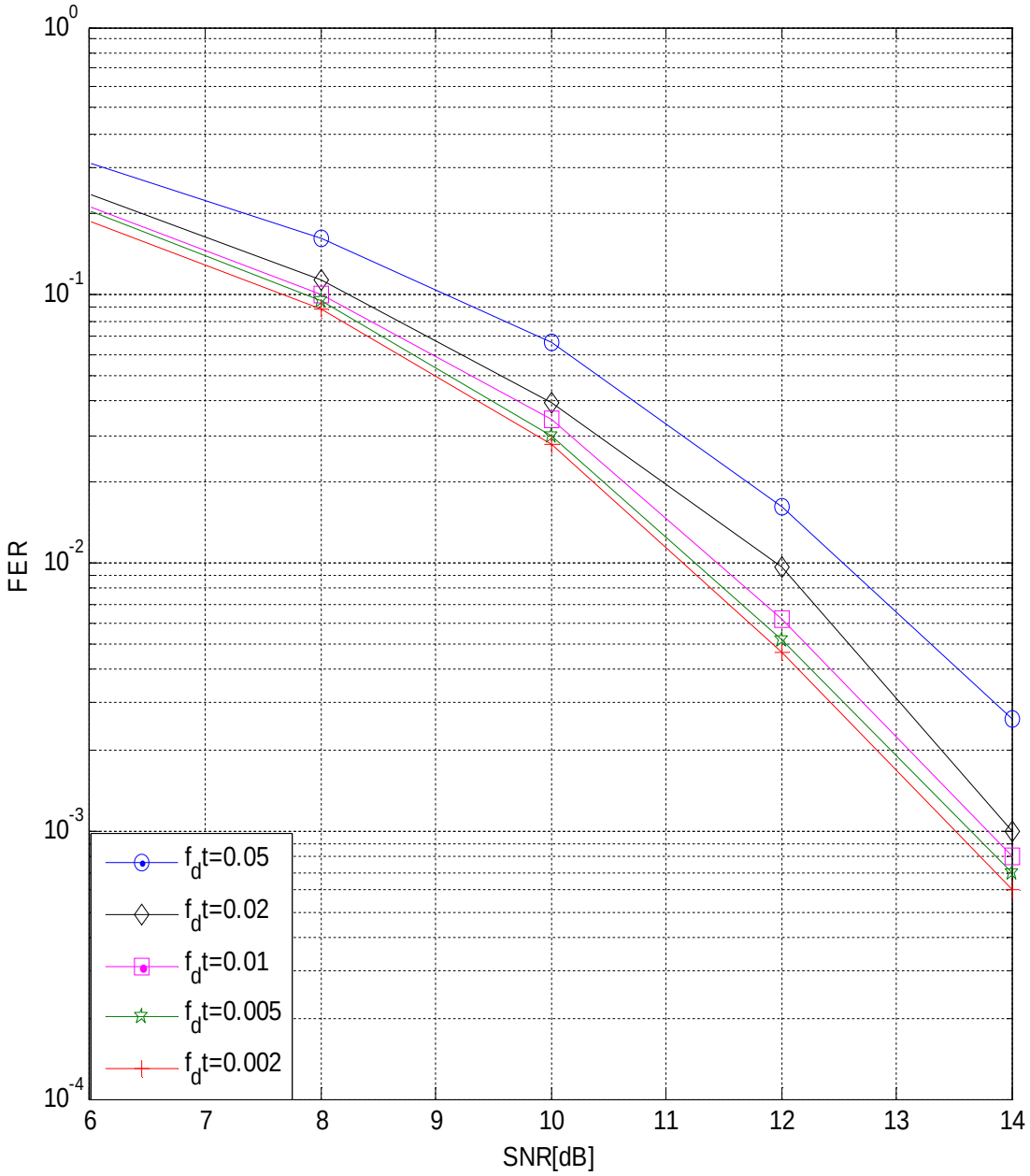

Fig. 6.5: FER performance of the Turbo-SOSTTC-OFDM with variation in mobile speed

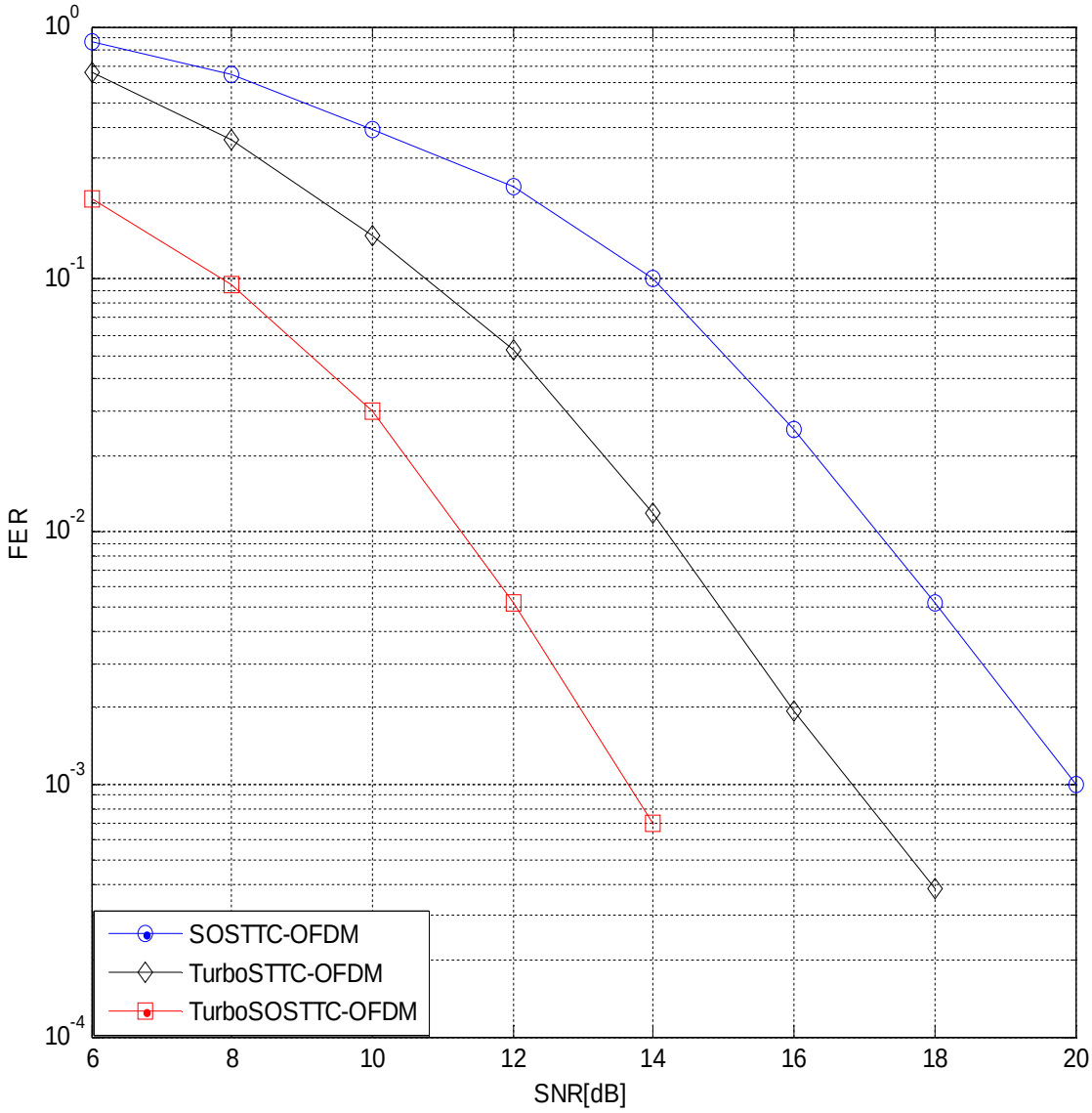

Fig. 6.6: FER performance of the Turbo-SOSTTC-OFDM (1 bit/s/Hz), Turbo-STTC-OFDM (1 bit/s/Hz), and SOSTTC-OFDM (2 bits/s/Hz)

6.4 Chapter Summary

In this chapter, a brief overview of turbo space-time coded systems was given and recent literature on turbo space-time coding and OFDM was reviewed. More importantly, a concatenated scheme for MIMO-OFDM system over a frequency-selective fading channel with only a constituent SOSTTC was proposed. The coding scheme was based on parallel concatenation of two SOSTTCs, interleaving and multiple-transmitter/receiver diversity systems. In order to exploit the multipath diversity advantage presented by the multipath channel, in addition to the spatial and temporal diversity of space-time coding, the 16-state SOSTTC designed in this thesis was employed as the constituent encoder. The system model for the proposed system was presented and the encoding and decoding processes were discussed. The decoding of the constituent codes was explained where the additive bitwise SISO algorithm was used.

Simulation results were presented and the system performance was evaluated over different channel scenarios. Simulation results were presented to determine the effect of the number of channel paths, delay spread and mobile speed on the system's performance. It was shown that the system exploited the multipath diversity of frequency-selective fading channels resulting in an increase in the diversity order when the number of channel paths increased. Also, it was shown that the diversity order of the scheme is preserved under the various mobile speeds. A comparative simulation result was provided for the case of concatenation involving STTC and un-concatenated SOSTTC-OFDM systems. The proposed scheme was shown to achieve substantial coding gain advantage over the uncoded counterpart and the scheme with STTC but with the same diversity order. The scheme achieves a high diversity order by exploiting available diversity resources provided by the frequency-selective fading channel and achieves high coding gain through turbo coding.

CHAPTER 7

CONCLUSION AND FUTURE WORK

A brief summary of the main contributions and the findings of this thesis are given in this concluding chapter. Suggestions on future research areas are discussed with a brief summary of the possible extensions of this work.

7.1 Conclusion

The design and performance of space-time coding and concatenated codes for MIMO and MIMO-OFDM systems with the objective of increasing the performance of these coding schemes over fading channel was studied in this thesis.

In literature, SOSTTCs are designed based on the rank and the determinant criterion for quasi-static Rayleigh fading channels. However, the performance of SOSTTC over a Nakagami-*m* fading channel was not known. In the first part of the thesis, the performance of SOSTTCs over Nakagami fading channels was investigated. The 16-, 32-, and 64-state SOSTTC from [72] was deployed over the Nakagami-*m* fading channel and it was discovered that the diversity of the SOSTTCs over a Nakagami fading channel is *m*-times the diversity in a quasi-static Rayleigh fading channel. Also, the coding gain achieved by the SOSTTC system in a Nakagami fading channel is a multiple of *m* of the coding gain over a Rayleigh fading channel.

In order to improve the coding gain of SOSTTC in a Rayleigh fading channel, two double concatenated schemes for flat-fading channels with a constituent code of SOSTTC and convolutional codes was proposed. The two topologies include serial concatenation of two parallel concatenated convolutional codes with SOSTTC, while the second involves parallel concatenation of two serial concatenations. In the serial concatenation, convolutional codes are serially concatenated with SOSTTC and the two are concatenated in parallel via an interleaver. The PEP for the two schemes was

derived, and it was shown that in quasi static fading channels, the concatenations add no diversity gain to the system but some coding gain. Over fast-fading channels however, the diversity gain of the concatenated topology is a multiple of the minimum Hamming distance of the outer convolutional code.

The design of space-time codes for MIMO-OFDM systems was also examined. Assuming CSI at the receiver, a rate-1 space-time code capable of achieving high coding gain and multipath diversity was proposed. For the sake of simplicity of designs, the channel was assumed to be quasi-static over two OFDM symbols duration and that the channel changed independently from frame to frame. Two new space-time coded-OFDM systems were proposed, one for two transmit antennas and the other for four transmit antennas. The first one used the rotated constellation concept from [73] and avoided parallel transition in the trellis design which, in the past, had restricted the performance in multipath designs. By proposing the ESOSTTC-OFDM system for 16, 32 and 64 states, the design of SOSTTC proposed in [65] for flat-fading channels was extended to a case of frequency-selective fading channels. Since there is no full-rate orthogonal code for a case of more than two transmit antennas, the SQOSTTC proposed for four transmit antennas for flat fading in [149] was extended for deployment in an OFDM system to give the SQOSTTC-OFDM for four transmit antennas using BPSK signalling. The scheme combined a quasi-orthogonal space-time block code with a trellis code to offer a full-rate, full diversity and high coding gain for four transmit antennas. The design of the SQOSTTC-OFDM was restricted to BPSK signalling because parallel transitions using QPSK modulation would require at least 256 trellis states which would make the system very complex.

SOSTTC-OFDM provides lower coding gain over frequency-selective fading channels. In order to further improve the coding gain of SOSTTC-OFDM, therefore, five concatenated schemes with constituent code of SOSTTC and convolutional code were also proposed for MIMO-OFDM systems. The system model together with the encoding and the decoding process of the various topologies were described in detail. The first topology involved a serial concatenation of convolutional code with inner SOSTTC for two transmit antennas while the second scheme which is also a serial concatenation involved serial concatenation of two outer convolutional codes with an inner SOSTTC. The third architecture involved two convolutional codes concatenated in parallel with SOSTTC in serial concatenation.

In the fourth scheme, two serial concatenations involving an outer convolutional code and an inner SOSTTC code were concatenated in parallel. The fourth scheme, called Hybrid SOSTTC-OFDM involved four transmit antennas and two receive antennas. All the propositions employed iterative decoding providing high coding gain and exploiting the multipath diversity of frequency selective fading channels. The PEP analysis and simulation results over various channel scenarios showed that the inbuilt diversity gain of the inner SOSTTC is multiplied by d_{free} of the outer convolutional code which determined the diversity order of the proposed schemes for MIMO-OFDM system. All the proposed schemes employed the MAP-log decoding algorithm and the decoding complexities of each of the topologies were calculated.

The turbo coding principle was also extended into parallel concatenation of two SOSTTCs for an MIMO-OFDM system. In this topology, bit interleaving was employed and the resultant code rate was halved. The scheme combines the coding gain benefits provided by turbo coding with the diversity advantage of SOSTTC and the bandwidth efficiency of coded modulation. The Turbo SOSTTC-OFDM offers improved coding gain over the conventional SOSTTC-OFDM system but no additional diversity is offered by the concatenations. The scheme without puncturing achieves higher coding gain but with half rate.

7.2 Future Work

Likely future pieces of work that extend the proposals presented in this thesis are hereby recommended. In the analysis that was done for the design of the space-time coded system, perfect channel estimation at the receiver was assumed. In reality, channel estimation is not perfect. In broadband wireless systems, the estimation error cannot be ignored because the number of training pilot symbols is limited as this has an impact of decreasing spectral efficiency. It would therefore be interesting to analyze the effect of channel estimation errors on the space-time trellis code OFDM system.

It was also assumed that no spatial correlation exists between the antennas. If there is spatial correlation, it is possible to analyze what happens with the error probability in order to derive the boundaries and design criteria for space-time coded OFDM with spatial correlation.

All the proposals in this thesis were designed for single-user systems only. For multiple access channels, the single-user space-time coded-OFDM is commonly applied to each user independently. There is little research on multi-user space-time coded OFDM systems designed for frequency-selective fading channels. Therefore, designing full diversity multi-user space-time coded OFDM for future broadband wireless systems would be an interesting area of research. Similarly, designing an ESOSTTC-OFDM-IDMA system for future high-rate multi-user communications over multi-path fading channels would also be interesting.

All the proposals in this thesis exploited the available spatial and frequency diversity over frequency-selective fading channels. In some situations however, the use of multiple antenna systems may be impractical because of the size and cost of the broadband mobile terminal. To overcome this, cooperative diversity has recently been proposed in which diversity gain is achieved via the cooperation of nodes. Cooperative diversity allows virtual antenna array to achieve spatial diversity gain in a distributed manner. This is obviously a new area, where the design of coding schemes which is able to exploit diversity at the space, time and frequency domain is necessary.

In the second part of the thesis, several concatenated topologies with constituent code of SOSTTC and CC for MIMO-OFDM were proposed. Variable length error correcting code (VLEC) is similar to block error correcting code in which a source symbol with a different length is mapped to a codeword. In VLEC, shorter codewords are assigned with the more frequent symbols. The design of VLEC codeword guarantees a minimum free distance and VLEC with a larger free distance has stronger error resilience capability. Extending the concatenated topology to a case of VLEC and SOSTTC for MIMO-OFDM would be interesting.

Low Density Parity Check (LDPC) code achieves great coding gain in AGWN channels. Extending the concatenated schemes to involve LDPC codes and SOSTTC in different topologies would also be an interesting area of research.

REFERENCES

[1] H. Jafarkhani, *Space-Time Coding, Theory and Practice.* New York : Cambridge University Press, 2005.

[2] *4G/IMT Advanced.* [Online] [Cited: 06 07, 2011.] http://www.4gamericas.org.

[3] *IMT-Advanced (4G) Mobile wireless broadband on the anvil New ITU radio interface standards to revolutionize mobile communication.* [Online] 2009. [Cited: 06 07, 2011.] http://www.itu.int/newsroom/press_releases.

[4] D. Tse, *Fundamental of Wireless Communications.* New York : Cambridge University Press, 2005.

[5] B. Sklar, "Rayleigh fading channels in mobile digital communication systems, Part I: Characterization,". *IEEE Commun. Magazine.* vols. 35, no.7 pp.90-100, July 1997.

[6] T. S. Rappaport, *Wireless Communication Principles and Practice.* New York : Prentice Hall, 1996.

[7] C. Oestage and B. Clerclex, *MIMO Wireless Communication; from real world propagation to space-time coding Design.* U.k : Elsevier Ltd, 2007.

[8] T. S. Rappaport, *Wireless Communication; Signal Processing Perspective.* U.K : Prentice Hall, 1998.

[9] B. Vucetic and J. Yuan, *Space-Time Coding.* John Willey and Son, 2003.

[10] C.-E.W. Sunberg and N. Seshadri, “Digital cellular systems for North America," *in proc. IEEE Global Telecommunications Conference, 1990, and Exhibition. 'Communications: Connecting the Future', (GLOBECOM '90),* pp.533-537 vol.1, 2-5 Dec 1990

[11] N. Balaban and J. Salz, "Dual diversity combining and equalization in digital cellular mobile radio," *IEEE Trans. Veh. Tech.*. vol. 40, pp. 342-354, May 1994.

[12] J. Winter, J. Salz and R.D. Gitlin, "The impact of antenna diversity on the capacity of wireless communication," *IEEE Trans. Commun.* vol .42. pp. 1740-1751, Feb. /Mar. /Apr. 1994.

[13] E. Telatar, "Capacity of multi-antenna Gaussian channels," *European Trans. on Telecommun,* . vol. 10, no. 6, pp. 585-595, Nov/Dec 1999.

[14] G. J. Foschini and M. J. Gans, "On limits of wireless communication in a fading environment when using multiple antennas," *Wireless Personal Commun.* vol. 6, no. 3, pp. 311-335, 1988.

[15] C. Shannon, "A mathematical theory of communications," *ACM SIG Mobile Computing and Communication Review.* vol. 5, no. 1, pp. 3-55, 2001.

[16] V. Tarokh, N. Seshadri, and A. R. Calderbank, "Space-time codes for high data rate wireless communication: performance criterion and code construction," *IEEE Trans. Info. Theory.* vol. 44, pp. 744–765, Mar. 1998.

[17] R. W. Chang**,** "Synthesis of band-limited orthogonal signals for multichannel data transmission," *Bell system Technical Journal.* vol. 45, pp. 1775-1776, Dec. 1966.

[18] B. R. Saltzberg, "Performance of an efficient parallel data transmission system," *IEEE Trans. Commun.* vol. 15, pp. 805-811, Dec 1967.

[19] L. Hanzo, M. Munster, B. J Choi, and T. Keller, *OFDM and MC-CDMA for Broadband Multi-user Communications, WLANs and Broadcasting.* Chichester: IEEE Press and John Wiley & Sons, Ltd., 2003.

[20] R. W. Chang and R. A. Gibby, "A theorectical study of performance of an orthogonal multiplexing data transmission scheme," *IEEE Trans. Commun.* vol. 16, pp. 529-540, Aug. 1968.

[21] Chang, R. W, *Orthogonal Frequency Division Multiplexing. 3,488,445* USA, January 6, 1970.

[22] S. B. Weinstein and P. M. Ebert, "Data transmission by frequency-division multiplexing using disrete Fourier transform," *IEEE Trans. Commun.* vol. 19, pp. 628-634, Oct.1971.

[23] L. J. Cinimi Jr, "Analysis and simulation of a digital mobile channel using orthogonal frequency division multiplexing," *IEEE Trans. Commun.* vol. 33, pp. 665-675, July 1985.

[24] I. Kalet, "The multitone channel," *IEEE Trans. Commun.*, vol. 37, pp. 119-124, Feb. 1989.

[25] K. Fazel and G. Fettweis, *Multi-carrier Spread Spectrum and Related Topics,*. MA: Kluwer, 2000.

[26] A. J. Vertibi CDMA, *Principle of Spread Spectrum Commuincation.* Reading : M.A: Addison-Wesley, 1995.

[27] R. Steele and L. Hanzo, *Mobile Radio Communications: Second and Third Generation Cellular and WATM Systems.* New York : IEEE Press and John Wiley &Sons. Inc., 2nd edn, 1999.

[28] L. Hanzo, L. -L. Yang, E. -L. Kuan, and K. Yen, *Single- and multi carrier DS-CDMA: Multi user detection, space-time spreading, synchronization and standards.* Chichester : IEEE Press and John Wiley & Sons, Ltd, 2003.

[29] L. E. Miller and J. S. Lee, *CDMA System Engineering Handbook.* London : Artech House, 1998.

[30] J. S. LEE "Overview of the technical basis of QUALCOMM's CDMA cellular telephone system design: a view of North American TIA/EIA IS-95," *In proc. Inter. Conf. Commun. Systems (ICCS), (Singapore),* pp. 353-358, 1994.

[31] K. Zigangirov, *Theory of Code Division Multiple Access Commuincation.* New York: IEEE Press and John Wiley& Sons, Inc., 2004.

[32] P. Xia, S. Zhou and G. B. Giannakis, "Bandwidth- and power- efficient multicarrier multiple access," *IEEE Trans. Commun.* vol. 51, pp. 1828- 1837, Nov. 2003.

[33] Z. Cao, U. Tureli and Y. Yao, "Deterministic multiuser carrier-frequency offset estimation for interleaved OFDMA uplink," *IEEE Trans. Commun.* vol. 52, pp. 1585-1594, Sept. 2004.

[34] A. Peled and A. Ruiz, "Frequency domain data transmission using reduced computational complexity algorithm," *In proc. IEEE International Conf. on Acoustic, Speech, and Signal Process.(ICASSP'80), (Denvar, USA), vol.* 5, pp. 964-967, 9-11 April 1980.

[35] T. May, H. Rohling and V. Engels, "Performance analysis of Viterbi decoding for 64-DAPSK and 64-QAM modulated OFDM signals," *IEEE Trans. Commun.* vol. 46, pp. 182-190, Feb. 1998.

[36] L. Lin, L. J. Cimini Jr., and C.-I. Chuang, "Comparison of convolutional and turbo codes for OFDM with antenna diversity in high-bit-rate wireless application," *IEEE Commun., Letters.* vol. 9, pp. 277-279, Sept. 2000.

[37] P. H. Moose, "A technique for orthogonal frequency division multiplexing frequency offset correction," *IEEE Trans. Commun.*, vol. 42, pp. 2908-2914, Oct. 1994.

[38] *European Telecommunications Standards Institute, Digital Audio Broadcasting (DAB); DAB to mobile, portable and fixed Receivers.* s.l. : ETSI ETS 300 401 ed.1, Feb 1995.

[39] *European Telecommunications Standards Institute, Digital Video Broadcasting (DVB); Framing structure, channel coding and modulation for digital terrestrial television (DVB-T).* ETSI ETS 300 744 ed. 1., March 1997.

[40] *European Telecommunications Standards Institute, Digital Video Broadcasting (DVB); Transmission system for handheld terminals (DVB-H)* ,ETSI EN 302 304 V1.1.1, Nov 2004.

[41] *European Telecommunications Standards Institute, Radio Equipment and System (RES); HIgh PErformance Radio Local Area Network (HIPERLAN) Type 1; Functional Specification,* ETSI ETS 300 652 ed. 1, Oct. 1996.

[42] *European Telecommunications Standards Institute, Broadband Radio Access Network (BRAN); Inventory of broadband radio technologies and techniques.* ETSI TR 101 173 V1.1.1, May 1998.

[43] M. Jankiraman, *Space-Time Codes and MIMO Systems.* Artech House, Inc., Norwood, 2004.

[44] A. F. Naguib, N Seshadri and A.R. Calderbank, "Increasing data rate over wireless channels," *IEEE signal process. magazine.* vol. 17, no. 3, pp. 76-92, May 2000.

[45] H. Bolcskel, "MIMO-OFDM wireless systems: Basic, perspectives and challenges," *IEEE Trans. Wireless Commun.,*vol. 13.pp. 31-37, 2006.

[46] W. Su, Z. Safar, K. Liu, "Towards maximum achievable diversity in space, time, and frequency: peformance analysis and code design," *IEEE Trans. Wireless Commun.,* vol. 4, no. 4, pp. 1847-1857, 2005,

[47] B. Lu and X. Wang, "A space-time trellis code design method OFDM systems," *Wireless Per. Commun.,* vols. 24, pp.403-418, 2003.

[48] D. Agrawal, V. Tarokh, A. Naguib and N. Seshadri, "Space-time coded OFDM for high data-rate wireless communication over wideband channels," *in proc. IEEE Conf. Vehicular Tech.* pp. 2232-2236, 1998.

[49] Y. Gong and K. Letaief, "An efficient space-frequency coded OFDM system for broadband wireless commuincation," *IEEE Trans. Commun.,* vol. 51. no. 11, pp. 2019-2029, 2003.

[50] Z. Liu, Y. Xin and G.B. Giannakis, "Space-time frequency coded OFDM over frequency selective fading channels," *IEEE Trans. on Signal Process., vol*. 50, no.10, pp.2465-2476, 2002.

[51] K. Aksoy and U. Aygolu, "Super-orthogonal space-time frequency trellis coded OFDM," *IET Commun.* vol. 1 no 3, pp. 317-324, 2007.

[52] B. L. Hughes, "Differential space-time modulation," *IEEE Trans. Info. Theory.* vol. 46, no. 7, pp. 2567-2578, Nov. 2000.

[53] J. G. Proakis and M. Salehi, *Digital Communications.* New York, NY, USA : Mc Graw- Hill 5th edition, 2008.

[54] K. Shr, Y. Huang. Kai-Ting Shr and Yuan-Hao Huang, "Low-complexity branch metric calculation for space-time trellis decoding," *in Proc. Asia-Pacific Conf. Commun., APCC 2007,* pp.73-76, 18-20 Oct. 2007.

[55] D. M. Ionescu, "On space-time code design," *IEEE Trans. Wireless Commun.,* vol. 2, no.1, pp. 20- 28, Jan. 2003.

[56] D. M. Ionescu, K. K. Mukkavilli, Y. Zhiyuan, J. Lilleberg, "Improved 8- and 16-state space-time codes for 4PSK with two transmit antennas," *IEEE Commun. Letters.* vol. 5, no.7, pp.301-303, July 2001.

[57] A. Viterbi, "Convolutional codes and their performance in communication systems," *IEEE Trans. Commun. Tech.* vol. 19, no.5, pp.751-772, Oct. 1971.

[58] G. D. Forney, Jr., "The Viterbi algorithm," *Proceeding of the IEE,.* vol. 61, no. 3, pp. 268-278, March 1973.

[59] H. L. Lou, "Implementing the Viterbi algorithm: Fundamental and real-time issues for processor designers," *IEEE Signal processing Magazine.* pp. 42-52, Sept. 1995,.

[60] S. M. Alamouti, "A simple transmitter diversity scheme for wireless communications," *IEEE J. Sel. Area Commun.,* vol. 16, pp. 1451-1458, Oct.1998.

[61] L. Hanzo, T. H. Liew, B. L Yeap, *Turbo Coding,Turbo Equalization and Space-Time Codes for Transmission in Fading Channels.* Chichster, England : John Wiley and Sons, 1st Edition, 2002.

[62] V. Tarokh, H. Jafarkhani, and A. R. Calderbank, "Space-time block codes from orthogonal designs," *IEEE Trans. Inf. Theory.* vol. 45, pp. 1456-1467, July 1999.

[63] H. Jafarkhani, "A quassi orthogonal space-time block code," *IEEE Trans. Commun.* vol. 49, pp. 1- 4, Jan.2001.

[64] G. Papadias and G. Faschini, “capacity-approaching STC for systems employing 4 transmit antennas,” *IEEE Trans. Info. Theory*. vol. 49, no. 3, pp. 726-733, March 2003.

[65] H. Jafarkhani and N. Sashadri, “Super-orthogonal space-time trellis codes,” *IEEE Trans. Inf. Theory*. vol. 49, no. 4, pp. 937-950, April 2003.

[66] J. N. Pillai and S. H. Mneney, “Super-orthogonal space-time trellis codes in rapid rayleigh fading channels," *in proc, South African Telecommunications Networks and Applications Conference(SATNAC* 2005),Central Drakenburg, Durban, South Africa, Sep.2005.

[67] O. Sokoya and B. T. Maharaj, “Performance of super-orthogonal space-time trellis cold in a multipath environment," *in proc. IEEE AFRICON*, Windhoek, Namibia, pp. 5, 26-28, Sept.2007.

[68] M. K. Simon and H. Jafarkhan, “Performance evaluation of super-orthogonal space-time trellis codes using moment generating function- based approach," *IEEE Trans. Signal Process.* vol. 51, no. 11, Nov. 2003.

[69] S. Siwamogsatham and P. Fitz, “Improved high–rate space-time codes via concatenation of expanded orthogonal block code and M-TCM,” *in Proc. IEEE wireless commun. Netw. Conf.*, pp. 264-270, Mar 2002.

[70] G. Ungerboeck, “Channel coding with multilevel/phase signal,” *IEEE Trans. Inf. theory*. vol. IT- 28, no.1, pp. 55-67, Jan. 1982.

[71] D. Disvalar and M. Simon, "Mutiple trellis coded modulation (MTCM)," *IEEE Trans. Commun.*, vol.36, no.4, pp.410-419, Apr 1988.

[72] M. Bale et al, “Computer design of super-orthogonal space-time trellis code,” *IEEE Trans. Wireless Comunm.*, vol. 6, no.2, pp. 463-467, Feb. 2007.

[73] Y. Zhu and H. Jafarkhani, “Differential super-orthogonal space time trellis codes,” *IEEE Trans. Wireless Commun.* vol. 5. no. 12, pp. 3634-3643, Dec. 2006.

[74] E. R. Hartling and H. Jafarkhani, "Design rules for extended super-orthogonal space-time trellis codes," *in Proc. Canadian Conf. Elect. and Computer Eng'g*, pp.001621-001626, 4-7, May 2008.

[75] S. Baro, G. Bauch and A. Hansmann, "Improved codes for space time trellis-coded modulation," *IEEE Commun. Letter,* vol. 4, no. 1., pp. 20-22, Jan. 2000.

[76] I. B. Oluwafemi and S. H. Mneney, "Performance of extended super orthogonal space-time trellis coded OFDM systems," *In Proc. Southern African. Telecommun. Netw. and Appl. Conf. (SATNAC), Spier Estate, South Africa.*, pp. 35-40, 2010.

[77] Y. Gong and K. B. Lataief, "Performance of space-time trellis coding over Nakagami fading channels," *in proc. 53rd IEEE Veh. Tech. Conf., 2001. VTC 2001 Spring*, vol.2, pp.1405-1409, 2001.

[78] C. Cheng, "A Nakagami-m fading channel simulator," *A thesis submitted to the Department of Electrical and Computer Engineering, Queen's University, Kingston, Canada.* Nov. 2000.

[79] M. O. Farooq, W. Li and T. A. Gulliver, "Performance of space-time trellis codes over Nakagami fading channel," *in Proc. IEEE/ ACES/ ICWCACE.* pp. 642-645, 2005.

[80] X. Wang and D. Yue , B. Lin and Y. Gong, "Performance results of space-time block coding over Nakagami-m fading channels," *in proc. Inter. Conf. on Wireless Commun., Netw. and Mobile Computing, 2005.* vol. 1, pp. 81- 84, 23-26 Sept. 2005

[81] M. Uysal, "Pairwise error probability of space-time codes in Rician-Nakagami channels," [Online] [Cited: November 10, 2010.] www.cslgreenhouse.csl.illnois.edu..

[82] K. A. Saaifan and E. K. Al-Hussaini, "Performance of MIMO systems through Nakagami fading channels with arbitrary fading parameter," *wireless pers. commun.*, no. 37 pp. 367-380, 2008.

[83] I. S. Gradshteyn and I. M Ryzhik, *Table of Integrals, Series and Products.* Burlington, USA : Elsevier Inc., 2007.

[84] A. Birol and U. Aygolu, "Super-orthogonal space-time trellis codes for two transmit antenna in fast fading channels," *Int. J. Commun. Syst.*, vol. 21, pp. 331-341, 2008.

[85] G. D. Forney, *Concatenated Codes.* Cambridge M.A : MIT Press, 1996.

[86] D. Cui and A.M. Haimovich, " Design and peformance analysis of turbo space-time coded modulation," *in Proc. IEEE Globecom' 00.* vol. 3, pp. 1627-1631, , San Franscisco, CA, Nov. 27-Dec.1 2000.

[87] D. Cui and A.M. Haimovich, " Error Performance analysis of turbo space-time coded modulation over fadng channel," *In Proc. IEEE Inter. Conf. Commun.(ICC'01),* Hesinki, Finland, June 2001

[88] D. Cui and A.M. Haimovich, "A new bandwidth efficient antenna diversity scheme using turbo codes," *in proc. 34th Annual Conf. info. Sc. and systems(CISS '00).* vol. 1, pp. TA-6.24-29, Printon, NJ, Mar.2000

[89] D. Tujkovic, "Space-time turbo coded modulation," *in proc. finnish wireless commun. workshop.* pp. 85-89, 2000.

[90] D. Tujkovic, "Recursive space-time trellis codes for turbo coded modulation,". *in Proc. IEEE global commun. conf. (GLOBECOM),* pp. 1010-1015, 2000.

[91] I. Altunbas and A. Yongacoglu, "Error performance of serially concatenated space-time coding," *J. Commun. and Netw (JCN).* vol. 3, pp. 135-140, 2003.

[92] H. J. Su and E. Geraniotis, "Space-time turbo codes with full antenna diversity," *IEEE Trans. Commun.,* vol. 49, pp. 47-57, 2002.

[93] X. Lin and RS Blum, "Improved space-time codes using serial concatenation," *IEEE Commun. Letter.* vol. 4, pp. 221-223, 2000.

[94] X. Lin, and R. S. Blum, "Guidline for serially concatenated space-time code design in flat Rayleigh fading channels," *in Proc. 3rd IEEE signal process*

workshop on signal process advances in Wireless Commun., , pp. 247-250, 2001.

[95] X. Lin, and R. S. Blum, "Guidline for serially concatenated space-time code design in flat Rayleigh fading channels," *in proc. 3rd IEEE signal process. workshop on signal process. advances in wireless Commun.,* pp. 247-250, 2001.

[96] L. Goulet and H. Leib, "Serially concatenated space-time codes with iterative decoding and performance limits of block-fading channels," *IEEE J. Sel. Areas Commun.,* vol. 21, pp. 765-773, 2003.

[97] R. H. Deng and D. J. Costello jr., "High rate concatenated coding systems using bandwidth efficient trellis inner codes," *IEEE Trans. Commun.* vol. 37, no.5 pp. 420-427, 1989.

[98] J. Hagenauer and P. Hoeher, "Concatenated Viterbi decoding," *in Proc. 4th joint Swedish-soviet international workshop on Info. theory, pp. 29-33.* Gotland, Sweden 1989.

[99] C. Berrou, A. Glavieux and P. Thitimajshima, "Near Shannon limit error correcting coding: Turbo-codes," *in proceedings IEEE inter. Conf. Commun (ICC).* pp. 1064-1070, 1993.

[100] S. Benedetto and G. Montorsi, "Serial concatenation of interleaved codes: performance analysis, design and iterative decoding," *IEEE Trans. Inf. Theory,* pp. 909-926, May 1998.

[101] S. Benedetto, D. Divsalar, G. Montorsi and F. Pollara, "Analysis, design and iterartive decoding of doulble serially concatented codes with interleavers," *IEEE J. Slect. Areas Commun.* vol. 16, pp. 231-244, Feb.1998.

[102] D. Disalar, and F. Pollara, *Hybrid concatenated code and iterative decoding. 6023783* USA, 2000.

[103] G. Bauch, "Concatenation of space-time block codes and turbo-TCM," *in proc. IEEE Inter. Conf. Commun.(ICC'99).* pp. 1202-1206, June 1999.

[104] K. R. Narayanan, "Turbo decoding of concatenated space-time code," *in proc. 37th Annual Allerton Conf. Commun, control and computing,* Sept 1999.

[105] H. Su and E. Geraniotis, "Spectrally efficient turbo codes with full antenna diversity," *in proc. Multicast Mobility and Teletraffic for wireless Commun.(MMT'99),* Oct. 1999.

[106] A. Stefanov and T. M. Duman, "Turbo coded modulation for systems with transmit and receive antenna diversity," *in Proc IEEE Globecom '99.* pp. 2336-2340, Dec. 1999.

[107] G. J. Byers and F. Takawira, "Double concatenated space-time trellis codes," *in Proc. IEEE AFRICON*, pp. 143-148, 2002

[108] K. Bon-Jin, C. Jong-Moon and K. Changeon, "Analysis of serial and hybrid concatenated space-time codes applying iterative decoding," *Inter. J. Electronics Commun.,* vol. 58, pp. 420-423, 2004.

[109] J. N. Pillai and S.H Mneney, "Concatenated super-orthogonal space-time Trellis codes in Rayleigh fading channels," *in Proc. Inter conf. computer as tool (EUROCON)* , pp. 1814-181, 2005.

[110] I. Altunbas, "Peformance of serially concatenated coding schemes for MIMO systems," *Int. J. Elctron. Commun.,* vol. 61, pp. 1-9, 2007.

[111] J. N. Pillai and S.H. Mneney, "Turbo decoding of super-orthogonal space-time trellis codes in fading channels," *Wireless Pers. Commun.*, vol. 37, no 3-4, pp. 371-385, 2006

[112] A. J. Viterbi, "Error bound for convolutional codes and an asymptotically optimum decoding algorithm," *IEEE Trans. Commun.* vol. IT-13, pp. 260-269, April 1967.

[113] L. R. Bahl, J. Cocke, F. Jelinek and J. Raviv, "Optimal decoding of linear decoding for minimizing symbol error rate," *IEEE Trans. Info. Theory,* vol. IT-20, pp. 284-287, March 1974.

[114] J. Hagenauer and P. Hoeher, "A Viterbi algorithm with soft-decision outputs and its applications," *in proc.IEEE conf. Global Telecommun., (GLOBECOM '89),* pp.1680-1686, vol.3, 27-30, Nov 1989

[115] L. Papke, P. Robertson and E. Villebrun, "Improved decoding with the SOVA in a parallel concatenated(trubo-code) scheme," *in proc. IEEE International Conf. Commun. (ICC 96),* pp.102-106 vol.1, 23-27 Jun 1996.

[116] C. Berrou and A. Glavieux, "Near optimum error correcting and decoding: turbo code," *IEEE Trans. Commun., COM-44: 1261-1271, Oct.1996.*

[117] J. P. Woodard and L. Hanzo, "Comparative study of turbo decoding techniques: An overview," *IEEE Trans. Veh. Techn.* vol. 49, pp. 2208-2232, Nov. 2000.

[118] B. Vucetic and J. Yuan, *"Turbo Codes: Principles and Applications,"* Kluwer Academic, 2000.

[119] S. Benedetto, D. Divsalar G .Montorsi and F. Pollara, "A soft-input soft-output APP module for iterative decoding of concatenated codes," *IEEE Commun. Letter.* vol. 1, no.1, pp. 22-24. Jan 1997.

[120] Y. Wu, Implementation of parallel and serial concatenation convolutional codes, *PhD dissertation,* Faculty of the Virgina Polytechic Institute and State University, July 1999.

[121] J. N. Pillai, Super-orthogonal space-time turbo codes in Rayleigh fading channels. *Master Dissertation.* Submitted to Sch. of Electrical, Electronic and Computer Engineering, University of kwaZuluNatal, South Africa, Nov. 2005.

[122] I. B. Oluwafemi, S. H. Mneney, "Hybrid concatenated super-orthogonal space-time trellis codes applying iterative decoding," *in proc. IEEE AFRICON, 2011 , pp.1-6, 13-15, Sept. 2011.*

[123] V. Branka and Y. Jimhong, *Space-Time Coding,* England : John Willey and son , 2003 1st edition.

[124] B. Lu and X. Wang, "Space-time code design in OFDM systems," *in proc. IEEE Global Commun. Conf.(GLOCOM).* pp.1000- 1004, 2000.

[125] Y. Li and J. Moon, “Performance analysis of bit-interleaved space-time coding for OFDM in block fading channels,” *in proc IEEE VTC 2004*. pp. 684-692, 2004.

[126] D. Tujkovic, M. Junti, M. Latva-aho, “Space frequency coded OFDM for future high data rate wide band radio systems,” *in proc. IEEE Veh. Tech. Conf.*, pp. 2304- 2308, 2001.

[127] W. Su, Z. Safar, M. Olfat, and K.J.R. Liu, “Full diversity space frequency codes for MIMO-OFDM systems," *in proc*. Inter. Symposium Info. Theory 2003, pp.325, June 29-July 4, 2003

[128] Y. Hong and Z. Y. Dong, “Performance analysis of space time trellis coded OFDM system," *Inter. J. of applied Math and Comp. Sc.* vol. 2. no. 2 pp. 59-65, Spring 2006.

[129] H. Boleskei, and A. J. Paulraj, “Space-frequency coded broadband OFDM systems,*" in proc. IEEE wireless commun. and Netw. conf. WCNC*, Chigaco,II, USA,. pp.1-6, Sept.2000.

[130] J. Yue, and J. D. Gidson, “Performance of OFDM Systems with space-time coding,*" in proc. IEEE Wireless Commun. Netw. Conf.*, pp. 280-284, 2002.

[131] I. Dagres, A. Zalonis and A. Polydoros, “An efficient adaptive space-time coding scheme for MIMO- OFDM systems,*”* *in proc*. Inter. Symposium on Info. Theory, 4-9 Sept. 2005.

[132] T. H. Liew and L. Hanzo, “Space-tme block coded adaptive modulation aided OFDM,*" in proc. IEEE Global Telecommun. Conf., 2001. (GLOBECOM '01).* vol.1, pp.136-140, 2001.

[133] Y. Zhang and H. Liu, “Decision-feedback receiver for quasi-orthogonal space-time coded OFDM using correlative coding over fast fading channels," *IEEE Trans. wireless Commun.*, vol. 5, no.11, pp. 3017-3022, Nov. 2006

[134] R. S. Blum, Ye (Geoffrey)Li, J. H.Winters, and Q. Yan, "Improved space -time coding for MIMO-OFDM wireless communications," *IEEE Trans. wireless Commun.* vol. 49, no.11, Nov 2001.

[135] Z. Liu, G. B. Giannakis, S. Barbarossa and A. Scaglione, "Transmit antenna space-time block coding for generalized OFDM in the presence of unknown multipath," *IEEE J. Select Area Commun.* vol. 19, no7, pp. 1352-1364, July 2001.

[136] Z. Liu, Y. Xin, and G. B. Giannakis, "Space-time-frequency coded OFDM over frequency selective channels," *IEEE Trans. signal process.* vol. 50, no. 10, pp. 2465-2476, Oct. 2002.

[137] K. Fang, G. leus and L. Rugini, "Alamouti space-time coded OFDM systems in time -and frequency-selective channels," *in proc. IEEE Global Telecommun. Conf., 2006. (GLOBECOM '06)*, pp.1-5, Nov. 27-Dec. 1, 2006,

[138] B. Lu, X. wang, K. R. Narayanan, "LDPC-based space-time coded OFDM systems over correlated fading channels: performance analysis and receiver design," *IEEE Trans. Commun.*. vol. 50, no.1, Jan.2002.

[139] K. Fang, G. Leus and L. Rugini, "Alamouti space-time coded OFDM systems in time-and frequency-selective channels," *in proc. IEEE Conf. on Global Telecomm. (GLOBECOM '06) pp. 1-5, 2006.*

[140] J. Kim, L. J. Ciminni, Jr. and Justin C. Chuang, "*Coding strategies for OFDM with antenna diversity for high bit rate mobile data applications," in proc. IEEE Vehicular Technology Confenrence (VTC '98)* pp. 763-767, 1998.

[141] A. S. Ibrahim, M. M. Khairy, and A. F. Hussein, "Multilayered space-time block codes for OFDM systems," *in proc. Inter. Conf. on Electrical, Electronic and Computer Engineering, 2004. (ICEEC '04.)* pp. 623- 625, 5-7 Sept. 2004

[142] Y. Hong, J. Yuan and X. Shao, "Robust space-time trellis codes for OFDM systems over quassi-static frequency selective fading channel," *in Proceedings IEEE in Inter. Symposium on personal indoor and mobile radio commun.* pp. 434-438, 2003.

[143] J. Flores, J. Sanchez, and H. Jafarkhani, "Quasi-orthogonal space-time frequency trellis codes for two transmit antenna," *IEEE Trans. wireless commun.*, vol.9, no.7, pp. 2125-2129, July 2010

[144] O. Sokoya and B. T. Maharaj, "Performance of space time coded orthogonal frequency division multiplexing scheme with delay spreads," *in proc. The 14th IEEE Mediterranean Electrotechnical Conference (MELECON 2008)*, pp.198-203, 5-7, May 2008.

[145] O. Sokoya and B. T. Maharaj, "Super-orthogonal block code with channel equalization and OFDM in frequency selective fading," *EURASIP J. Wireless Commun. and Netw*, . 10.1155:153846, 2010.

[146] S. Liu and J. Chong, " Improved design criterion for space-frequency trellis codes over MIMO-OFDM systems. *ETRI Journal*, vol. 26 no. 6 pp. 622 - 634, 2004

[147] H. Jafarkhani, "A quasi-orthogonal space-time block code," *IEEE Trans. Commun.*, vol. 49, no.1, pp.1-4, Jan. 2001.

[148] O. Tirkonen, A. Boariu, and A. Hottinen, "Minimal nonorthogonality rate 1 space-time block code for 3TX antennas," *in proc. IEEE 6th Int. symp. Spread-Spectrum Tech. Appl.* pp. 429-432, Sep. 2000.

[149] H. Jafarkhani and N. Hassanpour, "Super-quasi-orthogonal space-time trellis codes for four transmit antennas," *IEEE Trans. Wireless Commun.*, vol. 4 no. 1, pp. 215-227, Jan. 2005.

[150] A. Birol and U. Aygolu, "Super-orthogonal space-time BPSK trellis code design for 4 tramsmit antennas in fast fading channels," *in proc. 5th Inter. Symp. on Commun. Sys., Net. and Digital Signal Process. (CSNDSP'06)Patras Univ. Conference Centre, Patras, Greece.* July 19-21, 2006.

[151] I. B. Oluwafemi, S. H. Mneney, "Super-quasi-orthogonal space-time BPSK trellis coded OFDM system for four transmit antennas," *in Proc. 2nd Inter. Conf. on Wireless Commun., Veh. Tech., Info. Theory and Aerospace &*

Electronic Systems Tech. (Wireless VITAE). vol., no., pp.1-5, Feb. 28 2011-March 3, 2011.

[152] *"Digital Land Mobile Radio Communications,"* Luxembourg, Belgium : Commission of the European Communities COST 207, 1989.

[153] D. Agrawal, V. Tarokh, A. Naguib and N. Seshadri, "Space-time coded OFDM for high data-rate wireless communication over wideband channels," *in proc. IEEE Veh. Tech. Conf.,* pp. 2232-2236. 1998.

[154] P. Patcharamaneepakor, R. Rajathera and K. Ahmed, "Performance analysis of serial concatenated space-time code in OFDM over frequency selective channel," . *in proc. IEEE Veh. Tech. Conf. (VTC),*. vol. 1, pp. 746-750, 2003.

[155] T. Liew and L. Hanzo, Space-time trellis and space-time block coding versus adaptive modulation and coding aided OFDM for wideband channels. *IEEE Trans. Veh. Tech.* vol. 55, no. 1, pp. 173-187, Jan 2006.

[156] *"Digital Land Mobile Radio Communications,"* Luxembourg, Belgium : Commission of the European Communities. COST 207, 1989.

[157] W. Firmanto, B. Vucetic, J. Yuan and Z. Chen, "Space-time turbo trellis coded modulation for wireless data communication," *Eurasip J. applied signal process.* 2002, vol. 5, pp. 459-470.

[158] C. Dongzhe and A. M. Haimovich, "Performance of parallel concatenated space-time codes," *IEEE Commun. Letters,* vol. 5, no. 6, pp. 236-238, 2001.

[159] Y. Liu, M. P. Fitz and O.Y Takeshita, "QPSK space-time turbo codes," *In proc. IEEE Inter. Conf. Commun. (ICC'00),* June 2000.

[160] Y. Liu and M. P. Fitz, "Space-time turbo codes," *in proc. 37th Annual Allerton Conf. Commun, contrl and computing.* Sept. 1999.

[161] H. J. SU and E. Geraniotis, "Space-time turbo codes with full antenna diversity," *IEEE Trans. Commun.* vol. 49, pp.47-57, 2000.

[162] Y. Hong, J. Yuan, Z. Chen and B. Vucetic, "Space-time turbo trellis codes for two, three, and four transmit antenna," *IEEE Trans. Veh. Tech.* vol. 53, no. 2, March 2004.

[163] V. Gulati and K. R Narayanan, "Concatenated codes for fading channels based on recursive space-time trellis codes," *IEEE Trans. Wireless Commun.* vol. 2, pp. 118-128, 2003.

[164] G. Ferre, J. P. Cance, V. Meghdadi and J. M. Dumas, "New construction rules for space time trellis codes by set partitioning: (turbo) super-orthogonal space-time trellis codes," *in Proc 2nd Inter symp. Commun, control and signal process.* March 2006.

[165] I. B. Oluwafemi and S. H. Mneney, "Peformance of turbo-super orthogonal space-time trellis coded OFDM system," *in proc. 19th Telecom Forum Telfor 2011, 22nd-24th Nov 2011, Belgrade Serbia.*